UNIVERSITY OF SOUTHAMPTON

FACULTY OF ENGINEERING, SCIENCE AND MATHEMATICS,
SCHOOL OF ENGINEERING SCIENCES

NATIONAL CENTRE FOR ADVANCED TRIBOLOGY SOUTHAMPTON

ELECTROCHEMICAL SENSING OF AEROBIC MARINE BACTERIAL BIOFILMS AND THE INFLUENCE OF NITRIC OXIDE ATTACHMENT CONTROL

By

Stéphane Werwinski

Dstl contract of

“Sensor Actuated Smart Interfaces Incorporating Bio-Hybrid Materials (Biofilm Sensing)”

THESIS SUBMITTED FOR THE DEGREE OF

DOCTOR OF PHILOSOPHY

NOVEMBER 2010

UNIVERSITY OF SOUTHAMPTON

ABSTRACT

FACULTY OF ENGINEERING, SCIENCE & MATHEMATICS,
SCHOOL OF ENGINEERING SCIENCES

Doctor of Philosophy

ELECTROCHEMICAL SENSING OF AEROBIC MARINE BACTERIAL BIOFILMS AND THE INFLUENCE OF NITRIC OXIDE ATTACHMENT CONTROL

By Stéphane Werwinski

An attractive alternative to ineffective and inefficient biocide dosing strategies for seawater piping systems would be to monitor, quantitatively evaluate and then induce biofilm disruption when necessary using an environmentally friendly biocide. The aim of the present Dstl and EPSRC funded project is to *(i)* sense for the presence of bacterial biofilms on metallic surfaces within seawater handling systems (*e.g.* heat exchangers, pipework, pumps and valves) by deploying a sensor technology to ultimately disrupt biofilms matrix and to *(ii)* qualitatively and quantitatively assess the extent of bacterial fouling.

An electrochemical sensor using a 0.2 mm diameter gold electrode was characterised in abiotic and biotic media within a modified continuous culture flow cell under a controlled laboratory environment. Herein, electrochemical measurements by imposing electrical cathodic polarisations have demonstrated enhancement of the oxygen reduction reaction within aerobic bacterial biofilms. Importantly, electrochemical impedance spectroscopy at open circuit potential, *i.e.* without electrical imposed polarisation, was successfully employed to monitor initial bacterial biofilms growth and extent. An important parameter of the sensor response (capacitive component) can provide insight into quantitative evaluation of the interface, where for the first time *in situ* quantifiable EIS data were in good agreement with *ex situ* confocal microscopy analyses. Consequently, a relationship for the surface charge density (capacitive component / estimated number of sessile bacterial population) has outlined its potential use for in-service conditions. Uniquely, the electrochemical performances of a 72 h-old biofilmed gold surface dosed with nanomolar concentration; 500 nM, of the nitric oxide donor sodium nitroprusside were presented. Corroborative confocal microscopy studies have revealed effective and efficient dispersal of aerobic bacterial biofilms exposed to nitric oxide.

Overall, this unique qualitative and quantitative bacterial biofilm investigation utilising a modified once through flow cell, *i.e.* combining microbiological and engineering expertise, represents an important first step in controlling of marine biofouling within seawater piping systems. Gold multi-microelectrode arrays located on likely biofouling positions within the seawater piping systems should be used for enhanced effectiveness of the biofilm sensing / disruption strategy.

Table of contents

List of Figures

List of Tables

List of acronyms

Abbreviation	Meaning
AAS	Atomic Absorption Spectroscopy
ads	Adsorbed
AFM	Atomic Force Microscopy
Ag	Silver
AgCl	Silver Chloride
Al	Aluminium
Al_2O_3	Alumina
ANH	Anhydrous
Ar	Argon
ASW	Artificial Seawater
ATP	Adenosine Triphosphate
ATR	Attenuated Total Reflectance
Au	Gold
BES	Bioelectrochemical System
BGE	Bacterial Growth Efficiency
C	Element Carbon
Ca^{2+}	Calcium ion
CE	Capillary Electrophoresis
Cl^-	Chloride ion
CLEM	Correlative Light Electron Microscopy
CLSM	Confocal Laser Scanning Microscopy
CO_2	Carbon Dioxide
CPE	Constant Phase Element
CTD	Conductivity-Temperature-Depth
Cu	Copper
Cu^+	Copper (I) ion
Cu^{2+}	Copper (II) ion
CuCl	Cuprous Chloride
$CuCl_2^-$	DichloroCuprous anion complex

Cu-Ni	Copper-Nickel
CuO	Cupric Oxide
Cu_2O	Cuprous Oxide
CuOH	Copper (I) Hydroxide
$Cu_2(OH)_3Cl$	Atacamite
$Cu_2S(NiFe)_3S_4$	Copper (I) sulphide-violarite complex
CV	Cyclic Voltammetry
dc	Direct-current
DGGE	Denaturing Gradient Gel Electrophoresis
DIC	Differential Interference Contrast
dis	Dissolution
dis'	Dissolution
DNA	Deoxyribo Nucleic Acid
DO	Dissolved Oxygen
Dstl	Defence Science and Technology Laboratory
DTM	Differential Turbidity Measurement
e^-	Electron
EC	Equivalent Circuit
EDIC	Episcopic Differential Interference Contrast
EDS	Energy Dispersive X-ray Spectroscopy
EDTA	Ethylenediaminetetraacetic acid
EET	Extracellular Electron Transfer
EF	Epifluorescence
EIS	Electrochemical Impedance Spectroscopy
ELISA	Enzyme-Linked Immunosorbent Assay
EN	Electrochemical Noise
EPA	Environmental Protection Agency
EPS	Extracellular Polymeric Substance
EPSRC	Engineering and Physical Sciences Research Council
EQCM	Electrochemical Quartz Crystal Microbalance
EQUIVCRT	Equivalent Circuit software
ESEM	Environmental Scanning Electron Microscopy
FACSort	Fluorescence-Activated Cell Sorter

FCS	Fluorescence Correlation Spectroscopy
Fe	Iron
FFF	Field Flow Fractionation
FISH	Fluorescent In Situ Hybridisation
FLIM	Fluorescence Lifetime Imaging Microscopy
FRA	Frequency Response Analyser
FRAP	Fluorescent Recovery After Photo-bleaching
FRET	Förster Resonance Energy Transfer
FTIR	Fourier Transform Infrared
GC	Gas Chromatography
GE	Gel Electrophoresis
GFP	Green Fluorescent Protein
H^+	Proton or Hydrogen ion
H_2	Hydrogen
H_2CO_3	Carbonic acid
H_2O	Water
H_2O_2	Hydrogen Peroxide
HS^-	Hydrogen Sulphide ion
H_2S	Hydrogen Sulphide
H_2SO_4	Sulphuric Acid
IFREMER	Institut Francais de Recherche pour l'Exploitation de la Mer
IR	Infrared Radiation
ISA	Image Structure Analyser
K^+	Potassium ion
KCl	Potassium Chloride
Kr	Krypton
LC	Liquid Chromatography
LCS	Leica Confocal Software
LSCM	Laser Scanning Confocal Microscopy
MATLAB	MATtrix LABoratory
MFC	Microbial Fuel Cell
Mg^{2+}	Magnesium ion
MIC	Microbiologically Influenced Corrosion

MRI	Magnetic Resonance Imaging
MSS	Mechatronic Surface Sensor
N	Element Nitrogen
N_2	Nitrogen
Na^+	Sodium ion
NaCl	Sodium Chloride
Na_2CO_3	Sodium Carbonate
$NaHCO_3$	Sodium Bicarbonate / Sodium Hydrogen Carbonate
nCATS	national Centre for Advanced Tribology, Southampton
NCIMB	National Collection of Industrial, Marine and Food Bacteria
NEXAFS	Near-Edge X-ray Absorption Fine Structure
NH_4^+	Ammonium ion
Ni	Nickel
$(NiFe)_3S_4$	Violarite
NIH	National Institutes of Health
NMR	Nuclear Magnetic Resonance
NO	Nitric Oxide
N_2O	Nitrous Oxide
NO_3^-	Nitrate ion
NOC	National Oceanography Centre
O_2	Oxygen
O_2^-	Superoxide anion
OCP	Open Circuit Potential
OCT	Optical Coherence Tomography
$OH^\bullet$	Hydroxyl radical
OH^-	Hydroxyl ion
ORR	Oxygen Reduction Reaction
OTEC	Ocean Thermal Energy Conversion
P	Element Phosphorus
PCR	Polymerase Chain Reaction
PC	Polycarbonate
Pd	Palladium
PEEK	Polyetheretherketone

PEMC	Piezoelectric-Excited Millimetre-sized Cantilever
PFGE	Pulsed Field Gel Electrophoresis
PTFE	Polytetrafluoroethylene
PhD	Doctor of Philosophy
PHLIP	PHobia Laser scanning microscopy Imaging Processor
ppm	Parts Per Million
Pt	Platinum
PZC	Potential of Zero Charge
QCM	Quartz Crystal Microbalance
RAPD	Random Amplified Polymorphic DNA
RDE	Rotating Disk Electrode
Rh	Rhodium
RLC	Resistors, inductors, and capacitors
rms	Root Mean Square
RNA	Ribo Nucleic Acid
RNS	Reactive Nitrogen Species
RFLP	Restriction Fragment Length Polymorphism
RSNO	S-nitrosothiols
S^{2-}	Sulphide ion
SAW	Surface Acoustic Wave
SBS	School of Biological Sciences
SCLM	Scanning Confocal Laser Microscopy
SEC	Size Exclusion Chromatography
SECM	Scanning Electrochemical Microscopy
SEM	Scanning Electron Microscopy
SES	School of Engineering Sciences
Si	Element Silicon
SICM	Scanning Ion Conductance Microscopy
SNP	Sodium Nitroprusside
SO_4^{2-}	Sulfate ion
sol	Solution
SR	Synchrotron Radiation
SRB	Sulphate Reducing Bacteria

SS	Stainless Steel
STED	Stimulated Emission Depletion
STXM	Scanning Transmission X-ray Microscopy
TBT	Tri-*n*-butyultin
TEM	Transmission Electron Microscopy
TRB	Thiosulphate Reducing Bacteria
Ti	Titanium
UK	United Kingdom
UNS	Unified Numbering System
UoS	University of Southampton
USA	United States of America
UV	Ultra Violet
w/v	Weight / volume percentage or percentage solution
3D	Three-Dimensional

Nomenclature

Term	Meaning	Unit
A'	Cross sectional area of the flow chamber	m^2
a_i	Activity of species i	dimensionless
b	Depth of the flow chamber	m
c	Concentration of a relevant species	mol cm^3
C_{ADS}	Capacitive component for adsorbed biological material and / or organic material (normalised)	F cm^{-2}
C_{con}	Capacitance of the conditioning film (normalised)	F cm^{-2}
C_{dl}	Double layer capacitance (normalised)	F cm^{-2}
C_{eff}	Effective capacitance (normalised)	F cm^{-2}
C_{EPS}	Capacitance of the EPS matrix (normalised)	F cm^{-2}
C_{ref}	External reference capacitance (normalised)	F cm^{-2}
d	Pipe diameter or diameter of the circular flow chamber	m
D	Diffusion coefficient of a species	m^2 s^{-1}
D_f	Diffusion coefficient in the biofilm	m^2 s^{-1}
D_h	Hydraulic diameter	m
D_i	Dilution rate	h^{-1}
E	Potential measured at the interface (*vs.* Ag/AgCl, 3.5 M KCl)	V
$E^{0'}$	Formal potential of the electrode converted into potentials (*E vs.* Ag/AgCl, 3.5 M KCl)	V
E_p	Peak potential (*vs.* Ag/AgCl, 3.5 M KCl)	V
E_{pa}	Anodic peak potential (*vs.* Ag/AgCl, 3.5 M KCl)	V
E_{pc}	Cathodic peak potential (*vs.* Ag/AgCl, 3.5 M KCl)	V
E_r	Reduction potential of the corresponding reaction converted into potentials (*E vs.* Ag/AgCl, 3.5 M KCl)	V
f	Frequency	Hz
F	Faraday constant	96,485 C mol^{-1}
f_D	Darcy frictional resistance to fluid	dimensionless
$F(w'/b)$	Function used to calculate the pressure drop in **Equation 4.6**	dimensionless

$G(w'/b)$	Geometric factor used to compute the Darcy frictional resistance to fluid in **Equation 4.7**	dimensionless
h	Overall heat transfer coefficient	W m^{-2} K^{-1}
i_{anodic}	Anodic current across an electrochemical interface	A
$i_{cathodic}$	Cathodic current across an electrochemical interface	A
$i_{faradaic}$	Faradaic current of the cathodic branch	A
$i_{non\text{-}faradaic}$	Non-faradaic current of the cathodic branch	A
i_{obs}	Observed current across an electrochemical interface	A
j	Imaginary number (**Equation 2.26**)	dimensionless
j	Current density (**Equation 5.14**)	A cm^{-2}
j_{OCP}	Current density at the open circuit potential	A cm^{-2}
j_p	Peak current density	A cm^{-2}
j_{pa}	Anodic peak current density	A cm^{-2}
j_{pc}	Cathodic peak current density	A cm^{-2}
k^0	Standard heterogeneous rate constant	cm s^{-1}
K	Loss coefficient	dimensionless
k_F	Coefficient for $F(w'/b)$ in **Equation 4.10**	dimensionless
K_m	Mass transfer coefficient	m s^{-1}
k_β	Reaction rate constant at step β (I to IV) for order n ≥ 0	mol^{1-n} L^{n-1} s^{-1}
l	Pipe length	m
l'	Length of the flow chamber	m
L	Characteristic length	m
L_e	Entrance length through a rectangular cross-section	m
n	Empirical exponent of the CPE	dimensionless
n_b	Number of generations between t_0 and t	dimensionless
P	P-value	dimensionless
Q	Flow rate	m^3 s^{-1}
Q_a	Anodic surface charge density	C cm^{-2}
Q_{ADS}	Surface charge density	C cm^{-2}
$Q_{ADS(abiotic)}$	Surface charge density for the abiotic condition	C cm^{-2}
$Q_{ADS(biotic)}$	Surface charge density for the biotic condition	C cm^{-2}
r	Microdisk electrode radius	cm

r^2	Square of the sample correlation coefficient	dimensionless
R	Molar gas constant	8.3144 J K^{-1} mol^{-1}
R_a	Surface roughness	μm
R_{ct}	Charge transfer resistance (normalised)	Ω cm^{-2}
R_e	Reynolds number	dimensionless
R_f	Film resistance (normalised)	Ω cm^{-2}
R_h	Heat transfer resistance	m^2 K W^{-1}
R_k	Roughness Reynolds number	dimensionless
R_{rms}	Root mean square roughness	μm
R_s	Solution resistance (normalised)	Ω cm^{-2}
t	Time representative of the beginning of the stationary phase	h
T	Temperature of the solution	K
t_d	Average generation time	h
t_r	Residence time	s
t_0	Time representative of the beginning of the exponential growth	h
t_1	Time representative of 0.080 V (*vs.* Ag/AgCl) in **Equation 5.14**	s
t_2	Time representative of 0.150 V (*vs.* Ag/AgCl) in **Equation 5.14**	s
u	Mean velocity	m s^{-1}
V	Volume of solution	m^3
V_t	Total volume inside the flow channel	m^3
x	Cell density	cells mL^{-1}
x_t	Cell density at t	cells mL^{-1}
x_0	Cell density at t_0	cells mL^{-1}
ω	Angular frequency	rad s^{-1}
w'	Width of the flow chamber	m
w'/b	Side ratio of a straight rectangular channel	dimensionless
W'	Wetted perimeter of the flow chamber cross-section	m
Y_0	Admittance constant	Ω^{-1} cm^{-2} s^n
z	Number of electrons involved in an electrochemical reaction	dimensionless

Z_{CPE}	Impedance of a CPE (normalised)	$\Omega\ \mathrm{cm}^{-2}$
Z_W	Warburg impedance (normalised)	$\Omega\ \mathrm{cm}^{-2}$
α	Transfer coefficient	dimensionless
α_{a}	Anodic transfer coefficient	dimensionless
α_{c}	Cathodic transfer coefficient	dimensionless
β	Step (I to IV) of the reaction rate constant k_β	dimensionless
Γ_{ADS}	Amount of adsorbed biological material and / or organic material (normalised)	$\mathrm{mol\ cm}^{-2}$
δ_{b}	Biofilm thickness	$\mu\mathrm{m}$
δ_{d}	Diffusional / diffusion boundary layer thickness	$\mu\mathrm{m}$
δ_{l}	Viscous sublayer thickness	$\mu\mathrm{m}$
δ_{t}	Thermal boundary layer thickness	$\mu\mathrm{m}$
ΔE_{p}	Peak potential separation (*vs.* Ag/AgCl, 3.5 M KCl)	V
ΔP	Pressure drop	Pa
θ	EIS phase angle (between the applied voltage and the induced current)	deg
θ_{K}	Included angle	deg
λ	Wavelength	nm
μ	Dynamic viscosity	$\mathrm{kg\ m}^{-1}\ \mathrm{s}^{-1}$
μ_{b}	Specific growth of a bacterial species	h^{-1}
ν	Scan rate	$\mathrm{V\ s}^{-1}$
$\nu^{1/2}$	Square root of the scan rate	$\mathrm{V}^{1/2}\ \mathrm{s}^{-1/2}$
ν_{k}	Kinematic viscosity	$\mathrm{m}^2\ \mathrm{s}^{-1}$
ρ	Density	$\mathrm{kg\ m}^{-3}$
σ	Electrical conductivity	$\mathrm{mS\ cm}^{-1}$
$\sigma_{C_{\mathrm{eff}}}$	Measurement uncertainty for the C_{eff} value	$\mathrm{F\ cm}^{-2}$
$\sigma_{R_{\mathrm{ct}}}$	Measurement uncertainty for the R_{ct} value	$\Omega\ \mathrm{cm}^{-2}$
σ_{Y_0}	Measurement uncertainty for the Y_0 value	$\Omega^{-1}\ \mathrm{cm}^{-2}\ \mathrm{s}^{\mathrm{n}}$
τ	Shear stress	Pa
τ_{w}	Average wall shear stress	Pa
χ^2	Error for equivalent circuit best-fit	dimensionless

Declaration of authorship

I, Stéphane Werwinski, declare that the thesis entitled **"Electrochemical Sensing Of Aerobic Marine Bacterial Biofilms And The Influence Of Nitric Oxide Attachment Control"** is an account of the work carried out by me as part of the national Centre for Advanced Tribology, Southampton (nCATS), School of Engineering Sciences, University of Southampton, UK.

The work presented in this thesis is my own, and has been generated by me as the result of my own original research. I confirm that:

- this work was done wholly or mainly while in candidature for a research degree at this University;
- where any part of this thesis has previously been submitted for a degree or any other qualification at this University or any other institution, this has been clearly stated;
- where I have consulted the published work of others, this is always clearly attributed;
- where I have quoted from the work of others, the source is always given. With the exception of such quotations, this thesis is entirely my own work;
- I have acknowledged all main sources of help;
- where the thesis is based on work done by myself jointly with others, I have made clear exactly what was done by others and what I have contributed myself;
- parts of this work have been published as:

Journal publication

M. Salta, J.A. Wharton, P. Stoodley, S.P. Dennington, L.R. Goodes, S. Werwinski, U. Mart, R.J.K. Wood and K.R. Stookes, Designing biomimetic antifouling surfaces, *Philosophical Transactions of the Royal Society A*, **368**(1929), 4729-4754 (2010).

Conference publications

S. Werwinski, J.A. Wharton, R.J.K. Wood, M.D. Iglesias-Rodriguez and K.R. Stokes, *Electrochemical sensing of aerobic marine bacterial biofilms and the influence of nitric oxide attachment control*, MRS Spring Meeting - Symposium KK: Microbial Life on Surfaces – Biofilm-Material Interactions, San Francisco, California, 25 – 29 April, 2011.

S. Werwinski, J.A. Wharton, R.J.K. Wood, M.D. Iglesias-Rodriguez and K.R. Stokes, *Electrochemical Sensing for Aerobic Marine Bacterial Biofilms within Seawater Piping Systems*, Presented at:

- The 216th Electrochemical Society Meeting, Vienna, Austria, 4 – 9 October, 2009.
- Eurocorr 2009, Nice, France, September 6 – 10, 2009.
- The XXth International Symposium on Bioelectrochemistry and Bioenergetics, the Bioelectrochemical Society Meeting, Sibiu, Romania, 10 – 14 May, 2009.

Poster

S. Werwinski, J.A. Wharton, R.J.K. Wood, M.D. Iglesias-Rodriguez and K.R. Stokes, *Electrochemical Sensing for Marine Bacterial Biofilms,* The 14th International Congress on Marine Corrosion and Fouling, Kobe, Japan, July 27-31, 2008.

Signed: **Date:** 6th November 2010

Stéphane Werwinski

Acknowledgements

When embarking on a PhD, *i.e.* what I describe as a *'mental marathon'*, I would have never imagined (*good grief now I can realise!*) the long period of thinking and persistence required to achieve my own modest contribution to the science. On the top of that, differences in approach along with the barrier language between UK and France were somewhat challenging. Overall, I am extremely delighted the way things turned out.

First at all, I would like to thank especially my principal supervisor Dr Julian Wharton for his guidance, persistence and endless support throughout this PhD project. I personally recommend Dr Wharton for his excellent supervision, experience on engineering projects and for his scientific skills.

I would like to express my gratitude to my charismatic supervisor Prof Robert Wood, director of the national Centre for Advanced Tribology, Southampton (nCATS), to whom I have great admiration for his willingness to buildup a cohesive and highly qualified research group, for his wise words, intellect, and also passion for research.

Funding from the Defence Science and Technology Laboratory (Dstl) and the Engineering and Physical Sciences Research Council (EPSRC) are gratefully acknowledged. In particular, I would like to express my appreciation to my industrial supervisors; the enthusiastic Prof Keith Stokes and Prof Richard Jones (Dstl) for their guidance and financial support for the project.

My special thanks to my advisor Dr Debora Iglesias-Rodriguez for her enthusiasm, endless energy, advice, encouragement and willingness to share laboratory facilities at the National Oceanography Centre (NOC), Southampton. Likewise, I am grateful to Dr John Gittins and Mr Ross Holland from the NOC for the technical support and advice on the bacteria culture protocol and the marine flow cytometry.

I am also very appreciative to Dr Mengyan Nie (nCATS) and Dr Guy Denuault from the School of Chemistry, University of Southampton (UoS) for the discussions on electrochemistry. Similarly, I must not forget Dr Paul Stoodley (nCATS) for his invaluable technical support and advice on my confocal microscopy images.

I wish to thank Dr Hans Schuppe from the School of Biological Sciences (SBS), UoS for his technical support and expertise on the confocal microscopy technique. In addition, thank you to Dr Jeremy Webb and Prof Bill Keevil from the SBS, UoS for the discussions on flow cell devices, chemostats and fluorescence microscopy. Also, thanks to Dr Claire Hellio from the SBS, University of Portsmouth for the discussions on biofouling.

I would like to acknowledge the work done by members of staff at the University of Southampton and in particular: Miss Sue Berger, Mrs Alessia Plutino, Mrs Dawn Attree, Mrs Sonya Manton, Mrs Gwyneth Skiller, Mrs Julia Zimbler, Mr Robert Barnes, Mr Chris Williams, Mr Steve Pilcher, Mr Erik Roszkowiak and Mr David Brennan.

I am particularly grateful to all my PhD mates from Room 4061 with whom I tried to keep my mental health in a safe state (Dr Shiva Rajahram, Dr Lily Chambers, Dr Ramkumar Penchaliah and Dr James Booth). Special thanks to the Tribology UK V Organising Committee (Dr Dan Sun, Dr Jennifer Ang, Dr Mark Craig, Dr Fitri Ismail, Dr Nick Chen, Mr Apostolos Patatoukas and once again Dr Shiva Rajahram) I had the

pleasure to chair and to my friends, nice and / or interesting people I met at Southampton, in particular: Dr Cédric Floquet and Dr Peggy Courtois (thanks for offering me free accommodation for more than two weeks during the final stage of my writing-up), Dr David Barat, Mr Sylvain Boyer, Dr Alex Dickinson, Mr Robert Hanzal, Dr Guillaume Charria, Miss Maria Salta, Dr Peter Glynne-Jones, Dr Laure Grignon, Dr Mandar Thakare, Dr Manuela Hartmann, Mr Guillaume Monin, Dr Aude Bouchier, Dr Gaelle Delaizir, Dr Mamadou Bah, Dr Georges Limbert, Dr Rakesh Barik, Miss Jonee Zunega, Dr Takamasa Tsubouchi, Dr Terry Harvey (thanks for kindly processing my Agresso forms and driving me down to NOC), Dr Simon Dennington, Mr Liam Goodes, Dr Martin Brown, Dr Jurgita Zekonyte, Dr John Walker, Dr Ilaria Corni, Dr Bethan Jones, Prof Frank Walsh (thanks for the relevant feedback used to support this thesis), Prof Mark Spearing (thanks for asking challenging questions), etc...

Thank you to the Southampton Aikikai (Dr Alex Megann, Dr Jim Anderson, Dr Adam Blaker, Mr Robert Lemmen, Mr Karl Baverstock among many others) for sharing with me my passion: aikido. In particular, thanks to my Senseis, Alex Megann and Jim Anderson, for teaching me the concept of '*a maximum effect for a minimum effort*', how to relax my shoulders (*too much typing*) and extend my uke (*more amplitude*).

Last but not the least, I wish to thank my parents for their love, support and patience. The extent of their contribution to materialise this thesis cannot be expressed in a few words, thus this work is dedicated to my family.

In loving memory of my grandmothers, **mémé Rolande** and **mémé Marie**

'It doesn't matter how beautiful your theory is, it doesn't matter how smart you are. If it doesn't agree with experiment, it's wrong.' Richard P. Feynman

Chapter 1 – Introduction

1.1. Project scope

Marine bacteria are ubiquitous and are usually reported to be the primary colonisers on metallic surfaces in seawater handling systems, *e.g.* copper (Cu) alloys, titanium (Ti), and play a pivotal role in the initial microbial biofilm development, and also the maintenance of a biofouling community [**1.1**]. The engineering issues of this troublesome phenomenon in naval applications and in merchant shipping are numerous and can cause excessive capital costs, *e.g.* material costs associated with the replacing header castings alone are in excess of £100k each and heat exchanger fouling alone costs the UK up to £300 – 500 million per annum [**1.2**,**1.3**]. To combine reasonable expenses and higher operational availability, ship owners need enhanced preventive maintenance schedule of marine platforms [**1.2**,**1.4**].

Biofilms and fouling within seawater handling systems can affect the hydrodynamic properties (surface frictional resistance and cause flow restrictions) and reduce heat transfer performance of operating marine heat exchangers leading to frequent failures and blockages of components [**1.2**,**1.5**,**1.6**]. In addition, marine organisms can interact with metallic surfaces and be involved in corrosion pathways through biocorrosion mechanisms [**1.2**,**1.7**]. Although the problems of biofouling in marine heat exchangers are abundant, reliable and accurate techniques capable of sensing for the presence and extent of biofilms on metallic surfaces are still required [**1.2**,**1.8**]. Also, the proposed interfacial process / mechanism attributed to aerobic biofilm action to enzymatic processes needs to be better understood [**1.9**].

Biofilm inhibition strategies based on biocides for killing organisms are often ineffective, inefficient and costly. In this instance, effective cleaning is usually not achieved and dead organisms can be substantial biomass for further biofouling formation and extent [**1.2**]. In addition, the environmental impact is becoming important since the use of biocides is being restricted due to increased ecological concerns and legislature [**1.1**,**1.2**]. For instance, biocides for seawater piping systems such as chlorine, hypochlorite and chloride dioxide can react with the biomass to produce toxic by-products, which will eventually be discharged from the outflows of the marine systems. It has also been reported that biocides may lead to the buildup of microorganism resistance [**1.2**]. As a consequence, there is an increasing focus on both smart sensing surfaces and early warning systems that can quantitatively evaluate the metal / seawater interface and provide information of the extent of biofouling in order to establish a suitable and effective biocide dosing strategy.

1.2. Project outline

This thesis will focus on these two key areas: bacterial biofilm sensing and disruption, where the ultimate long-term objective would be to link new robust sensor technology with novel biofilm control to produce smart surfaces that are capable of a quantitative evaluation of the interface. This investigation has drawn on and strengthened existing collaborations at the University of Southampton (UoS) between the national Centre for Advanced Tribology, Southampton (nCATS) within the School of Engineering Sciences (SES), and with other research groups within the School of Biological Sciences (SBS) and the National Oceanography Centre (NOC).

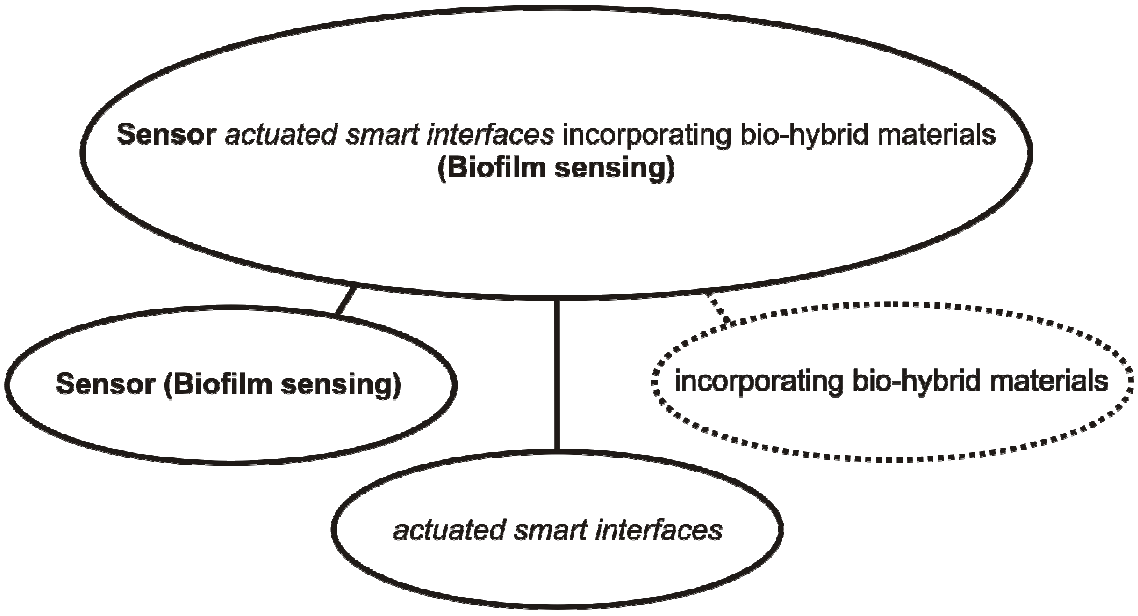

Figure 1.1. Dstl project title interpretation.

As outlined in **Figure 1.1**, three distinguishable project components have been identified for the ultimate goal of this Dstl funded project:

- "**Sensor (Biofilm sensing)**" refers to the detection of bacterial biofilms using a sensor technology [**1.2**], which excludes conventional biological techniques relying on sampling of defined surface areas or on exposure of test surfaces, *i.e.* coupons with subsequent time lag between laboratory analyses and results [**1.2**].
- "*actuated smart interfaces*" means an integrated structure similar to a transducer [**1.10**,**1.11**] that will respond to the sensor signal aiming to quantify the extent of bacterial biofilm and disrupt its integrity.
- "incorporating bio-hybrid materials" (bio-hybrid materials are often utilised for therapeutic devices and are based on a variety of natural biological recognition elements [**1.12**]) in this instance would refer to the capability of using biofilm precursor chemicals and biochemicals in an engineered application for quantitative evaluation of disruption [**1.13**-**1.15**].

1.3. Thesis structure

This thesis aims to sense for the presence of marine biofilm in the field and ultimately clean marine piping systems using an engineering approach. To define the strategy that will support the thesis objectives, a detailed literature review on marine biofouling in nature and within operating marine heat exchangers, biofilm sensing, microscopic and inhibition techniques is addressed in **Chapter 2**. The physico-chemical properties of seawater and the biological background are presented in **Chapter 3**. **Chapter 4** concerns the experimental details used to support the results and discussion in **Chapter 5**. Finally, **Chapter 6** highlights the main conclusions of this thesis and it summarises the potential key routes that may assist in defining a work programme in the future (further work).

Chapter 2 – Literature review

A broad literature review of biofilm sensing and inhibition has been undertaken to define a combined marine bacterial biofilm sensing / disruption strategy for marine piping systems. The starting point was to address a fundamental understanding of overall marine biofouling, bacterial biofilm growth rates and extent on metallic surfaces. To diagnose biofouling in-service, marine heat exchangers represent the overall engineering systems for the thesis, where metallic surfaces are directly exposed to seawater and thus subject to biofouling. Then, biofilm sensing, microscopic and inhibition techniques were presented with an emphasis on the key aspects that have supported the chosen engineering approach. Likewise, marine environmental concerns and legislature are of crucial importance. Thus, **Table 2.1** represents the keyword summary that has assisted in defining the search strategy for the literature review.

Table 2.1. Project keyword and phase classification.

System	Sensor for marine piping systems, where metallic surfaces are directly exposed to seawater
Aim	Detect bacterial biofilm growth and extent onto sensor surface
	Disrupt biofouling by complying to marine environmental terms and legislature
	Give quantitative information on biofilm formation and development, and also its disruption
Characteristics	*In situ* (*i.e.* detect and disrupt exactly in place where it occurs)
	Smart
	Real time
	Easy to use
	Sensitive
	Rapid time response
Application	Marine biotechnology applications
Target	Marine, aquatic bacterial cells / biofilms
Scale	Laboratory (short-term)
	In-service (long-term)
Cost	Affordable price – facile supply of component materials and scale-up

Metallic surfaces used for marine applications (*e.g.* heat exchangers, offshore structures, condenser tubes or pipelines) can undergo a series of undesirable accumulation of microorganisms, algae and animals in a process termed marine biofouling [**2.1**-**2.4**].

In addition, competing formation of non-biological deposits can occur on metallic surfaces:

- corrosion (*e.g.* corrosion product deposits),
- precipitation or scaling / chalking, *e.g.* deposition of inorganic material such as calcareous deposits: calcium carbonates, magnesium hydroxides and products of chemical reactions,
- particulate, *e.g.* deposition of organic material such as oil, humic substances, proteins, detritus, silica, clay and other suspended particles.

Marine biofouling is often divided into micro and macrofouling stages. Microfouling refers to a microbial colonisation step and subsequent developments of microorganisms, for instance bacteria, microalgae, phytoplanktons, unicellular fungi and protozoa on a metallic surface. On the other hand, macrofouling represents a biofouling stage where macroorganisms, such as macroalgae, sponges, barnacles, mussels, tubeworms and other animals settle on the colonised surface [**2.1**,**2.2**,**2.4**].

2.1 Marine biofouling: initiation by bacterial biofilms?

Although there is still much debate on the exact sequence of biofouling formation on metallic surfaces, it is often reported that the microbial adhesion precedes the macrofouling stage [**2.1**,**2.4**]. Many published articles even suggest that bacteria (within the microbial fouling) are the primary colonisers of a metallic surface (especially in heat exchangers [**2.5**]) and play a pivotal role in the initial biofilm development and the maintenance of a biofouling community [**2.1**,**2.6**,**2.7**]. For instance, the development of a bacterial microfilm, *i.e.* bacterial biofilm from *Pseudoalteromonas* (*Pseudomonas* for the ex-taxonomic name) *sp.* S9, on the inner walls of heat exchangers can initiate the settlement of *Ciona intestinalis* larvae [**2.7**,**2.8**]. In addition, the development of modern analysis methods, in particular confocal laser scanning microscopy (CLSM), has resulted in the appreciation that biofilms are highly heterogeneous, three-dimensional (3D) structures that contain complex communities of bacteria in an extracellular polymeric substance (EPS) matrix [**2.9**,**2.10**].

These previous considerations have led marine scientists to study the interaction between bacteria and metallic surfaces. To date, neither the strains of bacterial biofilms that facilitate the settlement of invertebrate larvae nor the signals inducing this settlement have been characterised and identified in great details [**2.7**]. Also, most of the studies have focused on bacterial adhesion and the nature of the EPS supporting that polysaccharides can act as adhesives for cells. However, the nature of these adhesives and their interactions with metallic surfaces remains an open question [**2.4**]. The challenge is still to fully understand the influence of the bacterial metabolism on the corrosion rate of metals, a research area defined as biocorrosion or microbiologically influenced corrosion (MIC), *i.e.* referring to corrosion of metals caused by biological organisms or microbes [**2.11**,**2.12**]. These microbes are categorised by common characteristics such as their by-products, the EPS matrix or compounds they affect, *e.g.* sulphur oxidising. The microbes can be classified into one of two groups based upon their oxygen (O_2) requirements: aerobic, which require O_2, such as sulphur oxidising bacteria; and anaerobic, requiring little or no O_2, such as sulphate reducing bacteria (SRB). The most studied case of MIC has been attributed to anaerobic bacteria on metallic surfaces, *i.e.* the corrosion of mild steel caused by SRB [**2.1**,**2.3**]. However, this mechanism of MIC is closely related to the type of microorganisms active in the biofilm (*i.e.* SRB) and to their metabolic reactions. Overall, mechanisms of MIC that depend on the physiology of sessile microbes are specific. Consequently, this consideration and similar approaches, which aim to establish non-universal mechanisms of MIC, may be inappropriate in a more complex environment with biofilms in the field (aerobic species). According to the published literature [**2.1**,**2.2**,**2.4**,**2.6**-**2.8**,**2.13**], marine bacteria are the most likely species to initiate and develop biofouling and biocorrosion on metallic surfaces.

2.2 Marine bacterial biofouling: the background and context

Marine bacterial biofilms are reported to form and develop on any exposed metallic surfaces, *e.g.* offshore platforms, naval and commercial vessels, and also submerged structures in seawater [**2.1**,**2.4**,**2.5**,**2.14**]. However, a general understanding of this troublesome phenomenon – precursor in the attachment of macrofouling organisms, and its control in seawater systems is scarce [**2.4**,**2.7**,**2.15**]. Consequently, it is increasingly essential to establish a detailed knowledge of the mechanisms that govern the interaction of bacterial biofilms and marine metallic surfaces. This will help to avoid the damaging degradation caused by biofouling and biocorrosion to ensure the operational effectiveness of many marine systems.

There are numerous reports detailing the important role played by the initial bacterial settlement, both on the onset and propagation of localised corrosion and on the enhancement of galvanic corrosion of less noble material [**2.2**,**2.16**,**2.17**]. MIC can also cause serious corrosion damage, which is often associated with metal rupture in pipelines, water tanks and many other industrial systems [**2.18**]. In addition, frequent failures due to biofouling are attributed to the reduction in heat exchanger performance (caused by the insulating nature of the biofilm), fluid impediment and blockages of fluid-handling components – pumps, filters, valves and condensers [**2.3**,**2.19**]. Thus, reliable and accurate techniques capable of sensing for the presence of bacterial biofilm and extent on metallic surfaces are required for marine systems, *e.g.* submarines, ships, docks and jetties.

Classical microbiological methods commonly used to detect and characterise bacterial biofilms, *e.g.* the Robbin device consisting in plugs inserted into pipe walls in order to experience similar shear stress as the wall itself, are typically based on *ex situ* measurements (requiring sample removal and identification) [**2.20**]. These techniques can potentially affect field bacterial biofilms and involve time-lag between analyses and results, and are, as a consequence, not appropriate for *in situ* sensing (to detect exactly in place where biofilm forms an develops). Similarly, biofilm inhibition strategies based on biocides are often neither appropriate nor a completely acceptable option for marine piping systems as biofilms can develop resistance to biocides [**2.3**,**2.21**,**2.22**]. This results from the biofilm capability (due to the development of 3D structures intrinsic to biofilms) of using an adaptive response for survival to changing environment, and also the failure of the most popular biocide (*i.e.* chlorine) to penetrate into deep biofilm layers for enhanced disruption efficiency [**2.3**,**2.23**]. These features of

biofilms make them particularly difficult to control and current treatment strategies involve large biocide quantities, which are often undesirable because they are expensive, have a short half-life and present additional downstream problems, such as corrosion and by-product accumulation.

Consequently, marine structures frequently lose their operational performance and laborious maintenance procedures are required [**2.18**]. For instance, docking and materials associated with the removal of macrofouling, *e.g.* submarine heat exchangers, headers and the corrosion of Cu alloy piping through the generation of sulphides by microfouling, is both high and repetitive. Increased costs are also incurred by component inaccessibility, which is especially true for submarine systems [**2.1**,**2.13**]. The environmental impact represents also a major issue, for instance, heat exchanger biocides, *e.g.* chlorine, chloride dioxide and hypochlorite, can make nutrients more bioavailable and produce toxic by-products that can interact with the process fluid of seawater systems [**2.3**,**2.18**,**2.21**]. As a result, there is currently considerable concern worldwide over the potential loss of marine biodiversity due to the contamination by toxic substances, which include chlorine-based biocides, plus organotin compounds, such as tri-*n*-butyultin (TBT) and Cu-based compounds [**2.24**,**2.25**]. Indeed, in any engineering field involving bacterial biofilm formation and extent, the need to effectively control this serious phenomenon is becoming increasing paramount, as the more traditional means of control are being restricted due to the increased environmental concerns and legislature. As a consequence, there the focus has been placed on the protection of the marine environment and the development of new antifouling agents / strategies that are not only effective and but also environmentally benign. Bacterial biofilm control by disrupting the cohesiveness of the biofilm matrix using naturally occurring compounds, *e.g.* biochemicals or even predator species, is an attractive alternative [**2.26**].

2.3 Bacterial biofilm formation stages

Qualitative assessments of marine biofouling processes on metallic surfaces have been described in the literature [**2.1**,**2.2**,**2.23**,**2.25**]. Nevertheless, there is still much debate since understanding the interaction between metallic surfaces and biofilm remains a significant scientific challenge, see **Section 2.1**. **Figures 2.1** to **2.5** present the classic and simplistic biofilm formation stages by bacterial microfoulers. This successional description of the fouling process is didactic and more complex patterns with other microfoulers such as, diatomic biofilms and macrofouler, *e.g.* macroalgae, barnacles, mussels, tubeworms and bryozoans, can also interact with time on metallic surfaces in nature [**2.4**]. From an engineering perspective, a timescale has been taken into consideration in order to qualitatively assess the extent of bacterial biofouling formation with time. However, this concept is still the subject of much discussion within the biological science research community since it depends on numerous interrelated parameters, such as the bacterial growth rate, which can be regulated by several factors including physical and chemical parameters: salinity, temperature, turbidity, nutrient levels, flow rates or actions of the waves on the metallic surfaces and the intensity of solar radiation. These factors can also vary seasonally, spatially and with depth [**2.1**,**2.4**,**2.23**].

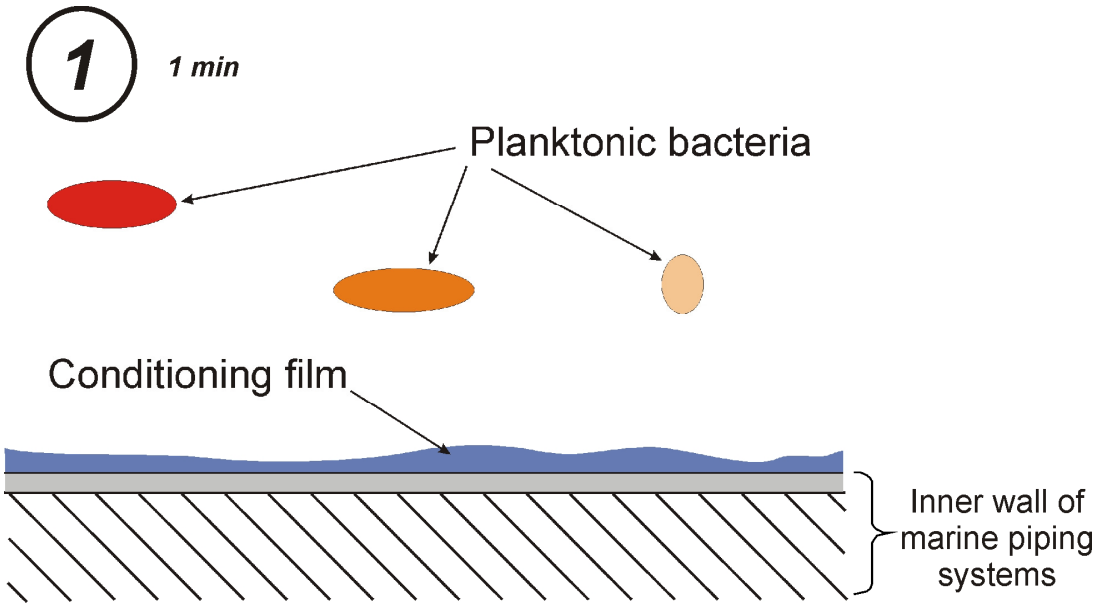

Figure 2.1. Bacterial biofouling: conditioning film formation.

Bacteria can modify their immediate environment by forming EPS, also referred to in the literature as slime, mucilage or glycocalyx [**2.23**] and, in seawater this varies broadly depending on temperature, degree of pollution and availability of organic matter [**2.13**]. After the initial molecular fouling or conditioning layer, which is a thin layer of adsorbed organic matter (polysaccharides, proteins, humic acids, nucleic and amino acids) that serves as a nutrient source (see **Figure 2.1**) [**2.27**], the EPS is generally reported to form within minutes to one hour (see **Figure 2.2**) which develops and grows into a mature biofilm (see **Figure 2.3**). However, the extent, the composition and physiology of bacterial populations, and also timescales of biofilm aggregation will ultimately depend on the environmental conditions nearby the metals and overall on the location and season [**2.1**,**2.4**,**2.25**,**2.28**,**2.29**].

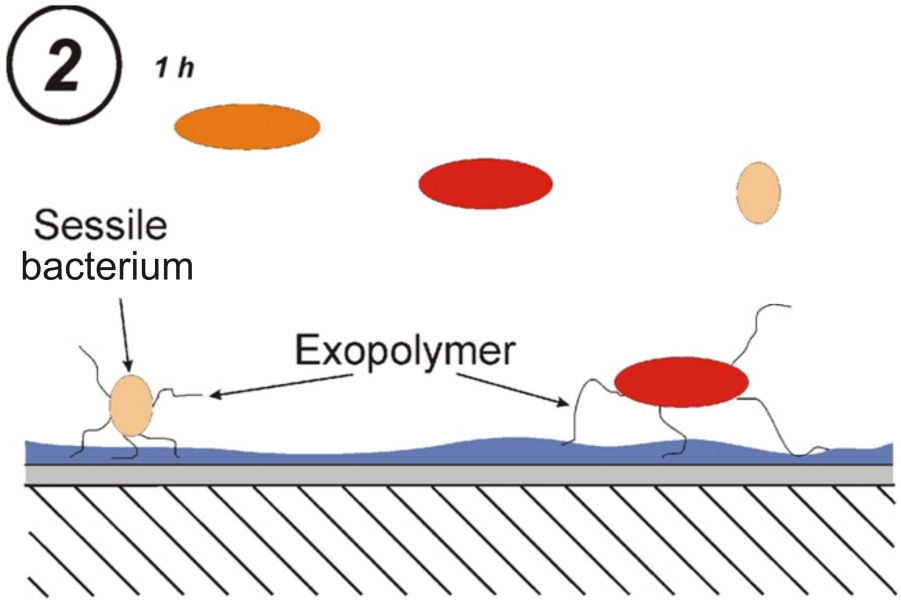

Figure 2.2. Bacterial biofouling: pioneering attachment, cell encapsulation.

Planktonic bacterial cells attach onto the conditioning film in a heterogeneous manner, see **Figure 2.2**. At this stage, they become sessile bacteria by producing adhesive exopolymers (*i.e.* EPS) to physically bind to the surface. In field biofilms, primary colonisers such as, yeasts and diatoms can compete with bacteria to establish more complex protective biofilm structures [**2.4**].

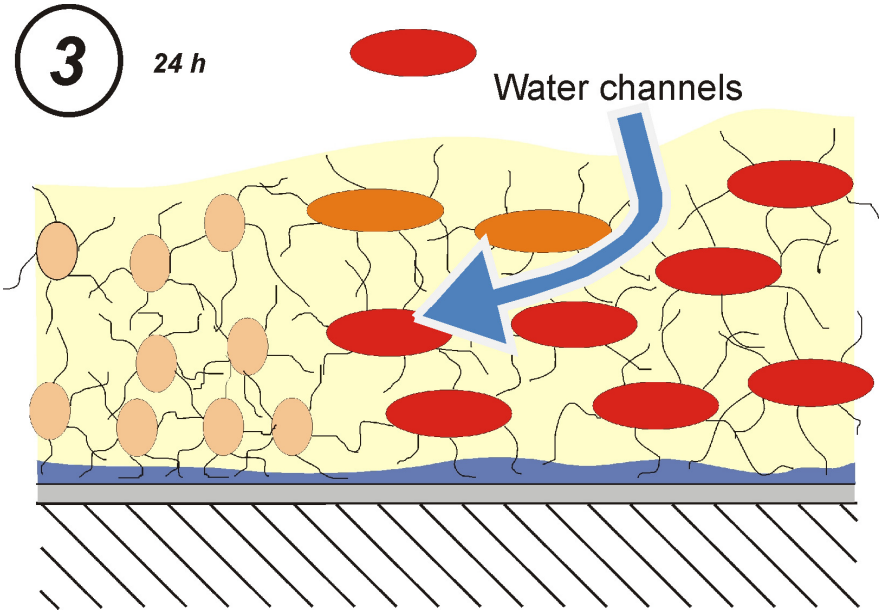

Figure 2.3. Bacterial biofouling: mature biofilm formation.

These sessile bacteria then form microbial clusters as a consortia and replicate, see **Figure 2.3**. The EPS, or slime, is composed of polysaccharides, enzymes and water where the slime volume can be 100 times higher than the bacteria volume. The matrix is a complex structure with planktonic bacteria, non-living particles and nutrients. Mature biofilms in seawater may form in a few days on passive metals on account of simultaneous inorganic processes (oxide layer formation) occurring within the same time period, *e.g.* between 3 – 7 days reported for biofilms to form on stainless steel (SS) UNS S31600 and UNS S30400 surfaces [**2.30**,**2.31**].

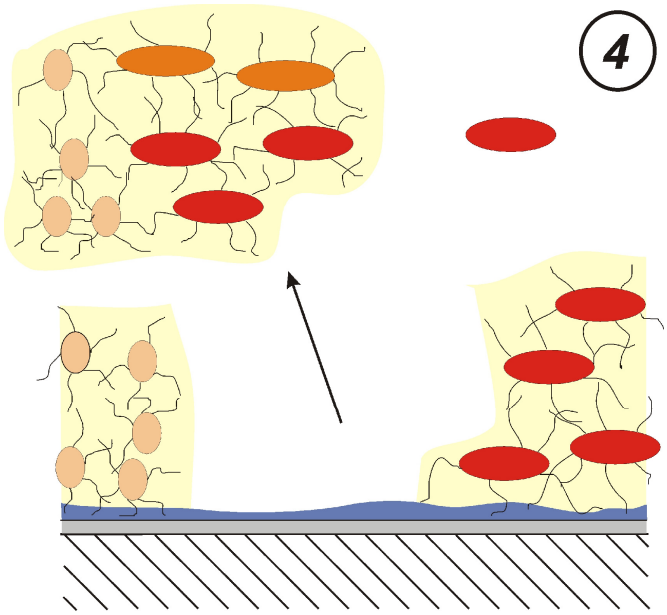

Figure 2.4. Bacterial biofouling: partial biofilm sloughing.

With time, areas of the biofilm may slough away from the surface exposing these localised bare surfaces to the bulk fluid, see **Figure 2.4**. This process of biofilm dispersal is directly correlated to natural dispersion mechanisms (not well understood) for potential inhibition strategies discussed later in **Section 2.9**. This step of the bacterial biofouling process is of major importance since the ultimate objective of this thesis is to enhance this mechanism.

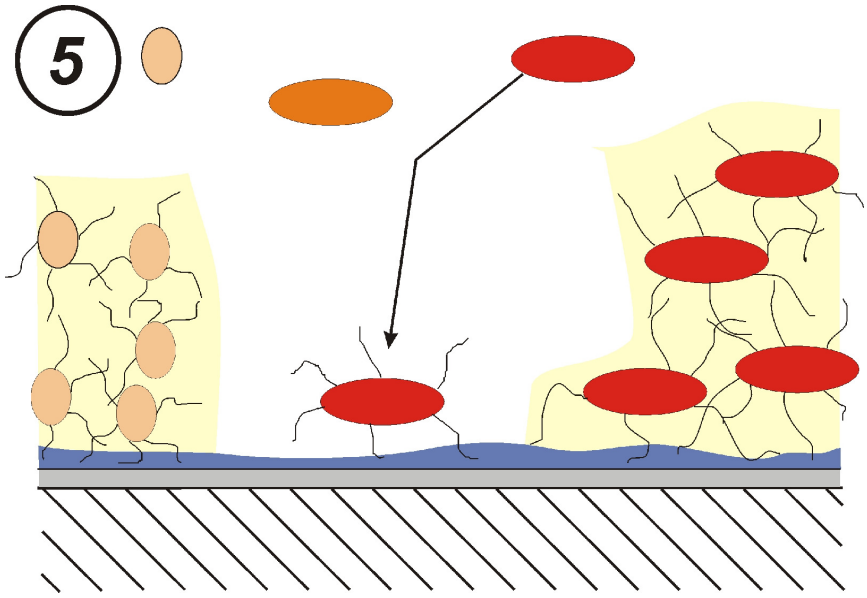

Figure 2.5. Bacterial biofouling: bacterial recolonisation.

Finally, the freshly exposed surface can be recolonised by pioneering planktonic bacteria, see **Figure 2.5** (similar to **Figure 2.2**). Thus, the process of bacteria biofilm formation is a continuous and dynamic process [**2.1**]. In nature, secondary colonisers, spores of macroalgae, fungi and protozoa, can settle with time after a 1 week immersion during favourable environmental conditions. After prolonged exposure, about 2 – 3 weeks, invertebrate larvae are usually reported to complete the marine biofouling process during the spawning season [**2.4**].

2.4 Marine heat exchangers

2.4.1 Heat exchanger working principle

Marine diesel engines are cooled by circulating coolant / seawater through the engine [**2.32**], see **Figure 2.6**. Two different types of cooling systems are commonly used in these engines: the standard seawater cooling system and the closed cooling system [**2.33**-**2.35**]. The former is a simple system where a seawater pump can be housed in a number of different locations depending on engine type and size. Traditionally, in most cases, the pump is inside the outdrive or inside the boat and driven by a V-belt or directly off the crankshaft for larger and inboard engines [**2.33**-**2.35**]. While for the latter, the closed cooling systems have more complex configurations which may include heat exchangers to give greater engine performance and reduce fuel consumption [**2.32**]. Heat exchanger devices ensure efficient heat transfer from one fluid to another and usually operate in the temperature range 28 – 45 °C for auxiliary cooling systems and 60 – 70 °C for condenser cooling [**2.3**]. Typical shell and tube marine heat exchangers have an external jacket / casing of about 250 mm in diameter and are composed of a bundle of 15 – 30 mm diameter internal tubes [**2.33**-**2.35**]. Surprisely, bacterial biofilms have been diagnosed even at these high temperatures [**2.3**], thus emphasising the resistive nature of the EPS matrix against adverse environments.

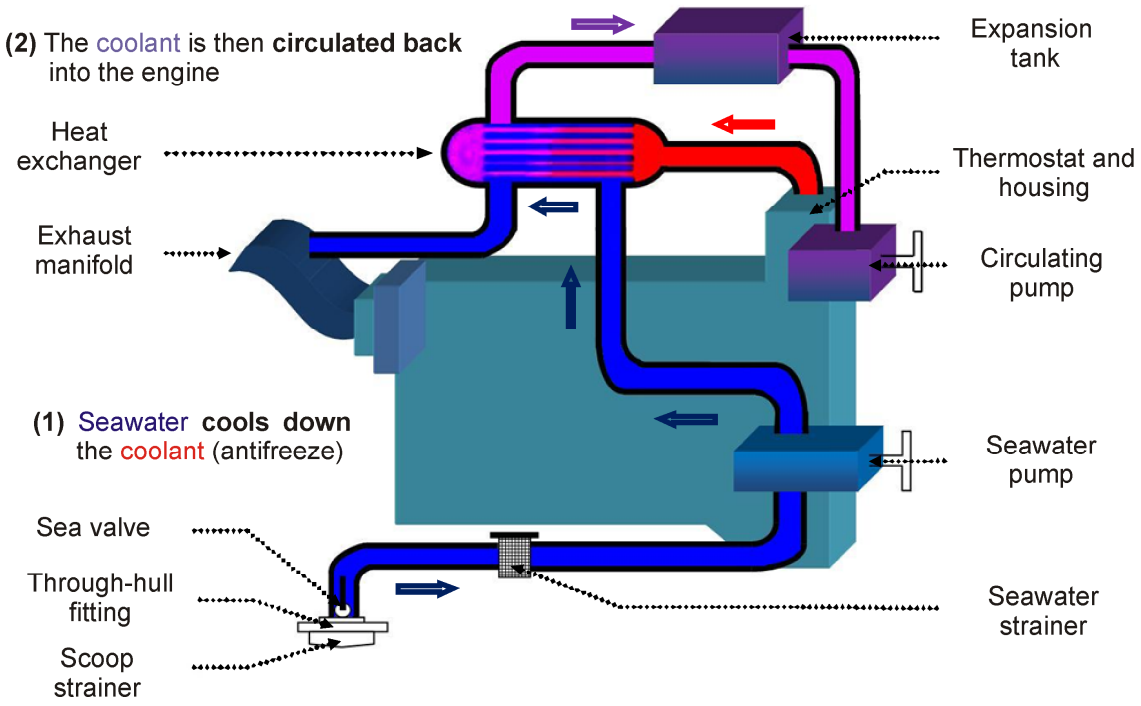

Figure 2.6. Closed cooling system for a marine engine, adapted from [**2.36**].

Certain precautions can limit, to a certain extent, damages incurred to the engineering marine systems. For instance, the non-use of seawater as a coolant can minimise heat exchangers failure. In addition, pre-treatments; microfiltration using strainer or biocide application, may eliminate 99.99 % of all bacteria [**2.3**]. However, a few surviving cells can still enter the system regardless of measures taken, colonise metallic surfaces and develop using biodegradable substances dissolved in seawater, thus clearly indicating that biofouling and biocorrosion are still major problems within standard marine closed cooling systems [**2.32**].

2.4.2 Copper-nickel alloys

Cu-based materials, for instance copper-nickel (Cu-Ni) alloys, are traditionally used for marine heat exchangers due to their corrosion (not susceptible to stress corrosion) and erosion resistance, and also biocidal action against marine organisms [**2.17**,**2.37**]. The corrosion resistance of Cu-Ni alloys can be explained by their low corrosion rate: initial formation (over the first couple of days) of a thin, adherent and protective oxide layer (Cu_2O) on the surface, which takes 2 – 3 months to become mature, see **Section 2.4.3**. Shear forces in flowing seawater systems can be sufficient to damage this protective surface film (flow-induced corrosion) if the velocity regime is above the breakaway velocity: 3 – 4 m s^{-1}, *i.e.* typical values in design of Cu-based pipes depending on the local geometry and pipe dimensions (100 mm diameter pipes) [**2.37**]. In the presence of entrained sand particles, the critical velocity range can be reduced due to solid particle erosion, which is related to the particle size (μm), the sand concentration in parts per million (ppm) and the local geometry of the fluid-handling component exposed to erosion. Conversely, if a minimum seawater velocity of 0.5 m s^{-1} is not maintained, build-up of sediments can form on the bottom of piping systems, as a result of initiation sites for corrosion underneath the deposits [**2.37**]. Consequently, the erosion resistance of the Cu-Ni alloys depends on the operating flow regimes and design of the marine heat exchangers. Despite their good corrosion resistance properties, Cu-Ni alloys can suffer from localised corrosion (pitting) when exposed to sulphide-polluted seawater [**2.17**,**2.37**]. More precisely, hydrogen sulphide (H_2S) is a corrosive metabolite formed by SRB using sulphate (SO_4^{2-}) ions and hydrogen (see **Equation 2.1**) and can dissociate in alkaline solution to sulphide (S^{2-}) ions, see **Equation 2.2** [**2.2**,**2.3**].

$$H_2SO_4 + 4H_2 \rightarrow H_2S + 4H_2O \quad (2.1)$$

$$H_2S + 2OH^- \rightarrow S^{2-} + 2H_2O \quad (2.2)$$

The significance of the corrosion incurred by sulphide-polluted seawater depends on the concentration of S^{2-} (accelerated attacks have been observed at low concentration of 0.01 ppm) and the sequence of exposure: polluted and clean seawater [**2.37**]. A mechanism of corrosion by SRB in seawater polluted with sulphides has been proposed with a modification of the oxide layer of Cu-based materials by S^{2-}, leading to a grey layer of $Cu_2S(NiFe)_3S_4$ / Cu_2O, and with a cathodic process that can include H_2S [**2.2**,**2.3**]:

$$2H_2S + 2e^- \rightarrow H_2 + 2HS^- \quad (2.3)$$

In addition, ammonia is a pollutant that may cause intensive corrosion (thermogalvanic corrosion attacks) by denickeling of the Cu-Ni alloys [**2.37**]. The resistance of Cu-based alloys to macrofouling has been attributed to the continuous release of Cu ions within the protective oxide film, thus affecting many marine organisms (inhibition of macromolecule synthesis and enzymatic reactions, effect on bacterial growth and decrease of cell numbers) and the overall process of microfouling [**2.17**,**2.37**]. Similarly, it was proposed that the top oxide layers of the Cu-Ni alloys formed during secondary corrosion reactions with compounds in seawater, *e.g.* $Cu_2(OH)_3Cl$, can be fouled and also subsequently removed from the surface. This can be explained by the weakly adherent porous structure of the top layers formed during secondary corrosion reactions and ensuing periodic biofouling formation and development, and also sloughs off, thus revealing the inner Cu oxide layer, Cu_2O [**2.38**,**2.39**].

However, certain genera of bacteria protected by a polysaccharide barrier, *e.g. Pseudomonas syringae* which can mediate sequestration of Cu by extracellular and periplasmic proteins [**2.40**], can be resistant and accommodate the toxic effect of Cu ions, thus affecting the overall biofouling process. The common Cu-Ni alloys used for marine applications are 90-10 and 70-30 Cu-Ni with corrosion rates in the order of 0.040 and 0.025 mm y^{-1}, respectively [**2.41**]. They can both be installed on different marine engineering structures, *e.g.* piping systems and tubes in heat exchangers. In particular, 90-10 Cu-Ni (UNS C70600) is mainly used for surface ships since it combines both good resistance to corrosion and macrofouling, thus minimising the propelling energy consumption of ships to a low level. Whereas 70-30 Cu-Ni (UNS C71500) is predominantly used for military submarines, where the nickel (Ni) reinforced Cu alloys ensure higher strength, maximum allowable flow rate, and also low magnetic permeability (essential to minimise detection of submarines) [**2.17**,**2.37**]. Overall, Cu-Ni alloys offer a unique combination of high resistance performance to both biofouling and

corrosion in marine environment with a potential of more than 20 years of life expectancy in-service [**2.37**].

More expensive metallic surfaces such as, Ti and certain SS, *e.g.* UNS S31254 and UNS S31603, may also be used for their corrosion resistance properties [**2.37**]. However, Ti used in electrical contact with dissimilar metals or alloys, *e.g.* Cu-Ni alloys, can lead to galvanic corrosion: one of the most common and damaging forms of corrosion, see **Table 2.2**. As a consequence, Ti is not used in submarines. Noble SS are also susceptible to significant potential changes, *i.e.* up to a 1.000 V in variation (depending on O_2 and chlorine content, temperature, and also the presence of a biofilm), in marine environment [**2.37**]. In contact with Cu-based alloys, galvanic corrosion can therefore occur (**Table 2.2**). To minimise galvanic corrosion, it is hence recommended to use compatible materials, as Cu-Ni alloys lies midway in the galvanic series (**Table 2.2**), it is thereby a good candidate. However, the combination of different metals in-service is often unavoidable, and in many instances as Ti is a poor cathode for reducing O_2, it can be coupled with Cu-based alloys [**2.37**]. Consequently, protection measures should be taken to limitate and ultimately avoid galvanic corrosion: use of a non-conducting distance spool between the dissimilar metals. Aluminium (Al) alloys, which are relatively lower in cost and more thermally efficient than the other candidates, can also be used in shell-and-tube designs [**2.32**]. Once again, incorrect assembly of Al alloys in an engineering system made of more noble material can result in galvanic corrosion.

Table 2.2. Galvanic series in flowing seawater (conditions: 2.5 – 4.0 m s^{-1} and 10 – 25 °C, 1 atm) – Values in brackets indicate low velocity or poorly aerated water, and at shielded areas, adapted from [**2.41**-**2.43**].

Metal / alloy or mineral	*E vs.* Ag/AgCl, 3.5 M KCl / V (Approximate)
Graphite	+0.240 to +0.340
Platinum	+0.220 to +0.290
Gold	+0.140 to +0.240
Ni – Cr – Mo alloy C	+0.010 to +0.130
Titanium	–0.010 to +0.100
Ni – Cr – Mo – Cu – Si alloy B	+0.060 to +0.080
Ni – Fe – Cr alloy 825	+0.020 to +0.080
Alloy 20 stainless steels, cast and wrought	0.000 to +0.100
UNS S31600, UNS S31700 stainless steel	+0.040 to –0.060 (–0.310 to –0.410)
Nickel copper alloys 400 and K-500	0.000 to –0.110
UNS S30200, UNS S30400, UNS S32100, UNS S 34700 stainless steel	–0.010 to –0.060 (–0.430 to –0.540)
Silver	–0.060 to –0.110
Nickel 200 (UNS N02200)	–0.060 to –0.160
Silver braze alloys	–0.060 to –0.160
Nickel chromium alloy 600 (UNS N06600)	–0.085 to –0.135
Nickel aluminium bronze	–0.110 to –0.180
70-30 copper nickel (UNS C71500)	–0.140 to –0.185
Lead	–0.160 to –0.200
UNS S43000 stainless steel	–0.160 to –0.240
80-20 copper nickel (UNS C71000)	–0.180 to –0.240
90-10 copper nickel (UNS C70600)	–0.185 to –0.250
Nickel silver	–0.220 to –0.240
UNS S41600, UNS S41000 stainless steel	–0.220 to –0.290 (–0.420 to –0.520)
Tin bronze	–0.225 to –0.280
Silicon bronze	–0.230 to –0.250
Manganese bronze	–0.250 to –0.300
Admiralty brass, aluminium bronze	–0.250 to –0.310
50-50 Lead tin solder	–0.250 to –0.335
Copper	–0.260 to –0.320
Tin	–0.260 to –0.280
Naval brass, yellow brass and red brass	–0.260 to –0.350
Aluminium bronze	–0.280 to –0.370
Austenitic nickel cast iron	–0.380 to –0.490
Low alloy steel	–0.530 to –0.590
Mild steel, cast iron	–0.560 to –0.680
Cadmium	–0.660 to –0.690
Aluminium alloys	–0.710 to –0.950
Beryllium	–0.930 to –0.950
Zinc	–0.950 to –0.980
Magnesium	–1.560 to –1.600

2.4.3 Biocorrosion in heat exchangers

2.4.3.1 Uniform corrosion of the Cu matrix in seawater

In **Section 2.4.3**, the author will assume that the seawater environment is free of pollutants including sulphides and ammonia. Uniform corrosion occurs on metal surfaces, *e.g.* Cu matrix, which have homogeneous microstructures [**2.44**]. At the microlevel, uniform corrosion is found to be an electrochemical reaction between adjacent closely spaced micro-anode and micro-cathode areas, see **Figure 2.7**. In this instance, five essential components are required for corrosion to occur: anode region, cathode region, electrical contact between regions, seawater and cathode reactant: dissolved oxygen (DO), with micro-galvanic effects between adjacent metal grains and / or microstructures.

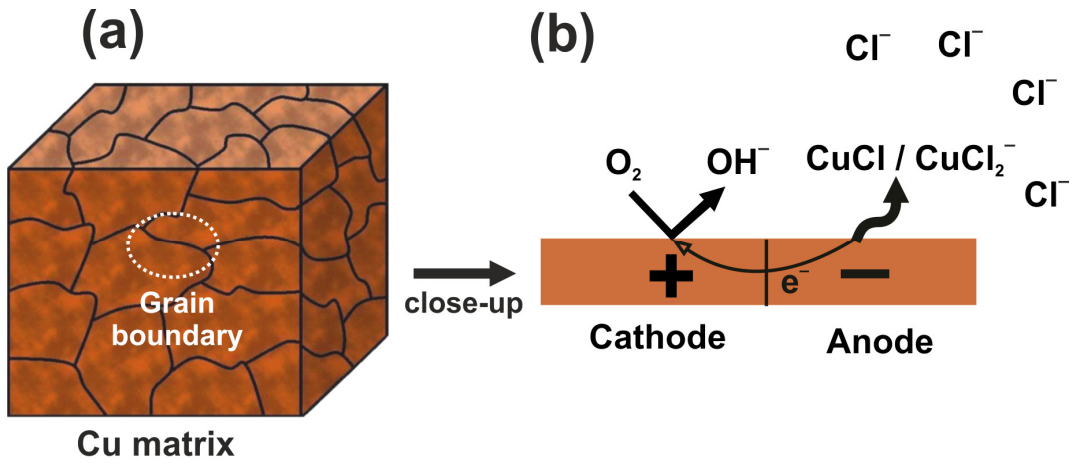

Figure 2.7. Corrosion in marine heat exchangers (*e.g.* Cu-based alloys): **(a)** grain boundaries in Cu matrix and **(b)** corrosion within the Cu matrix.

However, the corrosion of Cu alloys (often used for marine applications) in seawater is more complex than that shown in **Figure 2.7**. It has been established that the main corrosion process in aerated chloride media, *e.g.* seawater, is the anodic dissolution of Cu to form a dichlorocuprous anion complex [**2.45**-**2.47**], which is generally simplified to **Equations 2.4** and **2.5**:

$$Cu + Cl^- \rightarrow CuCl + e^- \quad (2.4)$$

$$Cu + 2Cl^- \rightarrow CuCl_2^- + e^- \quad (2.5)$$

The predominant cathodic reaction in aerated seawater is the oxygen reduction reaction (ORR) [**2.42**,**2.44**]:

$$O_2 + 2H_2O + 4e^- \rightarrow 4OH^- \quad (2.6)$$

Chloride (Cl^-) ions play an important role in the formation and properties of protective oxide films on Cu-based alloys. Indeed, Cu_2O may form via a number of processes in Cl^- containing environments, see **Equation 2.7**. The extent of Cu_2O formation depends on the relative concentration of Cl^- and pH, with higher pH favouring Cu_2O. Although these processes only relate to the formation of the first monolayers of Cu_2O, they are nevertheless important in determining the properties of the passivating interfacial Cu_2O. Beyond the first several monolayers, *i.e.* for films of the order of 1 – 10 nm in thickness, thicker Cu_2O layers in **Figure 2.8** are probably formed by a dissolution / precipitation process [**2.45**,**2.46**]:

$$2CuCl_2^- + 2OH^- \rightarrow Cu_2O + H_2O + 4Cl^- \quad (2.7)$$

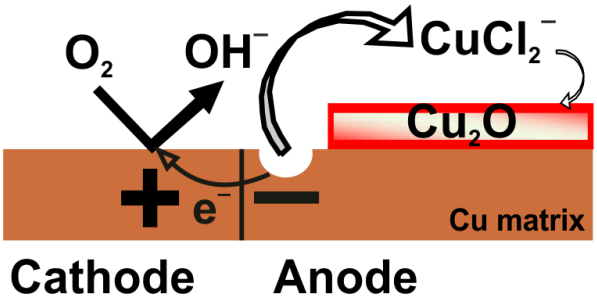

Figure 2.8. The initial corrosion of Cu-based alloys and formation of the protective oxide film.

Cl^- ions will also affect the properties and stability of the protective oxide films. The substitution of monovalent Cl^- ions for divalent superoxide anion (O_2^-) in the Cu_2O lattice creates defects and enhances the semiconducting properties of the film. Thus, Cu_2O films formed in chloride media may support electrochemical processes such as the ORR and the anodic dissolution of Cu, and be less protective, compared with the more-strongly passivating Cu_2O films formed in the absence of Cl^- ions. Depending on the chloride concentration, however, Cu_2O films formed in Cl^- media may be more susceptible to localised breakdown. At sufficiently high chloride concentrations, the surface layer may become so defective that it no longer protects the surface and the Cu actively dissolves. Thus, the stability of Cu_2O is inversely dependent on the

concentration of Cl^- ions [**2.45**,**2.46**], *i.e.* as the concentration of Cl^- ions increases the stability of Cu_2O equilibrium shifts to $CuCl_2^-$.

2.4.3.2 MIC of Cu-based alloys in seawater

Proliferation, aggregation and random attachment of bacteria are driven by microstructural features such as inclusions [**2.1**,**2.2**]. It has been reported that biofilm-forming bacteria may selectively colonise at grain boundaries [**2.1**,**2.2**]. This can cause long-term patchiness in the biofilm coverage leading to the initiation of localised corrosion. While initially immune from biofouling due to the toxic Cu-ion release within the protective oxide film, this immunity diminishes over time. Additionally, certain Cu resistant bacteria species, such as *Pseudomonas syringae*, can secrete proteins that sequester Cu ions [**2.40**]. Consequently, exposure to natural seawater for several months will inevitably lead to a multilayered structure of microorganisms, where EPS is usually found entrapped between layers of the Cu corrosion products. **Section 2.4.3.1** has described the primary reaction of the natural corrosion process of Cu alloys resulting in the formation of a cuprous oxide film, Cu_2O. The anodic and cathodic sites of the reaction take place at the metal / oxide and seawater / oxide interfaces, respectively and subsequently **Figure 2.8** leads progressively to **Figure 2.9**.

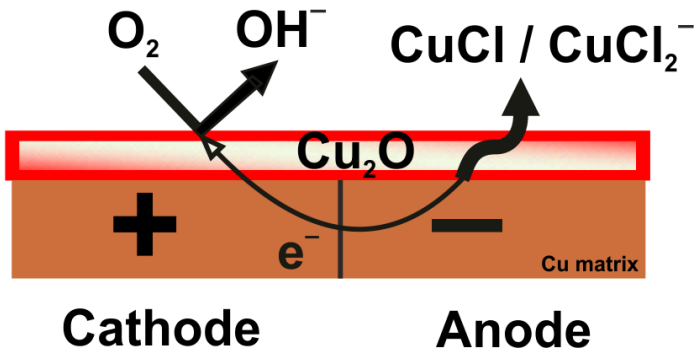

Figure 2.9. Formation of Cu_2O via a potential number of processes.

The Cu_2O film does not consist of a completely dense layer as a consequence the Cu matrix can continuously release Cu ions within the primary oxide film, thus having potential antifouling effects [**2.37**]. The resistance of the Cu matrix to macrofouling can thereby be controlled by the release of Cu ions within the Cu_2O film. After a prolonged exposure, the corrosion film thickens and another oxide layer is generated. It was shown that atacamite, $Cu_2(OH)_3Cl$, in **Figure 2.10(a)** can form on the outside surface of the Cu_2O layer by oxidation process [**2.41**]:

$$Cu_2O + 2H_2O + Cl^- \rightarrow Cu_2(OH)_3Cl + H^+ + 2e^- \quad (2.8)$$

The top layer oxide, $Cu_2(OH)_3Cl$, is usually thick and porous and can act as a diffusion barrier for Cu ions into seawater whereas the kinetic of the cathodic process remains relatively unchanged [**2.41**]. Similarly, Cu_2O is known to be thermodynamically unstable and a redox transformation of Cu_2O to cupric oxide, CuO can occur [**2.41**]:

$$Cu_2O + H_2O \rightarrow 2CuO + 2H^+ + 2e^- \quad (2.9)$$

The presence of protons in **Equation 2.9** can lead to localised acidification of pores within the film, thus resulting in pitting formation on Cu-based alloys. It has also been reported that this localised corrosion process may contribute to the production of atacamite (**Equation 2.10**), with evidence of $Cu_2(OH)_3Cl$ compounds in pitted areas on the Cu surface [**2.41**].

$$2CuO + H^+ + Cl^- + H_2O \rightarrow Cu_2(OH)_3Cl \quad (2.10)$$

The release of H^+ ions coincides with low pH values (< 6), which can allow the formation of light grey translucent cuprous chloride, CuCl, when the corrosion process initiates [**2.41**]. Likewise, CuCl can be an unstable intermediate in the formation of $CuCl_2^-$ as the corrosion potential moves to more positive values. This results in **Figure 2.10(b)** in the formation of $Cu_2(OH)_3Cl$ by hydrolysis of CuCl at the bottom of the pores located in the growing film [**2.41**]:

$$2CuCl + 3H_2O \rightarrow Cu_2(OH)_3Cl + Cl^- + 3H^+ + 2e^- \quad (2.11)$$

As the diffusion of Cu ions through the atacamite layer becomes increasingly difficult, the Cu-alloys can be affected by biofouling. Subsequently, the poorly adherent $Cu_2(OH)_3Cl$ layer will undergo sequential biofilm formation and extent, **Figure 2.10(c)**, and also removal, thus leaving a freshly exposed primary oxide layer resistant to macrofouling [**2.38**,**2.39**], see **Figure 2.10(d)**.

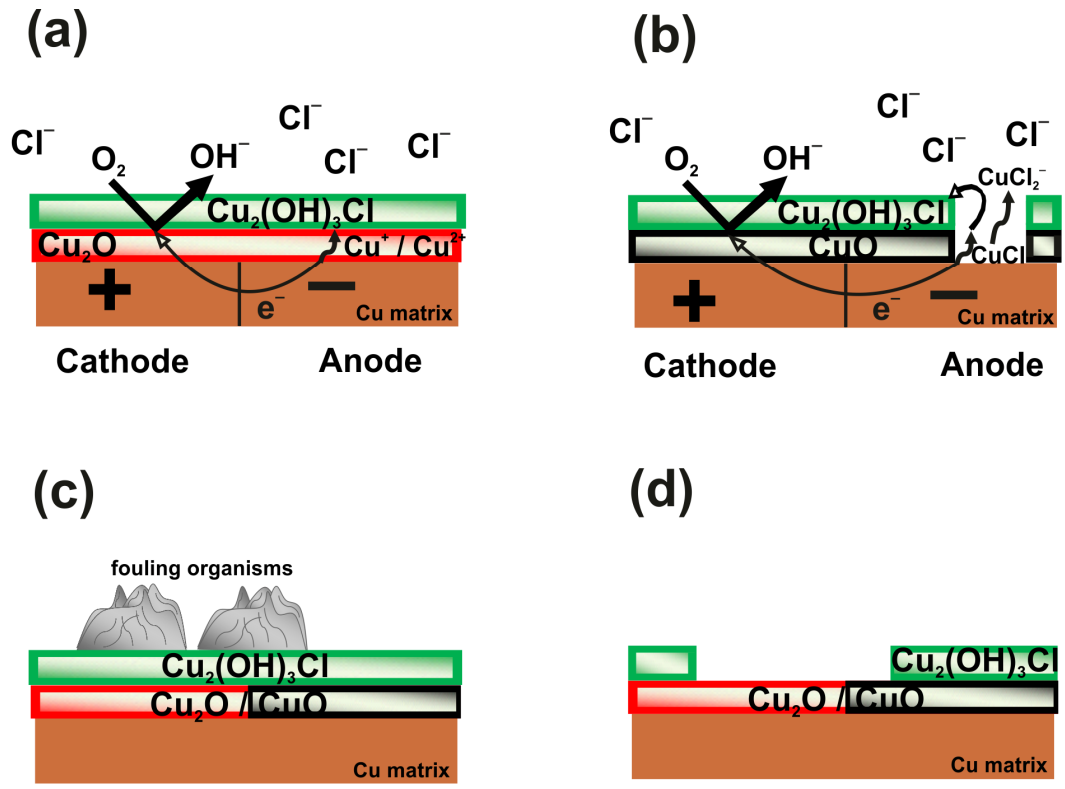

Figure 2.10. Establishment of a non-toxic top layer oxide, $Cu_2(OH)_3Cl$, on an inner **(a)** Cu_2O and **(b)** CuO films, **(c)** settlement of fouling organisms on the surface and **(d)** fouling organisms dispersal revealing the inner oxide layer, Cu_2O or CuO.

However, the inner Cu_2O layer (where Cu_2O has been identified as the main corrosion product of Cu-Ni alloys in alkaline solutions [**2.41**]) is still susceptible to microfouling and bacterial biofilms can form and extend on the Cu surface. **Figure 2.11** shows the influence of the complex redox processes within and nearby the EPS matrix.

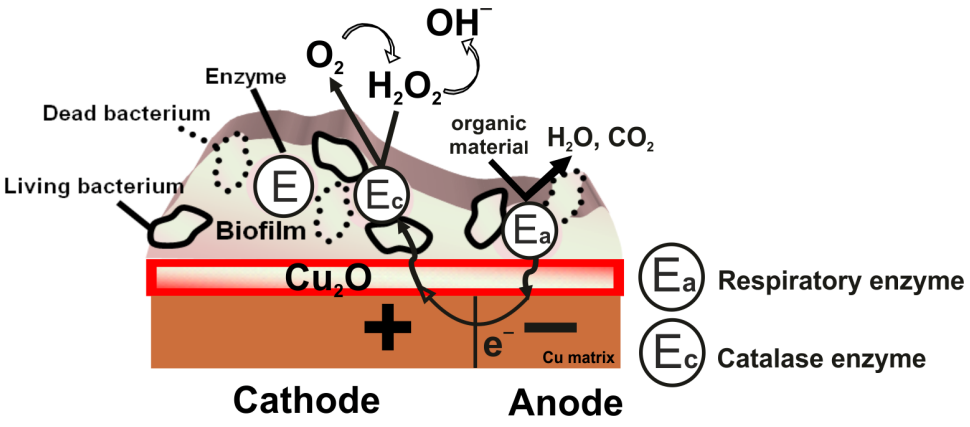

Figure 2.11. Establishment of Cu surface coated with EPS matrix and redox processes involved.

The interfacial Cu / EPS matrix in **Figure 2.11** becomes increasingly acidic due to the presence of carboxylic acid groups (pK_a in the range of 4.2 to 5.6) and also via the formation of corrosion products Cu_2O and eventually CuOH [**2.48**], see **Equations 2.12** and **2.13**.

$$2Cu + H_2O \rightarrow Cu_2O + 2H^+ + 2e^- \quad (2.12)$$

$$Cu + H_2O \rightarrow CuOH + H^+ + e^- \quad (2.13)$$

Consequently, the presence of a heterogeneous biofilm on the Cu matrix results in the formation of pH gradients underneath biofilms, whereas the phase boundary EPS / seawater corresponds to alkaline pH [**2.48**]. In particular, values lower that pH 5 can be expected underneath aerobic biofilms and pH in the range of 1 – 2 may be assessed under discrete biodeposits. The passive layer of metal alloys may be affected by marine biofilms for pH values below 3. In addition, pH values in the range of 2 to 5 were measured at discrete locations within marine biofilms using microelectrodes [**2.49**]. Similarly, localised measurements of DO levels within 180 μm biofilms using microelectrodes have indicated that the DO can decrease to zero [**2.31**]. Overall, the presence of a biofilm on a metallic surface can therefore coincide with a galvanic cell, in analogy with the most extensively described bioelectrochemical system (BES): the microbial fuel cell (MFC) [**2.50**-**2.54**]. At the anode, where O_2 is deficient, soluble organic material in seawater can be oxidised by respiratory enzymes, thus forming H_2O and carbon dioxide (CO_2). The resulting electrons can transfer into the bacteria with subsequent charge transport inside the cell [**2.53**].

Although the exact contribution of bacterial cells to electron transfer process at a metal interface needs to be addressed, it has been suggested that the electric current can be conducted using three extracellular electron transfer (EET) mechanisms [**2.54**], see **Figure 2.12**.

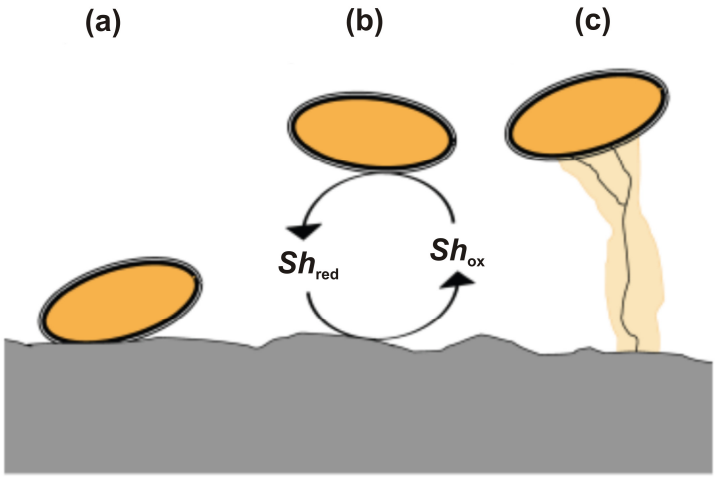

Figure 2.12. Schematic of three EET mechanisms for aerobic bacteria on a metallic surface: **(a)** direct electron transfer, **(b)** a reduced electron shuttle (Sh_{red}) that is oxidised (Sh_{ox}) and *vice versa*, and **(c)** a solid conductive matrix, from [**2.54**].

The first EET mechanism in **Figure 2.12(a)** involves a direct electron transfer utilising outer-membrane cytochromes (membrane-bound proteins, which contain heme groups / carboxylate functions and carry out electron transfer [**2.50**,**2.51**,**2.55**]) [**2.53**]. In the second EET mechanism in **Figure 2.12(b)**, soluble electron shuttles (simultaneously oxidised and reduced chemical compounds involved in the biodegradation of organic material by facilitating the transfer of electrons to and from bacteria [**2.50**,**2.51**,**2.55**]) are mediators for electron transfer process. Whereas, a solid conductive matrix, *i.e.* a component of the EPS matrix support for electron transfer such as bacterial nanowires / pili (hairlike appendage on the surface of bacteria) [**2.50**,**2.51**,**2.55**] can be used in **Figure 2.12(c)** [**2.54**].

In this scheme, it has also been reported that free electrons at the surface of bacterial cells can be exchanged with a metal surface during initial adhesion, where the charge transfer between bacteria and metallic surfaces can play a predominant role [**2.55**]. For instance, a charge of approximately 10^{-14} C per bacterium can be transferred on average during initial adhesion, thus corresponding to a small portion of the total surface charge for one bacterium, *i.e.* 10^{-12} C (see **Section 5.13.3**) [**2.55**,**2.56**]. As part of the redox process, electrons collect at the cathode, where enzymatic assisted reduction of O_2 occurs at the outer biofilm areas, see **Figure 2.11**. Overall, evidence of electrochemically improved biofilmed electrodes, with better catalytic effects than a bare electrode, has been demonstrated [**2.50**]. The electrochemical performance of the biofilmed surfaces across the interface, showing substantial potential losses and larger current densities, were enhanced in comparison with the control bare electrode [**2.50**]. Importantly, the performances of MFC-based reactors have revealed that successive microbial interactions and its extent can lead to electrochemically competent BES biofilms. In this instance, bacterial biofilms have shown capable of regulating the diffusion influx of nearby electro-active species / substrates and the corresponding discharge of electrons to the electrode [**2.50**].

Although a detailed and complete understanding of the interfacial processes involved has not been established yet, theoretical considerations published in the literature state that [**2.48**]:

- Neutral components, anions and cations, *e.g.* H_2O, O_2, and Cl^-, can pass through the EPS matrix, thus allowing the formation of Cu oxides / hydroxides, $CuCl_2^-$ and CuCl.
- Transport of Cu-ions (Cu^+ / Cu^{2+}) via electrochemical processes through the exopolymeric matrix is influenced by the gradient of electrochemical potential of ions due to the Cu oxidation reaction.
- The dissociable protons from the hydroxyls of the carboxyl groups of the anionic polysaccharides are oriented towards the Cu_2O layer.

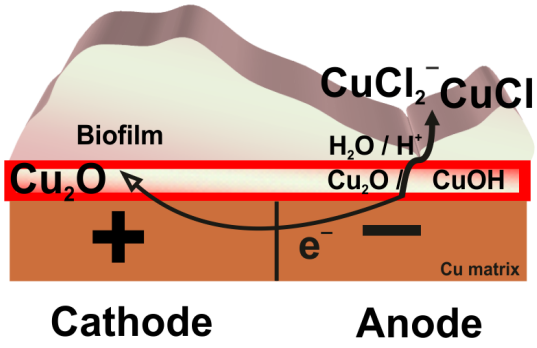

Figure 2.13. Anodic reactions and species diffusion through the biofilm.

Schiffrin and de Sánchez have demonstrated the modification of the O_2 reduction kinetics by bacteria of genus *Pseudoalteromonas*, and have proposed the role of bacterial metabolites as electrocatalysts [**2.57**]. Similarly, it has been proposed that specific enzymes entrapped in the EPS of aerobic bacteria could be responsible for an increase in cathodic currents, *e.g.* catalase [**2.58**,**2.59**]. Catalase is an integral component of bacterial cells response to oxidative stress and is believed to limit the accumulation of reactive O_2 species such as hydrogen peroxide (H_2O_2) that readily diffuses through cell membranes damaging their structures [**2.60**,**2.61**]. The mechanism requires the electrochemical production of H_2O_2 during the O_2 reduction process (**Equations 2.14** and **2.15**) and involves electron recycling during the enzymatic decomposition of H_2O_2 to H_2O and O_2 by the catalase enzyme, see **Equation 2.16** [**2.61**].

$$O_2 + 2H_2O + 2e^- \rightarrow H_2O_2 + 2OH^- \quad (2.14)$$

$$H_2O_2 + 2e^- \rightarrow 2OH^- \quad (2.15)$$

$$2H_2O_2 \rightarrow 2H_2O + O_2 \quad (2.16)$$

A schematic representation of the proposed catalase mechanism coupled with the O_2 reduction process of a metal surface is shown in **Figure 2.14**. The O_2 generated by the enzyme can be electrochemically reduced in addition to the O_2 reaching the surface by diffusion, thus, resulting in higher cathodic currents. For information, k_β is the reaction rate constant at step β (I to IV), where dis and dis' stand for dissolution. Species in solution (sol) or adsorbed to the surface (ads) are indicated in **Figure 2.14**.

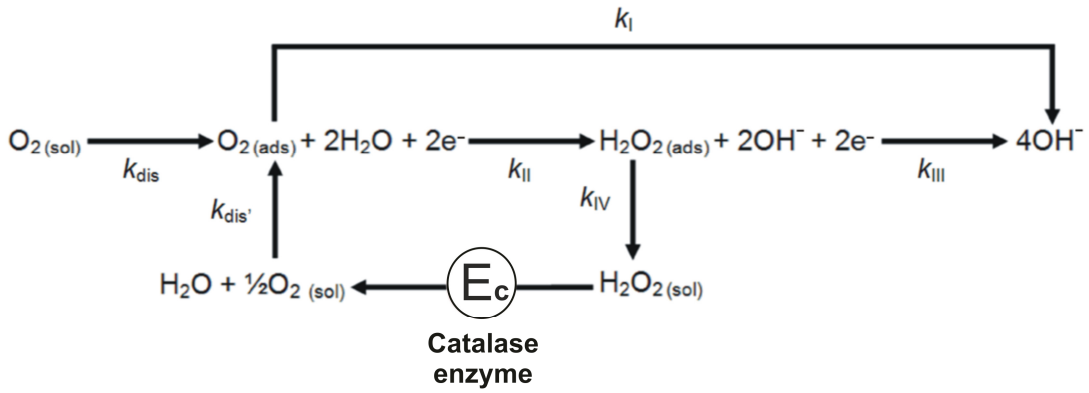

Figure 2.14. Catalase mechanism involved in the cathodic reaction, adapted from [**2.59**].

Schiffrin and de Sánchez have also investigated the effect of Cu^{2+} ions on *Pseudoalteromonas* species identified in the bacterial slimes present in marine condenser tubes made of Cu alloys [**2.57**]. They observed that *Pseudoalteromonas* bacteria can be tolerant to Cu^{2+} ions, *i.e.* no evidence of both a decrease of the bacterial activity and corrosion rate. Likewise, it was proposed that the *Pseudoalteromonas* genus may be more aggressive and cause enhancement of the corrosion rate (5 to 10 times more significant than for a mixed culture of bacteria) [**2.57**]. Metal-catalysed oxidation systems are reported to readily form H_2O_2 and free radicals such as the O_2^- anion and hydroxyl radical ($OH^{\cdot}$) [**2.62**]. These processes can inactivate enzymes and lead to the fragmentation of proteins. In biological systems on Cu surface (pH 3 – 5), it is probable that $OH^{\cdot}$ radicals can form when Cu^+ ions react with H_2O_2 via a 'Fento-type' reaction [**2.62**]:

$$Cu^+ + H_2O_2 \rightarrow Cu^{2+} + OH^- + OH^{\bullet} \qquad (2.17)$$

This reaction presumably coincides with the enzymatic decomposition of H_2O_2 in **Equation 2.16** by catalases (H_2O_2 scavengers) within *Pseudoalteromonas* biofilms, thus preventing the subsequent formation of $OH^{\cdot}$ radicals in **Equation 2.17** (potentially directly involved in proteins and DNA damages) and similarly enhancing the overall corrosion rate, see **Figure 2.14**. Nevertheless, the exact role of catalase in the corrosion process on a biofilmed Cu surface remains an open question [**2.61**]. Recently, Nercessian *et al.* have suggested that the catalase could be expressed inside aerobic bacterial biofilms by release of toxic Cu ions, electrochemical generation of H_2O_2 and biological oxidative stress [**2.61**]. More precisely, newly formed O_2 via the autocatalytic mechanism of H_2O_2 decomposition using catalase can support the electrochemical generation of H_2O_2 during the cathodic ORR (see **Figure 2.14**), thus

promoting the anodic dissolution of both the Cu_2O layer and Cu matrix at acidified sites under bacterial clusters (see **Figure 2.13**) [**2.61**].

2.4.3.3 Significance of biocorrosion on Cu alloys for the current study

The biocorrosion mechanisms on a biofilmed Cu matrix (**Figures 2.10**, **2.11** and **2.13**) have been outlined in **Section 2.4.3** to support the discussion for a biofilmed Au surface in **Chapter 5**, where in contrast to passive metals, substantial knowledge of biofilm growth and extent on a noble metal surface is limited. Alongside with the importance of microfouling in the overall biofouling process (**Figure 2.11**), the fundamental role played by the catalase in the ORR enhancement has been addressed, see **Figure 2.14**. This represents understanding on how the ORR kinetics can be affected at the Au / aerobic bacterial biofilm interface, see **Chapter 5**.

2.4.4 Biofouling within heat exchangers

Previous studies have concentrated on monitoring the fluid transport properties and carrying out mathematical calculations to discover the values of two parameters that indirectly define biofouling deposited on the inside of tubes: f_D the (Darcy) frictional resistance to fluid, such as seawater and R_h the heat transfer resistance [**2.63**,**2.64**].

2.4.4.1 Frictional resistance to fluid flow

In order to understand the influence of biofouling with regard to the frictional resistance to fluid flows, it is necessary to apply Darcy's formula (for fluid flow) through circular straight pipes (with d and l the diameter and length of the tubing) [**2.65**]:

$$f_D = \frac{2d\Delta P}{l\rho u^2} \tag{2.18}$$

Seawater (with ρ = 1025 kg m^{-3}) flowing through heat exchanger pipes, *e.g.* 21 mm diameter Cu-Ni tubes at u =1.5 m s^{-1} (with u the mean velocity) loses energy due to friction, f_D. This energy loss manifests as an increase in pressure drop (ΔP) within a pipe system. As marine biofilms attach and grow on the internal surfaces of pipes, they form a gel (secrete EPS matrix) which increases the frictional resistance to seawater flow. Thus, according to **Equation 2.18**, the energy loss characterised by a pressure drop also increases. Overall, skin friction and pressure drag are the two main

contributions of ΔP [**2.66**]. At low flow velocity, skin friction is predominant, thus suggesting that the total surface area of the biofilm may have a significant influence on the pressure drop. Conversely at high flow regime where the pressure drag is dominant, the shape of the biofilm structures will potentially have a great effect on the pressure drop. A previous study on the effect of ΔP with u under a controlled turbulent condition, has demonstrated that 7 day-old biofilms inside a flow cell device resulted in a 16 % decrease of the maximum achievable flow rate [**2.66**].

In addition, investigations of the frictional losses in a piping system due to biological fouling have been carried out by Eguia *et al.* [**2.63**,**2.64**]. In particular, biofouling has been described as an operational definition, when the extent of biofilm development interferes with technical, economical and aesthetic requirements [**2.3**]. In this instance, a threshold of interference has also been defined corresponding to a critical stage of biofouling when the operational performances of the engineering system are affected. The overall significance of the threshold of interference depends on the in-service operational conditions of marine heat exchanger design. Consequently, a detailed knowledge of the engineering system under investigation is fundamental in establishing the most efficient countermeasures against biofouling. **Figure 2.15** shows the three main stages; Induction, Log Accumulation and Plateau and their corresponding influence of frictional resistance [**2.1**,**2.3**,**2.4**].

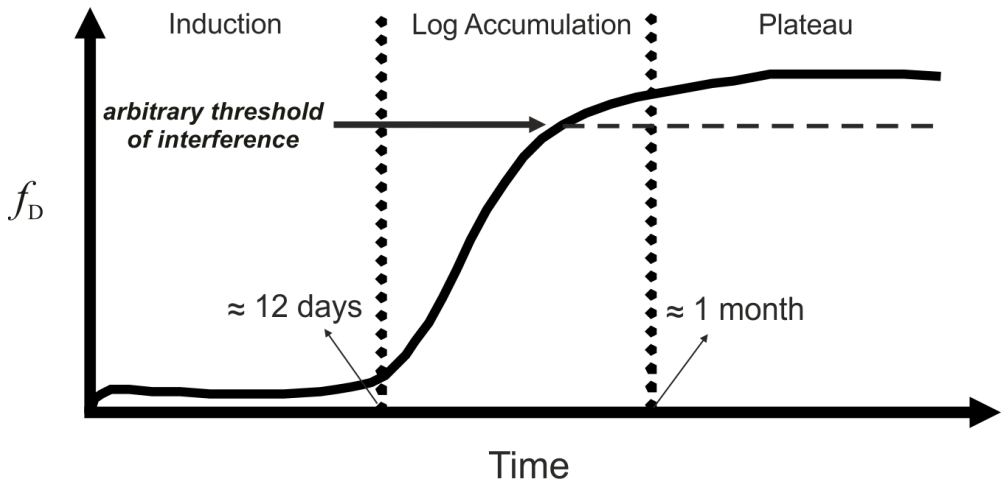

Figure 2.15. Qualitative evolution of the Darcy frictional resistance to fluid in marine heat exchangers over a period of biofouling development, adapted from [**2.3**].

It has been reported that a biological film of *circa* 10 μm thick can double the frictional resistance in a smooth pipe [**2.67**]. Likewise, the evolution of the frictional resistance to fluid motion within 10 mm diameter SS tubes (UNS S31603) of 3,165 mm in length was monitored over a 40-day biofouling growth seawater flowing at u = 1.9 m s^{-1} [**2.63**]. It was shown that f_D remained relatively constant (f_D = 0.025 ± 0.005) during the initial 12 days and then increased to level off at f_D = 0.045 ± 0.005 after approximately 24 days, thus corresponding to an 80 % increase in frictional resistance to fluid. Overall, biofouling deposits on the inside of tubes decreases the effective tube diameter (d), thus reducing the cross sectional area. For instance, biofouling build-up on a large 200 mm diameter carbon steel pipe has been reported to reduce the cross-sectional area by about 50 % over a 2.5 year exposure [**2.68**], restricting the pipe flow rate (Q) and subsequently the performance of the heat exchange (heat transfer).

2.4.4.2 Heat transfer resistance

The heat transfer resistance or R_h is defined as the sum of the resistance to heat transmission by convection (due to the motion of seawater) or conduction (resulting from the agglomeration of insulating layers formed by the biofouling deposits) [**2.18**,**2.69**]. Marine biofilms (where 95 % of the EPS matrix is made of water, only allows diffusive heat transport to occur) are reported to provide significant thermal insulation to heat exchanger surface from seawater [**2.18**,**2.69**]. In contrast, heat transfer by convection is inhibited, which is problematic since convective transport reduces biofouling agglomeration within the pipe surface [**2.69**].

Alongside with R_h, the overall heat transfer coefficient (h) represents the overall ability of convective and conductive barriers to transfer heat. An experimental study carried out in the Institut Francais de Recherche pour l'Exploitation de la Mer (IFREMER) for the French Ocean Thermal Energy Conversion (OTEC) programme focused on the evolution of the overall heat transfer coefficient (h) and the pressure drop with time within a 25 mm diameter Ti tube (at 1.5 m s^{-1}) [**2.70**]. The results showed that h remained constant (values similar to typical heat transfer coefficients around 5,000 W m^{-2} K^{-1}) during the initial 15 days and decreased twice as less after 30 days. The corresponding ΔP along a 1 m length distance was also monitored with time: a detectable increase in pressure drop at around 1,200 Pa was assessed after 20 days of exposure and ΔP was 2.5 times (≈ 3,000 Pa) more significant than the initial value after a 50 days time duration. Overall, studies on OTEC plants have revealed that a 55

μm thick biological film would lead to unacceptable reduction in the heat transfer of heat exchanger tubes [**2.71**]. This value of biofilm thickness is consistent with about 10 times thicker films (compared to thin biological layers), where the thermal boundary layer (δ_t) due to the difference of temperature between the wall and free stream can be affected [**2.33**-**2.35**]. In addition, the heat transfer performance of 90-10 Cu-Ni (UNS C70600) tubes with regard to biofouling have been evaluated in flowing seawater (at 1.8 to 2.4 m s^{-1}) over a 180-day period [**2.72**]. It was shown that biofouling significantly reduced the heat exchange after 90 – 110 days of exposure.

2.4.4.3 Estimate of biofilm / biological film thickness (δ_b)

Devices that measure total solid matter deposited inside surfaces of the tubes can be fitted at the outlet of heat exchanger tubes. These devices are usually composed of test-tube holders made of polyvinyl chloride that can house small portions of the test tubes; *e.g.* 6.5 mm in length, mounted on the heat exchanger unit [**2.63**]. In these configurations, both the test- and heat exchanger tubes have similar diameter, composition and surface finish. The test-tubes are extractable and allow assessing an estimate of the thickness of adhered biological films (δ_b) [**2.63**]. In practice, a biofilm thickness of 100 μm was reported after a 50 days exposure within the OTEC programme at IFREMER (25 mm diameter Ti tube at 1.5 m s^{-1}) [**2.70**]. Characklis suggested that an increase in ΔP is due to the presence of biofilms only when δ_b reaches the viscous sublayer (δ_l) [**2.68**], where in turbulent regime δ_l results from the very thin region in contact with a metal surface experiencing turbulent mixing impediment (δ_l represents about 1 % of the diffusion boundary layer, δ_d, which in turn is indicative of a concentration gradient of reactants at the surface due to mass transport and whose thickness decreases when u increases [**2.65**]). In this instance, δ_d is a parameter of relevance since it corresponds where the majority of the modifications in the fluid stress characteristics, turbulence, mass transfer and fluid interaction at the wall surface can occur [**2.65**]. Under low flow regime, bacterial cells must traverse δ_d, where bacterial biofilm formation and development depend on cell size and motility [**2.27**]. It is usually assumed that about 7 s are required for species to diffuse across δ_d (typical thickness of 6.0 μm for a microelectrode) regardless of fluid flow [**2.74**]. In contrast, planktonic bacteria are affecting by turbulence and mixing at higher flow conditions, thus associated with rapid surface colonisation until flow velocity reaches values relevant to substantial shear forces leading to biofilm dispersal [**2.27**]. However, Stoodley et *al.* measured a 3 times lower biofilm thickness (causing substantial pressure drop) than δ_l within a flow cell device [**2.66**]. Overall, this suggests that

considerations on biofilm thickness assessment need to be further addressed with suitable standard methods communally agreed.

2.4.4.4 Characteristics of hydrodynamic and diffusion dependent systems

Dimensionless numbers, such as the Reynolds number (R_e) are generally used to characterise hydrodynamic and diffusion dependent flow conditions [**2.65**]. The R_e value can represent a flow regime indicator from laminar to turbulent conditions and can be defined in **Equation 2.19** for circular straight pipes as the ratio of inertial to viscous forces in the fluid [**2.65**,**2.74**]:

$$R_e = \frac{ud}{\nu_k} \tag{2.19}$$

where u is the mean flow velocity, d the characteristic diameter and ν_k the kinematic viscosity of the fluid. In practical engineering conditions, the flow in circular pipes is usually laminar for $R_e \leq$ 2,300, turbulent for $R_e \geq$ 4,000, and transitional in between [**2.74**]. Typical values of R_e used by heat exchangers in-service conditions are beyond 10,000; *e.g.* flow regimes of $R_e \approx$ 35,700 (1.5 m s^{-1}) within a 25 mm diameter Ti tube in the French OTEC programme at IFREMER [**2.70**]. It is assumed that when R_e is less than 10,000, the deposition rate, on the heat exchanger internal walls is much greater than the removal rate. This leads to emergency shut downs and reduce the extent of the period of operation [**2.64**]. Likewise, running the heat exchanger systems at high flow regimes is not a viable solution since it would result in both an increase in the overall heat transfer coefficient and pressure drop, and also potential erosion of material surface [**2.3**]. Consequently, these engineering problems would cause enhanced energy consumption, systems failure and increased capital costs. In addition, studies on the effect of R_e on the biofilm thickness by Pujo and Bott, under nutrient limited conditions at R_e = 11,000, suggested that δ_b was 10 times thicker at 0.5 m s^{-1} than at 2 m s^{-1} over a 15-days exposure [**2.3**,**2.5**]. Similarly, biofilm density (dry mass / wet volume) has been reported to be affected by the mean velocity: increases from 0.1 to 0.5 m s^{-1} resulted in densities between 26 – 76 kg m^{-3} [**2.3**,**2.5**]. Velocity profile measurements within biofilms have also proven the existence of a transition between smooth to turbulent flow using the roughness Reynolds number (R_k) for $R_k >$ 3.5 – 5.0 [**2.66**]. In this instance, R_k represents the critical condition, which causes a wedge of turbulence due to roughness, *i.e.* depending on roughness height and the velocity in the laminar boundary layer at the roughness height [**2.75**].

The mass transfer due to bulk convection (net transport of fluid along the pipe) and turbulent convection (exchange of the fluid between δ_d and the bulk) are important concepts in hydrodynamics, thus can affect biofouling processes. In this instance, Schiffrin and de Sánchez [**2.57**] have argued that the mass transfer coefficient (K_m) derived from the rotating disk electrode (RDE) geometry can facilitate comparisons between different geometries / flow conditions, *e.g.* comparison with a circular straight pipe, thus consistent with Pletcher and Walsh [**2.42**].

This approach can be extended to the RDE developed by Herbert-Guillou *et al.* to monitor biofilm formation and growth [**2.76**,**2.77**]. This technique developed to assess biofilm thicknesses *in situ* is based on two fundamental properties inherent to change of mass transport associated with biological films: (*i*) biofilms behave as an inert porous layer and (*ii*) the diffusion coefficient in the biofilm D_f is the same as that for the electrolyte solution [**2.77**]. Measures of biofilm thicknesses were monitored using a RDE embedded inside a tube under a controlled turbulent flow at 0.5 m s^{-1} in a seawater environment [**2.77**]. After a 28-day exposure, the biofilm thickness varied between 80 and about 60 μm for rotation speeds of 100 and 1,100 rpm. Overall, the comparison between the RDE geometry and any hydrodynamic configuration, *e.g.* circular straight pipes, using K_m relies on the assumption that the reaction kinetic rate is limited by diffusion [**2.57**]. However, mechanical effects inherent to fluid motion, which are predominant at high flow regimes would have an influence on biofilms that is not addressed using this comparison. At a smaller scale, Stoodley *et al.* have proposed a relationship between K_m and u in a biofilm void using the combination of a microelectrode measuring the local mass transfer coefficient distribution and the particle tracking technique to characterise the velocity profile [**2.78**]. Whereas the tip of the microelectrode is capable of characterising a transport-limited reaction, the overall reaction rate inherent to bacterial cells in a biofilm may be more complex in nature, *i.e.* limited both by nutrient flux and by mass transport [**2.78**].

The flow effects on biofilm growth and extent are not as evident as these concluding remarks: thinner biofilms and higher removal rate with increased u and R_e, respectively and the mechanical properties of biofilms will also play a pivotal role to adapt from adverse flow conditions. Using the RDE configuration, Herbert-Guillou *et al.* have also shown that biofilms can readily deform with increased rotation speeds and that the biofilm structure is dependent on the hydrodynamic conditions of growth, *i.e.* greater deformations for biofilms grown under laminar in comparison with turbulent regimes [**2.77**]. These results are in good agreement with the conclusions drawn by Dunsmore

et al. who have demonstrated the viscoelastic characteristics of (anaerobic and aerobic) biofilms that depend on the flow regime at which biofilms are established [**2.79**]. Biofilms grown under turbulent conditions had enhanced mechanical properties including higher elastic modulus and a favourable propensity to recover its original shape after release of strain induced by increased flow regime. Conversely, biofilms established under laminar regimes were less rigid and presented an irreversible mechanical response (damage) upon exertion of strain [**2.79**]. Overall, the viscoelastic properties of biofilms can strengthen their mechanical structures (more stable) to resist detachment resulting from fluid shear [**2.3**]. To achieve greater hydrodynamic performance, it was shown that biofilms developed under turbulent conditions can adopt streamlined / filamentous structures to keep the flow attach nearby and minimise wakes at the rear [**2.79**]. Whereas, biofilms formed under laminar flow regimes are usually reported to consist of cell clusters separated by interstitial voids, thus having an overall mechanical structure less favourable with regard to profile drag [**2.3**].

2.4.4.5 Momentum transfer: fluid shear force

The shear stress-velocity gradient can account for the fluctuating turbulent motions of the fluid [**2.80**]:

$$\tau = \mu \frac{\mathrm{du}}{\mathrm{dy}} \tag{2.20}$$

with μ the dynamic viscosity, u and y representative of the velocity and the distance measured from the pipe wall, respectively. In industrial systems, high shear forces can influence EPS production and induce biofilm deformation, plus it can lead to both an increase in nutrient flux and mass transport of biocide at surfaces, enhanced shearing of biofilms, and also result in biofilm diversity and detachment [**2.3**,**2.81**]. In the published literature, typical values of τ reported in channels within biofilms can range from 0.0642 to 0.321 Pa [**2.73**]. Stoodley *et al.* have demonstrated that wall shear stress of 1.32 Pa within a flow cell device operating under a high flow regime (u = 0.505 m s^{-1} and R_e = 3,351) can result in cell clusters sloughing away and filamentous biofilms failure [**2.66**]. Using similar flow systems, theoretical τ values of 0.1 Pa at 0.04 m s^{-1} (R_e = 120) and 1.0 Pa at 0.4 m s^{-1} (R_e = 1,200) were reported by Dunsmore *et al.* [**2.79**].

Based on a comparative study on the influence of shear stresses on bacterial biofilms (leading to differences of the biofilm structure for similar flow regimes), Mehdi Salek *et al.* have recently addressed the importance of flow cell geometry on biofilm colonisation [**2.81**]. This study revealed that flow cells with different geometries operating at similar flow conditions had various wall shear stress distributions, thus affecting established biofilms under these conditions, which in turn showed different surface distributions, structures and responses to biocide. Thicker biofilms and higher surface coverage were predominant at low shear regions near the corner, whereas thin layers and reduced attachment were more pronounced within the middle of the flow cell, *i.e.* favourable higher shear stress conditions (enhanced interfacial mass transfer and less effective diffusive barrier) for a biocide to penetrate across the biofilm [**2.81**]. Overall, these results were consistent with previous works reported by Duddridge *et al.* using a corrosion flow loop, where maximum adhesion was observed at low surface shear stress on SS UNS S31600 tubes.

However, the significance of these shear stress values at the laboratory scale needs to be fully addressed with regard to industrial systems. **Figure 2.16** shows typical shear stress values at the interface between flowing seawater and the pipe surface. The values in **Figure 2.16** are taken from [**2.72**] and published τ values corresponding to channels within biofilms in [**2.73**] have been added to be able to predict the range of shear stress values required to slough biofilms away within heat exchanger tubes.

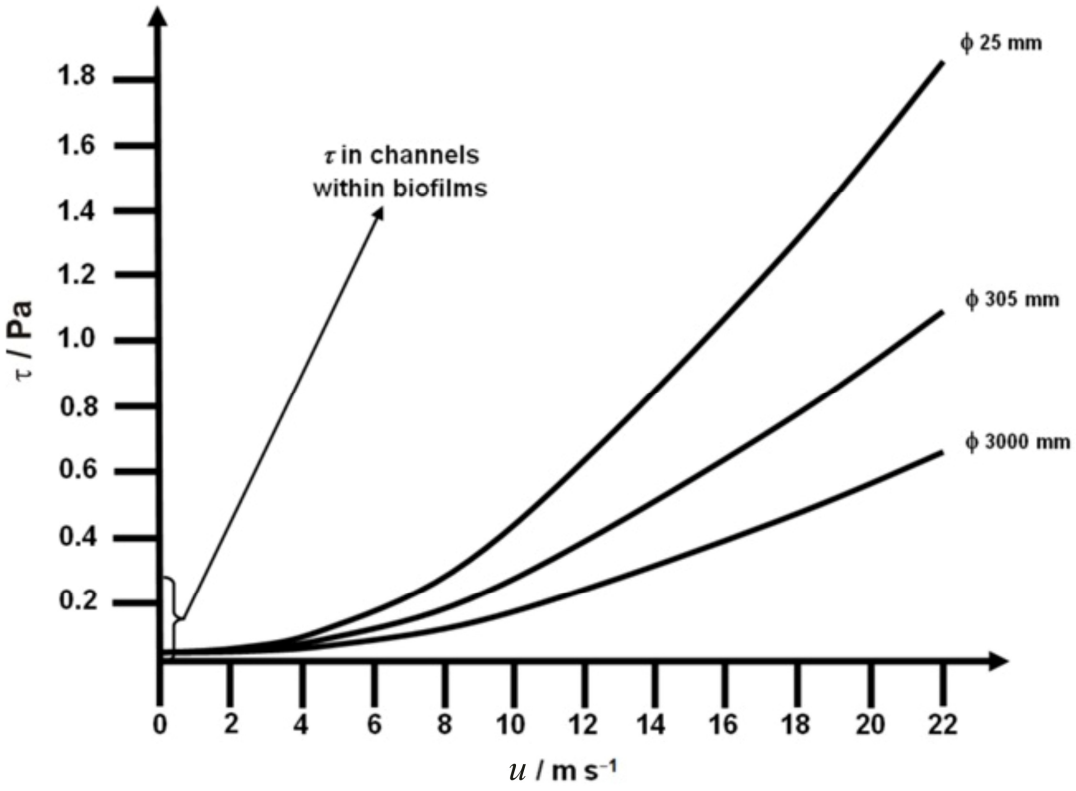

Figure 2.16. Evolution of the wall shear stress with the mean velocity in flowing seawater inside Cu-based alloys of different diameters, adapted from [**2.72**].

Up to u = 2.0 m s^{-1}, it is important to notice that the shear stress values are independent of the pipe diameter. By considering u = 3 – 4 m s^{-1}, *i.e.* the breakaway velocity (see **Section 2.4.2**) beyond which the passive oxide layer may suffer from fluid shear induced damage, it can be predicted that the corresponding τ values may not be sufficient to successfully remove / slough off the entire biofilm. Conversely, a rough estimate of τ (**Equation 2.20**) can be calculated with the mean velocity u and the half diameter of the tube using values reported in the published literature. For instance, using the hydrodynamic conditions of the French OTEC programme ($R_e \approx$ 35,700 at 1.5 m s^{-1} within a 25 mm diameter Ti tube) with μ = 1.07 $\times$ 10^{-3} kg m^{-1} s^{-1} for seawater at 20 °C, $\tau \approx$ 0.13 Pa [**2.70**].

2.4.4.6 Significance of the hydrodynamic conditions for the current study

Since the flow induced effect on biofilms is not trivial and debatable, a controlled low laminar flow regime ($R_e \approx 1$) indicative of a smooth flow within biofilms [**2.66**] represents a good alternative for the experimental tests in **Chapter 4**. Herein, the hydrodynamic parameters such as f_D ,ΔP, u, R_e and τ have been addressed in order to uniquely review flow-through biofilm culture devices in the published literature and characterise the once-through flow system used for the current approach, see **Section 4.6.2**. Similarly, the concept of biofilm thickness consists in an important physical parameter to quantify bacterial biofilm, *i.e.* using accurate confocal microscopy technique (**Section 5.12.3**) as opposed to rough measurements of biomass deposits inside metallic surfaces (**Section 2.4.4.3**).

2.5 Overview of bacterial biofilm analysis

Bacterial biofilm research, both formation and inhibition, is by its very nature highly interdisciplinary involving a diverse range of scientific and engineering fields [**2.20**,**2.82**]. However, previous biofilm studies have mainly focused on functional, structural and ecological aspects, for instance:

- biofilm attachment / formation stages [**2.1**,**2.83**] and biofilm cohesiveness [**2.1**],
- the microbial and biochemical composition [**2.1**], genetic and physiological considerations [**2.84**],
- the complex multicellular interactions based on cell-to-cell signalling (quorum sensing [**2.85**]),
- the protective and adsorption properties of biofilm upon exposure to organic and inorganic pollutants [**2.86**], and
- detergents, chemical substances such as biocides, synthetic surfactants and xenobiotics (chemicals such as drugs antibiotics found in an organism but not normally produced or expected to be present inside) combined with heavy metals, reactive O_2 species and biodegradation processes [**2.87**].

Biofilm analysis methods have recently been extensively reviewed for a range of research fields and are summarised in **Table 2.3** [**2.20**]. Although a detailed assessment of the biofilm analytical techniques is beyond the scope of this PhD thesis, they can, however, be classed into (A) Physical, (B) Microscopy, (C) (Bio)-chemical and (D) Molecular microbiological methods.

Table 2.3. Biofilm research fields and analytical techniques, adapted from [**2.20**,**2.82**].

Research fields			
Biofouling	Biocorrosion	Biodegradation	Ecology
Biofilm structure and function	*Community composition, metabolic activity and regulatory systems*		*Pathogenesis and hygienic relevance*

Biofilm (analytical methods)

Molecular techniques	Separation techniques	Detectors (C)	Surface and interface characterising techniques
***D**enaturing **G**radient **G**el **E**lectrophoresis (**DGGE**)* ***F**luorescent **I**n **S**itu **H**ybridization (**FISH**)* ***G**reen **F**luorescent **P**rotein (**GFP**)* *Immunoassays* *Oligonucleotide probes* ***P**ulsed **F**ield **G**el **E**lectrophoresis (**PFGE**)* ***P**olymerase **C**hain **R**eaction (**PCR**)* (D)	***C**apillary **E**lectrophoresis (**CE**)* *Extraction* ***F**ield **F**low **F**ractionation (**FFF**)* ***G**as **C**hromatography (**GC**)* ***G**el **E**lectrophoresis (**GE**)* ***L**iquid **C**hromatography (**LC**)* ***S**ize **E**xclusion **C**hromatography (**SEC**)*	*Atomic spectrometer* *Electrochemical detectors* *Mass spectrometer* *Optical detectors*	***A**tomic **F**orce **M**icroscopy (**AFM**)* ***C**onfocal **L**aser **S**canning **M**icroscopy (**CLSM**)* ***I**nfrared **R**adiation (**IR**)- and **A**ttenuated **T**otal **R**eflection (**ATR**)-IR- spectroscopy* ***N**uclear **M**agnetic **R**esonance (**NMR**)* *Photoacoustic spectroscopy* *Reflectance spectroscopy* ***S**canning **E**lectron **M**icroscopy (**SEM**)* ***E**nvironmental **S**canning **E**lectron **M**icroscopy (**ESEM**)* ***T**ransmission **E**lectron **M**icroscopy (**TEM**)* ***S**canning **T**ransmission **X**-ray **M**icroscopy (**STXM**)* ***X**-ray fluorescence spectroscopy* ***E**nergy **D**ispersive X-ray **S**pectroscopy (**EDS**)* (B)
Spectrometry	Microsensors		
***A**tomic **A**bsorption **S**pectroscopy (**AAS**)* *Fluorescence spectrometry* *Mößbauer spectrometry* *Spectrophotometry* (A)	*Electrochemical microsensors* *Fibre-optic microsensors*		

Microbiological and molecular methods, which apply molecular and separation techniques, are generally used in microbiological research. These methods are also highly technical and often too expensive, most notably for the genetic techniques involving nucleic acids [**2.88**]. Microscopy methods, such as atomic force microscopy (AFM), scanning electron microscopy (SEM) and CLSM also called scanning confocal laser microscopy (SCLM) or laser scanning confocal microscopy (LSCM) in the literature can be included in surface and interface characterising techniques [**2.89**]. Chemical techniques are typically methods based on a chemical reaction, adsorption or host-guest recognition, for instance, electrochemical microsensors and detectors are in this category. Whereas, biochemical techniques differ from chemical-based procedures by using a biological substance / bio-receptor (identification of specific enzymes, antibodies, nucleic acid sequences) [**2.90**,**2.91**]. Overall, physical methods include all the techniques which rely on a physical working principle, *i.e.* it encompasses virtually all surface and interface characterising techniques, microsensors (excluding bio-chemical sensors) and spectrometry methods [**2.91**].

Within the framework of this current review, the emphasis will primarily focus on microsensors, plus corroborative microscopic methods, in order to sense for the presence / formation, and also to provide characterisation of bacterial biofilms. Thus, three key components in the interdisciplinary bacterial biofilm research [**2.20**,**2.82**] will be considered: (*i*) biofilm attachment / formation stages (biofilm sensing and quantification), in addition to (*ii*) the protective and adsorption properties of biofilm upon exposure to (*iii*) environmentally friendly substances (biofilm disruption to comply with environmental concerns and legislature).

2.6 Analytical detection techniques

Several common analytical techniques in **Table 2.3** have been used to detect and characterise microorganisms (bacterial cells), biofilms, and also biological components (polysaccharides, proteins, nucleic acids, phospholipids and humic substances) over the last twenty years [**2.20**]. These techniques have proven to be reliable, sensitive and specific to the target bacteria. Generally, however, the majority of these techniques rely on preparation methods and/or sampling procedures, which are time-consuming, complex and often require highly trained operators.

According to biofilm and microbiological sampling definitions, indirect sampling (*ex situ* sampling) refers to sample analysis in which the sample is withdrawn from the bulk material, *e.g*. seawater, and transported to the external analytical testing area [**2.2**]. For instance, culture techniques, activity measurements and estimation of biomass are indirect methods of detection and biofilm characterisation [**2.2**]. In the culture methods, bacteria can be routinely tracked and identified using specific growth media (liquid or solid agar). Similarly, dip sticks consist of plastic strips coated with a layer of nutrient agar that enable rapid detection of microorganisms (when immersed in a liquid environment) and cell counts (after incubation in a warm space for 24 h) using a calibration chart. In addition, field detection kits for bacteria species, *e.g.* SRB or iron oxidizing bacteria, have become commercially available to diagnose MIC. After immersion in specific liquid media and incubation, the targeted microorganisms responding to these specific growth environments can be enumerated and their metabolic activity can also be measured [**2.2**]. Likewise, activity measurements using radiorespirometric methods (total heterotrophic activity and sulphate-reducing capacity) allow determining microbial activity in bacterial biofilms. Although microscopic assessment can provide information on biofilm biomass, its indirect determination can be performed using adenosine triphosphate (ATP) measurements used as an indicator of total microbial biomass using immunological techniques such as marker, fingerprint, enzyme-linked immunosorbent assay (ELISA), and gene probes (*i.e.* segment of genetic material specific to a bacterial species of interest that is labelled with a radioactive substance, such as a radioactive form of phosphorus, or an enzymatically detectable molecule). Conversely, direct sampling (*in situ* sampling) is the analysis that is conducted directly in the bulk material without a sample being removed [**2.20**].

Usually, direct sampling devices used to study biofilms are either (*i*) directly implanted in the engineering system or (*ii*) side-stream devices [**2.2**,**2.3**]. For instance, devices directly embedded into pipe walls, *e.g.* Petrolite Bioprobe^{TM}, are housed with high pressure access fittings compatible with the metallic structure to minimise shutdown and depressurisation. Side-stream sampling devices, *e.g.* a Robbins device that consists of a plug inserted flush with the pipe wall, are used in parallel with the sensing system under investigation as these will experience similar wall shear stresses. Although complex designs and alternative sampling coupons to actual pipe surface are necessary, these devices can offer greater flexibility than directly implanted configurations.

The detection techniques with external preparation methods include molecular microbiology, surface and interface characterising techniques and to a large extent the new applied microbiology spectroscopy techniques. Overall, only the microsensing techniques do not typically require any preparation methods, although sensor calibration may be necessary [**2.89**,**2.90**]).

2.6.1 Advantages of *in situ* microsensors

By taking into account the criteria of appropriate design and manufacture procedures, the *in situ* microsensors generally have better performance characteristics which ultimately best relate to the experimental details for the current investigation [**2.20**,**2.92**]. These characteristics / criteria include:

- good time-response (in the order of minutes required for EPS formation [**2.1**]),
- real-time: in-line (analyses done with a direct interface of the detector to the process), on-line (using a recirculation loop or an automatic sample transport system from the process to the detector), and at-line (using a detector located close to the process) as opposed to off-line (analyses on samples removed from the process) measurements [**2.20**,**2.91**]),
- low-cost (compared to other analytical methods [**2.20**]),
- smart (actuated and data displayed by means of a convenient interface without operator repetitive procedure [**2.90**,**2.91**]),
- easy-to-use (does not require highly-trained operators), and
- remote measurements (in comparison with cumbersome equipment in other categories in **Table 2.3**).

2.6.2 Fundamental requirements of microsensors

In general, the development of an appropriate sensor is linked to its operational robustness and its analytical response. In particular, *in situ* microsensors for marine biofilm applications must tolerate extreme conditions of prolonged seawater immersion [**2.93**]. In addition, there may be a requirement for sterilisation (autoclaved process) and the sensors should maintain calibration with time. The dynamic range of the sensor must cover the range of variation of the measured process parameter [**2.90**,**2.91**]. Similarly, the sensor sensitivity, which is mainly dependent on the sensing

element of the sensor, needs to be in good order to observe a clear measurable signal [**2.90**,**2.91**]. Baseline drift (from the useful signal, *i.e.* meaningful signal corresponding to the measured quantity) due to artefacts, *e.g*. precipitation of marine deposits, both inorganic and organic, and surface poisoning of the sensor sensing area are common problems [**2.90**,**2.91**]. Overall, microsensing techniques may be considered as being less precise and accurate than molecular microbiological and microscopic methods. Indeed, molecular techniques have the ability to measure the gene expression of bacterial cells [**2.20**] and microscope techniques are of interest to calibrate sensors for biofilm analysis [**2.94**]. Nevertheless, the flexibility of the sensor approach for bacterial biofilms can be a good alternative to the limitations associated with precision and accuracy. To date, only a few sensors for biofilm analysis have been commercialised and accepted by industrial [**2.2**,**2.3**,**2.82**], thus there is scope for novel sensing strategies / methodologies to contribute to the bacterial biofilm research [**2.20**,**2.93**].

2.6.3 *In situ* microsensing corroborated using microscopy techniques

In this project, the surface and interface characterising techniques in **Table 2.3** are the more apparent methods to corroborate *in situ* applied sensor technology microsensing approaches. Among the reliable techniques to characterise bacterial biofilms, surface and interface characterising methods are more convenient in terms of surface engineering approach, cost and accessibility. This is not the case for costly molecular biology, which requires a deep level of biological understanding and background. As spectrometry techniques are less mature methods (compared to the other candidates in **Table 2.3**) for bacterial biofilms [**2.20**], their use for corroborative investigations may need to be fully addressed. Importantly, microscopy techniques are probably the most convenient methods to examine microorganisms, especially bacterial species [**2.2**]. Historically, microscopic characterisations have allowed advanced progresses in the bacterial biofilm research using cutting-edge confocal microscopy equipments [**2.2**,**2.3**,**2.23**]. Novel considerations proving the existence of a three dimensional heterogeneous structure of biofilm with water channels (as opposed to a simplistic planar structure) have revolutionised the biofilm research field [**2.2**,**2.23**,**2.78**]. This represents evidence on the capability of advanced microscopy techniques to physically characterise the presence of bacterial biofilms on metallic surfaces. Overall, a more detailed review on microscopy techniques for bacterial biofilms is proposed in **Section 2.7**.

2.6.4 Review of sensor-based technology for biofilm sensing

Among the wide range of different analytical methods, the sensor technology approach is distinct from that of the various detection techniques described in **Table 2.3**. Indeed, sensor devices typically require a sensing element, which responds by means of a transducer and signal conditioner to an input quantity by generating a functionally related output, *e.g.* electrical or optical signals [**2.90**,**2.91**]. In order to assess the appropriateness of *in situ* microsensor measurements, the technology should be compared with the other candidate methods. Also, the scope of the sensor devices discussed in the published research literature for biofilm sensing (pros and cons) should be investigated to select an appropriate microsensing technique for the proposed experimental work programme.

2.6.4.1 Suitability of microsensors

For microbiology purposes, the worldwide research for biofilm sensing / monitoring is mainly based on biological microsystems [**2.95**]. The reason for the use of microscale sensor relies on different viewpoints discussed in the literature, see **Table 2.4**. Current limitations of the application of microsensors in biofilm characterisation from the literature [**2.17**] are detailed as follows:

- Limited commercial availability, which is to be expected since bacterial biofilm microsensing involves multidisciplinary expertise in an emerging biotechnology field.
- Isolated information caused by the heterogeneity on the microscale. However, this characteristic is inherent to the decomposition of EPS by the surface-associated microbial cells, which changes the surface charge and free energy and transforms the surface into a highly heterogeneous milieu [**2.1**]. For information, the patchy microstructure of the bacterial films can range from 1 – 2 μm (single bacteria) to $\geq$ 50 μm thick (colonies) according to simulations established by a ceramic based gradient flow cell [**2.96**].
- The lack of suitable mathematical models for biofilm development and growth.

Table 2.4. Characteristics of microsensors of interest for bacterial biofilm sensing.

Microsensors characteristics	Explanations and significance
Measurements at specific positions within biofilms / manipulation of microorganisms	Biofilms are heterogeneous with a complex chemistry [**2.9**,**2.10**]. Localisation by electric fields, which can be indirectly used for bacterial biofilm disruption in this project. High spatial resolution providing by the small tip size diameter (≤ 20 µm) of optical microelectrode [**2.89**]. Suitable to measure chemical gradients across thin biofilm layers (≤ 100 µm) [**2.97**], which are required for optical bacterial biofilm sensing. However, the shape of a tip relative to a metal flat surface is not appropriate with respect to bacterial biofilm formation at the metal / biofilm interface.
Faster rate of mass transport, steady-state current rapidly established, shorter time measurements	The diffusional mass efficiency is better with a smaller surface area of a microsensor and occurs even in the absence of convection (energy transfer through a fluid with molecule displacements) [**2.92**,**2.98**]. Surface areas (within $\approx cm^2$) related to conventional electrodes are therefore not appropriate. The long time taken for the measurements is subject to drift especially in the presence of living bacterial biofilms [**2.99**]. According to Dexter and Chandrasekaran who verified this property, this phenomenon is likely to happen if the measurement takes longer than about 30 s [**2.99**], which is very short and quasi-certain to occur within the scale of laboratory experiments. In addition, if the mass transport rate increases, the measurement can be done at high speed, limiting water ingression problems (mechanisms by which water penetrates into cracks and pores of the metal surface [**2.100**]).
No significant change of the chemistry	Due to the small area of a microelectrode, the quantity of chemicals reacted at the electrode surface will not change the chemistry significantly within the measurement pool [**2.99**].
Reduction of non-faradaic current	Capacitive charging currents (double layer capacitance) can be reduced to insignificant proportions as the electrode size is diminished, thus resulting in a small time constant [**2.92**,**2.98**]. Conventional electrodes undergo this dielectric phenomenon which often limits detection of faradaic currents [**2.99**].
Decrease of the detection limit	For impedance microbiology, the detection limit refers to the detection time, *i.e.* the time required for the threshold concentration of the target microorganisms to be reached. The threshold concentration represents the smallest concentration of microorganisms which can induce a detectable impedance change (resolution of the sensor [**2.90**,**2.91**]) [**2.101**]. Consequently, shorter detection limits correspond to finer and more reliable measurements provided by the microelectrode.

Table 2.5 shows the recent qualitative evolution of the sensing area over the last decade (2000 to 2010). It outlines a description of the sensor technology (optical, electrochemical, piezoelectric and magnetoelastic described in more details in **Section 2.6.4.2**) used with the scale achieved with respect to the sensing element area. A complete review of all sensor technology based techniques for biofilm is outside the scope of this study and will not be further addressed here. In addition to the sensor working principle or technology, the scope of application for microbiology, *i.e.* direct or indirect biofilm / bacterial cells detection, is highlighted. In this instance, 'direct' detection stands for sensing a measurand directly representative of the biological film, *e.g.* thickness, biomass. Conversely, 'indirect' detection is associated with monitoring characteristics that change upon the presence of a biological film or due to metabolic / redox processes within biofilms, *e.g.* mass transport, CO_2, pH.

The finest scale ranges of the sensing element area achieved are below 100 μm^2 [**2.102**]. However, such microsensors with very small sensing areas are appropriate for cell-surface interaction applications as opposed to investigations of biofilms formation. The studies of cell interactions via single macrophage cell-based sensors are of importance for pure microbiology purposes [**2.102**]. For instance, it may be applicable for quorum sensing to study multicomplex cells interaction, see **Section 2.5**. Thus, understanding the single cell behaviour in a specified chemical or biological environment is outside the scope of the proposed research since it is unrealistic to the scale of a real system where a biofilm (a more developed structure which encompasses a consortia of cells, organic and inorganic matter, see **Section 2.3**) can form and develop. As the biofilm chemistry along a metallic surface is non-uniform on a scale below 100 µm [**2.99**], the sensing area should be dimensioned accordingly. The characteristic length (L), *e.g.* the diameter for a cylindrical-shaped microsensor, corresponding to one sensing area (single-array system) should ideally range below 100 µm. This would enable a complete map of the biofilm chemistry on a metallic surface using for instance, several single arrays with $L \leq 100$ µm.

.

Table 2.5. Sensing element area evolution over the last past decade with respect to worldwide research groups and biofilm sensing and analysis – list non-exhaustive.

Authors / Country	Reference	Scale (sensing element area)	Sensor working principle / sensing application	Year
Herbert-Guillou *et al.* (France)	[**2.122**]	≈ 80 mm^2	Biofilm detection by mass transport modification / biofilm thickness (*electrochemical*)	1999
Beyenal *et al.* (USA)	[**2.97**]	≈ 300 μm^2	Measure spatially resolved profiles of backscattered light within biofilm / correlation with local effective diffusivity (*optical*)	2000
Philip-Chandy *et al.* (England, France)	[**2.113**]	≈ 80 mm^2	Biofilm detection at the core-cladding interface (evanescent field attenuation by refractive index and absorption / scattering modulation) / biofilm thickness) (*optical*)	2000
Le Coq *et al.* (France)	[**2.111**]	≈ 2.5 mm^2	Biochemistry function detection associated with bacterial growth using evanescent wave spectroscopy (*optical*)	2002
Bressel *et al.* (Germany, South Africa)	[**2.96**]	≈ 30,000 μm^2	Biomass monitoring / change in the open circuit potential (*electrochemical – piezoelectric*)	2003
Keirsse *et al.* (France)	[**2.112**]	≈ 1.5 mm^2	Biochemistry function detection associated with bacterial growth using evanescent wave spectroscopy (*optical*)	2003
Beyenal *et al.* (USA)	[**2.108**]	≈ 300 μm^2	Measure of CO_2 concentration profiles within biofilm (*electrochemical*)	2003
Ruan *et al.* (USA)	[**2.104**]	≈ 28,000 μm^2	Biomass monitoring / binding properties (*biosensor – magnetoelastic*)	2003
Basu *et al.* (USA)	[**2.123**]	≈ 18 mm^2	Biofilm detection (change in interfacial properties) / binding properties (*biosensor – electrochemical*)	2004
Beyenal *et al.* (USA)	[**2.110**]	≈ 300 μm^2	Detection and quantification of fluorescent light intensity distribution within biofilm (*optical*)	2004
Reipa *et al.* (USA)	[**2.116**]	≈ 3 cm^2	Biomass monitoring (*piezoelectric*)	2006
Spiller *et al.* (Germany)	[**2.124**]	≈ 2.5 mm^2	Cell growth detection / biomass monitoring (*biosensor – electrochemical*)	2006
Oliver *et al.* (Northern Ireland)	[**2.125**,**2.126**]	≈ 1 mm^2	Biofilm detection (change in interfacial properties) / biofilm formation stages (*electrochemical*)	2006
Guntupalli *et al.* (USA)	[**2.105**,**2.106**]	≈ 6,000 μm^2	Biomass monitoring / binding properties (*biosensor – magnetoelastic*)	2006/2007
Miečinskas *et al.* (Lithuania)	[**2.117**]	≈ 0.5 cm^2	Biomass monitoring (*piezoelectric*)	2007
Veiseh *et al.* (USA)	[**2.102**]	≈ 25, 100 and 400 μm^2	Cell-based detection / binding properties (*biosensor – optical*)	2007

2.6.4.2 Type of transduction-based sensor technology

Applied microorganism sensors reported in the research literature (in **Table 2.5**) are outlined below with regard to the transduction used (the action of converting the measurand such as the measured quantity, property or condition into a usable electrical / optical output [**2.90**,**2.91**]). The more mature approaches investigated are electrochemical and optical microsensors [**2.20**]. However, piezoelectric sensors using the quartz crystal microbalance (QCM) working principle have also been reported in 1993 to monitor the growth of a *Pseudomonas cepacia* biofilm for several days [**2.103**].

Magnetoelastic

More recently, research has been carried out using magnetoelastic sensors [**2.104**-**2.106**]. Magnetoelastic thin film sensors can be considered as the magnetic analogue of surface acoustic wave (SAW) sensors or QCM devices [**2.90**,**2.91**]. The working principle of mass-sensitive magnetoelastic sensors is described as follows. In response to an externally applied time-varying magnetic field, steady-state or pulse, ribbon-like magnetoelastic sensors mechanically vibrate at a characteristic resonance frequency [**2.104**-**2.106**]. In this instance, the piezoelectric transduction is similar to that for the magnetoelastic sensor and both of the techniques are used for biomass monitoring, see **Table 2.5**. The advantage of the magnetostrictive platform is the capability of doing remote and wireless measurements [**2.104**-**2.106**]. However, the magnetoelastic sensor drawbacks for biomass monitoring are listed as follows:

- All the magnetoelastic sensors reported in the literature for bacterial biofilm monitoring / disruption are biosensors involving specific immunosensors (complex antibody / antigen) [**2.104**-**2.106**]. In this instance, biosensors are not really suitable for the very demanding working environment inherent to marine applications (very few of developed / commercialised biosensors have been reported in the seawater environment and applied in routine analysis) [**2.107**].
- Magnetoelastic sensors are composed of ribbons such as Metglas alloy 2826 (composition $Fe_{40}Ni_{40}P_{14}B_6$), which can potentially corrode in seawater (inducing another parameter to control in addition to the bacterial biofilm monitoring). Therefore, such sensors need to be pre-coated, *e.g.* with a $\approx$ 100 nm layer of gold (Au) applied by thermal evaporation [**2.104**].

- This technique for biofilm analysis has only recently been proposed, as such the reported high sensitivity needs to be interpreted with care (mass sensitivity of a magnetoelastic sensor with a fundamental frequency of ≈ 367 kHz comparable with the sensitivity of QCM having a fundamental frequency of 5 MHz) and detection limit (magnetoelastic biosensor: 10^2 cells mL^{-1}, bienzyme electrochemical biosensor: 6×10^2 cells mL^{-1}, electrochemical impedance immunobiosensor: 6×10^4 cells mL^{-1}) [**2.104**].

Overall, the limitations of magnetoelastic sensors mean that this type of transduction is not appropriate for the project. Work carried out using fibre-optic microprobes (in addition to electrochemical microelectrodes [**2.108**]) primarily focus on the study of biochemistry functions within the biofilm [**2.109**]. Usually, microelectrode tips are small, *i.e.* typically less than 20 µm tip diameter to coincide with the size of a bacterium, thus offering favourable conditions to measure the concentration distribution of various chemical species using interfacial changes in current or potential [**2.82**]. For instance, analyte-selective microelectrodes to detect O_2, pH, nitrate (NO_3^-) ions, S^{2-} ions, ammonium (NH_4^+) ions, nitrous oxide (N_2O), chlorine, CO_2 and glucose have been developed [**2.20**,**2.82**]. Although microelectrodes have enhanced characteristics (in **Table 2.4**) compared to macroelectrodes in terms of sensitivity, stability, selectivity, reproducibility, accuracy and response time, they are however fragile, difficult to manufacture, need calibration, and are subject to interferences and potential drifts of the signal, and also can be destructive to the biofilm. Nonetheless, microelectrodes have enabled to measure spatial and temporal concentration gradients to develop fundamental understanding of several physiological processes and structural heterogeneity within biofilms [**2.82**]. Although these investigations on biofilm biochemistry diverge from the biofilm monitoring on metallic surfaces (interfacial properties), they can provide insightful background to support the interpretations of the sensing response. These research works can include Beyenal *et al.* [**2.97**,**2.108**,**2.110**], Le Coq *et al.* [**2.111**] and Keirsse *et al.* [**2.112**], and are summarised in **Table 2.5**.

Optical

In operating systems, optical fibre devices that use the absorption and scattering of light by a biofilm have been integrated into pipe walls [**2.3**,**2.69**]. In practice, light is conducted by the sending fibre from underneath to the surface and scattered light by deposits is detected in return. Similarly, Beyenal *et al.* have developed a tapered fibre-optic microsensor using a 10 μm tip diameter to measure the distribution of backscattered light in biofilms [**2.20**]. The principle of detection (using optical fibre devices) has some limitations since the assessment of the deposit thickness depends on the intensity of back-scattered light, where optical losses across a deposit layer can affect the measures. Consequently, optical fibre devices are not suitable to investigate thick biofilms. These devices rely on the principle of differential turbidity measurement (DTM) readings between a turbidity meter in a clean and fouled environment. In this instance, the change measured between the devices operating in the control (clean) and turbid milieu is indicative of deposits. Similarly, apparatuses that measure heat transfer, pressure drop, and also biofouling thickness (described in **Section 2.4.4**) lie in the same category relevant to deposit measurements. Although these detection devices can be used to evaluate surface deterioration, their main drawback is probably their unability to provide essential information on the nature of fouling (inorganic such as clay / silt, corrosion and scale deposits, and also biological fouling) [**2.3**]. Likewise, the experimental configuration of Le Coq *et al.* [**2.111**] and Keirsse *et al.* [**2.112**] is such that the wave penetration depth only allows probing of the top surface (a few microns deep), which may also suggest some concerns to investigate thick biofilms. Another issue of relevance for bacterial biofilms adhered on a surface, is the requirement for the fibre-optic sensor tip to align measurements with the surface of the system investigated (exact position relative to the metal / biofilm interface) [**2.108**].

Although, an optical device has a number of advantages over an electrochemical system, for instance chemical inertness, immunity to electromagnetic noise, internal reference (thus, there is no need for reference and counter electrodes) and geometric versatility [**2.20**], its utilisation for the project is limited by the following reasons:

- Optical techniques using; for instance, a wavelength of light (λ = 660 nm) are subject to interference such as optical absorption in the UV-visible region of the spectrum due to the formation of algae, chlorophyll and coloured deposits [**2.113**,**2.114**], which makes interpretations difficult in order to explain the

significance of the sensing response with regard to marine bacterial growth and extent. However, adjacent spectroscopy methods to detect autofluorescence by biomolecules may support differentiation between organic and biological material in the deposit [**2.3**,**2.69**,**2.115**].

- The correlation between the core-cladding interface (in optical fibre devices) and the physical property of the optical sensor is not evident (evanescent field attenuation by refractive index and absorption and scattering modulation), where the core of the optical fibre represents a cylinder (usually plastic or glass) surrounded by a medium with a lower refractive index (cladding) for light to travel along the fibre's length [**2.91**].

Due to the discussed limitations of optical sensors (interferences, non-trivial correlation between the sensing response and biofilms), this type of transduction will not be considered further for the proposed work.

Piezoelectric

The QCM as discussed in **Table 2.5** [**2.96**,**2.116**,**2.117**] is a sensitive technique to study solid-solution interfaces based on a shift of the quartz crystal resonance frequency, which is typically a thin 300 μm circular plate oscillating at 5 MHz [**2.82**] due to interaction with solution components such as bacteria [**2.117**]. Interestingly for marine environment it was shown that QCM can be used as a gravimetric device since the mass sensitivity in a liquid environment can be comparable with that in air or vacuum [**2.117**]. The advantage of QCM devices relative to electrochemical sensors is the higher sensitivity ($\approx$ ng cm^{-2}). For instance, the mass of a single cell of *Escherichia coli* from QCM data was estimated to be 0.8 picograms [**2.117**]. This can correspond to the estimated detection limit for a standard QCM, *i.e.* 3×10^5 cells cm^{-2} [**2.82**,**2.118**]. However, the main disadvantage of this technique is probably the theory associated with the working principle of QCM. Indeed, the Sauerbrey's equation upon which QCM relies (relating the resonant frequency shift and the mass variation of the film deposited on a crystal surface) is valid only when the attached film is rigid (similar rigidity to that of the quartz [**2.82**]), thin and does not experience critical shear forces during crystal vibration. These considerations may underlie minimalist concepts for the reasons as follows:

- Biofilms are soft with potential time-dependent viscoelastic characteristics (accounting for the secretion of EPS matrix, pili / fimbriae) and their thickness can exceed the length of the shear wave (λ = 0.24 µm in pure water) that is radiated into the contacting fluid by the oscillating crystal surface, *i.e.* vibrational motion dampened with the distance from the surface [**2.82**,**2.96**,**2.116**,**2.117**]. Consequently, suspended cells (not directly attached to the surface) may not be affected by the shear wave and subsequently not detected [**2.82**].
- The response of QCM devices can potentially be influenced by hydraulic pressure or temperature and then lead to signal drifts (that could be misinterpreted as biomass changes) [**2.82**,**2.118**]. In flow-through devices maintained at constant temperature and pressure, additional non-linearity in the calibration curve due to biofilm mechanical behaviour (viscoelastic properties) have also been reported [**2.82**].
- Significantly, surface roughness (R_a), non-uniform mass sensitivity, chemical adsorption and longitudinal standing waves can also affect the frequency-dependent signal of the QCM [**2.82**].

Likewise, a few SAW microsensors have been proposed in the microbial biofilm research [**2.119**]. These sensors are wireless devices and usually consist of a SAW resonator (61 MHz) and a pair of conductive electrodes connected in the feedback circuit with a radio frequency amplifier [**2.119**]. They have already been employed in the bioanalytical research fields, for instance in the determination of urea, pancreatic lipase or total salt concentration in serum [**2.119**]. Based on this working principle, a novel system operating at ultra-high frequency (314.5 MHz) to minimise polarisation effects of the probe has been developed for the assessment of the microbial count in a biological culture [**2.119**]. It was shown that this device can offer better signal to noise ratio (after inoculation with *Escherichia coli*) than a piezoelectric quartz crystal sensor oscillating at 8 MHz, whereas the stability of the compared sensing techniques are equivalent. Similarly to the magnetoelastic sensors, the performance of the SAW microsensors for biofilm research need to be further addressed. Nevertheless, new QCM approaches have been developed such as piezoelectric-excited millimetre-sized cantilever (PEMC) sensors for bacterial biofilm monitoring (more sensitive and smaller) [**2.96**,**2.116**,**2.117**]. In addition, QCM can be combined with other electrochemical sensing approaches to form electrochemical quartz crystal microbalance (EQCM) devices [**2.117**]. Kreth *et al.* showed that real-time EQCM investigations can inform on the kinetics of biofilm formation [**2.120**]. Therefore, this technique may have potential interest to this multidisciplinary project as proposed in [**2.82**] the QCM technology with

temperature and pressure compensations could be a suitable detector for the presence of a biofilm. Nowadays, the piezoelectric devices are probably most relevant to the study of mechanical characteristics of biofilms, exploiting the non-linear relationship between the frequency dependent response and the mass of biofilm (biomass) attached [**2.82**]. In this instance, a mechatronic surface sensor (MSS) was developed by Pereira *et al.*, demonstrating that the MSS response was not only influenced by the presence but also on the viscoelastic properties of the adhered deposit [**2.121**]. Although further applications in biofilm research should emerge from piezoelectric sensors in the future, *i.e.* when advancements in the theory of soft films and transducer technology are made [**2.82**], piezoelectric techniques will not be considered within this project.

Electrochemical

Finally, the last sensing technique for consideration is an electrochemical sensing approach; [**2.96**,**2.108**,**2.122**-**2.126**] in **Table 2.5**, for the following reasons:

- It is a mature technique for bacterial biofilm monitoring [**2.20**].
- It may enable a more comprehensible correlation with bacterial biofilm formation on a metal surface (mass transport and interfacial changes discussed in **Section 2.6.5**).
- It has been employed to monitor variables that assess damage to the metal and it helps to determine the mechanism of attack in MIC [**2.82**].

Among the electrochemical techniques for biofilm sensing, the biosensors (using bio-receptors) used by Basu *et al.* [**2.123**] and Spiller *et al.* [**2.124**] are not suitable for this current project (for the same reasons as the magnetoelastic sensors). Likewise, electrochemical microsensors using a small tip diameter, *e.g.* Beyenal *et al.* [**2.108**], are not appropriate for this study (see the discussion on fibre-optic microprobes). In addition, open circuit potential (OCP) and electrochemical noise (EN) methods can be used as indicators for microbial activity, *e.g.* microbially influenced ennoblement of OCP on SS [**2.127**]. In the OCP technique, the potential difference between a metal probe and a reference electrode is measured, whereas the fluctuations in potential or current are monitored using EN at OCP. However, these techniques are qualitative, usually difficult to interpret without corroborative assessment (statistical evaluation and interpretation of the signal noise spectra for EN) and do not provide a direct correlation with the presence of a biofilm on a metallic surface [**2.118**]. Small changes in

electrochemical variables can be monitored when a biofilm forms on a metal surface and usually these changes can be indicative of biofilm induced surface processes [**2.82**]. In this instance, techniques used to investigate MIC primary focus on metabolic products (used as characteristic detectable substances to detect the occurrence of a particular organism) and not necessarily on the biofilm that can potentially be responsible for a corrosion process [**2.118**]. Dual-cells (two galvanically coupled electrodes separated by a selectively-permeable membrane but also connected by a continuous and constant flow of electrolyte through the cells) have been the first proposed method to study MIC [**2.128**]. In this configuration, a zero resistance ammeter can measure the modification of current flowing through the electrodes between a biotic and a sterile environments, *i.e.* one cell in the presence of microorganism while the other is sterile [**2.128**,**2.129**]. Overall, electrochemical techniques to study MIC concern specific laboratory scale experiments that should provide insight into more complex real systems.

Similarly, commercialised on-line electrochemical sensors using electrical polarisation methods, such as the BIoGEORGE and the BioX, are utilised for monitoring of biofilm and biocorrosion, and also the effectiveness of biocide dosing strategies within marine piping systems [**2.3**,**2.67**,**2.130**-**2.132**]. Biofilm formation and development on the sensing element of electrochemical sensors can be associated with the measured galvanic current between a SS pipe and an iron (Fe) anode (BioX) or with the change in current flowing between two SS, *e.g.* UNS S30400 or UNS S31600, or Ti electrodes (BIoGEORGE) [**2.2**,**2.67**,**2.128**]. Likewise, Bressel *et al.* [**2.96**] performed cyclic voltammetry (CV) used as a corroborative technique (in addition to confocal microscopy) for the QCM microsensor to study microbial biofilms. This work has outlined a detailed description of a series of electrochemical processes (**Section 2.6.5.3**), which can occur when a biofilm develops onto a noble surface. The RDE used by Herbert-Guillou *et al.* [**2.122**] (see **Section 2.4.4.4** for a description of the working principle) consists in an electrochemical method based on mass transport modification [**2.128**]. This well-established technique for biofilm sensing / thickness assessment (using changes in the steady-state current of cathodically polarised electrodes) has already been tested inside piping systems [**2.122**], thus will not be considered for this current study.

However, the main concern with polarisation methods is the application of high negative and positive potentials, *e.g.* −1.000 and +1.000 V *vs*. a reference potential, which can modify the biological growth environment [**2.82**] (discussed in **Section 2.6.6.2** for the Au surface). In this instance, it was shown that cathodic polarisation can interfere with the bacterial growth process and direct-current (dc) can affect the biofilm structure, thus suggesting that polarisation techniques are debatable for monitoring undisturbed biofilms [**2.133**,**2.134**]. Likewise, it was demonstrated that biofilm established on a cathodically polarised platinum (Pt) wire can expand, whereas an overall contraction was observed when the wire was anodic [**2.135**]. This was explained by changes in pH in the vicinity of the electrodes (polarised at ± 1.300 V with a current of 50 μA, thus corresponding to a current density of 3.1 mA cm^{-2}), *i.e.* anodic oxidation of H_2O favouring acid conditions (**Equation 2.21**) and cathodic reduction of H_2O producing hydroxyl (OH^-) ions (**Equation 2.22**) [**2.135**].

$$2H_2O \rightarrow 4H^+ + O_2 + 4e^- \quad (2.21)$$

$$2H_2O + 2e^- \rightarrow H_2 + 2OH^- \quad (2.22)$$

More precisely, bacterial cells can be influenced by external excitations greater than potential differences across biological membranes (+0.140 to +0.200 V potential drops for a 10 nm distance across the thickness of the cell membrane), which play a major role in biological metabolic and physiological processes [**2.136**]. Hence, applying high-intensity fields to the cells, *i.e.* in the kilovolt-per-centimetre range or superior to this potential window, can disturb the delicate cellular electrical equilibria and cause membrane perturbations routinely used in electroporation [**2.137**].

Conversely, small electrical perturbations (± 10 mV_{rms}) applied to biofilm systems are reported not to affect the activity and the number of sessile bacteria within a biofilm [**2.82**] (detailed in **Section 2.6.6**). Based on this concept, the impedimetric sensor developed by Oliver *et al.* [**2.125**,**2.126**] has been used for pathogenic bacterial biofilm sensing. Recently, Bayoudh *et al.* discussed, for the first time, the use of electrochemical impedance spectroscopy (EIS) within a flow chamber to detect bacterial adhesion [**2.55**]. The results in [**2.55**,**2.125**,**2.126**], although informative of an interfacial change in impedance over time, did not fully address the electrochemical reaction occurring at the interface in addition to the causes of this reaction. Similarly, recent studies have proposed that the interfacial capacitance can be sensitive to the bacterial adhesion and development on electrode surfaces, thus monitoring the initial and mature stages of biofilm growth [**2.138**-**2.140**].

2.6.4.3 Justification of the biofilm sensing strategy adopted

As mentioned in [**2.118**], the analysis in **Section 2.6.4.2** highlights that a high number of analytical detection methods can potentially be used for bacterial biofilm monitoring, whereas the suitability of these techniques in complex operating systems usually restricts the number of candidates for feasible methods. Also, most of online biofilm monitoring techniques (except bioluminescence signals generated by an enzymatic reaction within biological metabolisms) rely on passive responses (that are detected and subsequently processed for engineering purposes) to input signals transmitted to metal surfaces, where the presence of a biofilm can modify the investigated surface and its environment [**2.118**]. In the scope of research, monitoring biofilms is essential since it can help understand fundamental processes within biofilms, which may ultimately support the development of tailor-made devices suitable for operating engineering systems. As pointed out by Lewandowski [**2.118**] and Roßteuscher [**2.141**], the challenge is, however, to be able to understand the significance of the measured signal with regard to features describing biofilms and to clearly identify the parameters of relevance to gain knowledge in the biofilm field. These considerations should help industrials define both a consensus on appropriate biofilm monitoring techniques and threshold levels of interference for particular industrial systems, and also provide insight in biocide concentrations required to control biofilms in-service [**2.3**].

As a result of the analysis in **Section 2.6.4.2**, EIS has been selected as an electrochemical method capable of monitoring interfacial and mass transport changes on and nearby metallic surfaces without perturbing the environmental growth (non-destructive) [**2.82**], see **Section 2.6.5** for a detailed description of the EIS technique. Although electrochemical sensors using electrical polarisation have been adopted by industrials, they do not provide a full description of the biofouling mechanisms involved, when similarly (according to evidence addressed in the published literature [**2.133**-**2.137**]) they can disturb the biofilm, *i.e.* the measurand for this current project. In this instance, laboratory scale experiments using EIS (and CV to support the use of the EIS technique) in a well-controlled environment, *e.g.* continuous culture flow cell systems, may provide an important step in better understanding of the sensing response significance, which is to date not fully addressed in the published literature [**2.55**,**2.125**,**2.126**,**2.138**-**2.140**]. Subsequently, strong knowledge of the interfacial properties inherent to biofilm will help define a protocol for biofilm disruption to ultimately deploy a suitable *in situ* dosing strategy when required [**2.3**]. Therefore, this

current study represents a unique opportunity to develop a clear understanding between the marine bacterial biofilm (formation and development, and also disruption) on a metal surface and the corresponding electrochemical response (using the EIS technique scarcely used in the field of ocean sensing [**2.93**]), which overall would support the design, development and future deployment of non-invasive, robust, reliable (accurate and reproducible), intelligent and low maintenance biofilm monitoring devices for marine environment (concerns that were pointed out by Busalmen *et al.* [**2.133**] and Denuault [**2.93**]). As stated by Nivens *et al.* [**2.81**], a single monitoring technique may not be sufficient for a full understanding of the engineering system. Consequently, microscopy techniques described in **Sections 2.6.3** and **2.7** will be required to corroborate the EIS response in addition to the knowledge gained from the published literature, *e.g.* bacterial biofilm colonisation model on a metal surface developed by Bressel *et al.* [**2.96**] in **Section 2.6.5.3**, which was supported by confocal microscopy analyses plus cyclovoltammetry measurements.

2.6.5 Biofilm sensing using EIS

2.6.5.1 An electrochemical technique for biofilm sensing

The EIS working principle relies on the application of a small sinusoidal perturbation (potential or current) to an electrochemical cell, *i.e.* a potentiostat or an electrochemical interface, together with a frequency response analyser (FRA) or spectrum analyser, which covers a wide range of frequencies, typically in the order of 0.01 to 100,000 Hz [**2.142**,**2.143**]. The potentiostat connections consist of a counter electrode that provides current to the electrochemical cell, a working electrode, which allows measurement of the current through the cell and a reference electrode for potential measurements [**2.142**,**2.143**]. One important characteristic of the potentiostat is its ability to maintain dc conditions on the working electrode interface while the FRA is performing the impedance analysis. A dc steady-state current can be applied to the electrochemical cell (under load conditions) or an experiment can be run at the OCP to investigate the interfacial impedance [**2.142**-**2.144**]. The multi-frequency excitation allows: (*i*) the measurement of several electrochemical reactions, which occur at different rates and (*ii*) the study of electrochemical interfacial properties [**2.142**-**2.144**]. In EIS, by defining the relation between applied stimulus and output quantity, the system impedance and the phase angle (the phase difference between measured current and applied potential) are obtained [**2.142**-**2.144**]. The concept of impedance, originally introduced to describe the response of a system composed of capacitances, resistances and inductances, was extended to electrochemical systems, where

numerous processes contribute to the relation between the current and potential [**2.142**-**2.145**]. Thus, based on impedance and phase angle measurements, it is possible to evaluate several processes such as charge transfer (including determination of electron transfer rate), film conductivity, double layer and redox capacitance and charge carriers diffusion coefficients [**2.145**]. Rapid physical phenomena in **Figure 2.17** tend to occur at higher frequencies while slow physical mechanisms are observed at lower frequencies (*i.e.* the frequency is inversely proportional to the period). Charge transfer and ionic diffusion (**Figure 2.17**) are the most prominent physical phenomena likely to occur within the working range acceptable to make suitable electrochemical measurements [**2.142**-**2.145**].

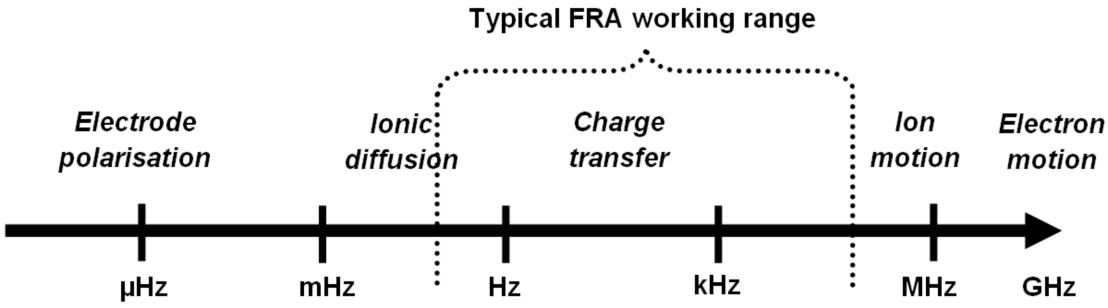

Figure 2.17. Physical frequency dependent phenomena in electrochemistry.

In practice, EIS has been used in the characterisation of biomaterial-functionalised electrodes and biocatalytic transformations / electrochemical reactions [**2.146**-**2.149**]. It has also been proven to be very effective in mechanistic studies of a wide range of corrosion phenomena involving MIC [**2.129**]. In addition, EIS provides repeatable and accurate measurements of surface conditions such as adsorption and desorption processes, charge transfer rate and redox-active centres determinations at the electrode surfaces, as well as information about biofilm behaviours (interactions of biological molecules to provide information such as surface loading, binding constants, rate constants and surface reactivity) [**2.53**,**2.146**,**2.149**], see **Section 2.6.5.3**.

2.6.5.2 Analysis of the EIS response

Analysis of the electrochemical impedance data can be achieved using different measurement models, specifically either equivalent circuit (EC) or mathematical models [**2.142**-**2.145**]. The application of EC models is based on the analogy between an electrochemical cell and an RLC electrical circuit of resistors, inductors, and capacitors [**2.142**]. The similarity of the electrical double layer to a parallel plate capacitor (Helmholtz model and non-faradaic processes) and the interfacial resistance to charge transfer (faradaic processes) to a resistance can lead to a representation of an electrode / electrolyte interface by a resistor, *e.g.* charge transfer resistance (R_{ct}) and a capacitor, *e.g.* double layer capacitance (C_{dl}) in parallel [**2.142**-**2.147**]. The current that flows through this electrochemical interface is conducted by the ions in solution [**2.142**]. The resistive effect on their migration (movement of charge species due to a potential gradient [**2.42**,**2.150**]) can be represented by the resistance of solution (R_s). Likewise, diffusion of species from the bulk solution (infinite diffusion due to the movement of species down a concentration gradient [**2.42**,**2.150**]) to the electrode surface can be defined as the Warburg impedance (Z_W) [**2.142**-**2.147**]. The difference in phase between current and potential is the result of the introduction of capacitive elements in a circuit. Because of this, a common representation for impedance in systems composed by resistors and capacitors is through a phase diagram in which the impedance shows a real (resistive) and an imaginary (capacitive) component [**2.142**-**2.147**]. This phase diagram representing the impedance in the complex plane, *i.e.* the Nyquist diagram, is also associated with a graph, which shows the modulus of the impedance and the phase shift, *i.e.* the Bode diagram, for different frequencies [**2.142**-**2.147**].

Both the Nyquist and Bode diagrams are used (**Figure 2.18**) to interpret the EIS data [**2.151**]. The Bode plot roughly indicates the number of elements / components constituting the total impedance of the related electrochemical cell while the Nyquist plots reveals their possible behaviour [**2.151**].

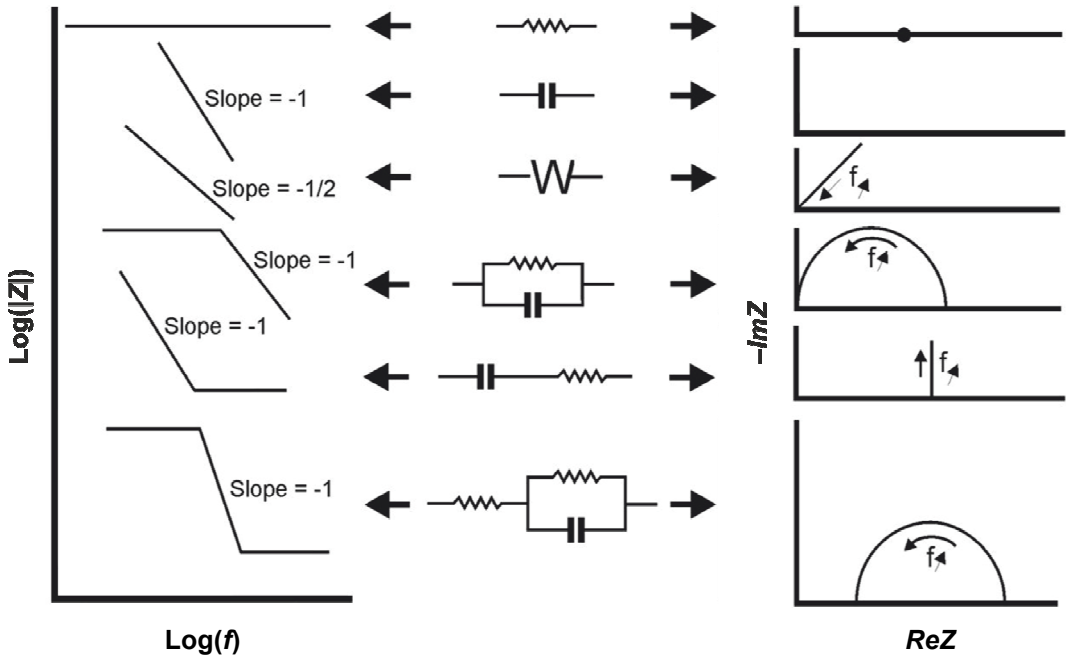

Figure 2.18. Interpretations of Nyquist and Bode diagrams using EC models, adapted from [**2.151**].

Usually, an EC model is used to fit the EIS data (utilising readily available programs such as EQUIVCRT by Boukamp or proprietary software [**2.142**,**2.152**]) in order to quantity the interface [**2.152**]. However, if care is not taken in the overall approach of representing the data and modelling the electrochemical cell, then errors and uncertainties can occur especially for the inexperienced user [**2.148**,**2.153**].

2.6.5.3 Schematic of bacterial biofilm for electrochemical detection

The presence of a bacterial biofilm in **Figure 2.19** can modify the electrochemical properties and the mass transport at and / or near the working electrode interface, thus ultimately altering the interfacial impedance response [**2.96**]. The mass transport induced by biological activity mostly accounts for diffusion (along concentration gradients) and migration (due to the electric field across the biofilm) processes [**2.42**,**2.53**,**2.150**]. Whereas, convection (the movement of species resulting from a mechanical force) although present results from the environmental hydrodynamic regimes (by stirring, agitating the electrolyte solution or flowing it through the electrochemical cell) [**2.42**,**2.150**].

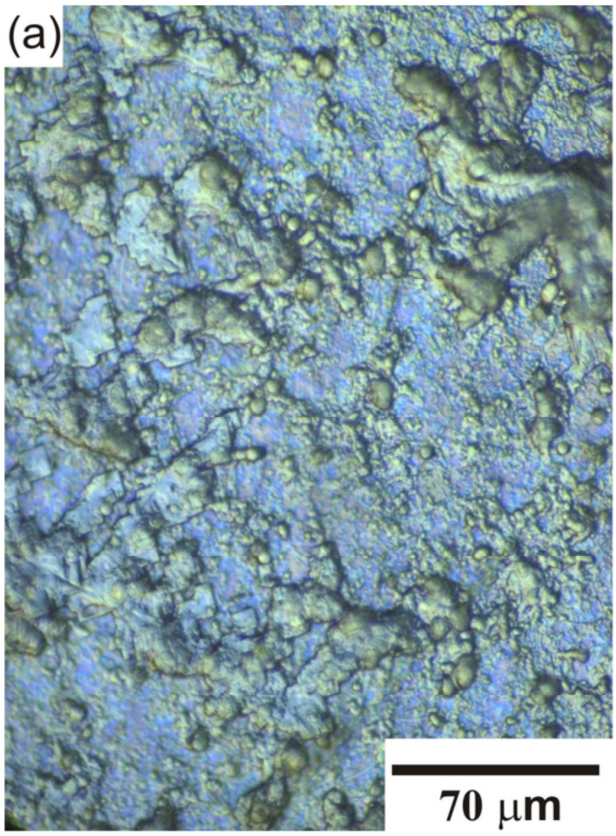

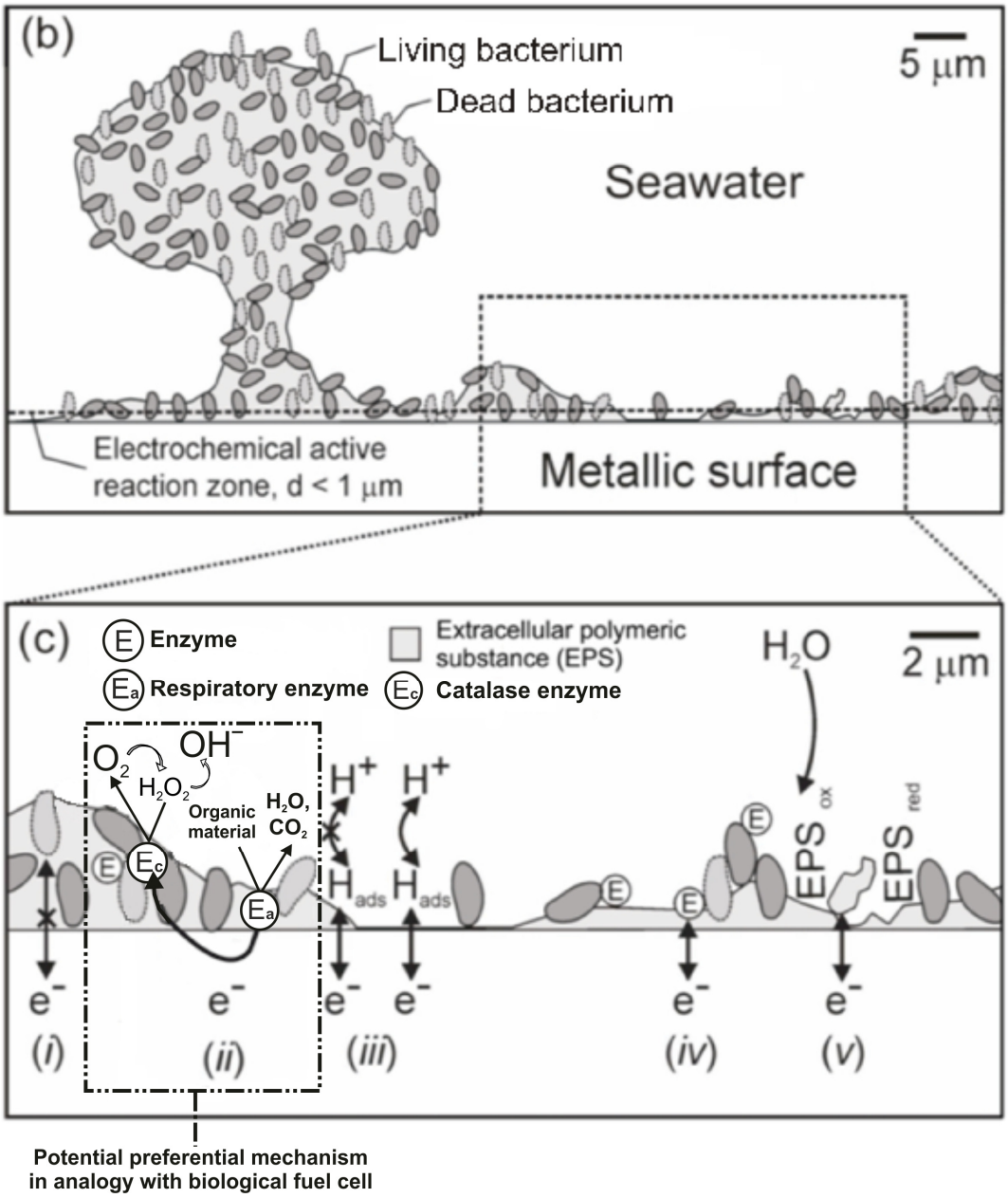

Figure 2.19. Bacterial biofilm colonisation: **(a)** a Ti surface immersed for 1 week in natural seawater at the NOC pontoon, **(b)** an overview of typical biofilm morphology and **(c)** processes detected by electrochemical measurements, **(b)** and **(c)** adapted from [**2.96**].

Figure 2.19(a) shows a bacterial biofilm attached to a metallic surface. Distinct bacterial clusters are clearly seen in the presence of EPS matrix. **Figure 2.19(b)** schematically illustrates that bacterial biofilms consist of a heterogeneous structure of EPS matrix and bacteria cells randomly distributed on a metallic surface [**2.1**], thus inducing different detectable interfacial responses [**2.96**]. A more detailed illustration of the metal / seawater interface in **Figure 2.19(c)** shows a range of competing electrochemical processes [**2.96**]. Overall, direct electron transfer to redox-active centres deep within the EPS matrix is generally not observed, see **Figure 2.19(c)*(i)***.

However, where the ORR is the prevailing reaction in neutral / alkaline conditions [**2.42**], mechanisms of enhancement of the ORR by enzymatic processes have been proposed [**2.59**]. They are associated with enzymatic catalysis by aerobic microorganisms with the decomposition of an intermediate reactant (H_2O_2 in **Equation 2.14**) resulting in an autocatalytic cycle through which the reduction current density is increased [**2.59**], see **Section 2.4.3.2**. The exact nature of the ORR mechanism still remains to be determined. One pathway in analogy with biological fuel cell [**2.50**-**2.54**] (see **Figure 2.12** in **Section 2.4.3.2**) is presented. The biofilm system on a metallic surface in **Figure 2.19(c)*(ii)*** can correspond to a galvanic cell composed of an anode and a cathode. In this instance, the anodic process is governed by the oxidation of soluble organic material via respiratory enzymes with H_2O and CO_2 the products of the anodic reaction. In contrast, an enhanced ORR by enzymatic activities at the outer biofilm region is prevalent at the cathode. Similarly, sessile bacteria can play a pivotal role in the charge exchange with a metallic surface, where the charge transfer occurs to or from the bacterium surface [**2.55**]. Whereas, hydrogen adsorption and reduction in **Figure 2.19(c)*(iii)*** has been reported to be inhibited by the colonization of the surface. After biocide treatments, results indicate a mechanism based on direct electron transfer to enzymes or other reductive agents entrapped in the EPS matrix may act as another pathway, see **Figure 2.19(c)*(iv)***. Also, bacterial EPS has been shown to be redox-active in **Figure 2.19(c)*(v)*** by allowing reductive and oxidative processes to occur.

Importantly, a suitable metallic surface utilised as an electrochemical probe operating in a well-defined seawater environment should be able to detect the predominant electrochemical reaction among the interfacial competing processes in **Figure 2.19**, see **Chapter 5**. For instance, it may be predictable that a noble metal electrode immersed a few days (to study initial microbial fouling) in continuous aerated (non polluted) seawater would probably undergo the overall reaction in **Figure 2.19(c)*(ii)***, *i.e.* the enzymatic enhanced ORR.

2.6.6 Au working electrode

2.6.6.1 Suitability of Au as a candidate-working electrode

The surface of the working electrode can be regarded as the sensing element of the sensor, see **Table 2.5**. Therefore, the selection of a suitable material is crucial for this PhD project. Metallic surfaces for marine applications are subject to corrosion mainly due to the saline properties of seawater, *e.g.* presence of aggressive Cl^- species. Likewise, metallic structures may suffer from surface degradation, resulting in the formation of corrosion products (hydrated oxides) deposit on the surface [**2.44**]. Subsequently, the corrosion plus hydrolysis reactions can lead to oxide fouling of the metallic surface, see **Section 2.4.3.2**. Ideally, the sensing element hence needs to be inert (to ensure stability of the sensing area and reliability of the electrochemical sensor) in order to monitor marine bacterial biofilms [**2.93**]. The electrochemical performances of passive metal surfaces, *e.g.* Cu alloys, SS and Ti (**Sections 2.4.2** and **2.4.3**) in seawater [**2.17**,**2.37**] or specific studies of MIC, *e.g.* SRB on mild steels (**Section 2.1**), have already been detailed in the literature [**2.1**,**2.2**]. Similarly, Ti and SS are currently used by the commercialised / patented electrochemical probes (**Section 2.6.4.2**) for marine biofouling and biocorrosion, and also biocide effectiveness assessment [**2.2**,**2.3**,**2.67**,**2.128**,**2.130**-**2.132**]. Consequently, this PhD thesis will not address the use of corrosion resistant metallic (passive oxide film) surfaces in **Table 2.2**.

Conversely, Au has been selected using **Tables 2.2** and **2.6** (where in addition to the galvanic series for alloys in **Table 2.2**, the electrochemical series in **Table 2.6** is informative on the corrosion properties of pure metals) as a good candidate since it is a noble metal, where (interestingly for noble surfaces) a linear relationship associated with the biofilm thickness has been proposed, thus suggesting a potential application for monitoring the growth of biological films [**2.133**]. In addition, Au substrates are commonly used in microbiology for their bio-compatibility properties [**2.134**,**2.154**,**2.155**]. The published research literature also mentions its use for biofilm sensing plus chloride media (seawater) applications using EIS [**2.96**,**2.99**,**2.123**,**2.125**,**2.126**,**2.138**,**2.156**]. Moreover, Au has often been utilised in a range of microtechnologies, *e.g.* multi / interdigitated microelectrode arrays [**2.93**,**2.154**,**2.155**,**2.157**-**2.159**]. In contrast to Au, Pt (**Tables 2.2** and **2.6**) has been proposed to minimise electrode oxidation processes in seawater when applying high positive potentials [**2.160**]. However, this consideration (for the anodic reaction) is

unlikely to affect the monitoring (for a non-polarised electrode) of a predominant cathodic reaction, *i.e.* the ORR in seawater [**2.42**]. An alternative low cost candidate to Au may be silver (Ag) but its electrochemical behaviour in seawater, *i.e.* electroformation of insoluble silver chloride (AgCl) [**2.161**-**2.163**], and its reported antifouling properties [**2.164**-**2.166**] would need to be addressed for this PhD project.

Table 2.6. Electrochemical series. Standard conditions (25 °C; 1 atm; H_2O; unit activities; metals present in their standard states), adapted from [**2.42**].

Electrode reaction:			E^0_e / V (SHE)
$Au^{3+} + 3e^-$	⇅	Au	+1.50
$O_2 + 4H^+ + 4e^-$	⇅	$2H_2O$	+1.23
$Pt^{2+} + 2e^-$	⇅	Pt	+1.20
$Pd^{2+} + 2e^-$	⇅	Pd	+0.91
$Ag^+ + e^-$	⇅	Ag	+0.80
$Cu^+ + e^-$	⇅	Cu	+0.52
$O_2 + 2H_2O^+ + 4e^-$	⇅	$4OH^-$	+0.40
$Cu^{2+} + 2e^-$	⇅	Cu	+0.34
$2H^+ + 2e^-$	⇅	H_2	+0.00
$Pb^{2+} + 2e^-$	⇅	Pb	−0.13
$Sn^{2+} + 2e^-$	⇅	Sn	−0.14
$Mo^{3+} + 3e^-$	⇅	Mo	−0.20
$Ni^{2+} + 2e^-$	⇅	Ni	−0.23
$Co^{2+} + 2e^-$	⇅	Co	−0.28
$Cd^{2+} + 2e^-$	⇅	Cd	−0.40
$Fe^{2+} + 2e^-$	⇅	Fe	−0.44
$Cr^{3+} + 3e^-$	⇅	Cr	−0.74
$Zn^{2+} + 2e^-$	⇅	Zn	−0.76
$Cr^{2+} + 2e^-$	⇅	Cr	−0.90
$V^{2+} + 2e^-$	⇅	V	−1.18
$Mn^{2+} + 2e^-$	⇅	Mn	−1.18
$Ti^{2+} + 2e^-$	⇅	Ti	−1.63
$Al^{3+} + 3e^-$	⇅	Al	−1.66
$Ti^{3+} + 3e^-$	⇅	Ti	−1.80
$U^{3+} + 3e^-$	⇅	U	−1.80
$Mg^{2+} + 2e^-$	⇅	Mg	−2.36
$Na^+ + e^-$	⇅	Na	−2.71
$Ca^{2+} + 2e^-$	⇅	Ca	−2.87
$K^+ + e^-$	⇅	K	−2.92
$Li^+ + e^-$	⇅	Li	−3.04

Overall, biofouling is dependent on the material surface [**2.2**,**2.3**], thus it is predictable that the fouling properties of Au would be different from that of other candidates, *e.g.* on passive alloys, where the formation of oxide films play an important role in the reaction kinetics [**2.2**,**2.17**]. For instance, it has been reported that biofilms of *Pseudoalteromonas fluorescens* were more extensive on Al plates than on either brass or Cu pipes (attributed to the toxic effects of Cu towards macrofouling in **Section 2.4.3.2**) [**2.3**]. Likewise, more biofouling was observed on Ti heat exchanger tubes than on brass pipes [**2.3**]. This suggests that corroborative tests (on various metallic

surfaces) and safety engineering factors would be necessary in-service to define the thresholds of interference for biofouling discussed in **Section 2.4.4.1**.

2.6.6.2 Preliminary concerns for Au prior testing

A major concern of biofilms on metals is the dependence of surface topography, where biofilm mass is usually reported to be more pronounced on rough surfaces (and conversely less important on smooth metals) [**2.3**]. This can be explained by a size criterion (individual cells are smaller than crevices) combined with a topographic-induced behaviour of biofilms against adverse flow conditions (irregular rough surfaces are suitable niches for bacterial cells exposed to high shear stress) [**2.3**,**2.27**]. Surface heterogeneities can have significant effects during the early stages of biofilm formation and development, however this influence becomes negligible when biofilm thickness exceeds the surface roughness (although the accumulation process can facilitate the anchoring of biofilms to rough surfaces) [**2.3**]. However, perfectly smooth industrial surfaces correspond to an idealistic concept (surface roughness depends on the manufacturing process) where no engineering surfaces (smooth or rough) can escape fouling [**2.1**-**2.3**].

With regard to these considerations, the Au electrodes will need to be ground and polished (to a final smooth surface roughness, R_a) before use (detailed in **Chapter 4**) to ensure controllability of the finished surfaces. Ideally, a further step of electropolishing, *e.g.* in an acid solution, to remove material from the metallic workpiece would be necessary for enhanced quality of the Au surface. However, this electrochemical step after the mechanical grinding and polishing method may be inappropriate in order to offer greater flexibility in material preparation for this PhD project. Alternatively, a suitable potential waveform (potential square wave by holding the potential at +0.800 V *vs.* a Cu anode for 1 s, whereas a potential switch to −0.450 V *vs*. a Cu anode is used for 12 s to monitor DO) can be used to electrochemically recondition the sensing surface, where electrodes continuously operating in seawater can lose their catalytic properties activity and / or be poisoned by heavy metals, *e.g.* electroplating at the potential for the ORR [**2.93**,**2.160**,**2.167**,**2.168**]. This represents a cleaning protocol that may be addressed for in service conditions.

Nevertheless, polarisation methods would be rejected for laboratory experiments (in this current study) to preserve the biological environment since dc excitations can affect biofilm and the bacterial metabolism, see **Section 2.6.4.2**. In this instance, it has been reported that the growth of bacterial cells attached to Au surface in sodium chloride (NaCl) media was primary affected under positive polarisation, *i.e.* an exponential growth was observed following an applied potential of +0.500 V *vs.* Ag/AgCl. Conversely, bacterial biofilm formation impediment was noticed after an excitation of +0.800 V *vs.* Ag/AgCl [**2.136**]. The condition of "unperturbed growth" (corresponding to potentials below +0.140 to +0.200 V across a 10 nm thick biological membrane [**2.136**], see **Section 2.6.4.2**) can coincide with the potential of zero charge (PZC) of Au in NaCl media ranging from zero to +0.070 V *vs.* Ag/AgCl-KCl saturated [**2.169**].

2.6.7 EC model at the Au / seawater interface

As the interfacial behaviour of an electrochemical reaction is analogous to an electrical circuit consisting for example of a specific combination of resistors and capacitors, the electrochemical systems (spectra) under study can be described in terms of their EC model [**2.141**].

In contrast to physical models established for polymer / organic coatings, *e.g.* waterborne protective coatings for marine applications [**2.28**,**2.142**,**2.170**-**2.174**] or porous metallic oxide coatings (alumina - Al_2O_3) [**2.175**], no consensus has been commonly agreed for reported EC models for biofilmed metallic surfaces [**2.55**,**2.125**,**2.126**,**2.129**,**2.138**,**2.139**,**2.156**,**2.176**-**2.182**] since the interfacial properties of a biofilmed metal surface (*e.g.* a biofilmed Au electrode) are complex. In analogy with MIC, there may be no universal model for biofilm on a metal surface but rather specific, well-defined mechanisms inherent to biofilmed metallic surfaces [**2.3**,**2.183**-**2.186**].

To represent the interfacial current exchange in the presence of diffusion, for instance inherent to the occurrence of a thin microbial film on the Au surface, all the interfaces using the Au electrode in alkaline media can be modelled (for the current study in **Section 5.13**) using an EC with mixed kinetic and charge control [**2.142**,**2.187**]. In this instance, the Randles model (R_s in series with a parallel branch with a C_{dl} and R_{ct} in series with W in **Figure 2.20**), which is indicative of a typical interface in electrochemistry, can be utilised [**2.99**,**2.142**-**2.147**,**2.153**].

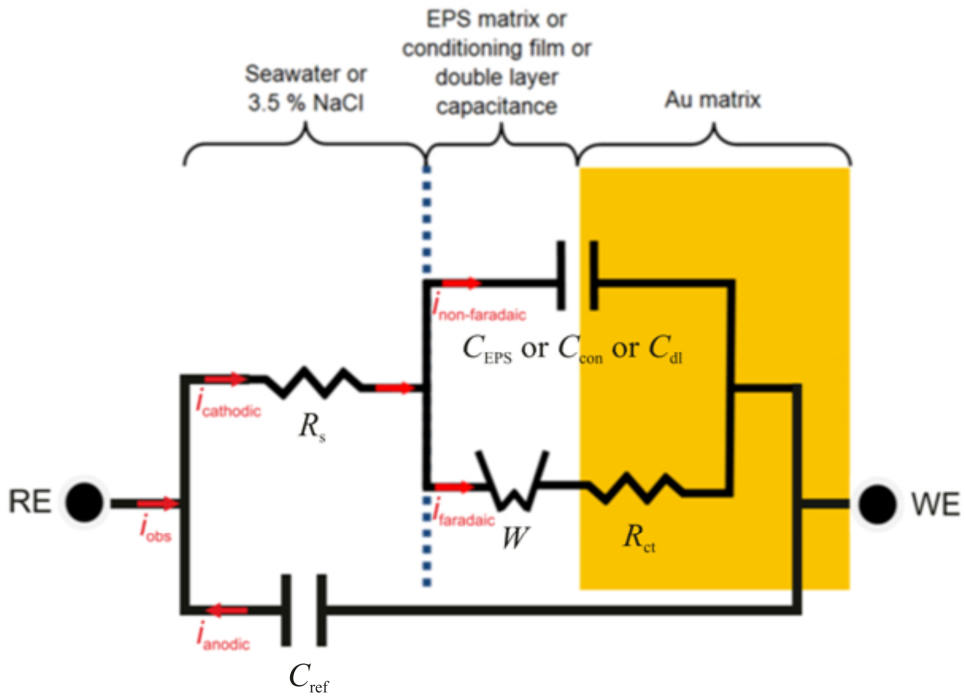

Figure 2.20. Schematic of the EC model for Au in a chloride medium.

The diffusion component (W) or Warburg impedance (Z_W) in series with the charge transfer resistance (R_{ct}) in **Figure 2.20** can be classified as faradaic processes (charge is transferred across the interface) with $i_{faradaic}$. Conversely, the capacitance component (C_{EPS} or C_{con} or C_{dl}) corresponds to charging effects (transient currents can flow without charge transfer), thus indicative of non-faradaic processes with $i_{non\text{-}faradaic}$ [**2.145**,**2.187**]. Overall, the observed current (i_{obs}) across an electrochemical interface (**Figure 2.20**) is given by [**2.42**,**2.142**]:

$$i_{obs} + i_{anodic} = i_{cathodic} \tag{2.23}$$

where at OCP, the zero current ($i_{obs} = 0$) corresponds to $|i_{anodic}| = |i_{cathodic}|$, thus showing the importance of the anodic branch (**Figure 2.20**) with the presence of an external reference capacitance (C_{ref}) having minimum effects (typical small magnitude values of *circa* zF) and whose values have been reported not to vary with biofilm growth on a Au surface [**2.156**,**2.178**].

In addition (see **Figure 2.20**):

$$i_{cathodic} = i_{faradaic} + i_{non\text{-}faradaic} \tag{2.24}$$

For a microdisk electrode, the Newman formula can be used to evaluate R_s (resistance of seawater or 3.5 % NaCl in **Figure 2.20**):

$$R_s = \frac{1}{4\sigma r} \tag{2.25}$$

where σ is the electrical conductivity of the electrolyte and r the radius of the microelectrode [**2.177**]. Whereas C_{EPS} is the capacitance of the EPS matrix inherent to the biofilm (**Figure 2.20**), C_{con} represents the capacitive component for the conditioning layer, and also C_{dl} is the double layer capacitance at the Au surface. C_{EPS}, C_{con} and C_{dl} in reality do not behave ideally as capacitors (due to a non-homogeneity – linked to surface roughness [**2.188**], distribution of reaction rates [**2.189**], varying thickness or composition [**2.190**] and / or non-uniform current distribution [**2.191**,**2.192**]) and consequently a constant phase element (CPE) [**2.142**,**2.145**] is used to model these components. The impedance of a CPE may be defined by:

$$Z_{CPE} = \frac{1}{Y_0(j\omega)^n} \tag{2.26}$$

where Y_0 has the numerical value of the admittance (1/|*Z*|) at ω = 1 rad s^{-1}. The factor n usually lies between 0.5 and 1. When n = 1, the CPE describes an ideal capacitance, where Y_0 is the capacitance value. For 0.5 < n < 1, the CPE represents a distribution of dielectric relaxation times in frequency space. When n = 0.5, the CPE stands for a Warburg impedance with diffusion character [**2.142**,**2.145**]. Although the impedance relations of a capacitor and CPE are similar, Y_0 does not have units of capacitance and relatively small deviations of n from 1 can lead to significant computational errors. Brug *et al.* have developed an expression of the effective capacitance (C_{eff}) of a CPE measured by EIS, which can be used for a normal distribution (*e.g.* with the occurrence of a thin biofilmed surface) assuming a minimum variation of the local resistivity [**2.193**,**2.194**]. This expression is preferred over the Hsu and Mansfeld's Equation with the presence of a characteristic frequency component at which the maximum in the imaginary part of the impedance occurs [**2.193**].

In this instance, **Equation 2.27** can be utilised to transform the CPE values into an effective capacitance [**2.193**,**2.194**] and R_f represents the film resistance:

$$C_{eff} = (R_f)^{(1-n)/n} Y_0^{1/n} \quad (2.27)$$

This will be used for the quantitative analysis of the EIS measurements in **Section 5.13.2**. The effective capacitance represents an average value of the interfacial capacitance (with the limitations associated with the concept of normal distribution), thus does not provide quantifiable information on the deconvoluted C_{EPS}, C_{con} and C_{dl} values in **Section 5.13.2**. Likewise, R_{ct} in **Figure 2.20** is the charge transfer resistance, which indirectly relates to the baseline ORR in alkaline media and / or the enzymatic enhanced cathodic reduction involving electron transfer at the Au / biofilm interface, or redox-active centre within the EPS matrix / seawater interface [**2.142**,**2.143**].

$$R_{ct} = \frac{RT}{zFj_{OCP}} \quad (2.28)$$

where R is the molar gas constant, T the temperature, z the number of electrons, F the Faraday constant and j_{OCP} the current density at OCP. Interestingly, R_f in **Equation 2.27** can correspond to R_{ct} (**Equation 2.28**) for a thin biofilm, see **Section 5.13.2**.

Similarly, the diffusion component (W) is representative of a competing process to the interfacial charge transfer, where electro-active species from the bulk solution (***e.g.*** DO) can diffuse across the Au interface [**2.142**-**2.147**].

In order to assess the quality of the EC fit *vs.* the EIS raw data, a number of standard procedures have been developed using software for EIS data analysis. These procedures rely on the following [**2.195**]:

- the χ^2 error has to be suitably low ($\chi^2 \leq 10^{-4}$),
- and the errors associated with each element have to range between 0 and 5 %.

2.7 Biofilm microscopy techniques

This section reviews potential corroborative microscopy techniques, which can be used to characterise the bacterial biofilm formed on a metallic surface. In this instance, Surman *et al.* [**2.89**] and more recently Denkhaus *et al.* [**2.20**] have published an extensive comparative study of microscope techniques for biofilm visualisation. Interestingly, flow cell systems (**Section 3.2.4.2**) have been reported to be convenient for examination of sessile microorganisms since they can be adapted for microscopic assessment under a wide range of operating conditions [**2.80**]. Similarly, a number of surface and interfacial spectroscopic characterising techniques (**Table 2.3**) such as infrared (-IR) and attenuated total reflection infrared (ATR-IR), Fourier transform infrared (-FTIR), nuclear magnetic resonance (NMR), photoacoustic, reflectance and X-ray analysis have the capability to be utilised in bacterial biofilm studies. A detailed description of these techniques for bacterial biofilm analysis is beyond the scope of this report and can be found in detail elsewhere [**2.20**,**2.80**,**2.118**]. Overall, these techniques can provide important information on the biochemical environment inherent to biofilm and are possibly too advanced for the immediate requirement to visually assess the bacterial attachment on Au surfaces. However, this does not exclude their potential use (*e.g.* spectroscopy techniques) for bacterial biofilm characterisation in the future.

2.7.1 Potential competitive microscopy techniques

SEM has been used for biofilm visualisation and characterisation of sessile bacteria in biofouling / biocorrosion studies for many years [**2.2**,**2.94**,**2.196**]. The main reasons were good image contrast, high depth of field and high magnification associated with the SEM technique. Conversely, a major SEM drawback is the sample preparation prior to biofilm examination using ultra-high vacuum: fixation, desalination when required, dehydration and critical point or freeze-drying [**2.2**]. This inevitably leads to induced artefacts and changes in structure (distorted and / or flattened biofilm), which make precise bacterial biofilm characterisation difficult [**2.94**,**2.141**,**2.197**,**2.198**]. Even the use of low vacuum (0.1 – 50 Torr) environmental scanning electron microscope (ESEM) can create problems due to the necessity to remove excess water on the surface, which may obscure underlying biological features and result in the collapse of the biofilm structure [**2.2**,**2.94**,**2.199**]. Alternatively, techniques such as transmission electron microscopy (TEM) for very high resolution imaging can be used for biofilm attachment on Au surface [**2.199**,**2.200**]. With TEM, high resolution

quantitative analysis of internal cross sections of individual bacteria and the corresponding overall biofilm can be assessed. Similar to SEM, TEM is costly requiring time-consuming sample preparation, where bacterial biofilms can be sensitive to harsh treatments on surfaces, *e.g.* mechanical sectioning of the biofilmed surface [**2.201**] and dehydration processes that can have a shrinking effect on the biofilm [**2.89**].

Alternative techniques, such as AFM capable of providing detailed structural information on a nanoscale [**2.2**,**2.202**], have been utilised to study naturally occurring biofilms on SS surfaces, *i.e.* selective metal-ion binding properties of EPS in the biocorrosion process [**2.2**,**2.203**]. Other applications for AFM involve adhesion load measurements of biofilms and force-distance plots [**2.203**]. Likewise, surface conditioning steps and bacteria adhesion were characterised on Au surfaces using AFM [**2.196**]. The results were in good agreement with fundamental studies on biofilm utilising AFM, which revealed the importance of chemical and topographic surface properties during the early stages of biofilm growth and extent, for instance on biofilmed Au surfaces [**2.204**]. However, AFM is potentially a destructive technique employing a cantilever tip with limited performances in aqueous solution [**2.196**,**2.202**], thus limiting its use to characterise biofilms in their native environment. In this instance, bacterial biofilm observations using the AFM tapping or acoustic resonant mode (to maintain an intermittent contact between the tip and the surface) may be a great alternative to minimise mechanical deformation on the biofilmed surface [**2.196**]. More recently, Flores *et al.* published a review on the future of the invaluable, high resolution AFM to address promising combination (of AFM) into hybrid devices, therefore suggesting greater routes for more complete description of biofilm processes and structures [**2.205**].

Nevertheless, the competing scanning ion conductance microscopy (SICM) has been developed to provide images of intact living cells with high resolution performance comparable to SEM and AFM [**2.206**-**2.211**]. In addition, SICM can provide 3D images, information on the dynamics and the structure of cell membranes [**2.207**,**2.211**], and also quantitative cell volume measurements [**2.210**]. Recently, scanning electrochemical microscopy (SECM), which relies on measurement of faradaic current changes during the displacement of a microelectrode [**2.212**,**2.213**], has been used to determine the spatial distribution of metals in microbial biofilms. SECM can enable non-invasive imaging of electro-active surface components at a microscale [**2.214**]. Similarly, Liu *et al.* uniquely reported the monitoring of redox activity of individual living cells using SECM [**2.215**], thus allowing further studies on the redox processes

inherent to cells [**2.216**-**2.219**]. However, SECM investigations of biofilm remain scarce [**2.220**].

Similarly, transmission light microscopy techniques could provide useful biofilm structure information such as biofilm thickness, *i.e.* biofilm thickness measurements of around ≈ 30 – 40 μm using a light microscope [**2.221**]. However, its use is limited to transparent surfaces such as glass and Perspex [**2.198**,**2.221**], thus is not applicable for metallic surfaces. In addition, the diffraction limit of light is a major drawback for transmission light microscopes [**2.141**].

More recently, episcopic differential interference contrast (EDIC) microscopy linked with epifluorescence (EF) microscopy, which is both more rapid and cheaper than most of the advanced competing microscopy candidates [**2.89**,**2.198**], has been developed by Prof Keevil, now working in the SBS at the UoS [**2.94**]. The EDIC version used by Keevil *et al.* consists of a reconfigured Nikon Labophot-2 microscope that combines a normal epifluorescence attachment with EDIC illumination above the specimen stage, thus allowing biofilm examination on opaque surfaces (in contrast with the conventional DIC microscope using transmitted light) [**2.94**,**2.170**,**2.198**,**2.222**]. Likewise, the path of light beam is influenced by the characteristics of the sample (shape, thickness and composition variability) [**2.198**]. The emerging EDIC microscopy can be used for film topography, growth features and biofilm viability, settling cue densities and composition on opaque surfaces such as metals [**2.94**,**2.170**]. In this instance, it has been successfully employed to visualise biofilm communities on metallic surfaces, *i.e.* Cu substrata [**2.41**,**2.94**,**2.198**]. In addition, the EDIC microscope has enabled a quantitative analysis of biofilm viability and formation on natural product based antifouling system [**2.170**].

Similar to the DIC technique, the Hoffman modulation contrast microscope can image biofilms with a high contrast resolution using opposite phase gradients to opposite intensities in the image, as a consequence the resulting image appears 3D with bright and dark features against a grey background [**2.89**]. Although the magnification and the quantitative analysis are limited, this cheap microscopy technique has been proven suitable to assess dense areas of the biofilm [**2.89**].

The advent of CLSM / SCLM rendered with 3D images has led to a new concept of bacterial biofilms (**Section 2.6.3**), *i.e.* the occurrence of complex 3D heterogeneous biofilms (aerobic films in waste water plants) containing interstitial voids and channels between these voids, thus facilitating convective mass transport and favouring higher

concentration of constituents (used for cellular metabolites) in void areas [**2.2**,**2.77**]. Importantly, this conceptual model of biofilm would have never emerged without the combined use of microelectrode measurements (**Section 2.6.4**), which has helped to address that the effective diffusion coefficient in aerobic biofilms was influenced by the flow regime and the biofilm structure, and also that mass transport by convection was predominant through the pores of the biofilm [**2.2**,**2.80**]. In practice, the CLSM technique can be used to obtain high resolution optical images at different depth, *i.e.* optical cross sectional images in the *x*-*y* plane captured along the *z*-direction for spatial imaging, with subsequent 3D reconstructions [**2.9**,**2.80**,**2.197**,**2.223**]. The high resolution of confocal microscopy in **Figure 2.21(a)** is achieved by reducing out of focus light using an aperture (detection pinhole), which is positioned (in the light path) in an optically conjugated plane to the point light source [**2.94**,**2.141**,**2.223**]. Consequently, the light in dotted gray line is obstructed by the detection pinhole, see **Figure 2.21(a)**.

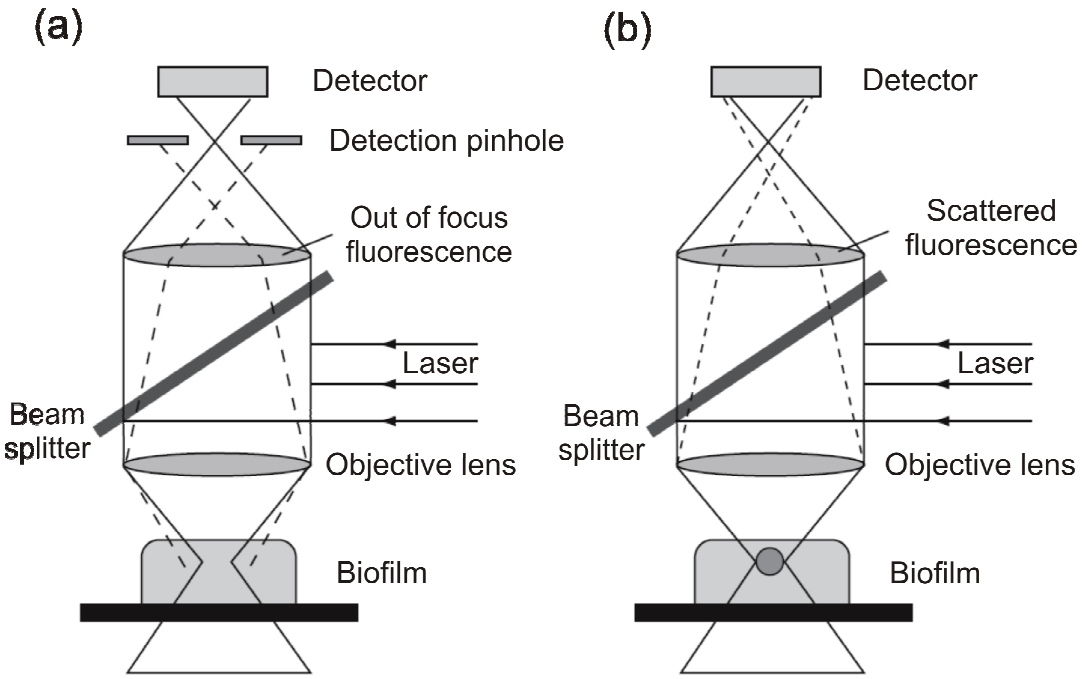

Figure 2.21. Comparison of **(a)** CLSM and **(b)** multi-photon fluorescence optics, adapted from [**2.94**,**2.223**].

As light reaching the detector is limited in the CLSM technique, high power lasers utilising argon (Ar) at λ = 488 and 568 nm or more expensive argon-krypton (Ar-Kr) at λ = 488, 568 and 647 nm sources can be used to excite a fluorophore in biological systems [**2.94**]. This in turn can cause irradiation below the planes where the

specimen is scanned, thus potentially generating photo-bleaching, -damages, cytotoxicity (toxicity towards the cells), and also photo-toxicity (leading to the selective death of the cells expressing the corresponding fluorophore) effects [**2.94**]. This has led to the development of the multi-photon microscope in **Figure 2.21(b)**, where out of focus light is limited (absence of detection pinhole) using a stream of strongly focused subpicosecond pulses of laser light in the red or near IR excitations (690 – 1,000 nm), therefore minimising all the photo-induced detrimental effects reported for the CLSM, *e.g.* photo-damages [**2.94**,**2.224**-**2.227**]. In this instance, the multi-photon in **Figure 2.21(b)** providing a better signal to noise ratio (whereas the filter range that can be used is limited) compared to the standard confocal system is suitable for the examination of thick films (from 50 – 100 μm towards 400 – 500 μm), living cells and UV sensitive surfaces [**2.94**,**2.224**-**2.227**].

Alternatively, advanced fluorescent methods (listed as follows) have been developed for measurements of exchange rates, molecular diffusion and / or structure:

- fluorescent recovery after photo-bleaching (FRAP) used to measure diffusion of fluorophores into a photo-bleached area,
- Förster resonance energy transfer (FRET) utilised to assess the radiation-less energy transfer between two fluorophores,
- fluorescence lifetime imaging microscopy (FLIM), where changes in fluorescence intensity of markers can be detected as well as energy states of fluorophores when combined with FRET, and
- fluorescence correlation spectroscopy (FCS) to enhance the resolution of CLSM images and for instance study molecular dynamics in living cells [**2.141**].

Moreover, correlative light electron microscopy (CLEM) and stimulated emission depletion (STED) microscopy can be used for imaging at the nanoscale [**2.141**]. In the CLEM technique, this is achieved utilising correlation between electron microscopic and CLSM images, but it requires time-consuming computation. In contrast with transmission light microscopy, the STED technique is an advanced fluorescent method, where a sample region under investigation is photo-bleached, therefore allowing microscopic assessment below the diffraction limit [**2.141**]. In addition, optical coherence tomography (OCT) has been used for biofilm characterisation, where non-invasive measurements of backscattered light from the biofilmed surface are performed, thus leading to evaluation of biofilm density and structure at the micrometer scale [**2.141**]. However, the applicability of CLEM, STED microscopy and OCT for

biofilm examination needs to be further addressed [**2.141**]. Besides investigations on the structure and architecture of biofilms, the use of magnetic resonance imaging (MRI) has been reported for the two-dimensional description of flow phenomenon at the biofilm / bulk solution interface [**2.228**]. In MRI, biofilm images are selectively computed with relaxation time weighted NMR technique, *i.e.* exploiting the difference in NMR relaxation time values of H_2O molecules arising from changes in mobility between the inner and outer biofilm layers [**2.228**,**2.229**]. Nevertheless, the MRI system is expensive and unhandy, where its use outside laboratories is not appropriate [**2.118**].

Recently, scanning transmission X-ray microscopy (STXM) using a near-edge X-ray absorption fine structure (NEXAFS) spectroscopy has been applied to study fully hydrated biological materials, thus being a competing technique to the ESEM, EDIC and CLSM [**2.20**,**2.141**,**2.230**]. The STXM technique relies on:

- soft X-rays to penetrate water,
- the presence of suitable analytical core edges in the soft X-ray region,
- reduced radiation damage compared to that caused by electron beam techniques such as SEM [**2.20**,**2.200**].

STXM is capable of mapping biofilmed metal (*e.g.* Au) surfaces [**2.20**,**2.200**,**2.231**]. In addition, there is no need for the addition of reflective, absorptive, or fluorescent probes and markers that may introduce artefacts or complicate the interpretation [**2.200**]. However, STXM limitations involve the following:

- requirement for very thin samples (< 200 nm equivalent thickness of dry organic components and < 5 μm of water for wet conditions),
- use of fragile silicon nitride windows,
- potential absorption saturation distortion of analysis in thick regions of a specimen,
- necessity for data acquisition without undue radiation damage, and
- suitability of the model compounds relative to biofilm material [**2.200**].

2.7.2 Preferred microscopy methodology

From **Section 2.7.1**, STXM, SEM and TEM are limited compared to CLSM and EDIC with regard to surface preparation (harsh treatments required for SEM and TEM, whereas encapsulation of biofilm in a wet cell can significantly reduce the applicability of the STXM technique for the current project). Likewise, other microscopy studies for biofilm examination have reported that TEM can introduce a significant higher number of artefacts than confocal microscopic systems [**2.89**]. Whereas the presence of the cantilever tip for the AFM can potentially cause damages to the biofilm [**2.2**,**2.202**,**2.203**], the reported more convenient SICM has shown promise in imaging living cells [**2.207**,**2.211**]. However, the use of a micropipette tip relative to the sample surface (for instance in the SICM technique) requires accurate and precise positions of the sensing probe [**2.2**,**2.82**], thus is a source of inconvenience to map an engineering surface. Similarly, the SECM technology needs to be fully addressed for bacterial biofilm studies [**2.220**]. Overall, the scanning probe methods such AFM, SICM and SECM suitable for imaging localised surface processes may find alternative routes of application in the field of MIC [**2.82**,**2.220**]. In contrast, both CLSM and EDIC, which do not involve a tip / surface interaction, can allow greater penetration and are non-invasive, and also non-destructive 3D imaging of biofilm [**2.94**,**2.200**]. For instance, the *z*-scan detection of the EDIC/EF with good depth of field is ideal for examination of biofilms of less than 10 μm in thickness [**2.94**], where the more affordable Hoffman modulation contrast microscope may only be limited to qualitative analyses of dense areas of the biofilm [**2.89**]. Similarly, EDIC/EF enables the detection of high extinction factor values (point at which a bacterial species experiences an abrupt change in density or number because of an important parameter such as habitat loss), can increase image contrast and brightness and define clear spatial relationships, thus resulting in good quality images [**2.94**]. Furthermore, the CLSM and EDIC techniques are appropriate for viewing biofilms on opaque materials, *e.g.* Au surfaces [**2.94**].

Ideally, a corroborative microscopic assessment for biofilm studies should be able to provide detailed information of biofilm spatial distribution and composition as demonstrated by Lawrence *et al.* using STXM, CLSM and TEM [**2.200**], Gamby *et al.* utilising SEM, AFM and spectroscopy methods [**2.196**], and also Yuan *et al.* with fluorescent microscopy, SEM and XPS investigations [**2.182**]. However, this valuable approach appears to be unrealistic for the current project, thus emphasising the necessity to select one suitable microscopy technique as opposed to a combination of potential microscopy candidates. As CLSM has proven to be capable of revolutionising

the field of biofilm using microelectrodes [**2.2**,**2.77**] and can provide quantitative information of biological material (**Section 2.8.1**), it will be used for the proposed project to corroborate the electrochemical sensing strategy. Not only CLSM is a valuable quantitative microscopy technique, but it has also been described as the most versatile, applicable and suitable technology for biofilm investigation [**2.27**,**2.230**]. In addition, the CLSM technique has allowed the development of action mechanisms of biocide [**2.2**], therefore relevant to address the effectiveness of a biofilm inhibition strategy (**Section 2.9**).

2.8 Quantification of bacterial biofilm

2.8.1 Microscope image processing

No single microscopy technique is completely satisfactory for quantitative evaluation of bacterial biofilms, *i.e.* each has a number of limitations and disadvantages that limit a full understanding of the microbial interactions on metallic surfaces [**2.82**]. For example, EDIC/EF provides only partial quantitative data (examinations and analyses of fluorophore-labelled cells with resulting images appearing 3D [**2.94**]), whereas optical cross-sections and 3D reconstruction of biofilm imaging can be obtained using CLSM, thus facilitating quantitative microscope image processing [**2.89**]. With the use of fluorophores (two nucleic acid stains, the green-fluorescent SYTO® 9 stain and the red-fluorescent propidium iodide stain) live / alive (live bacteria unable to reproduce in nutrient medium [**2.232**]) and dead bacterial cells can be clearly identified [**2.41**,**2.94**,**2.170**,**2.198**,**2.232**]. As a standalone, SYTO® 9 stain labels both live and dead bacteria [**2.41**,**2.232**]. Conversely, the propidium iodide can only stain bacteria with damaged membranes, therefore reducing the SYTO® 9 green fluorescence when both stains are utilised [**2.41**,**2.232**]. Overall, intact bacterial cells fluoresce green, whereas aging bacteria (with damaged membranes) appear red [**2.170**,**2.232**]. **Figure 2.22** illustrates the typical fluorescence emission spectra (excitation at 470 nm) of live and dead bacterial cells using a molecular probe technique Live / Dead® *Bac*Light™ (from Invitrogen), which contains the SYTO® 9 and propidium iodide stains [**2.232**].

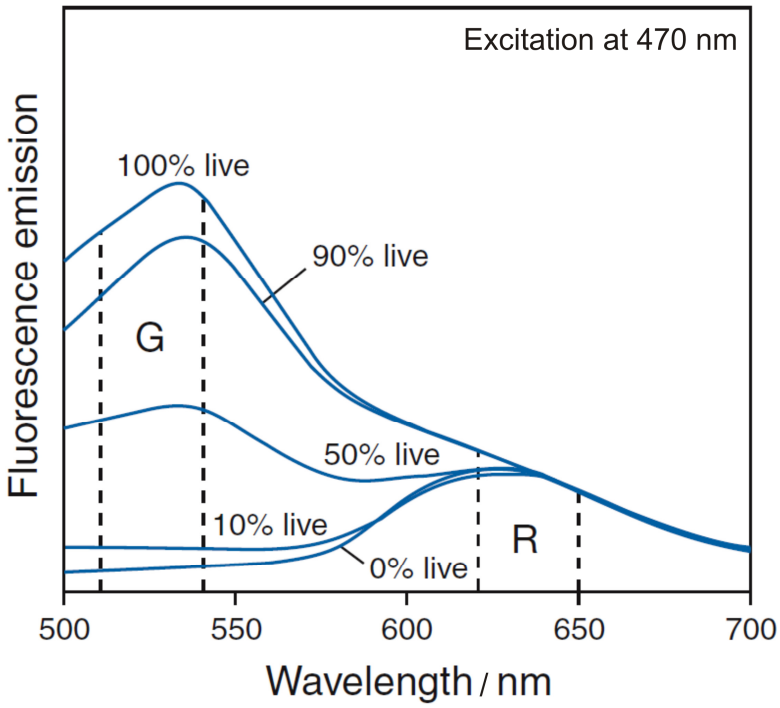

Figure 2.22. Typical viability analysis responses for bacterial cells, adapted from [**2.232**].

Using the Live / Dead® *Bac*Light™ bacterial viability kit (**Figure 2.22**), live bacteria fluoresce green (**G**) and dead bacteria are red (**R**) fluorescent. After exposure to isopropanol (effective reagent in killing bacteria), a fluorescence spectral shift is observed from **G** to **R** in **Figure 2.22** as the percentage of live bacteria is significantly reduced [**2.232**]. However, it may be difficult under certain circumstances, for instance in analogy with the acridine orange stain, to differentiate dead cells (with degraded single stranded DNA) from rapidly growing cells (with a high RNA content) because they can both fluoresce in the red part of the spectrum (around $\lambda \approx 620$ nm) [**2.94**]. Importantly, the *Bac*Light™ fluorescence-based assay has been successfully used on a variety of bacteria (*e.g. Escherichia coli* and *Pseudoalteromonas* species) [**2.67**,**2.232**-**2.234**] and biofilms [**2.41**,**2.67**,**2.170**,**2.232**-**2.234**].

Similarly, a qualitative assessment of the extent of biofouling and bacterial viability on metallic surfaces can be achieved using percentage coverage methods [**2.41**,**2.79**,**2.170**,**2.233**,**2.234**]. This can be performed utilising suitable image analysis thresholding of green / red (8-bit colour) and subsequent measurement of the corresponding fouled areas on binary (black and white) pictures with ImageJ (Java-based image processing and analysis software inspired by NIH-Image developed at the National Institutes of Health [**2.66**,**2.77**,**2.234**,**2.235**]), where black features are

indicative of biofilm (cells clusters) with surrounding white channels and / or bare surfaces [**2.66**,**2.77**], see **Section 5.12**. Alternatively, AxioVision software from Imaging Associates, Thame, UK can be used for percentage coverage analyses [**2.236**].

Specifically, recent research carried out using CLSM and 3D visualisation methods have resulted in quantitative evaluation of the microbial biofilm structures cultivated in a controlled medium [**2.237**], where previously it was limited to qualitative analyses, two dimensions observation or required operator-defined calibration [**2.238**]. Detailed maps of biofilm structures and composition have also been created with the combination of multi-microscopy analysis including STXM, CLSM and TEM [**2.200**]. This has led research to focus on powerful 3D image processing software utilising cross-sectional images obtained from microscopy techniques such as CLSM [**2.237**-**2.239**], with reported studies to describe in three-dimensions the biofilm heterogeneity, size and morphology of the biomass using CLSM images [**2.237**]. In this instance, the aim of these studies was to further develop existing software including:

- COMSTAT, *i.e.* program developed by the Department of Microbiology, Technical University of Denmark, written as a MATLAB script for quantification of 3D biofilm structures by analysing stacks of images acquired with a CLSM [**2.240**].
- Image Structure Analyser (ISA), *i.e.* program developed by the Biofilm Structure and Function Research Group, Montana State University, which can calculate textural entropy, homogeneity, energy, contrast, correlation, area porosity (measures the ratio of the void area to the total image), run lengths, diffusion distances and fractal dimension from digital biofilm images [**2.241**,**2.242**].

Whereas COMSTAT and ISA are used for quantitative analysis of single-channel CLSM data at a time, the PHobia Laser scanning microscopy Imaging Processor (PHLIP) is now a new image quantification package for multi-channel CLSM data, thus favouring processing of large quantities of data [**2.243**]. For example, the PHLIP program was used to describe the dynamic spatial and temporal separation of bacteria, diatoms, organic and inorganic matter during the changes incurred from bacteria- to diatom-dominated biofilms [**2.243**].

Overall, these studies have allowed a more comprehensive description of these biofilm-related parameters in three dimensions [**2.237**-**2.239**]. However, the two main factors limiting the full automation of quantitative analysis of CLSM biofilmed images are: (*i*) the large computational requirements inherent to 3D data processing and (*ii*) the lack of suitable mathematical solutions and the corresponding computational package [**2.238**,**2.239**].

2.8.2 Quantification using electrochemical techniques

2.8.2.1 Biofilm thickness assessment using the charge transfer resistance

The R_{ct} parameter has been proposed in the literature to quantify δ_b on a noble metal surface, where there is a debate over the validity of the derived parameters [**2.133**]. In most cases, a ferricyanide / ferrocyanide redox couple is used to maintain stable reaction kinetics at the interface during biofilm growth [**2.125**,**2.126**,**2.244**], thus allowing assessment of film thicknesses [**2.133**]. However, both the non-faradaic (capacitance) and faradaic (resistance) components of the EIS response play an important dual role in this current study (**Section 2.6.7**), therefore it is not appropriate when using a naturally occurring and electro-active bacterial biofilm (**Section 2.4.3.2**).

2.8.2.2 Evaluation of bacterial sessile population using the interfacial capacitance

Similar to **Section 2.8.2.1**, previous studies have shown that the interfacial capacitance can be informative of bacterial attachment (early and mature stages of biofilm formation and extent) on sensor surface [**2.67**,**2.123**,**2.139**,**2.156**,**2.178**], and in particular the changes in capacitance can be related to a magnitude coverage of sessile bacteria [**2.123**].

In analogy with electrochemical investigations of protein adsorption on metallic surfaces [**2.245**-**2.250**], the amount of adsorbed biological material and / or organic material Γ_{ADS} and the corresponding surface charge density Q_{ADS} can be associated in **Equation 2.29** [**2.249**]:

$$\Gamma_{ADS} = \frac{Q_{ADS}}{zF} \tag{2.29}$$

Likewise, the relationship between the corresponding effective capacitance C_{eff} (either C_{con} or C_{EPS} for an adsorbed conditioning layer or adhered biofilm, respectively) and Γ_{ADS} is defined in **Equation 2.30** [**2.249**]:

$$C_{\text{eff}} = \frac{F^2 \Gamma_{\text{ADS}}}{4RT} \tag{2.30}$$

As a result, the combination of **Equations 2.29** and **2.30** leads to **Equation 2.31**, thus showing the relationship between the calculated Q_{ADS} value and the experimental C_{eff} parameter:

$$Q_{\text{ADS}} = \frac{4zRT}{F} C_{\text{eff}} \tag{2.31}$$

Using the reported total surface charge (≈ 10^{-12} C per bacterium) involved in current exchange during adhesion [**2.55**], **Equation 2.31** can be exploited to address a relationship of the surface charge density of sessile cells to their adhered population (after subtraction of the abiotic response) using **Equation 2.32**, see **Section 5.13.3**.

$$\text{Number of cells} \cong \frac{Q_{\text{ADS(biotic)}} - Q_{\text{ADS(abiotic)}}}{10^{-12}} \tag{2.32}$$

where $Q_{\text{ADS(abiotic)}}$ and $Q_{\text{ADS(biotic)}}$ are the surface charge density for the abiotic and biotic media, respectively. However, the hypotheses herein can provide limited information of the overall interfacial adsorption process:

- There is no deconvolution between the biofilm and the conditioning film, *i.e.* between C_{EPS} and C_{con} for the calculation in **Equations 2.29** to **2.32** and as mentioned in analogy with protein adsorption on metallic surfaces [**2.245**-**2.250**].
- The z value is herein assumed to be 4 (for consistence with **Figure 2.14**), where the validity of **Equations 2.29** to **2.31** has been addressed for z = 1 in the studies on protein adsorption [**2.245**-**2.250**].
- The total surface charge (≈ 10^{-12} C per bacterium) is used as a general accepted value for a sessile bacterium [**2.55**], where the exact value for a

Pseudoalteromonas bacterium adhered on a Au surface may show substantial differences.

Although the significance of these assumptions needs to be further assessed, it will be used, together with the evaluation of bacterial sessile population utilising *ex situ* confocal microscopy studies, for comparison in **Section 5.13.3**. Likewise, it was shown that the charge transfer resistance was dependent of the surface charge density of adsorbed organic material, where a decrease of the R_{ct} parameter can be explained by favoured charge transfer between strongly adsorbed organic material (increase amount of organic matter) and the electrode [**2.245**,**2.249**]. Overall, this represents a corroborative quantitative assessment of bacterial biofilm for this current study (see **Section 5.13.3**).

2.8.3 Summary of the review of biofilm quantification

Sections 2.8.1 and **2.8.2** have outlined the unique approach for the current study (see **Chapter 5**) combining an electrochemical parameter (surface charge density) and the analysis of CLSM images (surface coverage and estimated number of adhered bacteria) to gain insight into biofilm quantification for online monitoring systems. The relevance of this strategy was reinforced by Keevil, who has argued that biofilm sensors are limited by calibration using suitable microscopy techniques to truly assess and quantify industrial biofouling [**2.94**].

2.9 Review of biofilm inhibition

Among the industrial cleaning procedures available for marine piping systems, such as marine heat exchangers, chemical and non-chemical methods are frequently used [**2.2**,**2.3**,**2.21**,**2.69**].

For the chemical techniques, routine oxidizing agents using chlorine, result in environmental concerns (chronic toxicity problems) and biofilm resistance increase (the reported concentration of antibiotic required to completely disrupt a biofilm on a metal is about 500 – 5,000 times higher to that for killing the corresponding planktonic cells) [**2.3**,**2.5**,**2.21**,**2.137**,**2.251**-**2.253**]. Thanks to CLSM, more is now known on the action mechanisms of oxidizing biocides such as chlorine, chlorine dioxide and ozone, whereas the modes of action for organic and synthetic biocides (bactericide) are to date not well understood [**2.3**]. Many years of research using biocides on biofilmed metallic surfaces demonstrated that formaldehyde, glutaraldehyde, ammonium

didecyldimethyl chloride, isothiazolinone mixtures, dissolved ozone and sodium hypochlorite were more effective in killing planktonic cells rather than sessile bacteria [**2.2**], thus demonstrating their limitation for the proposed project. In addition, Mexel® 432 is one of the most adopted antifouling solutions with a longstanding experience in industrial plants (*e.g.* used in the Gaz de France's 800 MWe DK6 plant in Dunkirk "Dunkerque", northern France) and in marine ships (*e.g.* utilised onboard the French nuclear aircraft carrier Charles de Gaulles plus onboard three UK nuclear submarines) [**2.254**]. Injected on average with 5 ppm for a 30 min duration once per day, the Mexel® 432 is a mixture of aliphatic amine surfactants (emulsion), which adsorbs onto exposed metallic surfaces and forms a very thin protective layer [**2.254**,**2.255**]. This protective film can act as a corrosion inhibitor, scale dispersant and it can affect fresh- and saltwater mussels, and also barnacles. Overall, Mexel® 432 is a non-oxidant (minimum impact on the environment), tensioactive emulsion that is not sufficiently toxic to kill organisms but it retards population growth and settlement including bacteria colonies: SRB, thiosulfate reducing bacteria (TRB) and *Legionella* spp [**2.254**-**2.257**]. Because Mexel Industries S.A. holds a patent on the Mexel® 432 technology [**2.254**] (*i.e.* the exact compositon of the Mexel® 432 emulsion is protected by commercial confidentiality [**2.255**]), it will not be addressed in this thesis. Alternatively, the electrolysis of seawater generating chlorine and hypochlorous acid has already been proposed as an electrochemical antifouling method (relevant to in-service applications) [**2.258**].

Most of the non-chemical methods commonly used are mechanical ones, *i.e.* using trash racks, rakes, screens, sponge (batch) balls and brush systems [**2.5**,**2.21**]. The main drawback of these cleaning procedures is the associated frequent long downtime for offline treatments, the risk of partial ball blockage inside tubing (sponge rubber ball) and the unacceptability of the flow reversal using oscillating brushes (when costs of the sponge ball system are prohibitive) [**2.5**,**2.21**]. Other techniques such as thermal backwash (by raising the cooling water temperature) [**2.3**], non-thermal energy (using ultraviolet, gamma and laser irradiations) [**2.3**,**2.21**,**2.258**,**2.259**] and hydraulic methods (using high velocity $\approx$ 1 – 2 m s^{-1}) [**2.3**] are less common since their viability for in-service conditions needs to be further addressed. Although Brizzolara *et al.* have shown promising results in microfouling inhibition, *i.e.* up to 95 % over a 4 week duration, using acoustic pulsed devices operating at 17 kV with a frequency range of 0.01 – 1 MHz (thus protecting a 6 m long section of 16 mm diameter Ti heat exchanger tubes from microfouling), industrial applications of studies using applied physical stimuli (*e.g.* acoustic pulses generated by an electrical discharge) are still in their infancy [**2.5**,**2.260**].

In analogy, antimicrobial strategy against pathogenic biofilms is a major concern for health care applications, where the combined use of antibiotics and weak electrical currents [**2.135**,**2.137**,**2.252**] or equivalent radio frequency currents [**2.261**] or low-intensity ultrasound [**2.251**] has shown promise in enhancing the overall efficacy of routine antibiotics. A probable explanation arising for the greater performances of the antibiotics results in their ability to traverse outer and inner bacterial membranes, which are significantly reduced or suppressed using suitable stimuli (*e.g. circa* 10 mA cm^{-2} current density for 12 h [**2.252**] or rms current of 150 mA at 10 MHz, with a power output of 5 W for 24 h [**2.261**] or 500 kHz ultrasound at 10 mW cm^{-2} for 2 h [**2.251**]). However, these valuable effects against biofilms do not apply to all antibiotics and the overall applicability to industrial piping systems is not obvious. In addition, research on biofilm removal and disinfection has focused on the alternative use of enzyme (*e.g.* proteases used in pipelines) [**2.262**-**2.265**]. Nevertheless, not only the overall cost incurred for potential in-service conditions remains prohibitive [**2.262**], but also enzymes are highly sensitive to pH and temperature changes (*i.e.* denaturation of proteins) [**2.263**,**2.265**].

As the USA, *e.g.* US Environmental Protection Agency (US EPA) 1992 [**2.3**] and European countries, *e.g.* Biocidal Product Directive 98/8/CR [**2.132**,**2.263**], have introduce directives to reduce the discharge of organochlorines into the aquatic environment, attractive environmentally benign biocides that are efficient and effective against biofouling represent a good alternative. Whereas preliminary works using biological signals have focused on preventing biofilm growth and evolution (*i.e.* interference with the natural cell signalling mechanisms inherent to biofilm formation and development) [**2.55**,**2.253**], one suitable disruption approach would be the use of nitric oxide (NO) biofilm dispersal as a natural antifouling strategy to comply with marine environmental concerns and legislature. The formation of a biofilm is a dynamic process that integrates metabolic activities and exhibits developmental stages often resembling those of higher multicellular organisms [**2.1**]. Compounds that regulate key multicellular behavioural traits, for instance, those that coordinate biofilm detachment dispersal have emerged as novel and exciting targets for manipulation and control technologies [**2.26**,**2.67**,**2.265**]. In particular, bacteria in biofilms often undergo coordinated dispersal events and revert to a free-swimming planktonic phenotype [**2.235**].

Recent research at Southampton has discovered that biofilms undergo programmed detachment during the course of normal development and that this detachment is linked to the accumulation of reactive nitrogen species (RNS) within biofilms [**2.131**,**2.132**]. NO was identified as an important factor in the regulation of biofilm dispersal [**2.267**,**2.268**]. Exposure to low, non-toxic concentrations of NO (in the nanomolar range, 500 nM) was found to induce dispersal in *Pseudomonas aeruginosa* biofilms and increase the sensitivity of cells to various antimicrobial treatments. Importantly, the concentration of NO that induces dispersal is substantially below that which would be toxic to biofilms [**2.131**,**2.132**]. NO signalling therefore exhibits considerable potential as a low-dose, economically attractive and environmentally benign technology for the control of biofouling. At concentrations that triggered dispersal in *P. aeruginosa* biofilms, NO was also found to enhance cell motility, a phenomenon correlated with active dispersal. Subsequently, it has been demonstrated that NO is able to induce dispersal in a broad range of other biofilm-forming microorganisms and, importantly for these studies, also in complex communities of microorganisms on surfaces [**2.131**,**2.132**,**2.269**]. Recently, it was shown that combined treatments with NO (*e.g.* chlorine with NO) were more efficient in removing multi-species aquatic biofilms, up to 20-fold increase in biofilm removal compared to the conventional chlorine treatment, therefore suggesting novel inhibition strategies [**2.267**]. One way of generating NO is to use the NO donor sodium nitroprusside (SNP) [**2.232**]. In this instance, SNP is composed of sodium (Na^+) ion linked with nitroprusside anion via ionic interaction [**2.268**-**2.271**]. In aqueous solution, the nitroprusside, which has an octahedral ferrous centre with five tightly bound cyanide ligands plus one linear NO ligand, readily decomposes to NO [**2.268**-**2.271**], see **Figure 2.23**.

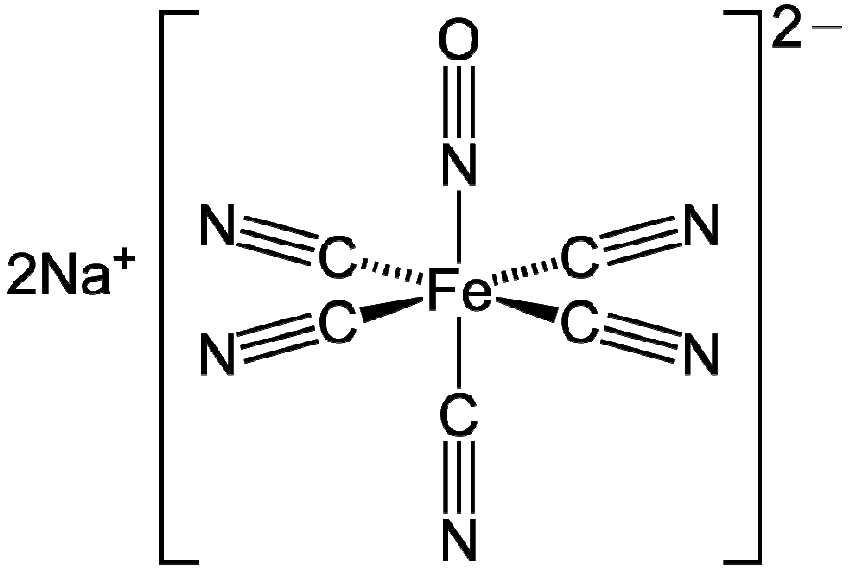

Figure 2.23. Chemical composition of SNP.

A preliminary study at Southampton (**Figure 2.24**), a collaboration between Dr Wharton from the nCATS and Dr Webb from the SBS at the UoS, involving the NO donor SNP, and a silane and glutaraldehyde immobilisation treatment on 3.5 cm diameter Ti specimens, has shown encouraging results after a 1 week immersion in natural seawater at the NOC pontoon. The dark areas in **Figure 2.24(b)** have been identified using Synchrotron Radiation – Fourier transform infrared (SR-FTIR) spectroscopy as having a biological signature similar to EPS in the fingerprint region, *i.e.* containing amides (1500 – 1750 cm^{-1}), phosphates (1200 – 1400 cm^{-1}) and carbohydrates (850 – 1100 cm^{-1}), which are characteristic of biofilm formation, see **Figure 2.24(c)** [**2.1**-**2.3**,**2.82**,**2.134**,**2.272**,**2.273**]. Significantly, the overall extent of the EPS coverage on the SNP treated surface can be seen to be considerably reduced in **Figure 2.24(d)**, thus indicating an effective biofilm inhibition performance.

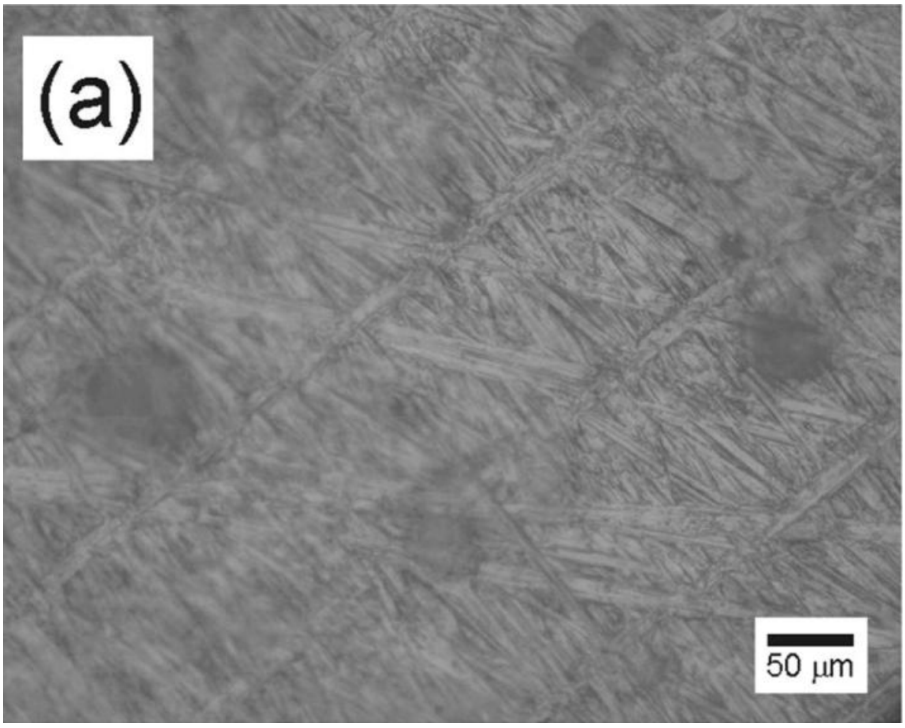
(a)
50 μm

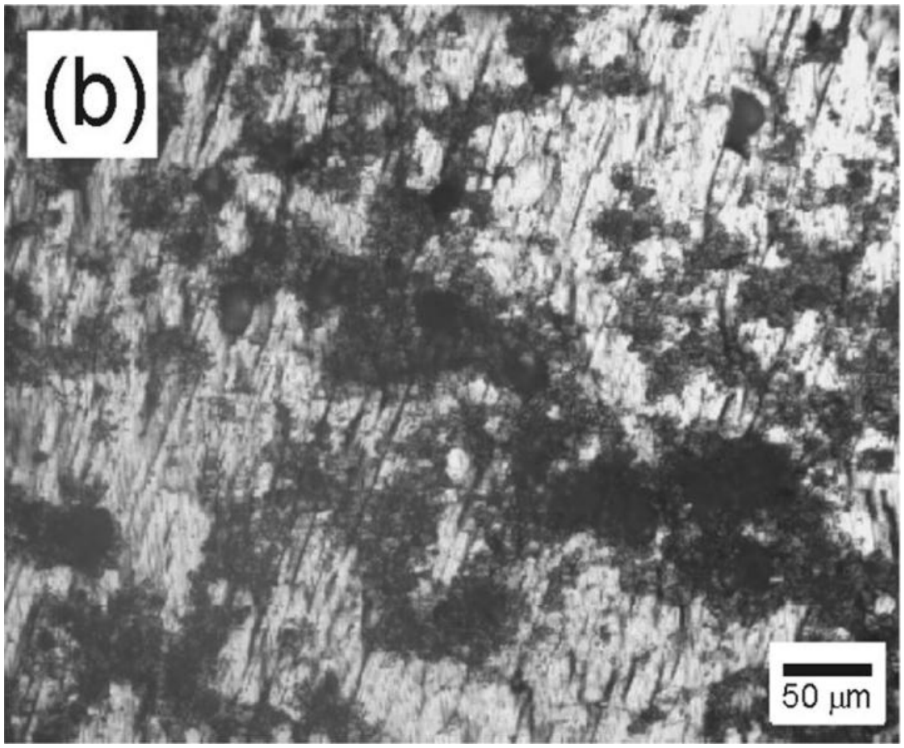
(b)
50 μm

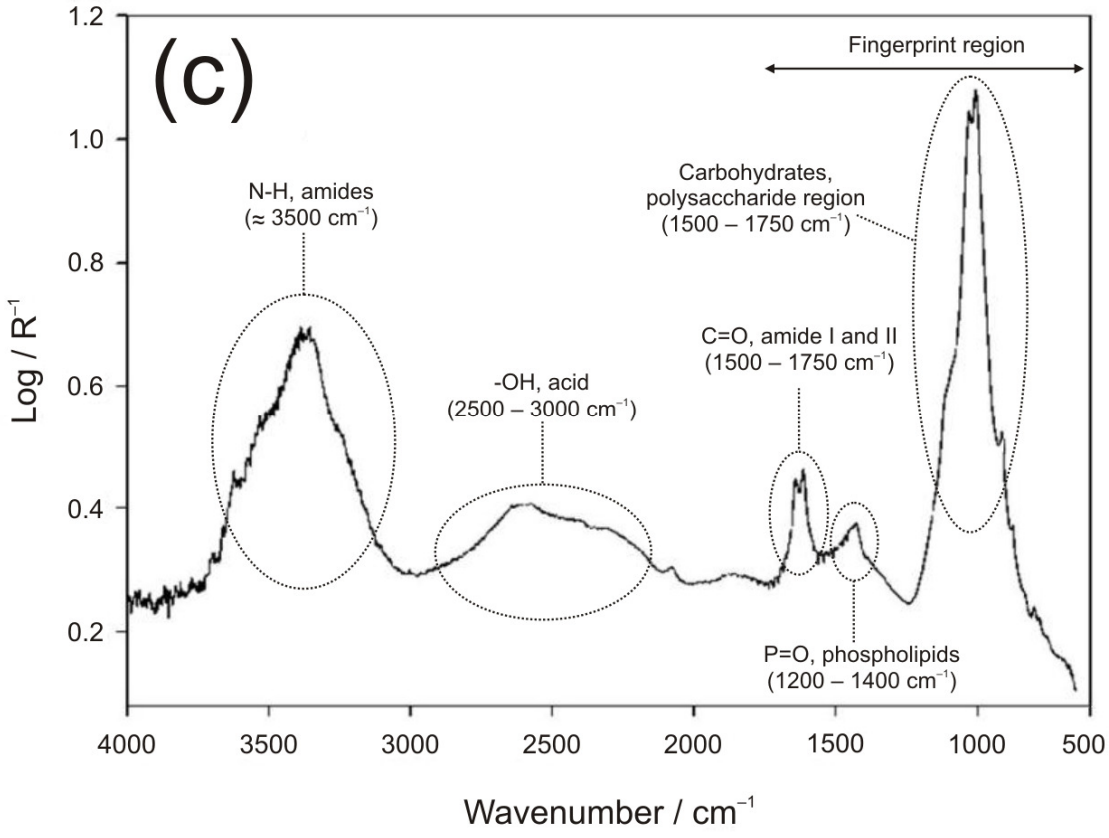

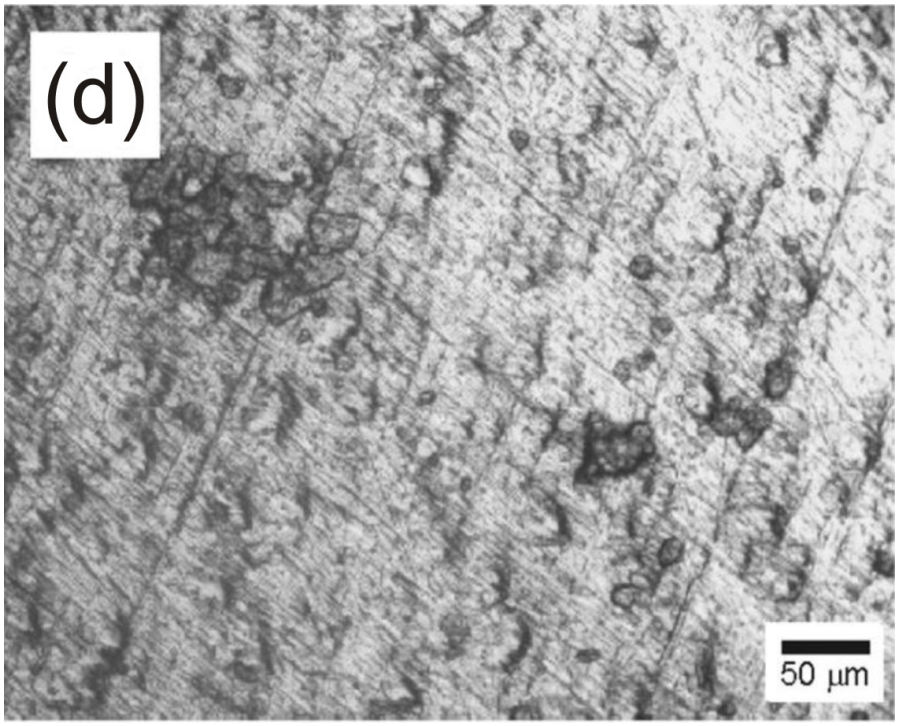

Figure 2.24. **(a)** The as-ground Ti surface. Seawater immersed: **(b)** silanised and glutaraldehyde treatment, **(c)** SR-FTIR spectra of bacterial EPS of the surface **(b)**, **(d)** silanised / glutaraldehyde treatment plus SNP immobilisation – courtesy of Dr Wharton and Dr Webb, University of Southampton.

The NO biofilm dispersal approach at Southampton has initiated a combination of basic and application-targeted research to investigate and exploit the interaction between NO and the detachment of fouling communities of microorganisms from surfaces. This corresponds to a completely novel area of application for the NO technology and therefore represents a unique opportunity for the control of marine biofouling. Although the study of the silanised / glutaraldehyde treatment plus SNP (NO donor) on Ti surfaces has shown insightful results into antifouling performance, this approach is not viable within marine piping systems directly exposed to seawater, and to a larger extent, no biofilm inhibition strategies using surface modification of Au surfaces [**2.274**] will be addressed for the current study. In contrast, NO donor SNP will be used as a biocide in seawater (for the proposed project) with the ultimate goal to generate the NO *in situ*. For that purpose, rapid screening of potential NO donors can include known NO donor molecules: SNP [**2.234**], diazeniumdiolate-based species and polymeric materials [**2.266**] where NO release can be controlled by selecting different molecular structures [**2.275**], or the *in situ* NO generation by catalytic decomposition of biofilm S-nitrosothiols (RSNO) via Cu corrosion [**2.276**]. Not only is the choice of a suitable biocide important, but also the duration (sufficient contact time [**2.3**]) and frequency of dosing (mostly on an intermittent or a continuous basis for industrial systems [**2.3**,**2.5**]), and also the flow regime can influence the overall fouling process [**2.277**], thereby emphasising the extremely difficult nature for effectively and / or efficiently combating biofouling in real systems [**2.3**].

Chapter 3 – Seawater environment

3.1 Physico-chemical properties of seawater

A diverse range of research fields including physical oceanography, marine chemistry, geology, biology and pollution are concerned with the physico-chemical properties of seawater [**3.1**]. This has resulted in the development of different simulanting test solutions, which are generally used to model in-service conditions at the laboratory scale. However, it is possible to focus on typical marine engineered case scenarios with well-defined parameters, *e.g.* a marine heat exchanger operating under a turbulent hydrodynamic flow regime.

3.1.1 Seawater chemical composition

Seawater consists of water with various dissolved materials [**3.1**]. Most of the salt ions in the sea (≈ 99 %) are Cl^-, Na^+, SO_4^{2-}, magnesium (Mg^{2+}), calcium (Ca^{2+}) and potassium (K^+). A detailed composition of the major ions in seawater is described in [**3.1**-**3.3**]. These ions are a semi-conservative property of seawater, *i.e.* they display little variation with time. Nutrient elements are scarce chemicals in surface seawater (open ocean) and are typically measured in ppm, however, these are essential for the environmental growth conditions [**3.3**]. Major nutrients are carbon (C), nitrogen (N), phosphorus (P) and silicon (Si), and are non-conservative in seawater. The major dissolved gases in the sea are nitrogen (N_2), O_2, CO_2 and noble gases, such as Ar [**3.3**]. Usually, the ratio of the molar concentration of C, N and P (to form the soft tissues of organisms) in ocean water is 106:16:1 and the absolute values depend upon biological activity, transport processes, and chemical equilibria [**3.3**,**3.4**]. N_2 and Ar are conservative whereas DO and CO_2 are non-conservative. Organic material in seawater is composed of relatively low concentrations of large complex molecules produced by marine organisms or resulting from biological decay, *e.g.* proteins, lipids (fats), fatty acids, carbohydrates, hormones and vitamins.

3.1.2 Physico-chemical properties of surface seawater

The physico-chemical properties of surface seawater (zero to 500 m in depth) of relevance for the proposed experimental programme and detailed in [**3.1**,**3.3**,**3.5**-**3.7**] are:

- temperature range of –2 to 28 °C (**Figure 3.1**),
- pH is slightly alkaline and between pH 7.5 – 8.3,
- salinity (representative of the amount of salts in g dissolved in 1 kg of seawater after all carbonate converted to oxide, all bromine has been replaced by chlorine and all organic matter destroyed) varies between 32 and 36 ‰ (parts per thousand or g kg^{-1}) in **Figure 3.1**,
- and the DO concentration is around 4 – 10 ppm.

Seawater density depends on temperature, salinity and atmospheric pressure. Usually, denser (more atoms or molecular mass in the same volume), colder and less salty water is overlain by less dense and high salinity warm water, where heat diffuses downwards more rapidly than the salt, thus resulting in instability in the system (convection patterns) [**3.1**,**3.3**]. However, the dependence is non-linear (**Figure 3.1**) for surface seawater equilibrated with the atmosphere.

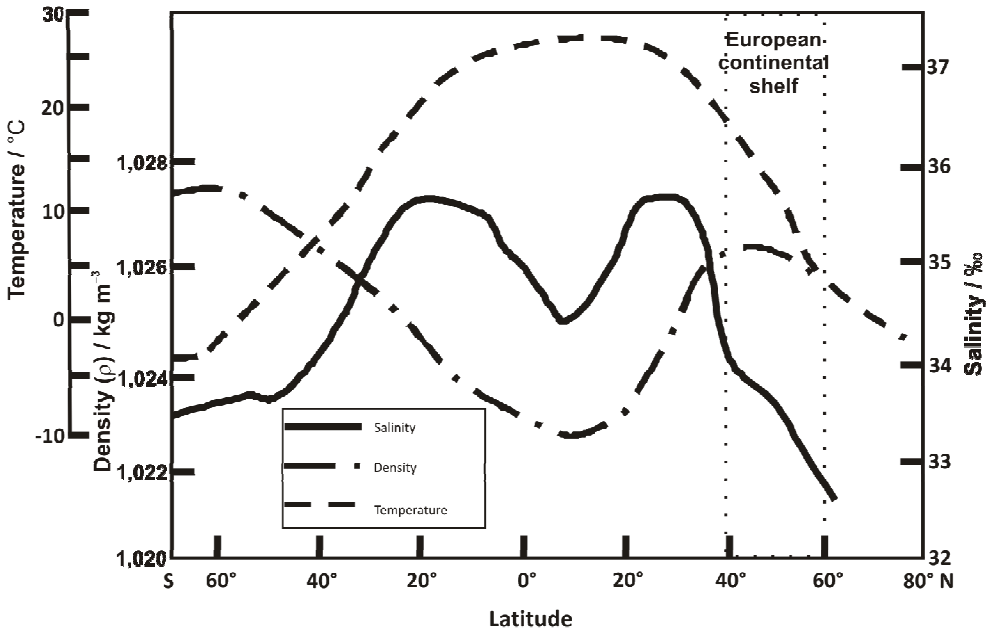

Figure 3.1. Average surface temperature, salinity, and density variation with latitude for all oceans, adapted from [**3.1**,**3.2**,**3.6**].

The latitude in **Figure 3.1** corresponds to the location on the Earth, where 0° is representative of the Equator. For instance, North Atlantic coastal ocean, which occurs above the European continental shelf, ranges from 40 to 60° North latitude [**3.1**]. Seawater salinity can be estimated by measuring its conductivity since the relationship salinity-conductivity used by salinometers is based on a polynomial law [**3.3**,**3.8**]. However, conductivity-temperature-depth (CTD) instruments are often used to provide more detailed descriptions of the seawater environment under investigation [**3.1**,**3.3**]. For instance, the conductivity of seawater of 35 ‰ salinity at 25 °C is reported to be 53.03 mS cm^{-1} [**3.7**]. Conductivity in seawater is mostly affected by the presence of inorganic ions, *e.g.* Cl^- and Na^+, as opposed to organic matter, *e.g.* carbohydrates and fatty acids [**3.1**,**3.8**]. The air-sea interaction is the primary source of the DO in seawater [**3.1**]. Because of this (gas-liquid) interaction, the surface seawater is usually close to saturation, *i.e.* it contains as much dissolved gas as it can hold in equilibrium at an existing temperature, salinity and pressure. The solubility of O_2 (its ability to be dissolved as DO in a solution) is dependent on the salinity, temperature and its partial pressure [**3.1**]. When either the temperature or salinity increases, the DO level in seawater decreases (see **Table 3.1** for surface seawater equilibrated with the atmosphere [**3.7**]) and increases with increasing pressure [**3.3**,**3.7**]. Conversely, cold and lower salinity seawater can maintain relatively higher DO levels [**3.3**,**3.7**]. All the above considerations regarding seawater properties result in the necessity of measuring the temperature, pH, salinity and DO level of the media for the EIS testing.

Table 3.1. Concentration of O_2 at various temperatures and salinity levels, from [**3.7**,**3.9**].

Temperature / °C	**Salinity / ‰**				
	0	10	20	30	35
	DO / ppm				
10	11.3	10.6	9.9	9.3	9.0
12	10.8	10.1	9.5	8.9	8.6
14	10.3	9.7	9.1	8.6	8.3
16	9.9	9.3	8.7	8.2	8.0
18	9.5	8.9	8.4	7.9	7.6
20	9.1	8.5	8.0	7.6	7.4
22	8.7	8.2	7.8	7.3	7.1
24	8.4	7.9	7.5	7.1	6.9
26	8.1	7.6	7.2	6.8	6.6
28	7.8	7.4	7.0	6.6	6.4

3.2 Biological background

3.2.1 Biofilm and biological processes

Any research programme using bacterial strains is not a straightforward task [**3.10**-**3.15**]. Due to the nature of this project, which is a surface engineering focused investigation applying marine microbiology, the microbiology component is liable to be the least controllable aspect and may lead to experimental problems if not carefully considered and planned (*e.g.* complexity of biological systems and reciprocal interactions between bacterial biofilms and the environment). For instance, just simply sampling from natural seawater requires attention with regard to seasonality, temperature, resilience (duration, natural and artificial light, nutrient levels) and aeration (significant potential for contamination from airborne pollutants and carbon sources) [**3.10**,**3.16**].

3.2.2 Biological considerations for biofilm monitoring

3.2.2.1 Environmental changes induced by bacterial metabolism

Bacterial metabolism may induce modifications in the growth environment / bulk solution, which can be detected by appropriate sensor technologies [**3.12**,**3.10**,**3.17**-**3.27**]. For instance, marine aerobic bacterial metabolism (where aerobic bacteria use DO present in seawater for respiration and are unable to live in its absence [**3.12**]) can affect the marine environment or the metal / seawater interface as follows:

- Bacterial metabolism for heterotrophs (derive energy from oxidation of organic matter [**3.28**]) involves the consumption of DO and organic material (*e.g.* glucose), resulting in the release of CO_2, H_2O, heat and organic acid production (lactic and acetic acid) [**3.29**,**3.30**], see **Figure 2.11** in **Section 2.4.3.2**. CO_2 generated by the bacterial metabolism hydrates to form carbonic acid (H_2CO_3), a weak acid which contributes to the acidification of seawater [**3.3**,**3.14**,**3.31**], see **Equation 3.1**.
- The differential aeration cell created by the bacterial biofilm on metallic surfaces can lead to localised corrosion [**3.17**]. This is consistent with the concept of a DO profile (a DO concentration gradient) across a mixed biofilm [**3.12**,**3.14**,**3.17**]. Similarly to **Section 2.4.3.2**, measurements of the pH profiles within the biofilms on SS UNS S31600 in a natural aqueous environment using a fibre-optic sensor have indicated pH values lower than 3 (at localised areas) to 8 (at the outer biofilm surface) [**3.32**].

$$CO_2 + H_2O \rightarrow H_2CO_3 \qquad (3.1)$$

As seawater can be considered as a naturally buffered solution (alkaline pH $\approx$ 8 due to the presence of sodium carbonate (Na_2CO_3), which acts as a pH regulator [**3.1**]), the influence of any localised changes in pH resulting from the bacterial metabolism may be negligle over a short-time duration of a few days. In addition, photosynthesis from phytoplankton (diatoms, dinoflagellates, coccolithophores [**3.10**]) contribute to CO_2 consumption (using energy from sunlight, phytoplankton assemble organic matter from CO_2 and nutrients dissolved in seawater) in marine environment [**3.31**].

3.2.2.2 Environmental stresses on biofilm growth and variability

Marine bacterial growth is influenced by physico-chemical parameters from the surrounding environmental conditions [**3.16**,**3.21**]. Each bacterial species has its own optimal growth conditions and thus bacterial biofilms will be affected by environmental factors such as temperature, sunlight levels, nutrient supply, pH, DO level, flow regime and osmotic effects in unique ways [**3.10**,**3.16**,**3.21**,**3.28**,**3.33**,**3.34**]. These parameters vary with the seasons, geographical location and with water depth (pressure levels) [**3.16**,**3.21**].

Temperature

The temperature of the biotic environment can affect living organisms in two ways: (*i*) as the temperature rises, the reaction kinetics of enzymatic and chemical processes can be enhanced and (*ii*) above a certain threshold temperature the biofilm proteins can be irreversibly damaged [**3.5**,**3.10**,**3.12**]. Alternatively, O_2 solubility declines as temperature increases in seawater (**Table 3.1**) [**3.7**,**3.9**], thus affecting respiration rates in aerobic organisms [**3.1**,**3.3**,**3.5**]. Similarly, the temperature of the environmental growth can influence the development of a diverse microbial community [**3.21**]. For example, an 80 % increase in biofilm thickness was reported with a temperature rise from 30 to 35 °C [**3.35**]. It was also shown that larvae of *Balanus amphitrite* and *Balanus trigonus* can settle on biofilms established at high temperatures (23 and 30 °C), whereas at lower temperatures (16 °C) their settlement was unaffected (*Balanus amphitrite*) or inhibited (*Balanus trigonus*), respectively. In addition, higher rates of larval metamorphosis was observed at higher temperatures (23 and 30 °C) while biofilms were predominant at lower temperatures (16 °C) [**3.21**]. This is in good agreement with the studies reported by Shams El Din *et al.*, where it was shown that the rate and extent of biofilm formation is dependent on the ambient seawater temperature, with more significant biofouling rates during the warmer periods [**3.36**].

Sunlight levels

UV radiation (particularly at λ = 260 nm) from the solar radiation spectrum can affect the genetic content of bacteria [**3.33**]. Certain types of enzymes are hence activated to repair possible damages caused by this UV radiation. The effects of sunlight on the decomposition of dissolved organic carbon, NO_3^- and phosphate (PO_4^{3-}) and bacterial metabolism in aqueous conditions has been studied in the published literature [**3.37**]. It is reported that the synergic effect of photochemical (interactions between atoms, small molecules and light) and microbial alteration of dissolved organic matter discussed in [**3.37**], may include:

- increase bacterial demand for inorganic nutrients,
- change the bacterial growth efficiency (BGE),
- and influence the contribution of carbon between bacterial biomass and respiration.

Hung *et al.* studied the effect of UV-A (315 – 400 nm) and UV-B (280 – 315 nm) on the biofilm bioactivity that can indirectly affect larval attachment of barnacles [**3.21**]. Applied UV radiation resulted in a decrease in the percentage of respiring bacterial cells with enhanced effects using higher UV energies. At fixed energy level, UV-B showed greater ability in reducing bacterial cell density than UV-A [**3.21**]. Conversely, a decrease of larval settlement of *Hydroides elegans* with increased UV radiation was observed, potentially indicating that UV radiation can affect a biofilm's inductive cues for *Hydroides elegans*. Overall, these considerations suggest that the influence of radiation on biofilm bioactivity may depend on the larval / spore's response induced by biofilms [**3.21**]. However, the sunlight-exposure within marine pipes and heat exchangers is very limited and bacterial biofilms usually develop under dark conditions. Consequently, an enclosed Faraday cage (dark conditions, *i.e.* at light irradiance values close to 0.0 µmol photons m^{-2} s^{-1}) has been chosen for the EIS laboratory experiments.

Season

The North Atlantic Ocean has marked seasonal changes in seawater temperature, as a consequence this affects the biofilm growth enhanced during the spring and summer months [**3.5**,**3.6**]. The reproduction and growth of marine organism are suppressed during the winter period (accounting for the reductions in seawater temperature, solar radiations and the numbers of spores and larvae [**3.16**]), resulting in an overall decrease in new attachment and biofouling [**3.6**,**3.7**].

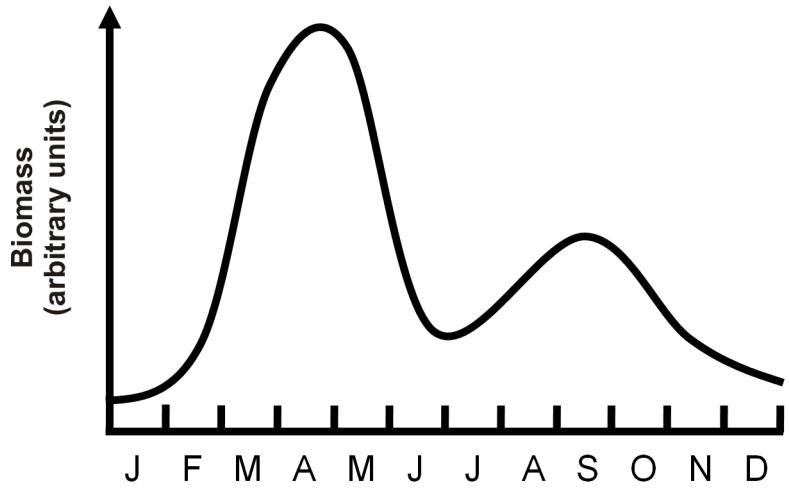

Figure 3.2. Seasonal cycle in (phytoplankton) biomass for the North Atlantic [**3.6**,**3.7**].

Two maxima are frequently reported for marine organisms (phytoplankton) in the North Atlantic Ocean, a large peak occurring in the spring and a smaller one in the autumn, see **Figure 3.2**. The sharp onset of colonisation in the spring suggests that a temperature threshold may exist, which can represent the time when attachment begins. The duration of the biofouling season is hence defined as the time over which the seawater temperature remains beyond this critical level [**3.6**,**3.7**]. However, it is more likely that the onset of bacterial growth for the spring season (**Figure 3.2**) is shifted compared to that for phytoplankton, *i.e.* it initiates when phytoplankton biomass is suppressed [**3.38**].

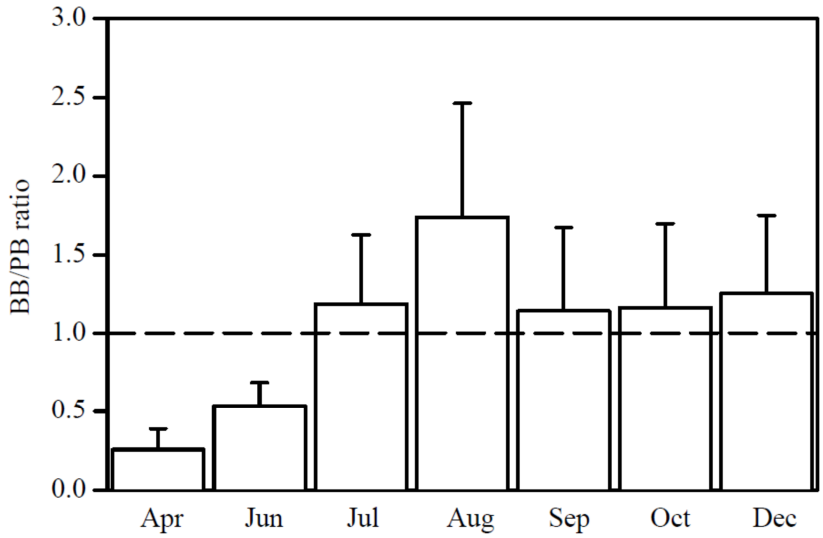

Figure 3.3. Monthly mean (+Standard Deviation) ratio of depth-integrated total bacterial biomass (BB) and depth-integrated phytoplankton biomass (PB). Dashed line indicates unity, from [**3.38**].

This is consistent with **Figure 3.3**, where phytoplankton biomass is about half of the bacterial biomass in August – the depth-integrated total biomass is representative of an average biomass value of measurements taken at 5, 15 and 25 m depth in the southern North Sea [**3.38**].

Nutrient supply and geographical location

Likewise, biofouling is influenced by the geographical location. For instance, a dominant fouling species in northern France and southern UK coastal areas is the barnacle *Semibalanus balanoides*, whereas the *Balanus amphitrite* species is prevalent in the Mediterranean Sea [**3.16**]. The chemical composition of the ambient seawater (**Section 3.1.1**) will also play an important role in the number, diversity and metabolic states of planktonic bacteria, and their ability to attach onto surfaces [**3.21**]. To date, the interactions between nutrients, biofilm properties and the colonisation process in nature still need to be addressed [**3.21**]. Recently, Hung *et al.* demonstrated that biofilms established at similar intertidal height in different ecological niches (experiencing contrasting environmental conditions) can activate diverse bioactivities for barnacle larval settlement. These findings suggest that the nutrient load at different habitats can be a key element triggering several biofilm bioactivies [**3.21**]. Because of the importance of temperature on bacterial growth and its complex seasonal and geographical effects, and also nutrient load, the EIS testing will be performed using

artificial seawater (ASW) of known chemical composition in a controlled room temperature (fixed location, absence of seasonal effects).

pH

Changes in the pH solution can degrade proteins, enzymes (required for the bacterial metabolism) and unbalance the stability of the cytoplasmic membrane of bacteria from the biofilms [**3.33**,**3.39**,**3.40**]. In addition, pH changes can affect adsorption onto surfaces, see **Figure 2.19** in **Section 2.6.5.3**. This reinforces the need of using buffer alkaline media or seawater with its naturally buffering due to the presence of Na_2CO_3.

DO level

Similarly, marine aerobes or aerobic bacteria require DO otherwise they can potentially die or go dormant without its presence in the growth environment [**3.1**,**3.10**,**3.33**]. Therefore, continuous aerated media will be required.

Flow regime

As discussed in **Sections 2.4.4.4** and **2.4.4.5**, the flow regime can affect biofilms. For instance, the effective diffusion coefficient in aerobic biofilms was found to be dependent on flow conditions and biofilm structure [**3.12**]. This mass transport process occurs preferentially by convection through pores in the biofilm [**3.12**]. In addition, CSLM observations under flow regimes have revealed that cell clusters from the biofilm can vary in shape (ranging from cylinders to filaments) [**3.12**,**3.21**,**3.41**], see **Section 2.4.4.4**. It was also observed that turbulent conditions can favour rapid adhesion of planktonic bacteria, thus facilitating secretion of EPS matrix resistant to high fluid shear and subsequent settlement and growth processes [**3.21**]. As a result, the EIS testing will be done under controlled flow conditions.

Osmotic effects

Seawater salinity can also play a pivotal role in the biofilm processes [**3.21**]. Osmosis is the mechanism by which water diffuses from a region of low (dilute) to high (dense) solute concentration [**3.33**]. Usually, cellular cytoplasm has a higher solute concentration (higher water activity) than the growth environment. As a result, the tendency is for water to diffuse into the cell or more generally through the biofilms. Marine microorganisms usually have specific requirement for the Na^+ ion and grow optimally at the water activity of seawater. These species are called halophiles (with affinity for salt). Consequently, the salinity of the test media will need to be constant and relevant to seawater environment.

Water depth

The development of the deep-water oil and gas industry has led to an increased focus on the study of deep biofilm / fouling species, thus supporting interest in the effect of pressure levels on these marine communities (a field area largely uninvestigated) [**3.16**]. Although deep waters can represent extremely unfavourable conditions for living organisms, it was reported that deep-sea organisms can adapt from adverse environments (lower light radiations, nutrient levels and water temperature, and also higher hydrostatic pressures) [**3.16**]. In this instance, certain types of marine bacteria, *e.g. Photobacterium* or *Shewanella* species can only grow under high pressure conditions (400 – 500 atm, representative of a 4000 – 5000 m depth) [**3.42**]. At such depths, the seawater temperature is on average about 2 °C [**3.42**]. Therefore, these conditions make methods for bacteria culturing difficult at the laboratory scale. In contrast, biofouling can occur in any marine engineered metallic systems at the atmosphere, *e.g.* offshore platform (truly ubiquitous problem detailed in **Section 2.2**). Thus, the EIS experiments will be performed under atmospheric pressure.

Biological considerations

Although beyond the scope of this current study, biological considerations such as availability and physiological condition of the colonising species, biological disturbance, competition and cooperation among species can play a pivotal role in biofilm community alterations [**3.21**]. In this instance, three main biological concepts may be of importance [**3.15**,**3.43**,**3.44**]:

- physiological adaptation: cells respond adaptively to local environmental conditions,
- genotypic variation and natural selection: mutation or chromosomal rearrangements,
- and stochastic gene switching: cells toggle between discrete physiological states by gene switching (random in nature).

3.2.3 Selection of marine bacterial species

Overall, marine planktonic bacterial cell populations range from 10^6 to 10^7, and 10^4 to 10^6 cells mL^{-1} for estuarine and coastal ocean waters, respectively [**3.1**,**3.28**]. Estimates of the density of sessile bacteria are in the range of 1 cell / 0.3 μm^2 to 1 cell / 400 μm^2 [**3.1**]. Similarly, the size of planktonic bacteria cell in the ocean is small ($\leq$ 0.4 µm in diameter), whereas, sessile bacteria generally have an average diameter of 0.6 µm [**3.1**]. As a complex and broad range of bacterial cells can be found in surface seawater, it is therefore necessary (for controllability reasons) to select a particular strain for the proposed study.

3.2.3.1 General considerations for bacterial strain selection

Specific bacterial species for this research work programme have been considered with regard to the published literature [**3.45**-**3.48**] and after discussions with Dr Hellio from the SBS at the University of Portsmouth and Dr Webb from the SBS at the UoS. Importantly, the bacterial strain selection criteria have to meet with engineering purposes such as biocorrosion and biofouling within marine heat exchangers, see **Section 2.4**. In biocorrosion, key research in **Figure 3.4** has primarily focused on investigating interactions of anaerobic marine bacteria such as SRB on steel and Cu alloys. However, MIC has been recognised to be a much more complicated process, where it is rarely associated with just one species, see **Section 2.1**. For instance, the SRB mechanisms are not necessarily appropriate when considering aerobic bacteria. In addition, there is a general lack of understanding into the behaviour of aerobic marine bacterial biofouling and their interaction on metallic surfaces [**3.49**]. This has led to recent emerging studies to determine how aerobic bacteria influence the corrosion behaviour of Cu alloys to provide helpful insight in controlling biofouling and MIC in a marine environment [**3.45**].

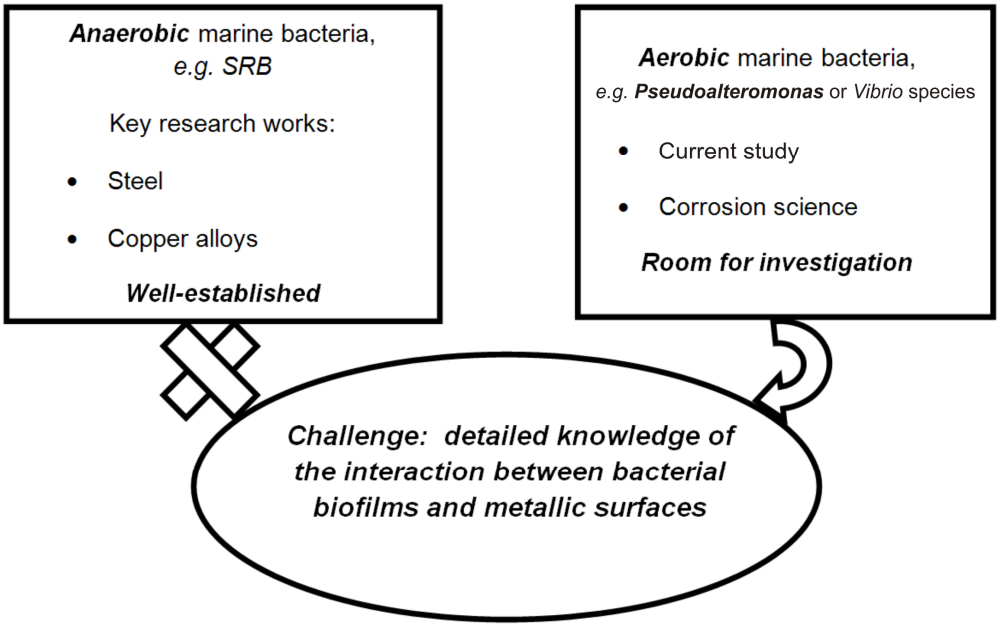

Figure 3.4. State-of-the-art in marine biocorrosion.

Based on these considerations, **Figure 3.4** shows the key components for this current project, which will focus on aerobic marine bacteria in an engineering context to develop understanding on the interactions of aerobic bacterial biofilms on metallic surfaces. This should help support future investigations for corrosion science using more realistic approaches with both anaerobic and aerobic species.

The most appropriate candidate strain (to study in this current study) has been identified as *Pseudoalteromonas* sp. NCIMB 2021 (**Table 3.2**) as it is probably the most prevalent bacterial species in seawater [**3.10**,**3.16**,**3.21**]. *Pseudoalteromonas* sp. has been found to be involved in the corrosion process of aluminium alloys (occasionally used in heat exchangers) in marine habitats [**3.45**]. This gram-negative rod is an aerobic slime-former and often grows in a patchy distribution over metal surfaces [**3.12**,**3.50**]. Similarly, Busalmen *et al.* have attributed the enhancement in the kinetics rate to the cathodic reduction by the catalase secreted by *Pseudoalteromonas* strain [**3.51**], see **Section 2.4.3.2**. Another species for possible consideration is *Vibrio* sp. strain S14, which can safely be cultured in a laboratory environment. Likewise, bacterial genera that may require further possible consideration include: *Achromobacter*, *Micrococcus* and *Flavobacterium* spp., which are widespread as fouling bacteria [**3.10**]. In contrast, the genera *Bacterium*, *Bacillus* and *Sarcina* are less common [**3.10**]. Bacterial species can be supplied freeze-dried in ampoules or as active cultures with a hazard sheet provided for each bacterial strain from the National Collection of Industrial, Marine and Food Bacteria (NCIMB) in the UK.

Table 3.2. Specification of bacterial strains.

Bacterial strain	***Pseudoalteromonas* sp. NCIMB 2021**	***Vibrio* sp. strain S14**
Main properties	Commonly considered a pioneer in terms of attachment / bacterial biofilm formation [**3.10**,**3.16**,**3.21**]	Biofilm development, cellular detachment, adhesion [**3.47**,**3.52**,**3.53**]
Growth T / °C	18 [**3.54**-**3.56**]	Ambient temperature [**3.48**]
Medium	Similar to seawater conditions [**3.45**,**3.54**,**3.55**,**3.57**-**3.59**]	Väätänen nine-salt solution agar: Lauria-Bertani plates – 20 g L^{-1} NaCl. Culture liquid using Marine minimal medium [**3.48**]
Advantages	Species widespread in seawater [**3.45**,**3.59**]	Remains 100 % viable after 2 weeks in unsupplemented ASW – culturable after 6 months in the starvation regime [**3.47**]
Why use this bacterial strain?	Few studies on bacterial biofilms directly formed on metallic surfaces / spatial repartition of biofilms [**3.45**,**3.49**]	
Supply	NCIMB [**3.45**,**3.52**,**3.59**-**3.61**]	
Storage	NOC	

3.2.3.2 Characteristics of *Pseudoalteromonas* sp. NCIMB 2021

A detailed description of the artificial growth environment of *Pseudoalteromonas* sp. NCIMB 2021, the parameters influencing its growth and colonisation on substratum, and SEM imaging to corroborate its fouling properties has been previously outlined in [**3.50**,**3.54**-**3.56**]. The 250 mL media used consisted of 0.1 % (w/v) peptone and 0.07 % (w/v) yeast extract powder in filtered seawater, pH 7.6 at 18 °C [**3.55**]. Peptone and yeast extract were used to enhance the organic carbon source content required by the bacteria (heterotrophic bacteria) for their metabolism [**3.1**]. It has been shown that the number of sessile bacteria is dependent on the cell density (planktonic cell population) and the growth stage (logarithmic, stationary and scenescent phases, see **Figure 3.5**) [**3.55**]. **Figure 3.5** corresponds to a batch culture in the absence of continuous flow of nutrients, representative of environmental conditions associated with the natural self-purification process of rivers and lakes [**3.12**]. In this instance, the bacterial growth starts after the addition of an inoculum (certain amount of microorganisms) to a culture medium of specific chemical composition. The lag period preceding the logarithmic phase (**Figure 3.5**) coincides with the time required for bacterial cells to adapt to the

new medium before the exponential growth begins [**3.15**]. Usually, the duration of the lag phase is influenced by the ability of cells to grow in a specific culture medium that may be different to that of the inoculums, *e.g.* a short lag period is correlated with fast growing cells when both the culture medium and inoculum are similar [**3.12**,**3.15**].

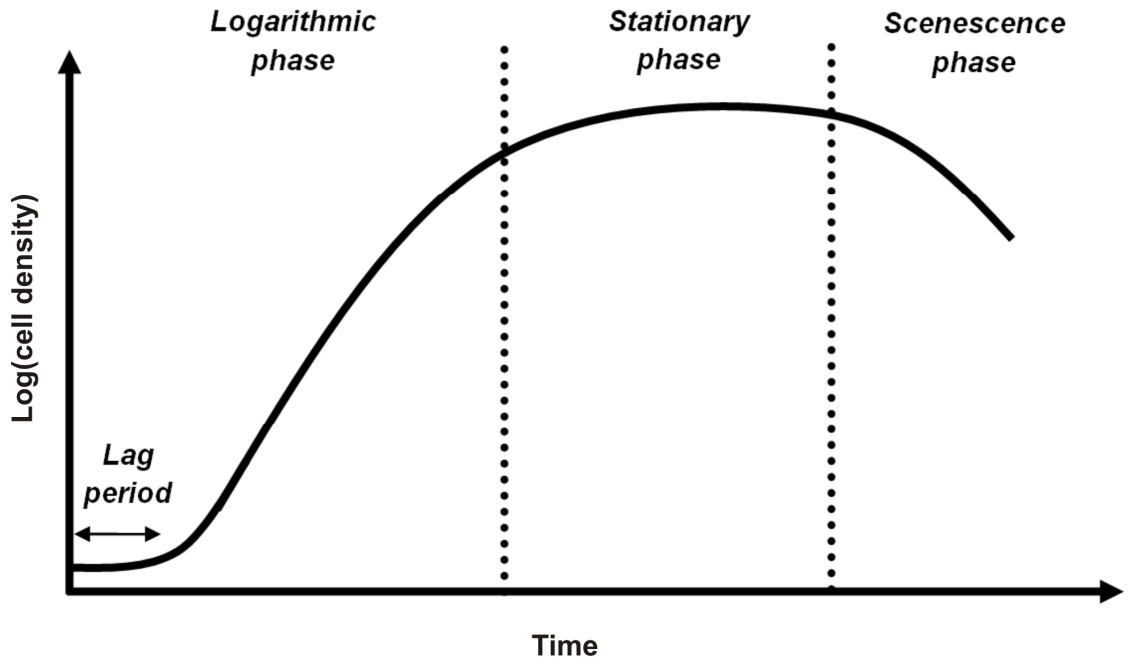

Figure 3.5. Typical growth curve of a bacterial culture, adapted from [**3.12**,**3.15**].

During the logarithmic phase (**Figure 3.5**), the species grow at a constant rate due to the constant division of each cell into two daughter cells [**3.12**]. Using this scheme, the average generation time (t_d) corresponding to the time interval for the bacterial population to duplicate can be computed, see **Section 5.1**. Values of t_d are largely affected by the nutrients concentration and the environmental conditions in the culturing system, for instance for heterotrophic bacteria t_d can range from 0.28 h (*Escherichia coli*) to 34 h (*Treponema pallidum*) [**3.12**]. Once the nutrients in the medium are depleted, the bacterial growth stops and the stationary phase starts (**Figure 3.5**). During this (stationary) phase, which can last a few hours / days for *Pseudoalteromonas* sp. [**3.55**], the number of cells remains stable. After prolonged exposure, the accumulation of toxic metabolic products can be an additional growth-limiting factor, thus explaining the occurrence of the scenescence phase. During this biological ageing / death phase, dying cells can undergo lysis [**3.12**].

Overall, cell attachment for *Pseudoalteromonas* sp. NCIMB 2021 occurred more readily when the cells were fresh and in significant numbers [**3.55**]. Recently, Salta *et al.* have studied the biofilm properties of *Pseudoalteromonas* sp. NCIMB 2021 on natural products incorporated in a paint system using a multidetection microplate reader (for real-time monitoring of biofouling rate and, together with a molecular probe technique, *in situ* quantifiable information of the vialability and extent of biofilm) [**3.62**]. It was reported that a significant biofilm occurred on the control paint coating, compared with the greater antifouling properties of coatings containing natural products [**3.62**].

The influence of culture growth stage on attachment (for the *Pseudoalteromonas* bacteria) was discussed by Fletcher using two factors: (*i*) changes in cell motility (planktonic bacterial cell ability to spontaneously move is altered with age) and (*ii*) modifications in the quantity or quality of cell surface polymers (the production or secretion of EPS by bacteria declines with time) [**3.55**]. Likewise, the effect of temperature on bacterial attachment has also been studied [**3.55**]. The results showed that fewer bacteria were attached at low temperatures (3 ± 1 °C) compared with cells at 20 ± 1 °C. It has been suggested that two major characteristics could be associated with the thermal effect on attachment:

- The viscosity of the media increases as temperature decreases and can affect the bacterial cell motility.
- The physiology of the organisms may be affected by changes in temperature (**Section 3.2.2.2**) and in particular, high temperatures result in greater adsorption on the surface suitable for bacterial attachment.

In contrast, it was reported that *Pseudoalteromonas* sp. is psychrophilic and can hence acclimatise to changing conditions, for instance it has the ability to thrive at relatively low temperatures [**3.55**]. Similarly, no obvious differences of the cell membranes were detected using microscopy techniques and additional investigations on the attachment of *Pseudoalteromonas* sp. on a noble metal, such as Pt, have also revealed ≈ 15 cells / 100 μm^2 after a 2 h exposure [**3.56**], plus SEM analysis has highlighted naturally attached bacteria of roughly 0.7 µm in diameter [**3.50**].

Based on the knowledge developed in [**3.50**,**3.54**-**3.56**], the EIS growth media (alkaline, pH 8) will contain similar composition of carbon source level in pH ≈ 8 media (relevant to seawater). In addition, bacterial cells will be kept at 18 °C and an estimate of the cell

density, and also the age of the bacterial growth phase / stage will be required before undertaking testing.

3.2.4 Monitoring bacterial biofilms under controlled conditions

3.2.4.1 Experimental controllability: the background and context

To suit the biological requirements, a more detailed understanding on bacterial colonisation and growth processes (from an engineering perspective) is required. Importantly, there are only a few investigations in which a comprehensive and detailed analysis of problems associated with bacterial colonisation has been reported [**3.12**,**3.21**-**3.24**,**3.63**]. In order to limit experimental effects, the following steps are proposed:

- The electrochemical sensor should work *in situ* (rather than *ex situ*), see **Section 2.6**.
- The tests should be conducted under well-defined and controlled conditions, *i.e.* use of one marine aerobic bacterium species of known growth phase (*Pseudoalteromonas* sp. NCIMB 2021), constant temperature (18 °C for the species) and media salinity (35 ‰ in open seawater), buffer media (pH 8.1 in open seawater), continuous aeration (saturated DO level of ≈ 7 ppm), Faraday cage (minimise electromagnetic interference and tests in dark conditions at light irradiance values ≈ 0.0 µmol photons m^{-2} s^{-1}), and a well-defined hydrodynamic flow regime (low laminar flow).
- Additional precautions are necessary in performing any kind of microbiology experimentation, above those normally associated with surface engineering. All laboratory equipment should be sterilised before use. Gloves, white coat and goggles have to be worn when UV lighting is used. Contaminated materials have to be stored in suitable disposable boxes that will be later autoclaved. The nCATS laboratory has limited experience of these requirements. Therefore, key collaborations with other research groups within the UoS, including the NOC (Dr Iglesias-Rodriguez) and the SBS (Prof Keevil and Dr Webb) will resolve the facility issues. Additionally, access to the tissue engineering laboratory strengthened by the expertise of Dr Stoodley from nCATS will add value to this project.

3.2.4.2 Chemostats / flow culturing systems and flow cytometers

Developing a laboratory system that can truly model the real world of biofilm growth and extent in addition to the inherent hydrodynamic conditions is a challenge. Such a system has to properly simulate the fluctuations of nutrient availability, growth and shear rates, changes incurred by predator-prey relationships and environmental conditions, the redox processes, pH, temperature, and also the physico-chemical properties of the surfaces investigated [**3.64**]. This section will address the suitability of two selected continuous culture systems (chemostat and flow cell devices) proposed for this study. Likewise, an established method to study the growth curve of a bacterial culture (marine flow cytometer) is considered.

A chemostat in **Figure 3.6** is a continuous monospecies culture vessel to which fresh nutrient medium from a sterile reservoir is added and excess liquid (the efflux of exhausted medium, living cells and cellular debris) is removed to keep the culture volume constant [**3.12**,**3.28**,**3.64**-**3.66**]. The advantage of chemostat relies on its capability of triggering the rate of removal of the organism once the species growth rate is well-defined, see **Equation 3.2** [**3.64**] used in **Section 5.1**.

$$\frac{\mathrm{dx}}{\mathrm{dt}} = \mu_{\mathrm{b}} x - D_{\mathrm{i}} x \text{ and } D_{\mathrm{i}} = \frac{Q}{V} \tag{3.2}$$

Rate of change of cell density in the vessel

Growth rate of the organism

Rate of removal of the organism

Consequently, a chemostat is a controlled bioreactor, which ensures good repeatability / reproducibility of the environment conditions. For instance, specific nutrient limitations with slow growth rates (as might be experienced in nature) can be setup using a chemostat [**3.64**]. **Equation 3.2** for a monoculture chemostat is derived from continuous culture theory laid by Monod in France and Novick and Szilard in the USA [**3.64**]. For a defined monoculture system without loss, the culture concentration in the vessel at a given time corresponds to that which has been generated minus that removed.

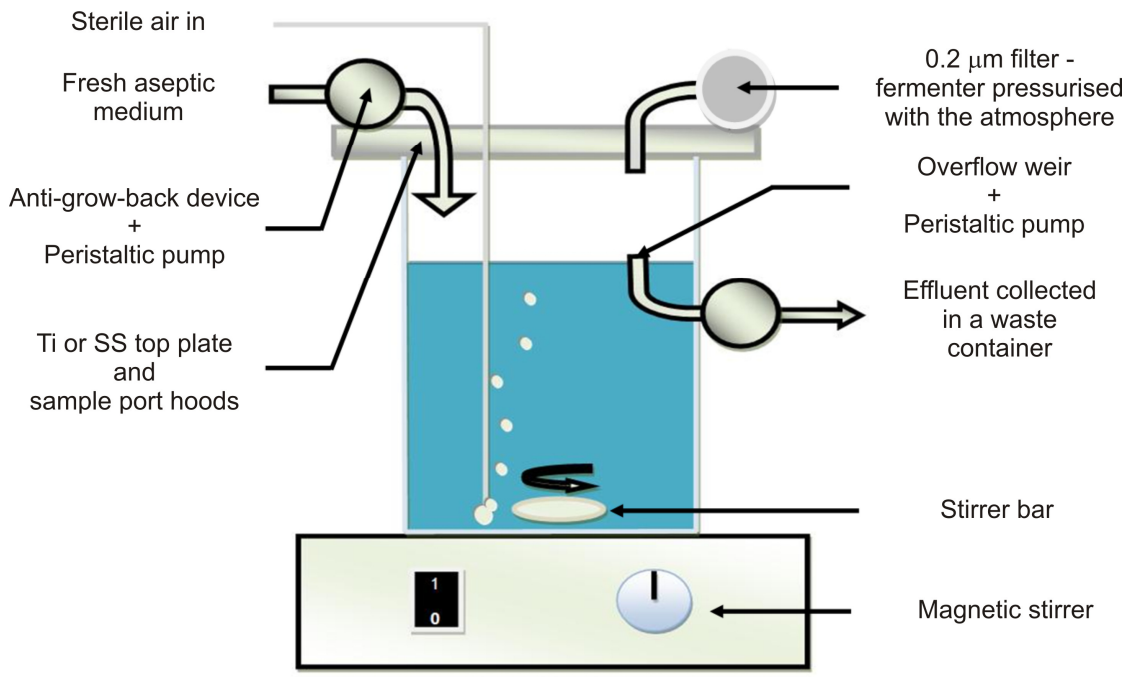

Figure 3.6. Schematic of a chemostat for marine applications.

Typical fermenter heads of chemostats in **Figure 3.6** are made of Ti or SS for seawater applications (avoid leaching of Fe inside the culture medium) and are approximately 150 – 200 mm in diameter to be accommodated by 1 litre glass / Pyrex fermenter vessels [**3.64**]. In addition, a number of ports (12 – 19 mm in diameter) for housing electrodes and the aseptically insertion and retrieval of coupons (for subsequent microbiological and microscopic analyses) on the top can be used. Operating chemostats can employ 500 mL cultures in which, for instance fresh sterile medium can be introduced at a constant rate of 25 mL h^{-1} using a peristaltic pump, thus allowing a dilution rate of 0.05 h^{-1} (representative of $t_d \approx 13.9$ h) [**3.64**,**3.67**]. The anti-grow-back system (**Figure 3.6**) is used to minimise grow-back of culture in the sterile medium reservoir. Typical stirrer speeds are 300 rpm to ensure liquid homogenisation. A continuous sterile air supply at 50 mL min^{-1} enables constant DO level in the chemostat pressurised with an atmosphere suitable for aerobes, see **Figure 3.6**. Likewise, Teflon-coated magnetic stirrer bars can be utilised, together with the heater pad, to both favour external heating and stirring maintained at 30 °C and 300 rpm, respectively [**3.64**,**3.68**]. Similarly, the culture volume inside the chemostat is kept constant using an overflow weir connected to a peristaltic pump. Importantly, a pH controller can automatically regulate the pH of the culture measured by an autoclavable pH electrode to maintain a pH 7.0 [**3.64**,**3.68**].

Ideally, the growth of *Pseudoalteromonas* sp. NCIMB 2021 strain should be controlled using a chemostat. However, it requires a costly experimental setup and needs expertise to run effectively, for instance to ensure a defined dilution rate with $D_i \leq \mu_b$ to avoid loss of cell population or washout. As there may be many microbiological factors that are not crucial for the preliminary understanding of the interfacial EIS response (when bacterial biofilms develop on the Au surface) an alternative culturing strategy may be more appropriate for this project.

Flow culturing systems are methods often used to study microbial adhesive interactions [**3.69**]. In particular, flow devices aimed at studying microbial adhesion to substratum surfaces under carefully controlled hydrodynamic and mass transport conditions [**3.69**]. After consultation on the pros and cons of chemostats and flow device systems with Prof Keevil and Dr Webb from the SBS, the flow culturing method has been identified as a suitable system to be combined with the EIS technique for the following reasons:

- Flow culturing systems setup is more straightforward than that for chemostat (no concern regarding $D_i \leq \mu_b$ and simple inoculation of the flow chamber with the species using a syringe). Similarly, Dr Webb from the SBS and Dr Stoodley from nCATS at the UoS have expertise on flow devices and associated experimental procedures [**3.40**,**3.70**,**3.71**].
- Flow devices enable the embedment of an electrochemical sensor to study bacterial attachment, and allow the control of the electrodes position and their relative distance within the flow channel dimensions [**3.69**,**3.72**].
- The flow culturing method is a potential first step approach to hydrodynamic operating systems, *i.e*. the fluid flow through a heat exchanger [**3.21**].
- The hydrodynamic properties of parallel plate flow chamber design are established [**3.69**]. An estimate of the thickness of the viscous sublayer (δ_l in **Section 2.4.4.3**) could be in good agreement with the size of biofilms [**3.10**,**3.71**].

Marine flow cytometers are used to characterise suspended particles (density, size and optical properties), within a hydrodynamically focused fluid stream, based on their individual fluorescence and light scattering properties where a single wavelength beam of light is used to excite the stream of fluid [**3.73**,**3.74**]. The flow cytometry technique can count, identify cells (based on their optical properties) and sort populations of interest from a heterogeneous sample, since similar particles usually exhibit common light scattering and fluorescence properties [**3.73**-**3.75**]. For instance, the fluorescence-activated cell sorter (FACSort), with λ = 488 nm for an Ar source, at NOC can be used to study particles ranging from the sub-micron level up to about 40 μm in size dimension [**3.73**]. The flow cytometer accuracy depends on the number of events per second rate (monitored within the sheath fluid)*, i.e.* the number of bacterial cells detected per second [**3.75**]. However, the more this rate exceeds 1000 events per second, the less reliable is the measurable signal [**3.73**]. In order to minimise this counter effect, the threshold, which distinguishes useful signals from artefacts can be increased to remove excess noise. The flow rate of the sheath fluid for the hydrodynamically focused particles can also be reduced. In addition, moderate dilution can enhance accuracy of the measurable signal [**3.73**]. The Sideward light Scatter and Forward light Scatter modes of the FACSort instrument can be selected to record small size bacterial cells and to visualise stained cells, respectively [**3.73**,**3.75**]. The FACSort does not automatically generate cell counting as flow rates. Therefore, the liquid volume to be analysed has to be well-defined to count cells and 0.5 μm microspheres or beads at a known concentration and volume have to be added to the samples [**3.73**]. By counting the number of beads in a given sample, the liquid volume can be assessed. Thus, the volumetric concentration of any particles of interest is deduced [**3.73**]. By repeating this procedure with time, it is possible to generate a growth curve for bacterial species and do subsequent analyses, such as define the growth phases, and determine the bacterial cell population and also calculate μ_b, see **Section 5.1**. Although flow cytometers are less accurate than chemostats, they are quick and straightforward to use for the proposed project. As a result, flow cytometry will be used to assess relevant microbiological factors of *Pseudoalteromonas* sp. NCIMB 2021, *i.e.* the growth phases, cell density and μ_b (**Section 5.1**).

3.2.5 Summary of experimental controllability

Section 3.2.4 has outlined the complexity incurred to the selection of a suitable continuous culture device that should meet biological and physico-chemical requirements with regard to real operating systems. A chemostat may be viewed as the most realistic laboratory scale approach to date but is probably an overly complex system to setup and fully address for the proposed engineering project. In this instance, a flow cell device in which an electrochemical sensor can be embedded offers flexible opportunities for bacterial biofilm monitoring in a controlled environment. The modified flow cell configuration incorporating the sensor will be similar to those used by Dr Webb (SBS) and Dr Stoodley (nCATS) at the UoS to ensure a reproducible method to study bacterial attachment within the flow chamber. In agreement with the concluding remark in **Section 2.4.4.6**, a low laminar flow regime ($R_e \approx 1$) will be used for the EIS testing (see **Chapter 4** for a detailed discussion). In accordance with **Sections 3.2.2** and **3.2.3** (complete description of the experimental protocol in **Chapter 4**), the EIS experiments will be made within a Faraday cage in NOC laboratory temperature controlled conditions at 18 ± 1 °C. Similarly, fresh, aseptic and continuously aerated, and also buffered ASW solutions (enriched with organic carbon source and of known chemical composition) will be prepared. Likewise, the physico-chemical properties of the media (conductivity, pH and DO level) will be measured before testing. In addition, the equipment such as the electrochemical sensors, flow chambers, reservoir vessels, tubes, and media will be sterilised and / or sealed to avoid air contaminants. The growth curve of *Pseudoalteromonas* sp. NCIMB 2021 will be studied using flow cytometry, thus allowing assessment of the corresponding cell population for a specific growth phase / stage and an estimate of the growth rate.

Although nature seawater is composed of many different microorganisms (which may affect the chemical properties of the surrounding environment), working with a single bacterial strain (not realistic to natural systems) is necessary in order to provide greater controllability. However, once the sensor response has been characterised and determined to be capable of detecting a well-defined bacterial species, the applicability of the measurement procedure will then be assessed for the more complex systems, for example sampled seawater.

Chapter 4 – Experimental details

4.1 Surface characterisation

Optical microscopy and surface optical profilometry were performed using an Olympus BH2-UMA with the digital images rendered using Motic MCCamera software (Camera: Moticam 1000, 1.3 million pixel, USB 2.0) and a Zygo NewView™ 7000 Series profiler to assess the performance of the Au electrode polishing.

4.2 Specifications of the Au electrode

The 0.2 mm diameter Au electrodes consisted of:

- a 0.2 mm diameter Au wire (Goodfellow) with metallic impurities determined as follows: 6 ppm Fe, 9 ppm palladium (Pd), 4 ppm Pt and 7 ppm rhodium (Rh),
- a 5 mm diameter glass housing in which the Au wire was embedded and,
- a Ni / Pt wire to make the electric contact, see **Figure 4.1**.

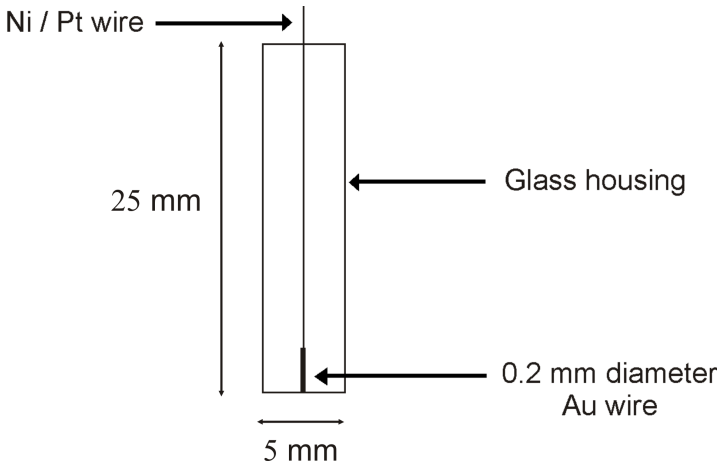

Figure 4.1. Schematic of the 0.2 mm diameter Au electrode.

4.3 Au surface preparation

The 0.2 mm diameter Au electrode surfaces were ground and polished before testing. **Table 4.1** shows the different grinding and polishing steps utilised. The electrodes were cleaned using an ultrasonic bath (Ultrawave cleaning solution, *i.e.* Ultraclean M Formula II with about 25 – 50 mL of detergent for 1 L of water) for 5 – 10 minutes between each grinding and polishing step to prevent contamination to successive cloths.

Table 4.1. Grinding and polishing method used for pure Au.

Process	**Grinding**		**Polishing**		
Step	1	2	3	4	5
Surface / Paste	#1200	#4000	6 μm	1 μm	0.3 μm
Lubricant Type	Water	Water	DP-Blue	DP-Red	DP-Red
Speed / rpm	300	300	300	200	200
Holder direction	→	↑	←	↓	→
Time / min	1-2	1-2	1-2	4	2-3

Struers DP-Blue and DP-Red lubricating liquids were used with the diamond polishing pastes. The final polishing step was achieved using a 0.3 μm Al_2O_3 powder. Polishing of the 0.2 mm diameter Au electrodes was not straightforward since Au is a ductile metal and great care is required to remove scratches without generating more. Thus, the polishing cloths needed to be clean and free of any contamination. Using the optimised procedure, as described in **Table 4.1**, a good electrode surface was obtained, see **Figure 4.2**.

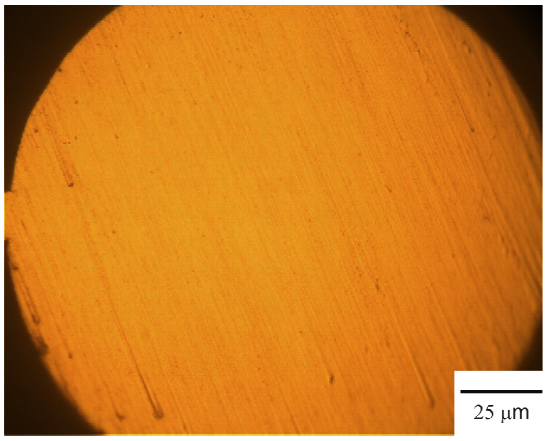

Figure 4.2. Optical microscopy image showing the 0.2 mm diameter Au electrode surface after grinding and polishing steps as detailed in **Table 4.1**. The scale was determined using a graticule, Tonbridge, Kent, England (100 x 0.01 mm).

The surface profile of the 0.2 mm diameter Au electrode obtained using the Zygo optical profiler shows a concave feature due to the ductile nature of the Au and harder glass at the edges of the surface electrode, see **Figures 4.3(a)** and **4.3(b)**.

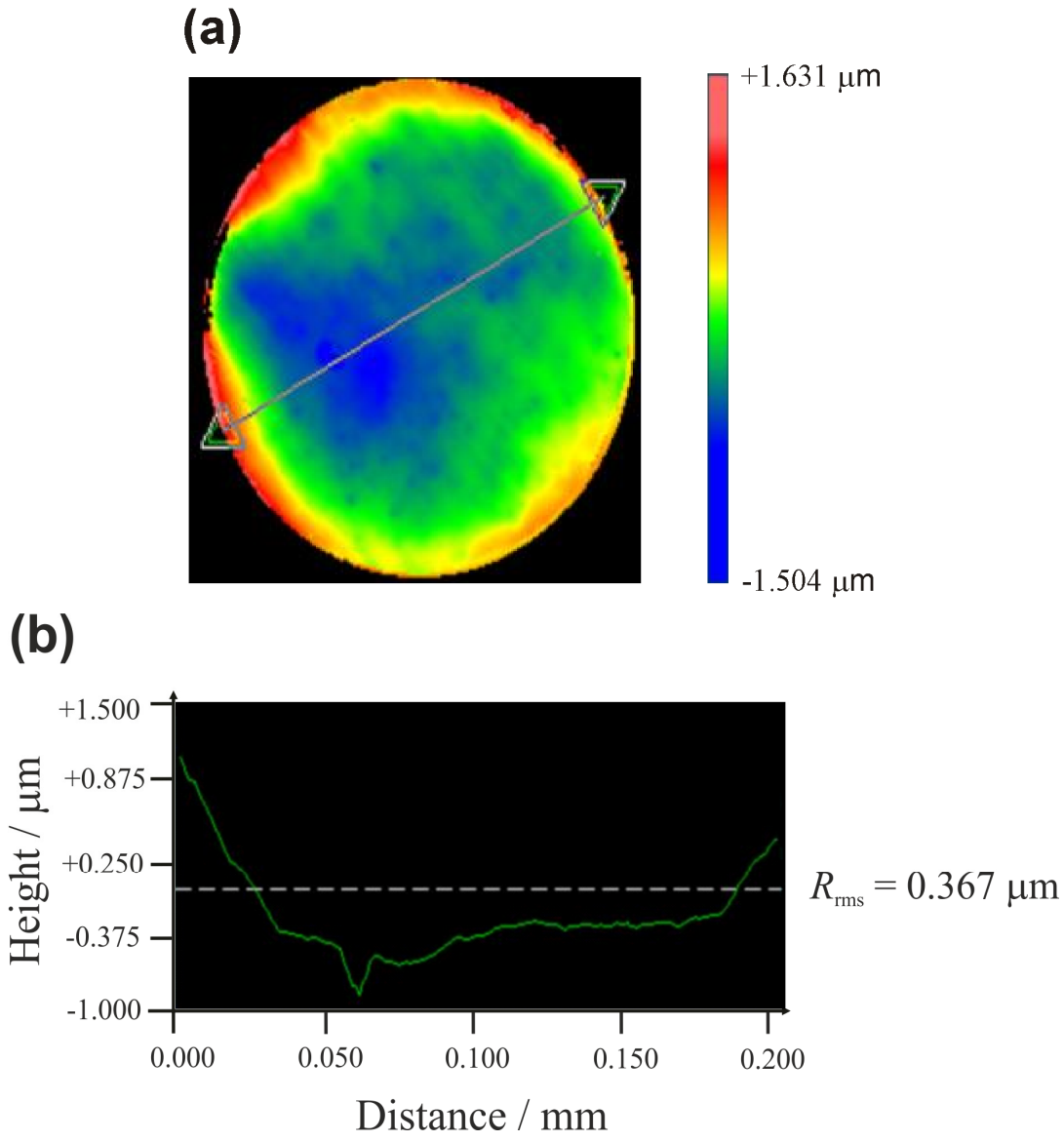

Figure 4.3. **(a)** Surface optical profile showing the 0.2 mm diameter Au electrode surface with pronounced glass edge effects after grinding and polishing steps in **Table 4.1** and **(b)** the root mean square roughness of the profile, R_{rms} = 0.367 μm.

However, the root mean square roughness R_{rms} = 0.104 μm of the Au surface (with limited glass edge effects) in **Figures 4.4(a)** and **4.4(b)** was about three times lower than that in **Figures 4.3(a)** and **4.3(b)** (with pronounced glass edge effects), R_{rms} = 0.367 μm.

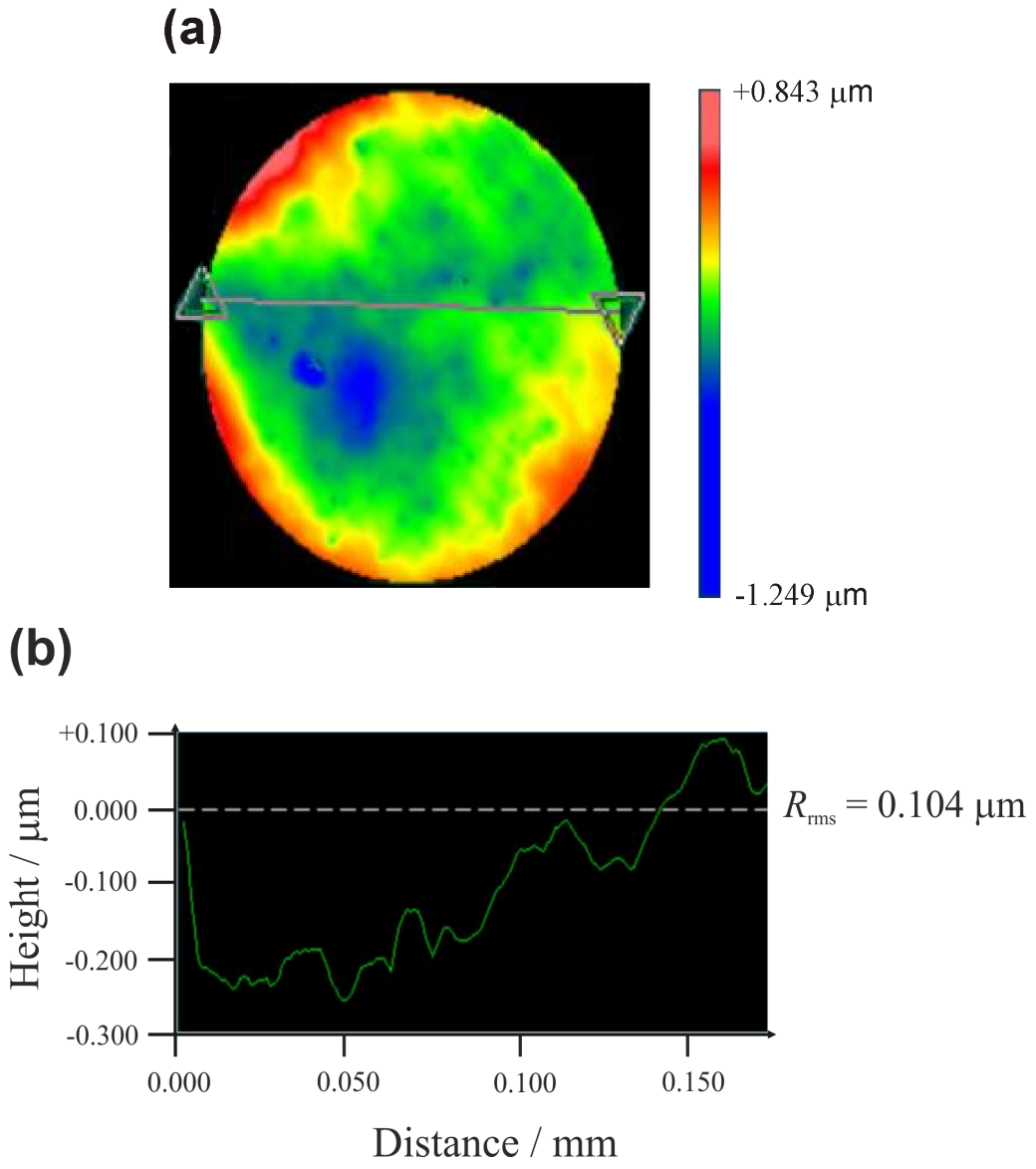

Figure 4.4. **(a)** Surface optical profile showing the 0.2 mm diameter Au electrode surface with limited glass edge effects after grinding and polishing steps in **Table 4.1** and **(b)** the root mean square roughness of the profile, R_{rms} = 0.104 μm.

Overall, the R_{rms} value of 0.104 μm was acceptable for the experimental work programme, since the roughness was both below the Al_2O_3 powder size (0.3 μm) of the last polishing step in **Table 4.1** and the actual size of a bacteria cell from the genus *Pseudoalteromonas* (which is typically about 1 μm in size [**4.1**]). After polishing, the 0.2 mm diameter Au electrodes were cleaned using an ultrasonic bath for 5 – 10 minutes, rinsed thoroughly with ethanol to remove any remaining organic material / debris and dried using a Metaserv specimen dryer.

4.4 Test solutions

The freshly prepared, 0.22 µm filtered and flush test solutions were (*i*) 3.5 % NaCl solution at pH 8.0, (*ii*) abiotic ASW, ASW with a single aerobic *Pseudoalteromonas* sp. strain NCIMB 2021, and also (*iii*) ASW with 500 nM of the NO donor SNP (using SNP crystals dissolved in ASW and flushed into the flow cell) on a 72 h-old biofilmed Au surface. In particular, the fresh SNP solution was protected against light (0.12 ± 0.01 µmol photons m^{-2} s^{-1}) and kept over a maximum 12 h duration before being changed to minimise light side effects [**4.2**,**4.3**]. The abiotic ASW at a pH 8.1 contained dissolved salts and metal-ions, vitamins and nutrients [**4.4**], see **Table 4.2**. Although the seawater composition by Riegman *et al.* (**Table 4.2**) has been commonly approved in the published literature, the concentration of sodium bicarbonate ($NaHCO_3$) may be twice as high as to that for natural seawater. After discussions with Dr Iglesias-Rodriguez (NOC), it was suggested that this bacterial growth environment can correspond to nutrient-replete conditions (as opposed to nutrient-limited conditions), thus favouring the exponential bacterial growth for heterotrophic bacteria (**Section 3.2.3.2**). In addition, 0.1 % (w/v) tryptone and 0.07 % (w/v) yeast extract were added to enhance the abiotic ASW organic carbon levels, resulting in a similar test condition to [**4.5**]. Alternatively, a control ASW (see **Chapter 5**) test solution made of dissolved salts and metal ions, and also ethylenediaminetetraacetic acid (EDTA) to keep metal ions in solution (**Table 4.3**), was used to support the discussion in **Section 5.8**. All the prepared solutions were made at the NOC using 18.2 MΩ cm Milli-Q water.

4.4.1 Bio-chemical characteristics of the test media

In comparison with the abiotic ASW and ASW with *Pseudoalteromonas* sp*.,* the 3.5 % NaCl solution was free of organic matter and represents a sterile condition, and also a typical control test to assess the ORR in alkaline conditions [**4.4**]. In addition, compared to ASW with *Pseudoalteromonas* sp., the abiotic ASW was free of living organisms but still contained organic matter, which was able to pass through the 0.22 µm filter. This coincided with a baseline for an adsorbed organic material (conditioning film) on the Au surface [**4.7**,**4.8**]. The *Pseudoalteromonas* sp. inoculated in ASW represented a more complex biochemical media, which contained organic material and living organisms (biotic). The environment for the test solution using ASW with the NO donor SNP was also biotic due to the presence of *Pseudoalteromonas* sp. biofilms on the Au surface, see **Table 4.4**.

Table 4.2. Composition of seawater: Riegman *et al.*, adapted from [**4.4**] – anhydrous (ANH) stands for a substance that contains no water.

Chemical	Molar mass / g mol^{-1}	Concentration / mol L^{-1}
NaCl	58.44	0.42
$MgCl_2.6H_2O$	203.31	54.4×10^{-3}
$CaCl_2.2H_2O$	147.02	10.5×10^{-3}
Na_2SO_4	142.04	22.7×10^{-3}
K_2SO_4	174.27	4.9×10^{-3}
$NaHCO_3$	84.01	4500×10^{-6}
d-Biotin	244.3	0.164×10^{-9}
Thiamine-HCl	337.3	59.3×10^{-9}
Cyanocobalamine	1355.4	0.59×10^{-9}
$FeCl_{3(ANH)}$	162.21	5.86×10^{-6}
$NaEDTA.2H_2O$	372.2	5.85×10^{-6}
$CuSO_4.5H_2O$	249.68	0.02×10^{-6}
$ZnSO_4.7H_2O$	287.5	0.038×10^{-6}
$CoCl_2.6H_2O$	237.9	0.021×10^{-6}
$MnCl_2.4H_2O$	197.9	0.46×10^{-6}
$Na_2MoO_4.2H_2O$	241.95	0.012×10^{-6}
KBr	119.01	92.4×10^{-6}
$SrCl_2.6H_2O$	266.62	13.4×10^{-6}
$AlCl_3.6H_2O$	241.43	0.1×10^{-6}
LiCl	42.39	0.071×10^{-6}
KI	166.01	0.06×10^{-6}
H_3BO_3	61.83	3.2×10^{-6}
RbCl	120.92	0.36×10^{-6}
$NaNO_3$	84.99	100×10^{-6}
NaH_2PO_4	119.98	6.24×10^{-6}

Table 4.3. Composition of the control ASW (see **Figures 5.10** and **5.11** in **Section 5.8**) medium based on Riegman *et al.*, adapted from [**4.4**].

Chemical	**Molar mass / g mol^{-1}**	**Concentration / mol L^{-1}**
NaCl	58.44	0.42
$MgCl_2.6H_2O$	203.31	54.4×10^{-3}
$CaCl_2.2H_2O$	147.02	10.5×10^{-3}
Na_2SO_4	142.04	22.7×10^{-3}
K_2SO_4	174.27	4.9×10^{-3}
$FeCl_{3(ANH)}$	162.21	5.86×10^{-6}
$NaEDTA.2H_2O$	372.2	5.85×10^{-6}
$CuSO_4.5H_2O$	249.68	0.02×10^{-6}
$ZnSO_4.7H_2O$	287.5	0.038×10^{-6}
$CoCl_2.6H_2O$	237.9	0.021×10^{-6}
$MnCl_2.4H_2O$	197.9	0.46×10^{-6}
$Na_2MoO_4.2H_2O$	241.95	0.012×10^{-6}
KBr	119.01	92.4×10^{-6}
$SrCl_2.6H_2O$	266.62	13.4×10^{-6}
$AlCl_3.6H_2O$	241.43	0.1×10^{-6}
LiCl	42.39	0.071×10^{-6}
KI	166.01	0.06×10^{-6}
H_3BO_3	61.83	3.2×10^{-6}
RbCl	120.92	0.36×10^{-6}

Table 4.4. Biochemical characteristics of the test media.

Media	Biochemical characteristics	Information
3.5 % NaCl, pH 8.0	Organic free – Sterile	Baseline for the ORR (3.5 % NaCl in **Chapter 5**)
0.1 % (w/v) tryptone and 0.07 % (w/v) yeast extract in ASW (**Table 4.2**), pH 8.1 [**4.4**,**4.5**]	Organic matter – Sterile – Abiotic	Baseline for a conditioning film (adsorbed organic layer) (Abiotic ASW in **Chapter 5**)
Control ASW test solution (**Table 4.3**)	EDTA – Sterile – Abiotic	Baseline for complex metal-ions (Control ASW in **Chapter 5**)
0.1 % (w/v) tryptone and 0.07 % (w/v) yeast extract in ASW (**Table 4.2**) with 200 µL aliquot of 2h-old *Pseudoalteromonas* sp. strain NCIMB 2021 culture, pH 8.1	Organic matter – Non-sterile – Biotic	Biofilm (Biotic ASW in **Chapter 5**)
500 nM of the NO donor SNP [**4.9**] in 0.1 % (w/v) tryptone and 0.07 % (w/v) yeast extract in ASW **(Table 4.2)**, pH 8.1 on a 72 h-old biofilmed Au surface	Organic matter – Non-sterile – Biotic – Environmentally friendly biocide	Biofilm dispersal (500 nM SNP in ASW, see **Chapter 5**)

4.4.2 Physico-chemical properties of the test media

The physico-chemical properties of the test media in **Table 4.4**: conductivity, DO, pH and temperature were assessed before each test (**Table 4.5**), thus allowing any variations to be identified with regard to typical values reported in nature in the North Atlantic Ocean, see **Section 3.1.2**. The conductivity, DO level and pH of the solutions were measured using an ATI Orion model 162 conductivity meter, a Hanna Instruments HI9145 DO probe with a water movement of about 0.3 m s^{-1} and a Hanna Instruments HI99129 Combo probe, respectively. All experiments were made under laboratory temperature controlled conditions at 18 ± 1 °C using the NOC facilities.

Table 4.5. Comparison of the physico-chemical properties of the media measured before testing (0 h).

Properties	**Test Media**				
	3.5 % NaCl, pH 8.0	0.1 % (w/v) tryptone and 0.07 % (w/v) yeast extract in ASW (**Table 4.2**), pH 8.1	Control ASW test solution (**Table 4.3**)	0.1 % (w/v) tryptone and 0.07 % (w/v) yeast extract in ASW (**Table 4.2**) with 200 µL aliquot of 2h-old *Pseudoalteromonas* sp. strain NCIMB 2021 culture, pH 8.1	500 nM of the NO donor SNP in 0.1 % (w/v) tryptone and 0.07 % (w/v) yeast extract in ASW (**Table 4.2**), pH 8.1 on a 72 h-old biofilmed Au surface
	3.5 % NaCl in **Chapter 5**	Abiotic ASW in **Chapter 5**	Control ASW in **Chapter 5**	Biotic ASW in **Chapter 5**	500 nM SNP in ASW, see **Chapter 5**
Conductivity / mS cm^{-1}	50.4 at 22 °C	49.5 at 21.5 °C	49.6 at 21.7 °C	49.9 at 21.8 °C	47.9 at 20.1 °C
DO level / ppm	6.90	6.90	6.90	6.90	6.90
pH	8.0	8.1	8.1	8.1	8.1
Temperature / °C	18.5	18.9	18.6	18.8	18.5

The conductivity measurements of the freshly prepared laboratory solutions (NaCl and ASW media) were consistent with a salinity of 35 ‰ and representative of typical values found in open surface seawaters. Overall, the test had an alkaline pH 8.0 ± 0.2, which is within the range normally cited for seawater, *i.e.* pH 7.7 to 8.3 for surface waters. The temperature of 18 ± 1 °C was acceptable for seawater since it can range in **Figure 4.5** between 5 and 22 °C (the winter and summer extremes). In addition, the average value of 6.90 ppm for the DO level was in agreement with aerated surface seawater (where it can vary substantially in **Figure 4.5**).

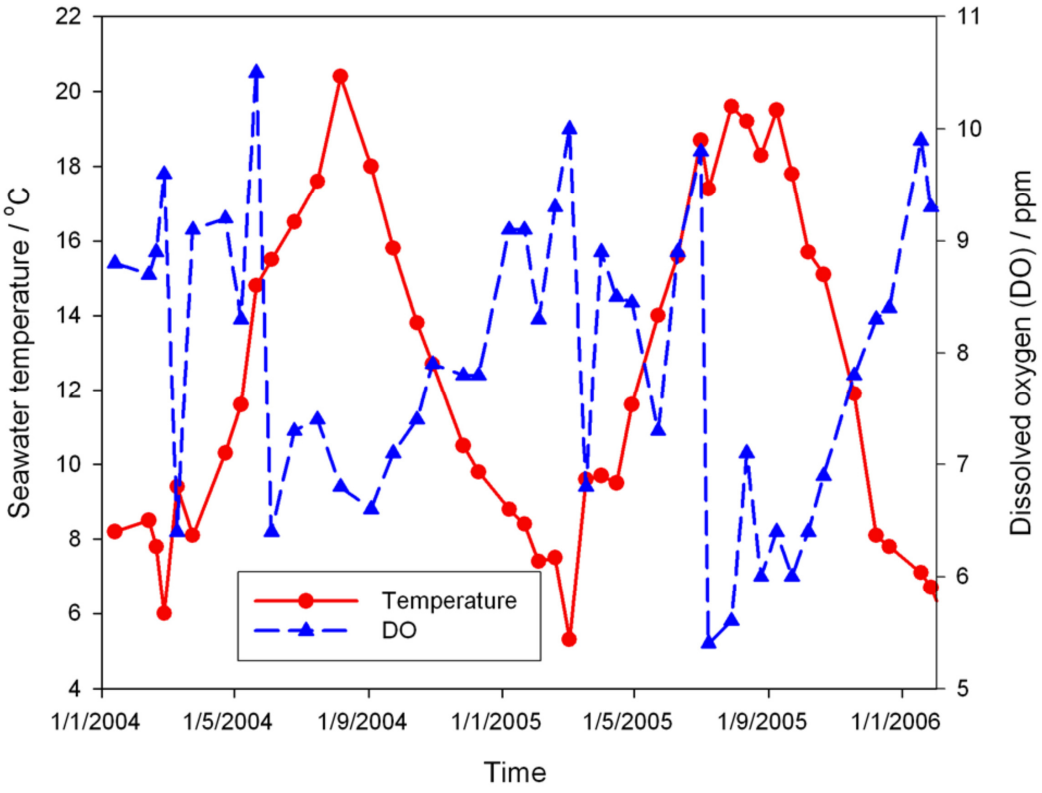

Figure 4.5. Seawater DO concentration and temperature measured at the NOC site, from [**4.10**].

The corresponding solutions in **Table 4.5** have remained clear over the entire test duration, thus showing the absence of backflow that could have affected the results in **Chapter 5**.

4.4.3 Summary of the test media analysis

Overall, the freshly prepared laboratory solutions, *i.e*. 3.5 % NaCl test solution, abiotic and biotic ASW media with a salinity close to 35 ‰, pH ≈ 8, temperature of 18 ± 1 °C and DO content of ≈ 6.90 ppm were representative of surface seawater from the North Atlantic equilibrated with the atmosphere [**4.11**]. The information obtained from these measurements in bulk water analysis have limited significance and cannot be representative of the Au / ASW interface, but should remain relatively constant to minimise an influence on a biofilm. This can be explained by the limited diffusion behaviour of biofilms, where the chemical composition within and nearby these biological systems can vary significantly within a few micrometers [**4.12**]. A suitable residence time should be used within the flow chamber, *i.e.* it should be long enough for bacterial adhesion (see **Section 4.6.2**) and sufficiently short to ensure constant supply of DO level (6.90 ppm) during bacterial biofilm growth and extent. Ideally, the physico-chemical properties of the test media should therefore be monitored *in situ* within and nearby the sensing site.

4.5 *Pseudoalteromonas* sp. NCIMB 2021 strain growth characteristics

4.5.1 Sub-culture of *Pseudoalteromonas* sp. into solid agar media

The marine aerobic bacterium *Pseudoalteromonas* sp. NCIMB 2021 strain was supplied in freeze-dried bacterial cultures from the NCIMB in Aberdeen, UK. The certificate of authenticity n°11479 for NCIMB parent cultures was provided by Dr Peter N Green, the NCIMB Curator. The contents were in a vacuum-sealed ampoule, which were to be opened for the germination of cultures under aseptic conditions using a flame. A small volume (0.5 mL) of an autoclaved agar solution, similar to the NCIMB Medium 210, was added to the ampoule and the contents mixed, avoiding frothing. The 1 L pH 7.3 agar solution contained: 3.0 g of yeast extract, 5.0 g of tryptone, 15.0 g agar, 0.750 L of 0.22 μm filtered aged seawater (seawater from the Solent kept 3 – 4 months in the dark in controlled temperature room at 6 ± 1 °C) and 250 mL 18.2 MΩ cm Milli-Q water. Then, 200 μL of media inocula, *i.e.* the initial content of the ampoule, plus agar solution, was dropped using a micropipette into a solid agar sterile Petri dish (made with 20 mL of agar solution using the NCIMB Medium 210 and dried at room temperature under aseptic conditions). A sterile bioloop was then used to spread the inoculum on the agar plate. The rest of the ampoule contents (not necessary for the

experiments) were autoclaved and safely disposed off in biohazard bags. The agar plates inoculated with *Pseudoalteromonas* sp. were cultured in a controlled temperature room of 18 ± 1 °C. After 2 – 3 days of growth, distinct microcolonies were observed on the agar plate. The procedure of subculturing was repeated more than once by picking-up one single microcolony from a culture plate and inoculating a sterile agar Petri dish, plus subsequent spreading using a sterile bioloop. As recommended by NCIMB, this is a precaution against accidents and ensures a viable culture (resuscitated freeze-dried cultures tend to exhibit a lengthened lag period).

4.5.2 *Pseudoalteromonas* sp. growth curve establishment

A continuously aerated and stirred sterile standard batch culture containing 250 mL agar NCIMB medium 210 solution was used to grow *Pseudoalteromonas* sp. strain NCIMB 2021 over 72 h in a controlled temperature room of 18 ± 1 °C. A series of three 2 mL samples were collected from the batch culture at different time intervals, *i.e.* 0 h, 4 h, 21 h and 72 h, to allow time-dependent bacterial cell populations assessment using a FACsort marine flow cytometer (Ar source at λ = 488 nm) at the NOC. Also, two series of three samples diluted 10 and 100 times were prepared. This ensured measurable signals from the flow cytometer (poor measurements due to either too dense or excessively diluted samples), see **Section 3.2.4.2**. A 1 % final concentration paraformaldehyde was used in each sample as a fixative to kill *Pseudoalteromonas* sp. cells and preserve their membranes. All the samples were mixed using a vortex and then stored at –20 °C. Prior to doing flow cytometry measurements, all the samples were defrosted in an oven at 35 °C for about 5 – 10 minutes. A series of 580 µL samples in polystyrene rand-bottom tubes were prepared with a 500 µL culturing solution, 5 µL DNA-Stain SYBr Green I (Sigma-Aldrich) at a ratio of 1:100, 50 µL potassium citrate solution at a ratio 1:10 and 25 µL of bead stock solution from NOC, *i.e.* containing 1,125,485 beads per mL. All contents were thoroughly mixed to ensure solution homogeneity. This procedure allowed the preparation of 200 µL aliquots of 2 h-old *Pseudoalteromonas* sp. culture (inoculum) for the electrochemical experiments in **Chapter 5**. Similarly, the protocol for growth curve establishment was repeated within the flow cell to address any variability in comparison with the standard batch culture, see **Section 5.1**. Ideally, the batch culture content should be identical to the ASW test solution to minimise environmental stresses toward bacterial cells. In that instance, however, the NCIMB Medium 210 was chosen and recommended by the NCIMB in Aberdeen, UK as a standard growth solution for *Pseudoalteromonas* sp. strain NCIMB 2021.

4.6 Flow cell arrangement

A modified once through flow cell device was designed to operate under a controlled low laminar flow condition ($R_e \approx 1$), see **Figure 4.6**. The overall system consists of a new engineering approach to study initial bacterial biofilms development and extent under a controlled flow cell environment. The flow cell arrangement hosted three embedded flush electrodes for the EIS experiments. EIS was chosen as a suitable non-destructive electrochemical method to monitor biofilm over time (see **Sections 2.6.4.3** and **2.6.5** for a detailed description of the EIS technique) [**4.13**]. The modified flow cell system had a 0.2 mm diameter Au working electrode mounted on the top surface to avoid gravitational effects, a homemade Ag/AgCl – saturated 3.5 M KCl solution reference electrode and graphite counter electrode mounted on opposing sides to ensure good repeatability of the electrodes position and their relative distance using the flow channel dimensions, see **Figure 4.6**. Whereas the Ag/AgCl reference electrode is appropriate for seawater systems [**4.14**,**4.15**], the graphite counter electrode is commonly used as an electrically conductive and high surface material (limitations of measurement interferences with the working electrode) [**4.16**]. The Au electrodes were sealed under reduced pressure in a soda glass pipette using a heating coil as described in [**4.17**] before being embedded in the flow cell device.

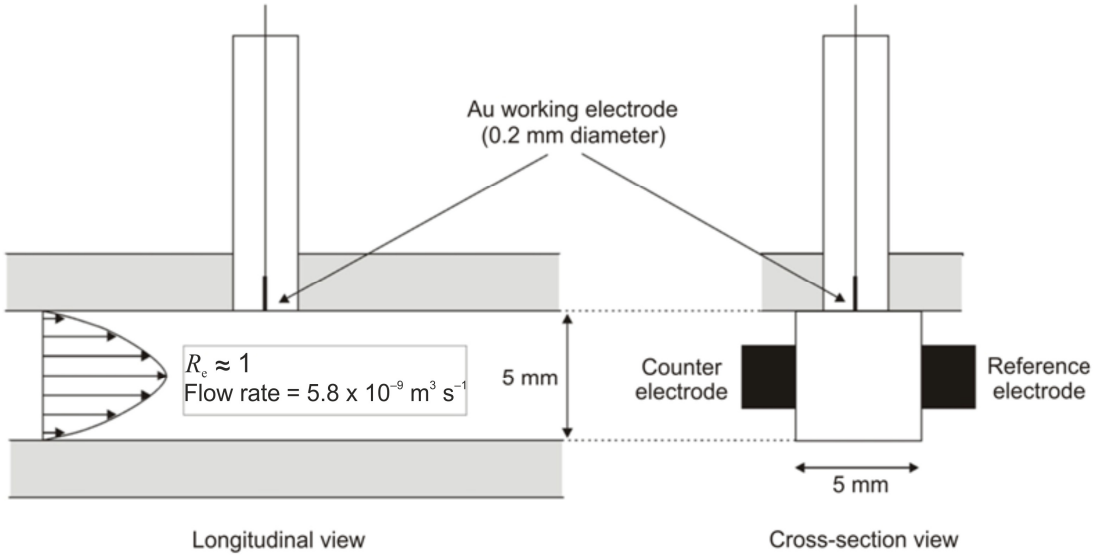

Figure 4.6. Schematic illustration of the flow cell electrode arrangement for EIS measurements.

The once-through flow cell (5 × 6 × 40 mm) was made of polycarbonate (PC) and was similar to a configuration utilised by Dr Webb from the SBS at the UoS. The PC material is generally not recommended for autoclaves since this can result in crazing or cracking due to moulding stresses. However, PC is often used for marine bacteria settlement studies in flowing seawater [**4.18**,**4.19**].

4.6.1 Flow cell channel design

The flow cell channel was designed to minimise abrupt fluid distortion of the ingoing and outgoing flow, which can lead to turbulence effects. A series of Upchurch connectors were used to enlarge and narrow the flow at the inlet and outlet, respectively. They were associated with two 6 degree conical angle diffusers to minimise flow separation and pressure losses incurred by sudden enlargements or contractions [**4.20**-**4.22**]. These configurations represent a good compromise, where the included angle θ_K is sufficiently small to limit separation, flow eddy, pressure losses, but large enough to minimise frictional losses, see **Figures 4.7** and **4.8**.

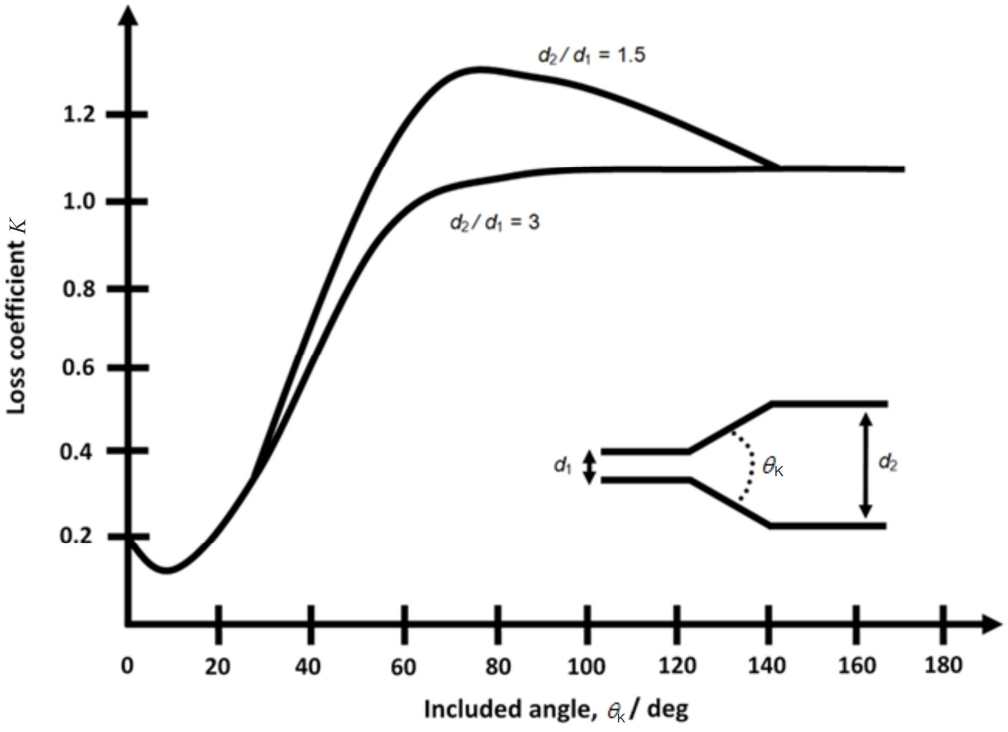

Figure 4.7. Loss of pressure in a conical diffuser, from [**4.20**].

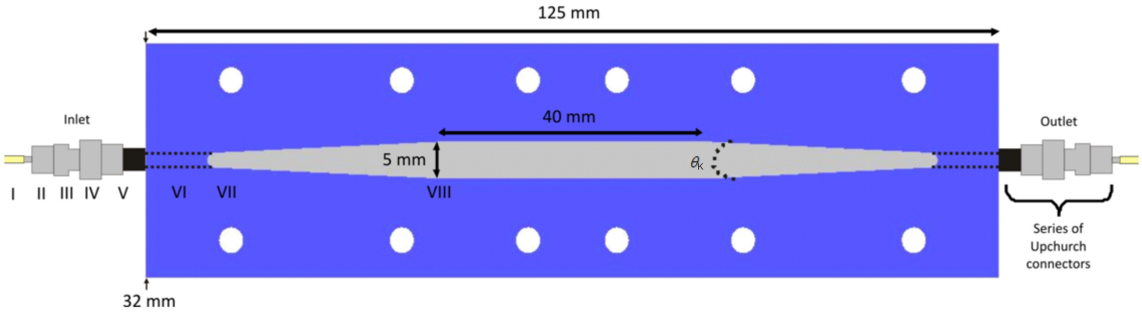

Figure 4.8. Plan view of the core plate showing the included angle, θ_K= 6 deg.

In this configuration (**Figure 4.8**), the theoretical mean velocity (u) decreased by a factor of ten (from 20 to 0.2 × 10^{-3} m s^{-1}) when the fluid entered the flow chamber, see **Table 4.6**. A silicone rubber (biocompatible elastomer) gasket was also used to seal the two flow cell sections.

Table 4.6. Calculations of mean velocities at different (inlet / outlet) positions.

I	II	III	IV	V	VI	VII	VIII
Marprene tubing	P-692	P-652	P-669-01	P-672 + 10-32 FB NanoPort			
Ø 0.63 mm (bore)	Ø 0.5 mm (through-hole)	Ø 0.75 mm (through-hole)	Ø 1.00 mm (through-hole)	Ø 1.25 mm (through-hole)	Ø 2.00 mm (through-hole)	D_h = 3.00 mm	D_h = 5.45 mm
20 × 10^{-3} m s^{-1}	30 × 10^{-3} m s^{-1}	13 × 10^{-3} m s^{-1}	7.5 × 10^{-3} m s^{-1}	5 × 10^{-3} m s^{-1}	2 × 10^{-3} m s^{-1}	0.5 × 10^{-3} m s^{-1}	0.2 × 10^{-3} m s^{-1}

4.6.2 Hydrodynamic regime

As the flow cell geometry can have a significant effect on biofilm thickness and morphology (**Section 2.4.4.5**), a comparative study of flow cell dimensions (from the published literature) and the corresponding hydrodynamic parameters is addressed in **Table 4.7**, thus allowing the justification of the flow cell channel design and the operating flow regime for the proposed project. In addition, this investigation is based on theoretical computations for clean tubes in a standard 35 ‰ seawater environment at 20 °C.

Table 4.7. Comparison of the dimensions and theoretical hydrodynamic parameters of different flow cell configurations – calculations representative of the conditions **VIII** in **Table 4.6** for a 35 ‰ seawater environment (μ = 1.07 × 10^{-3} kg m^{-1} s^{-1} and ν_k = 1.05 × 10^{-6} m^2 s^{-1} at 20 °C) – * is indicative of potential concerns for the flow cell dimensions and / or flow regime.

Flow cell geometry	**Dimensions**						
	b / (m) × 10^{-3}	w' / (m) × 10^{-3}	w'/b	l' / (m) × 10^{-3}	W' / (m) × 10^{-3}	A' / (m^2) × 10^{-6}	D_h or d / (m) × 10^{-3}
Webb *et al.* [**4.19**]	1.0	4.0	4	40.0	10.0	4.0	1.60
Stoodley *et al.* [**4.30**]	10.0	5.0	0.5	250.0	30.0	50.0	6.67
Stoodley *et al.* [**4.31**]	6.0	10.0	10/6	45.0	32.0	60.0	7.50
Stoodley *et al.* [**4.25**]	10.0	5.0	0.5	240.0	30.0	50.0	6.67
Stoodley *et al.* [**4.26**] and Dunsmore *et al.* [**4.29**]	3.0	3.0	1	200.0	12.0	9.0	3.00
Salek *et al.* [**4.24**]	1.0	5.0	5	100.0	12.0	5.0	1.67
	2.0	2.0	1	100.0	8.0	4.0	2.00
Bayoudh *et al.* [**4.23**]	N/A	N/A	N/A	35.0	N/A	154.0	14.0
Current study	**6.0**	**5.0**	**5/6**	**40.0**	**22.0**	**30.0**	**5.45**

Flow cell geometry	Hydrodynamic parameters								
	Q / m^3 s^{-1}	u / m s^{-1}	R_e	L_e / m	Percentage of chamber length corresponding to hydrodynamically fully developed conditions	τ_w / Pa	ΔP / Pa	f_D	t_r / s
Webb *et al.* [**4.19**]	2.50×10^{-9}	0.625×10^{-3}	0.95	91.43×10^{-6}	99.8	3.34×10^{-3}	95.26×10^{-3}	76.57	64.0
Stoodley *et al.* [**4.30**]	4.50×10^{-6}	90.0×10^{-3}	571.43	228.69×10^{-3}*	8.5*	0.12	4.01	0.10	2.8*
Stoodley *et al.* [**4.31**]	1.40×10^{-6}	23.3×10^{-3}	166.43	74.89×10^{-3}*	$L_e > l'$*	26.60×10^{-3}	0.15	0.36	1.9*
	2.40×10^{-6}	40.0×10^{-3}	285.71	128.57×10^{-3}*	$L_e > l'$*	45.65×10^{-3}	0.26	0.21	1.1*
Stoodley *et al.* [**4.25**]	1.20×10^{-6}	24.0×10^{-3}	152.38	60.98×10^{-3}	74.6*	30.80×10^{-3}	1.02	0.39	10*
	25.25×10^{-6}	0.5	3174.60*	112.51×10^{-3}	53.1*	N/A	N/A	N/A	0.5*
Stoodley *et al.* [**4.26**]	9.0×10^{-6}	1.0*	2857.14*	49.72×10^{-3}	75.1*	N/A	N/A	N/A	0.2*
Dunsmore *et al.* [**4.29**]	90.0×10^{-9}	10.0×10^{-3}	28.57	5.14×10^{-3}	97.4	28.53×10^{-3}	1.69	1.99	20.0*
	0.36×10^{-6}	40.0×10^{-3}	114.29	20.57×10^{-3}	89.7*	0.11	6.77	0.50	5.0*
	0.90×10^{-6}	0.1	285.71	51.43×10^{-3}	74.2*	0.28	16.91	0.20	2.0*
	3.60×10^{-6}	0.4	1142.86	205.71×10^{-3}*	$L_e > l'$*	1.14	67.66	0.05	0.5*
Salek *et al.* [**4.24**]	33.30×10^{-9}	6.67×10^{-3}	10.59	1.06×10^{-3}	98.9	34.19×10^{-3}	2.45	7.21	15.0*
	33.30×10^{-9}	8.34×10^{-3}	15.89	1.91×10^{-3}	98.1	35.70×10^{-3}	1.58	3.56	12.0*
Bayoudh *et al.* [**4.23**]	6.41×10^{-9}	41.6×10^{-6}	0.55	0.47×10^{-3}	98.7	25.43×10^{-6}	0.25×10^{-3}	115.38	840.9
Current study	**5.83×10^{-9}**	**0.195×10^{-3}**	**1.01**	**0.33×10^{-3}**	**99.2**	**0.31×10^{-3}**	**1.99×10^{-3}**	**56.03**	**351.6**

4.6.2.1 Flow cell dimensions

Apart from Bayoudh *et al.* [**4.23**] who used a relatively large 14 mm diameter circular straight channel, the flow cell dimensions were within the same order of magnitude in terms of cross sectional area ranging between 4.0 and 60.0 $\times$ 10^{-6} m^2, and hydraulic diameter (**Equation 4.1**), which ranged between 1.60 and 7.50 $\times$ 10^{-3} m. As result, this reinforces the suitability of the flow cell geometry (5 $\times$ 6 $\times$ 40 mm) for the current study.

$$D_{\mathrm{h}} = \frac{4A'}{W'} \tag{4.1}$$

where D_{h} is the hydraulic diameter utilised to compute hydrodynamic parameters for non-circular straight pipes (*e.g.* use of D_{h} in **Equation 2.19** to calculate the Reynolds number for rectangular straight pipes) [**4.20**-**4.22**], W' the wetted perimeter of the rectangular cross-section (**Equation 4.2**) [**4.24**] and A' the cross sectional area of the flow chamber.

$$W' = 2(b + w') \tag{4.2}$$

with b the depth and w' the width of the flow chamber. In addition, it must be emphasised that the D_{h} model is limited by side ratios, where w'/b values greater than 4 (when the rectangular cross-section departs further from a circular one) can potentially induce flow prediction errors [**4.22**]. This might be an issue for the configuration proposed by Webb *et al.* [**4.19**] and Salek *et al.* [**4.24**].

4.6.2.2 Flow regime and entrance length

Most of the flow cells in **Table 4.7** were operating in a laminar flow regime to study bacterial adhesion with the exemption of Stoodley *et al.* [**4.25**,**4.26**], where higher flow conditions ($R_{\mathrm{e}} \approx$ 3,000) were also employed in order to examine the effect of flow on a biofilm (oscillation of biofilm streamers under flowing conditions [**4.25**] and localised growth and detachment events [**4.26**]). In addition, significantly low R_{e} values < 10 were reported by Webb *et al.* [**4.19**] and Bayoudh *et al.* [**4.23**] to study bacterial attachment and colonisation at a very low laminar regime. These conditions (and in

particular for the proposed approach) may represent enhanced controllable flow cell systems for bacterial growth, where the flow will have minimum effect on a biofilm. In contrast, the use of high velocity, *e.g.* u = 1 m s^{-1} (relevant to marine heat exchanger pipes), may need to be further addressed. In this instance, the pipe needs to be long enough to ensure hydrodynamically fully developed conditions, *i.e.* it represents over *circa* 95 % of the chamber length when the entrance effects become insignificant in **Table 4.7**, see **Equations 4.3** and **4.4** [**4.27**,**4.28**].

$$L_e = 0.06 R_e D_h \text{ for } R_e < 2{,}000 \tag{4.3}$$

$$L_e = 4.4 R_e^{1/6} D_h \text{ for } R_e > 2{,}000 \tag{4.4}$$

where L_e is the entrance length for a straight rectangular segment. **Equations 4.3** and **4.4** can also be applied for circular straight pipes of diameter d. Most pumps, heat exchangers and filters are designed to operate in optimum fully developed flow conditions at inlets and area changes to minimise streamwise wall shear stress gradients and unnecessary pressure drops [**4.22**,**4.24**,**4.27**]. Flow cell channels proposed by Dunsmore *et al.* (operating at 0.4 m s^{-1}) [**4.29**] and Stoodley *et al.* [**4.30**,**4.31**] in **Table 4.7** may have limited length to ensure fully developed flow conditions, therefore enhanced designs may be necessary. In contrast, the flow cell channel for the current study (**Table 4.7**) has been designed accordingly (more than 95 % of flow cell length corresponds to fully developed flow).

4.6.2.3 Sherwood number

As pointed out by Pletcher and Walsh [**4.27**], it is usually too complex to address a detailed description of the fluid-mechanical interactions within a variety of cell geometries, types of electrodes and flow patterns. However, suitable analytical relationships exist, for instance using the Sherwood number (to measure the rate of the mass transport) in a parallel-plate cell in fully developed laminar flow [**4.27**]. In this instance (apart from Bayoudh *et al.* [**4.23**] for a circular pipe), this is not applicable due to the low side ratio (w'/b should be > 6 [**4.27**]) of flow cells in **Table 4.7** as opposed to flow between infinitely wide parallel plates [**4.32**]. An alternative way of calculating the Sherwood number involves the use of the limiting current density for an electrode, where the corresponding potential is held at a value favouring the electrode reaction, *e.g.* the cathodic ORR [**4.27**]. In a rectangular channel electrode (*i.e.* flow cell with a stationary embedded electrode as for the current study), the analytical solution

between the mass transport limiting current and the flow rate is known [**4.33**]. Nevertheless, corroborative empirical measurements of process parameters such as mass transport inside flow cell channels are scarce, as a consequence a reliable assessment of the Sherwood number is extremely difficult [**4.27**]. Measurements of the mass transfer coefficient distribution as proposed by Stoodley *et al.* [**4.31**] that can provide insight into flow cell characterisation may be an exemption, see **Section 2.4.4.4**.

4.6.2.4 Wall shear stress and pressure drop

In piping systems, it is frequently recommended to predict the pressure drop but a true assessment of the average wall shear stress (τ_w) is often difficult [**4.22**]. Nevertheless, an approximate of the τ_w value for a rectangular cross-section in a laminar flow can be computed [**4.24**]:

$$\tau_w = \frac{8\mu u}{D_h} \tag{4.5}$$

Where μ = 1.07 $\times$ 10^{-3} kg m^{-1} s^{-1} is the dynamic viscosity of 35 ‰ seawater at 20 °C. In addition, D_h can be replaced by d in **Equation 4.5** when using circular pipes. Overall, the calculated values of average wall shear stress (for a seawater environment) in **Table 4.7** were consistent with, for instance, the corresponding data reported by Dunsmore *et al.* [**4.29**].

Alternatively, the relationship between major head loss and friction factor can be used to evaluate both the pressure drop and average wall shear stress. However, the exact analytical solutions for the velocity and pressure fields for laminar flow in a rectangular or circular straight pipe are well-established [**4.22**]. Therefore, it is not necessary to use the head loss and friction factor concept in **Table 4.7**. Nevertheless, the Darcy frictional resistance to fluid has been added since it is customary to include the friction factor for discussion on fluid hydrodynamics [**4.22**].

For a rectangular pipe in a laminar flow, ΔP depends on u [**4.22**]:

$$\Delta P = \frac{3\mu l' u}{b^2 F(w'/b)} \tag{4.6}$$

and similarly the analytical solution for the friction factor is [**4.22**]:

$$f_{\mathrm{D}} = \left(\frac{96}{R_{\mathrm{e}}}\right) G(w'/b) \tag{4.7}$$

Equation 4.7 is equivalent to **Equation 4.8**, which is derived from the analytical solution for a straight rectangular pipe [**4.20**-**4.22**]:

$$f_{\mathrm{D}} R_{\mathrm{e}} = \frac{48(w'/b)^{3/2}}{\left(1+(w'/b)\right)\left[1-\frac{192}{\pi^5 (w'/b)}\tanh\left(\frac{\pi}{2}(w'/b)\right)\right]}\left(\frac{4\sqrt{A'}}{W'}\right) \tag{4.8}$$

where $F(w'/b)$ is a function (derived expression in **Equation 4.10**) that depends only on the side ratio (w'/b) and $G(w'/b)$ is a geometric factor defined in **Equation 4.9** [**4.20**]:

$$G(w'/b) = \frac{1}{\left(1+\frac{b}{w'}\right)^2 F(w'/b)} \tag{4.9}$$

$$F(w'/b) = \left(\frac{2}{k_{\mathrm{F}}(w'/b)^{1/2}}\right)\left[1-\frac{192}{\pi^5 (w'/b)}\tanh\left(\frac{\pi}{2}(w'/b)\right)\right]\left(\frac{W'}{4\sqrt{A'}}\right) \tag{4.10}$$

where k_{F} = {3.00, 2.20, 2.00, 1.60, 1.25 and 1.20} for (w'/b) = {0.5, 5/6, 1, 10/6, 4 and 5} in **Table 4.8**, respectively.

In addition, **Table 4.8** represents the corresponding values of $F(w'/b)$, $G(w'/b)$ and $f_{\mathrm{D}}R_{\mathrm{e}}$ for different values of (w'/b).

For a circular straight pipe in a laminar flow (*e.g.* Bayoudh *et al.* [**4.23**] in **Table 4.7**), ΔP can be assessed using **Equation 2.18** in **Section 2.4.4.1**. In this instance, f_{D} is necessary and can be obtained for laminar flow using **Equation 4.11** [**4.20**-**4.22**]:

$$f_{\mathrm{D}} = \frac{64}{R_{\mathrm{e}}} \tag{4.11}$$

An alternative relationship to determine ΔP (for a circular straight pipe in a laminar flow, *e.g.* Bayoudh *et al.* [**4.23**] in **Table 4.7**) without the use of the friction factor can be [**4.22**]:

$$\Delta P = \frac{32\mu l' u}{d^2} \tag{4.12}$$

Table 4.8. Values of $F(w'/b)$, $G(w'/b)$ and $f_D R_e$ as a function of the side ratio (w'/b) for a rectangular segment – * is indicative of estimated values computed using **Equations 4.7** to **4.10** and included for comparison with **Table 4.7**, adapted from [**4.22**].

	(w'/b)	$F(w'/b)$	$G(w'/b)$	$f_D R_e = 96G(w'/b)$
	0.5*	0.18*	0.63*	60.23*
Thesis	**5/6***	**0.35***	**0.59***	**56.75***
	1	0.42	0.59	56.91
	10/6*	0.63*	0.62*	59.76*
	4	0.84	0.76	72.93
	5	0.87	0.79	76.28
Infinitely wide parallel plates	∞	1	1	96.0

The ΔP values in **Table 4.7** were low ranging between 0.25×10^{-3} and 67.66 Pa, thus consistent with reported pressure drop values < 250 Pa in a clean flow cell operating below 0.5 m s^{-1} [**4.25**,**4.34**].

4.6.2.5 Residence time

The residence time (t_r) of the flow cell in **Equation 4.13** can be defined as the amount of time the medium (*e.g.* an ASW medium) can spend inside the flow channel [**4.35**].

$$t_r = \frac{V_t}{Q} \tag{4.13}$$

where V_t is the total volume inside the flow channel.

Usually relevant to mixing flow in reactor [**4.31**], the residence time is, for the current investigation, informative of the time available for bacterial attachment preceding a new cycle of fresh flush solution at the intlet. Therefore, a low t_r value (*e.g.* 64 s [**4.19**]) can represent a minimum time for bacterial adhesion per cycle of flush medium. However, Webb *et al.* [**4.19**] used a 1 h incubation without flow to ensure bacterial colonisation inside the flow cell. In addition, extremely low residence time values, which ranged between 0.2 and 20.0 s, are noticed in **Table 4.7**. Herein, batch cultures connected to flow cells are mostly employed [**4.25**,**4.26**,**4.29**-**4.31**]. For instance, a 6 h bacterial growth is used before switching to continuous culture, thus referring to t_r values *circa* 1,560 s for the whole reactor – flow cell system (as opposed to flow cell as a stand-alone in **Table 4.7**) [**4.30**]. Additionally, Salek *et al.* [**4.24**] utilised a bacterial culture pumped through a circulating tubing network to allow bacterial colonisation for 24 h. Similar to Bayoudh *et al.* [**4.23**], a relatively long residence time of 351.6 s can correspond, for the current study, to favourable low laminar flow conditions for pioneering microbial adhesion and subsequent development (**Section 2.3**) within the flow channel, thereby potentially resulting in a rapid and nutrient limited stationary regime [**4.36**]. In particular for a laminar flow, mechanisms of Brownian motion or molecular diffusion normal to streamlines, which are more pronounced near solid or biofilm surfaces (in contrast with the streamwise direction more influenced by bulk convection) are most likely to be the dominant transport processes [**4.24**].

4.6.2.6 Relevance of laminar and turbulent flow

Pioneering work by Cornish suggested that the laminar flow conditions in a straight rectangular pipe using w'/b = 2.92 could be similar to that for a corresponding circular section. For w'/b = 1, the laminar flow regimes were still in good agreement (and in particular for the proposed work using a side ratio of 5/6 $\approx$ 0.83), whereas a significant offset was observed for $w'/b \rightarrow \infty$ [**4.32**]. For a turbulent regime, there are no analytical solutions but rather an empirical Moody Chart (f_D *vs.* R_e) used to assess the (Darcy) frictional resistance to fluid and the corresponding pipe roughness [**4.22**].

4.6.3 Summary of the flow cell devices analysis

The review on flow cells (used for bacterial adhesion study) in **Section 4.6.2** has outlined the limited knowledge of hydrodynamic processes from a microbiological standpoint, where engineering expertise is also necessary to develop appropriate bacteria culturing systems. Ideally, greater consensus between microbiologists and engineers should be required to commonly agree flow cell devices for bacterial biofilms. In this thesis, it was decided to design a rectangular flow cell channel of comparable dimensions to that found in the published literature with:

- minimum pressure losses and flow separation at the inlet / outlet,
- fully developed flow conditions (*i.e.* L_e = 0.33 × 10^{-3} m for a 40.0 × 10^{-3} m flow channel length), low wall shear stress (0.31 × 10^{-3} Pa) and pressure drop (1.99 × 10^{-3} Pa) for a clean rectangular flow channel, and
- a relatively long residence time of 351.6 s suitable for bacterial biofilm growth and extent.

4.6.4 Watson-Marlow peristaltic pump

A Watson-Marlow series 323S peristaltic pump (**Figure 4.9**) combined with small 0.63 mm bore Marprene tubes was used to generate a low flow rate, *i.e.* 5.83 × 10^{-9} m^3 s^{-1} to minimise pulsative flow effects. This ensured a calculated R_e close to ≈ 1 within the rectangular section of the flow channel consistent with a low laminar flow regime, see **Table 4.7**.

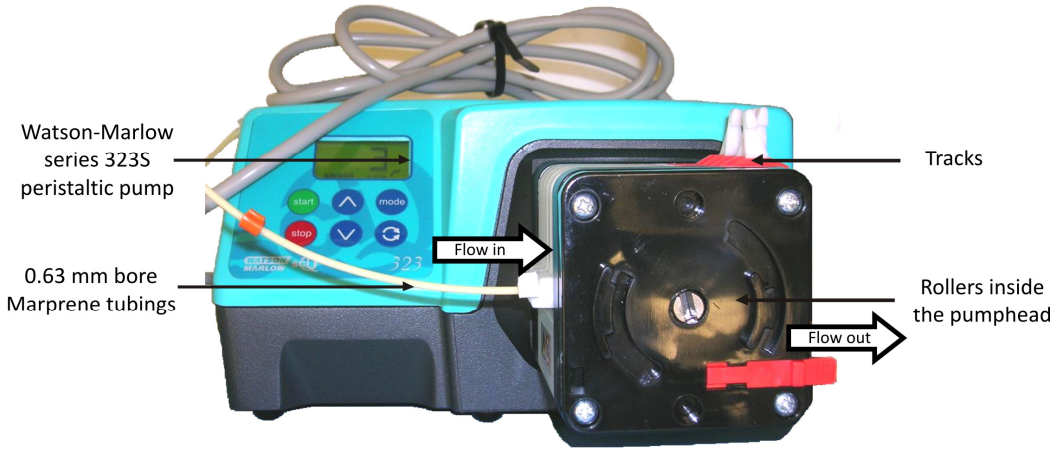

Figure 4.9. Watson-Marlow series 323S peristaltic pump working principle.

Although syringe pumps (more expensive) can provide continuous flow, Watson-Marlow Bredel peristaltic pumps are suitable for microbiology purposes since only the tubing is in contact with the fluid [**4.37**]. Consequently, this eliminates the risk of pump or fluid contamination. The liquid is drawn into the pumphead, it is then trapped between a system of rollers and a track. As the rollers move forward, liquid is expelled and a vaccum is created allowing more fluid to be drawn into the tubing (positive displacement) and so on [**4.37**], see **Figure 4.9**.

4.7 Electrochemical measurements

Cyclic voltammetry or CV at ν = 0.200 V s^{-1} in N_2 deaerated 1 M H_2SO_4 was used to characterise the surface state of the Au electrode. CV at ν = 0.100 V s^{-1} of the Au electrode in a 3.5 % NaCl solution was performed periodically or at 72 h under continuously air and N_2 sparging, aerated and deaerated conditions, respectively, to support the analysis of the cyclic voltammogram in the ASW media. Passing a stream of pure N_2 or Ar over the solution surface for about 30 min is often reported to be necessary to remove all residual O_2 [**4.38**,**4.39**]. However, a 5 – 10 min N_2 bubbling was sufficient for the current study to measure a detectable difference in bulk DO level, *i.e.* 6.90 and 0.20 ppm between the aerated and deaerated conditions (see **Chapter 5**). In addition, CV at ν = 0.100 V s^{-1} was utilised to electrochemically characterise the Au electrode in the abiotic and biotic media. Overall, the scan rates used were consistent with similar studies in [**4.17**]. A stable CV response was generally only obtained after 3 – 5 cycles. For clarity, E_r is the reduction potential of the corresponding reaction converted into potentials (*E vs.* Ag/AgCl, 3.5 M KCl). EIS measurements for the bacterial growth study (*i.e.* for the 3.5 % NaCl solution, the abiotic and biotic ASW) were made over 72 h at 18 ± 1 °C in the NOC using a Ref600 Gamry Instruments potentiostat and EIS300 software at the OCP. An additional 24 h was used for the biocide inhibition investigation, *i.e.* using 500 nM of the NO donor SNP on a biofilmed Au surface (see **Table 4.4**). The applied sinusoidal potential was 10 mV_{rms}, with a frequency range of 0.1 to 100,000 Hz. All the electrochemical tests were performed *in situ* in a Faraday cage both to minimise interference due to external electromagnetic fields and light irradiance. The light irradiance (inside the Faraday cage) was measured at 0.12 ± 0.01 µmol photons m^{-2} s^{-1} using a Li-Cor Li-189 Photometer [**4.40**]. The standard procedures for the selection of EC best-fit using the Gamry Echem Analyst software version 5.30 were followed: the χ^2 error was suitably low ($\chi^2 \leq 10^{-4}$), and the errors associated with each element were up to 5 %, see **Section 2.6.7**.

4.8 Experimental rig

Two vessels, a sealed 2 L reservoir pressurised with 0.2 µm filtered atmospheric air for test solution supply (see **Section 4.4**) and a waste container, were used for the experiments in **Tables 4.4** and **4.5**, see **Figure 4.10**. All the components of the whole system were sterilised. The glass vessels, Marprene tubings, Upchurch connectors made of polyetheretherketone (PEEK) were autoclaved at 120 °C. The flow cell device components (PC material, silicone rubber gasket), the polypropylene adapters for tubings were cleaned using bleach, whereas ethanol washes were used on the electrodes as an antiseptic. After cleaning, these elements were rinsed throughly with 18.2 MΩ cm Milli-Q water. The flow cell system (see **Figure 4.11**) was assembled under laminar flow chamber, *i.e.* under a particle-free and heated environment to perform microbiological or biotechnological procedures. The flush electrodes were clamped with screws embedded in the PC material. In addition, the N-008 Upchurch Scientific epoxy resin was carefully added and cured for 1 hour at 49 °C for enhanced sealing properties. Before running the experiments, attention were taken to full up the flow cell chamber with test solution by inclining the device and flushing away gas bubbles, thus minimising artefacts interfering with the useful signal of the electrochemical sensor.

Figure 4.10. Whole system for electrochemical testing under a controlled flow condition.

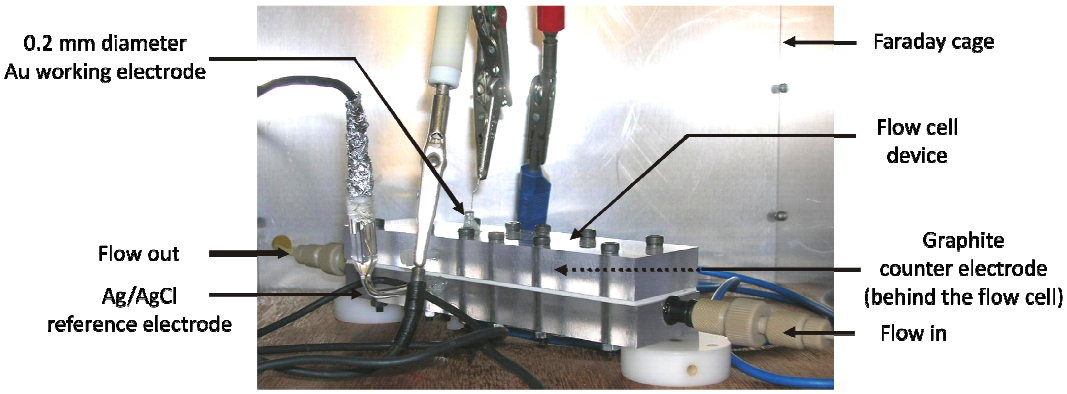

Figure 4.11. Modified flow cell device in sandwich configuration with an electrochemical sensor within the Faraday cage.

4.9 Confocal microscopy characterisation

Confocal microscopy (Leica TCS SP2) studies using a molecular probe technique Live / Dead$^{(R)}$ *Bac*Light^{TM} (from Invitrogen Ltd, Paisley, UK) were performed *ex situ* using an excitation wavelength of 470 nm (see **Section 2.8.1**) to assess the morphology of bacterial colonies, their distribution and the presence of EPS matrix on the Au surface, and also to corroborate the performance of the electrochemical sensor.

The main components of the Leica TCS SP2 in **Figure 4.12** are:

- **(1)** the motorised scan head,
- **(2)** the upright microscope stand,
- the *x*/*y* microscope stage with an additional **(3)** high precision *z*-stage,
- and **(4)** the anti-vibration table.

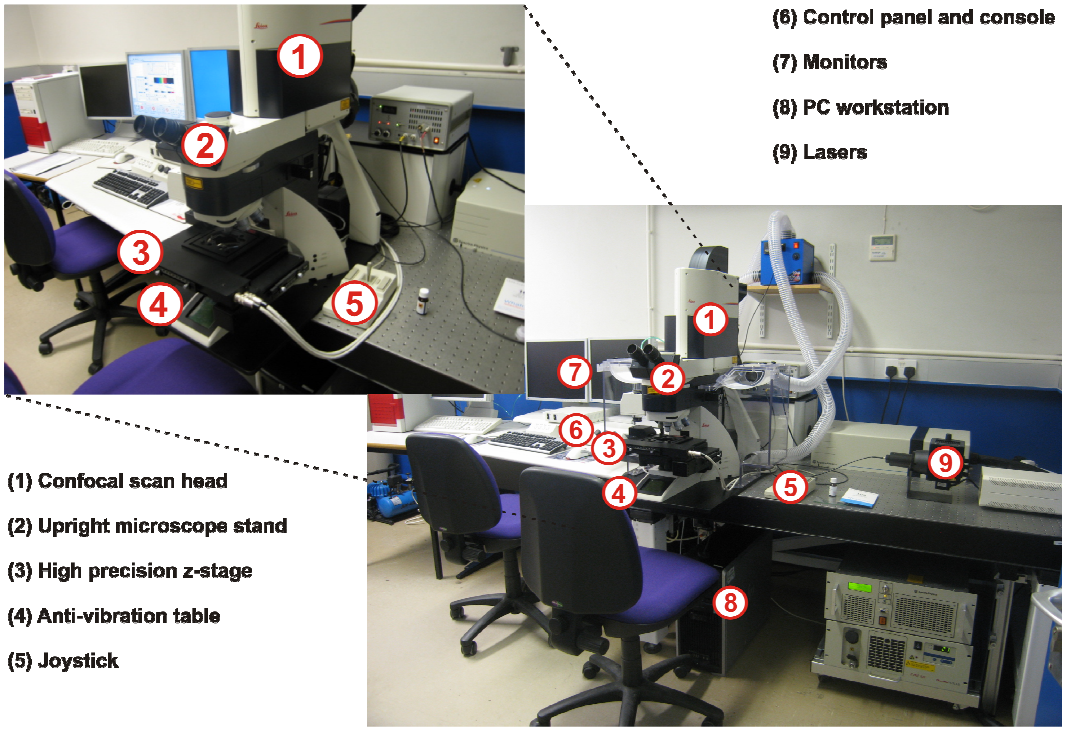

Figure 4.12. Leica TCS SP2 laser scanning microscope system.

The *Bac*Light consists in a green-fluorescent SYTO® 9 stain and a red-fluorescent propidium iodide dye [**4.41**] (see **Section 2.8.1** for a detailed description). The procedure chosen was similar to the staining method in [**4.41**]. The *Bac*Light was defrosted at room temperature and SYTO® 9 / propidium iodide stains at a ratio of 50:50 was utilised. For instance, 10 µL of SYTO® 9 was added to 10 µL of propidium iodide. Subsequently, 18 µL of the total was combined to 6 mL of 0.2 µm filtered test solution, *e.g.* NaCl or ASW. 0.5 mL droplets of the corresponding mixture were hence added to the Au surfaces. In between microscopy examinations, the samples were covered in tinfoil and left for 30 mins in the dark to avoid photo-bleaching. Using the Leica TCS SP2, a series of stacks of confocal images were collected at 0.5 µm intervals along the *z*-direction. Due to optical limitations, the resolution of raw data is always worse than the true spatial distribution of the fluorescent surface [**4.42**]. Consequently, subsequent deconvolutions were carried out using the Leica Confocal Software (LCS) version 2.61 resulting in a partial non-deterioration of the overall image resolution and a reconstruction of the original object structure under investigation. ImageJ was utilised for percentage coverage analyses on the Au surface images to qualitatively evaluate biofouling plus bacterial viability, *i.e.* Live and / or Dead bacterial cells. In this process, the biofilm stacks were projected to a view plane using the LCS version 2.61 prior to ImageJ analyses, *i.e.* it was representative of an underestima for

the presence of a thin biofilm. In addition, numbers of attached sessile bacteria cells were computed from the percentage coverage analyses (*i.e.* for the biofilmed surface areas) using a relevant size criterium for one adhered *Pseudoalteromonas* sp. NCIMB 2021 cell (1.0 – 2.5 μm long and 0.4 – 0.6 μm in diameter [**4.43**]), see **Section 5.12.6**. As discussed in **Section 2.8.1**, suitable thresholds were applied to Leica TCS SP2 images, thus rendering biofilm cell clusters in black and the corresponding channels in white [**4.31**]. Additionally, biofilm thickness measurements were performed using the stacks of confocal images. Similar to [**4.31**], the biofilm thickness was defined as the distance between the Au surface and the peaks of the highest cell clusters. For the current study, the inter-distance between two focused images, *i.e.* bare and biofilmed Au surfaces was assessed using the LCS version 2.61, therefore providing biofilm thickness measurements at ± 0.5 μm.

Chapter 5 – Results and discussion

5.1 *Pseudoalteromonas* sp. NCIMB 2021 growth curve

Figure 5.1 shows the 72 h growth curve of the *Pseudoalteromona*s sp. NCIMB 2021. Each point (**Figure 5.1**) represents the mean value at a given time of a magnitude of cells number detected per mL in the non-and diluted samples (*i.e.* with values corrected from the 10 and 100 dilution factor), see **Section 3.2.4.2**.

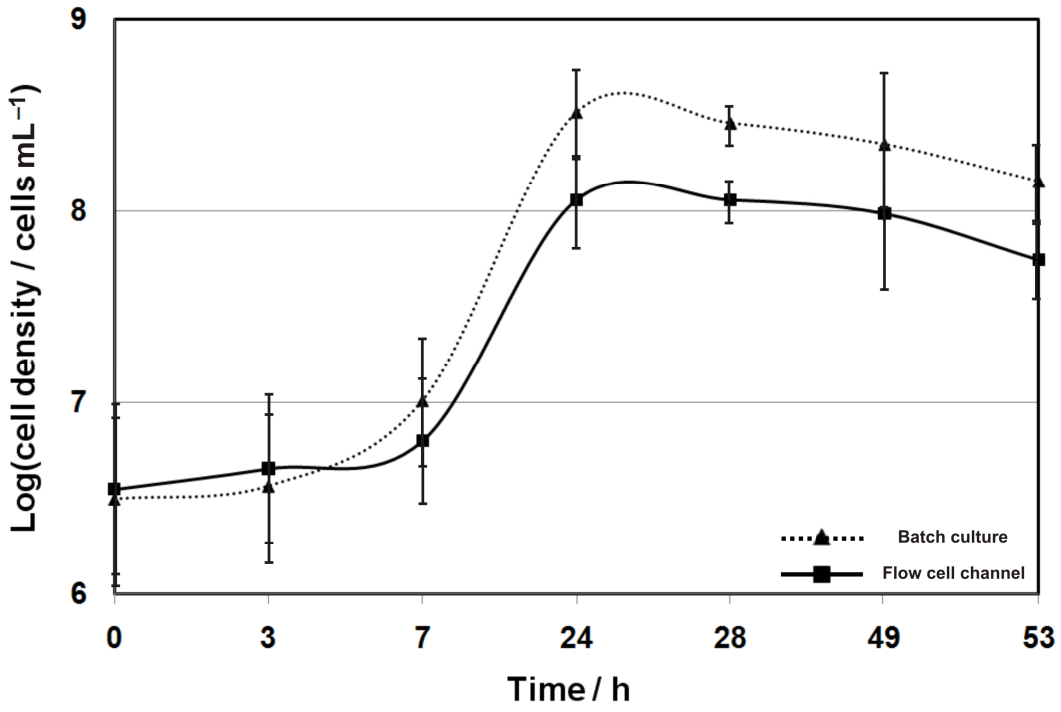

Figure 5.1. Bacterial growth curve for *Pseudoalteromonas* sp. NCIMB 2021: **(dashed line)** cultured in the 250 mL batch culture and **(solid line)** established inside the flow channel.

Relative large percentage of errors shown in **Figure 5.1** can be explained by the contribution of the 10 and 100 times dilution, which can greatly affect the precision of the measurement. Likewise, no useful signal was detectable after a 53 h exposure due to the presence of biological by-products in the samples, thus rendering the measurable signal not accurate (see **Section 3.2.4.2**). Overall, the shape of the growth curves in both the batch culture and flow cell (*i.e.* logarithmic, stationary and scenescence phase) were similar to that in **Figure 3.5**. Initially, the plot for the flow cell corresponds to a 2 h-old *Pseudoalteromonas* sp. NCIMB 2021 culture, therefore representative of the bacterial growth phase for the batch culture at 2 h with $\approx 3.5 \times 10^6$ cells mL^{-1}. However, the magnitude of the logarithmic growth phase was lower for the flow cell compared to that for the batch culture. This can be explained by greater

organic carbon source content substantially favouring bacterial growth in the batch culture than for the flow cell channel, see **Sections 4.4** and **4.5**.

In addition, the results (≈ 1.0 to 3.2 × 10^8 cells mL^{-1} at the plateau between 24 to 49 h) in **Figure 5.1** were in agreement with that reported by Fletcher (*i.e.* stationary and scenescence phase reached at around 21 – 22 h and between 45 and 50 h, respectively with ≈ 2.5 to 5.0 × 10^9 cells mL^{-1}) [**5.1**].

From **Figure 5.1**, it is possible to assess μ_b defined in **Section 3.2.4.2** using **Equations 5.1** and **5.2** [**5.2**]:

$$t_d = \frac{\ln 2}{\mu_b} \tag{5.1}$$

$$n_b = \frac{\log x_t - \log x_0}{\log 2} \text{ for } n_b \text{ generations (}i.e.\ n_b t_d\text{) between } t_0 \text{ and } t \tag{5.2}$$

where t_d is the doubling time or mean generation time. It represents the average time required for all the components of the culture to double. In addition, x_0 and x_t stand for the cell density at t_0 and t representative of the beginning of the exponential growth and the stationary phase, respectively. **Table 5.1** summarises the computations using **Figure 5.1** for biological characterisation of both the batch and flow cell culturing systems in terms of mean generation time and grow rate.

Table 5.1. Calculations of biological parameters for the batch culture and flow cell system between t_0 = 3 h and t = 24 h.

Biological parameters / computations	Batch culture	Flow cell
$\log x_0$ (at 3 h)	6.56	6.66
$\log x_t$ (at 24 h)	8.51	8.06
x_0 (at 3 h) / cells mL^{-1}	3,675,798	4,533,826
x_t (at 24 h) / cells mL^{-1}	327,223,465	114,092,842
n_b	6.47 generations in 21 h	4.65 generations in 21 h
t_d (*i.e.* 21 / n_b) / h	3.25	**4.52**
μ_b / h^{-1}	0.21	**0.15**

Between 3 and 24 h (as an example for the flow cell in **Table 5.1**), $x_0 \approx$ 4,533,826 cells mL^{-1} and x_t = 114,092,842 cells mL^{-1}, there are (8.06 – 6.66) / 0.30103 $\approx$ 4.65 generations in 21 h. This corresponds to t_d = **4.52** h, thereby μ_b = **0.15** h^{-1} (**Table 5.1**) using **Equation 5.1**. Likewise, the mean generation time (3.25 h) and grow rate (0.21 h^{-1}) values for the batch culture in **Table 5.1** were within the same order of magnitude to that for the flow cell. These growth rates can be related to typical μ_b values for standard batch culturing vessels (*i.e.* 0.5 – 0.7 h^{-1} [**5.3**]) or biofilm model system operating at a fast dilution rate of 0.2 h^{-1} [**5.2**], which are usually about 10 times higher than that for typical dilution rates using a chemostat (*i.e.* $\approx$ 0.05 h^{-1}) [**5.2**]. As a result, the μ_b value of 0.15 h^{-1} is acceptable for the current study.

5.2 Summary of the bacterial growth curve characterisation

Although different environmental conditions can cause biological variability in bacterial growth (see **Sections 3.2.2.2** and **4.5**), results in **Figure 5.1** have demonstrated that the bacterial growth curves for the the flow cell and the batch culture were similar with comparable mean generation time and growth rate. Hence, using different growth media in the flow cell and batch culture (**Sections 4.4** and **4.5**) has a minimum influence on the outcome of the electrochemical investigation in **Sections 5.10**, **5.12.3**, **5.12.4** and **5.13**. Additionally, the growth curve characterisation of the *Pseudoalteromonas* strain has shown that the flow cell device is a suitable culturing system for the proposed engineering approach, *i.e.* allowing microbial fouling colonisation and development to occur.

5.3 Overview of the cyclic voltammograms

The cyclic voltammogram investigation performed using 1 M H_2SO_4 was made in order to characterise and establish the behaviour of the 0.2 mm diameter Au electrode in an acidic solution often used in electrochemical studies. The CV plots for NaCl solution, abiotic and biotic ASW media (**Sections 5.6**, **5.8** and **5.10**, respectively) will be discussed in detail to provide fundamental insights into the interfacial electrochemical reactions monitored during 72 h, thus fully assessing the measurement accuracy and reliability.

5.4 Characterisation of the Au electrode in 1 M sulphuric acid

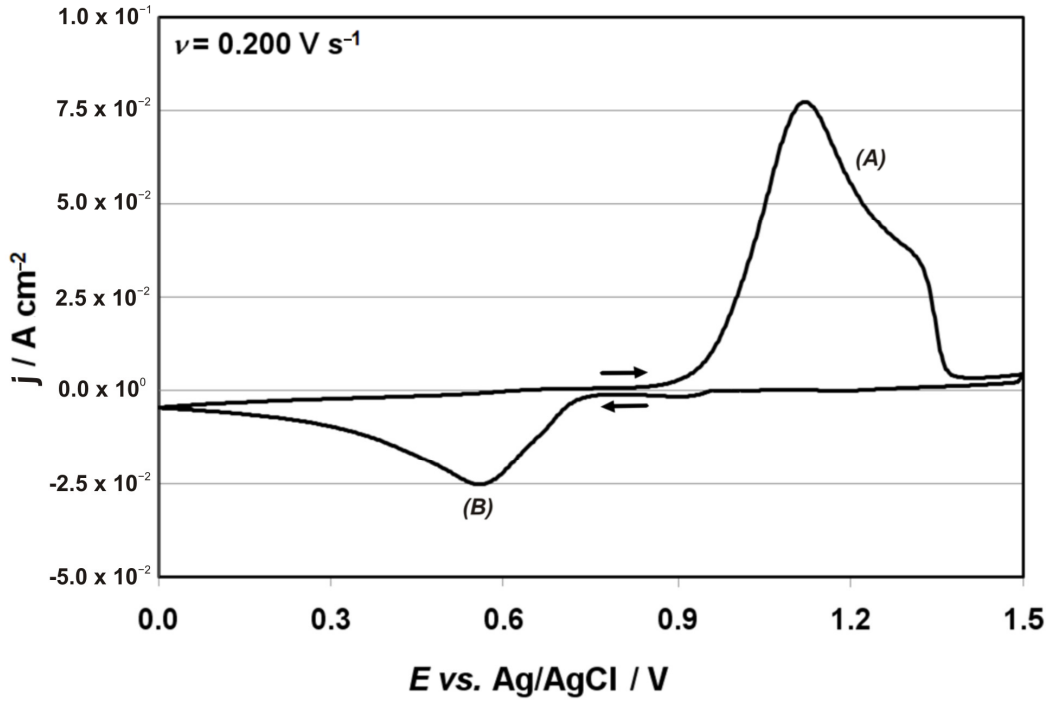

Figure 5.2. Cyclic voltammogram for a 0.2 mm diameter Au electrode in N_2 deaerated 1 M H_2SO_4 at a scan rate of 0.200 V s^{-1}.

The Au electrode CV in deaerated 1 M H_2SO_4 (**Figure 5.2**) is similar in behaviour to a previously reported typical Au electrode acid voltammogram [**5.4**,**5.5**]. The extended region ***(A)*** between +0.900 and +1.350 V (*vs.* Ag/AgCl) represents the Au oxide formation, see **Equations 5.3** and **5.4**.

$$Au + 3H_2O \rightarrow Au(OH)_3 + 3H^+ + 3e^- \quad E_r = +1.245 \text{ V (}vs.\text{ Ag/AgCl, 3.5 M KCl)} \qquad (5.3)$$

where the product $Au(OH)_3$ is the hydrated oxide,

$$2Au + 3H_2O \rightarrow Au_2O_3 + 6H^+ + 6e^- \quad E_r = +1.305 \text{ V (}vs.\text{ Ag/AgCl, 3.5 M KCl)} \qquad (5.4)$$

where the product Au_2O_3 is the anhydrous oxide.

The distribution of the anodic peaks in the region ***(A)*** along a potential range, between +0.900 and +1.350 V (*vs.* Ag/AgCl), can be explained by the formation of an oxide monolayer at the Au surface [**5.5**]. The hysteresis, *i.e.* the difference in the potential range between the peaks for oxide formation / reduction in regions ***(A)*** and ***(B)***, can be attributed to gradual changes in the nature of the oxide film. Dipolar ($Au^{\delta+}.OH^{\delta-}$) species are produced during the oxide growth process (during the positive potential

sweep) and cover the Au surface. The oxide coverage of the Au surface increases the overall electrostatic repulsion energy favourable for additional dipoles generation in the extended region ***(A)***.

The reduction peak in the region ***(B)*** around +0.550 V (*vs.* Ag/AgCl) was not well-defined. This is unusual since a conventional Au electrode acid voltammogram should ideally exhibit a relative sharp cathodic peak. This can be explained by the non-complete release (negative sweep) of lateral repulsion or stress in the surface layer of the manually polished Au electrode [**5.5**]. Ideally for a complete reduction of the electrostatic repulsion barrier, the post-electrochemical process of the Au oxide formation is governed by place-exchange reaction, *i.e.* rotation of surface dipoles resulting in the release of lateral residual stresses in the surface layer. As part of the place-exchange reaction in **Figure 5.3**, some Au atoms (unshaded circles) can switch positions with adsorbed O_2 species (shaded circles) [**5.5**].

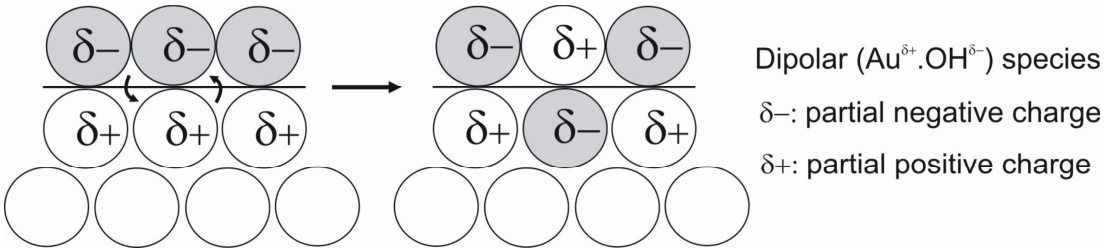

Figure 5.3. Schematic representation of the place-exchange reaction in a monolayer oxide formation, from [**5.5**].

5.5 Summary of the CV analysis for the 1 M sulphuric acid

The electrochemical response for the 1 M sulphuric acid in **Figure 5.2** was consistent with typical Au electrode acid voltammogram [**5.4**,**5.5**], *i.e.* Au oxide formation / reduction in regions ***(A)*** and ***(B)***, see **Table 5.2**.

Table 5.2. Summary of detectable electrochemical process at the Au / 1 M H_2SO_4 interface (**Figure 5.2**) for a potential range of 0.000 to +1.500 V (*vs.* Ag/AgCl).

Potentials	Regions	Description
between +0.900 and +1.350 V (*vs.* Ag/AgCl)	***(A)***	Au oxide formation
around +0.550 V (*vs.* Ag/AgCl)	***(B)***	reduction of the Au oxide

5.6 CV for the NaCl solution

For clarity, only the 72 h data has been presented in **Figure 5.4.** Over the entire test duration, cyclic voltammograms were found to be time-independent for the NaCl test solution. The time-independent behaviour can be explained by no overall change / modification of the reaction kinetics at the Au / 3.5 % NaCl interface.

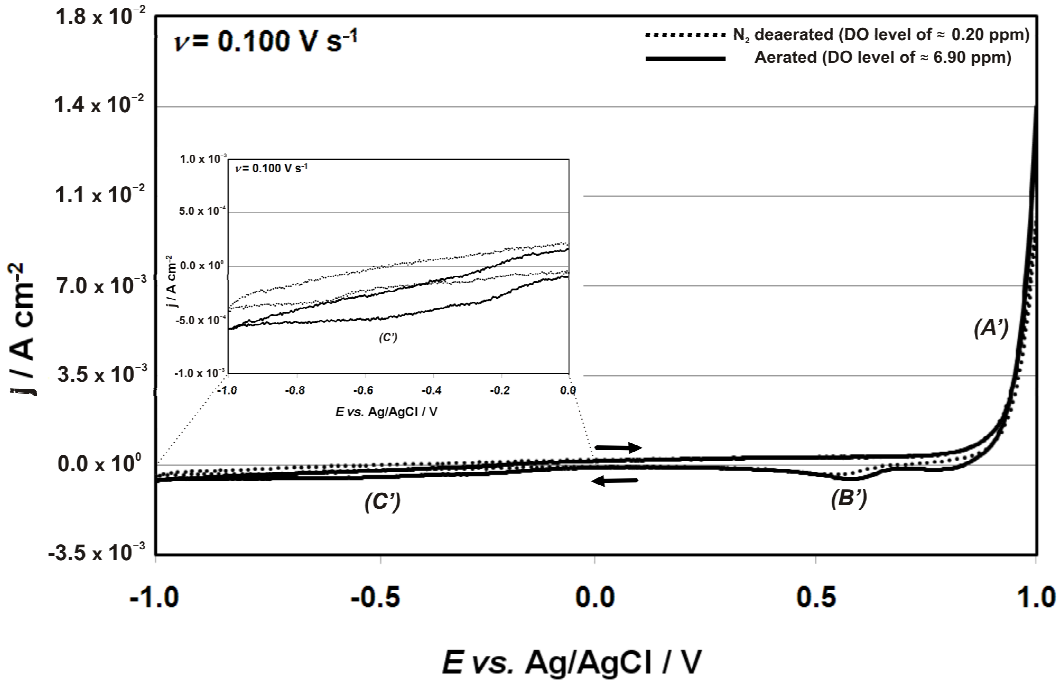

Figure 5.4. Comparison of cyclic voltammograms for a 0.2 mm diameter Au electrode in N_2 deaerated **(dashed line)** and aerated **(solid line)** 3.5 % NaCl at a scan rate of 0.100 V s^{-1}.

Overall, **Figure 5.4** was in agreement with conventional cyclic voltammograms of Au in 3.5 % NaCl solution [**5.4**]. At positive potentials, the oxidation of Au begins around +0.750 V (*vs.* Ag/AgCl) in the region ***(A')***. The presence of Cl^- can also influence Au dissolution, in parallel to Au oxide formation on the surface, leading to the formation of tetrachloroaurate ions ($AuCl_4^-$) [**5.4**].

$$Au + 4Cl^- \rightarrow AuCl_4^- + 3e^- \quad E_r = +0.797 \text{ V (}vs.\text{ Ag/AgCl, 3.5 M KCl)} \qquad (5.5)$$

As part of the Au oxide layer formation process, the surface may be covered by Au-oxygen species, such as Au(OH), $Au(OH)_3$ or AuO(OH) [**5.4**]. The associated cathodic (stripping) peak of the Au oxide formation in the region **(B')** around +0.550 V (*vs.* Ag/AgCl) is not evident in **Figure 5.4**. This is indicative of a process that is essentially irreversible [**5.6**]. Using the Pourbaix diagram for Au in chloride-water system in **Figure 5.5**, two possible reaction pathways can be deduced to determine the origin of the Au oxide dissolution [**5.4**].

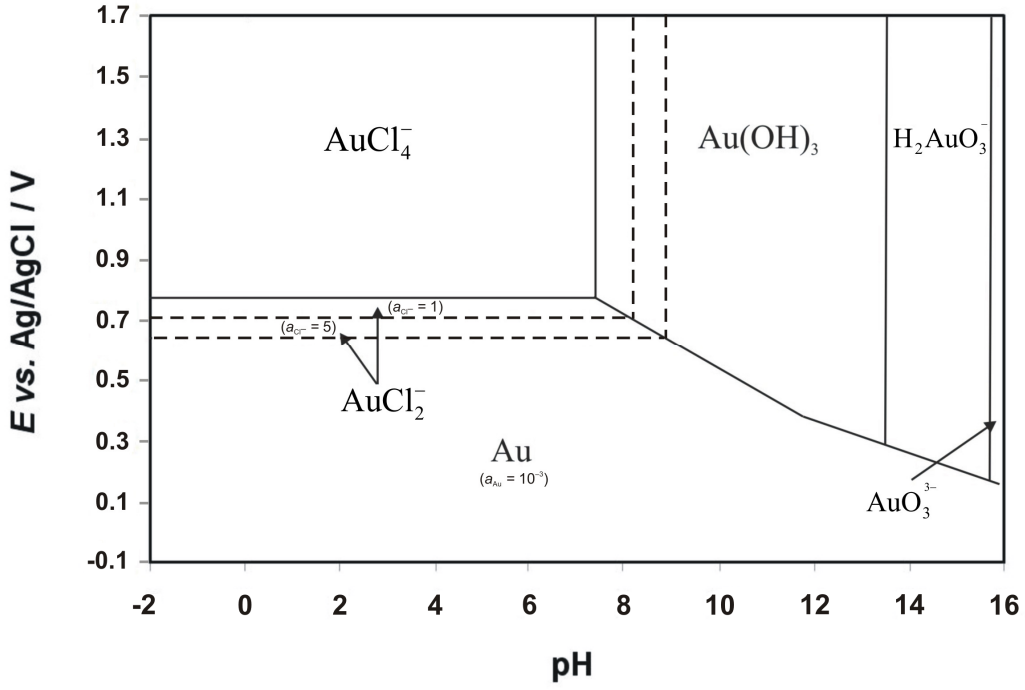

Figure 5.5. Pourbaix diagram for an Au chloride-water system at 298 K with $a_{Au} = 10^{-3}$ and $a_{Cl^-} = 1$ **(solid line)**, $a_{Cl^-} = 5$ **(dashed line)** where a_i is the activity of species i, adapted from [**5.4**].

The first mechanism in **Figure 5.6** suggests that Au can initially dissolve in the presence of Cl^- to form the $AuCl_2^-$ complex. The $AuCl_2^-$ stability depends on the chloride and Au activity ratios (stable at high values). With a chloride deficiency at the Au / NaCl solution interface, $AuCl_2^-$ can undergo disproportionation to simultaneously form both Au and $AuCl_4^-$, see **Equation 5.6** [**5.4**].

$$3\,AuCl_2^- \rightarrow 2Au + AuCl_4^- + 2Cl^- \qquad (5.6)$$

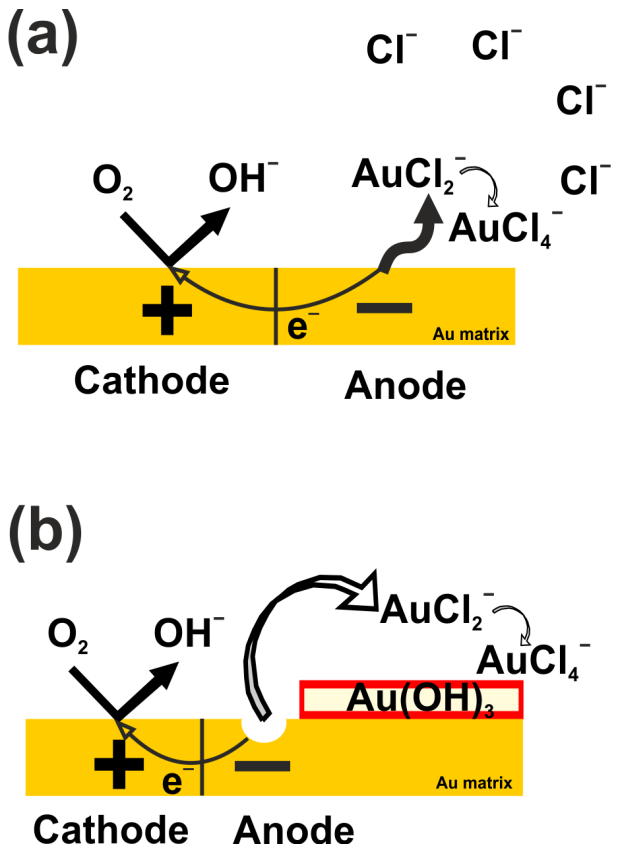

Figure 5.6. First mechanism of Au dissolution: **(a)** initiation of corrosion within the Au matrix and formation of the $AuCl_2^-$ and $AuCl_4^-$ complex **(b)** yielding to $Au(OH)_3$.

The second mechanism in **Figures 5.7(a)** and **5.7(b)** suggests that Au dissolution in a NaCl solution can proceed by the reaction of $Au(OH)_3$ with Cl^- to form mixed chlorohydroxo Au complexes, such as $AuCl(OH)_3^-$, see **Equation 5.7** [**5.4**].

$$Au(OH)_3 + Cl^- \rightarrow AuCl(OH)_3^- \qquad (5.7)$$

A further exchange of hydroxyl ligands of the $AuCl(OH)_3^-$ complex can occur to yield $AuCl_4^-$, see **Figure 5.7(c)**.

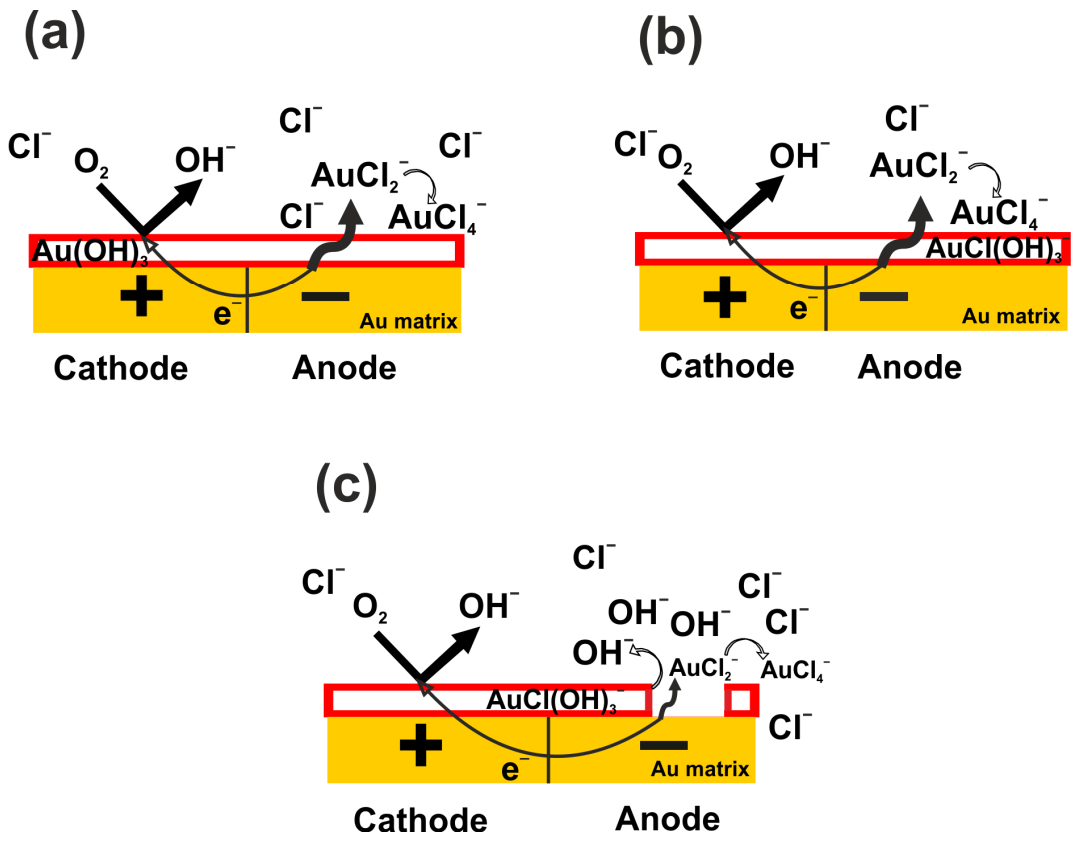

Figure 5.7. Second mechanism of Au dissolution: **(a)** reaction of $Au(OH)_3$ with Cl^- to form **(b)** $AuCl(OH)_3^-$ and subsequent **(c)** exchange of hydroxyl ligands resulting in the formation of the $AuCl_4^-$ complex.

It has been demonstrated that the ORR on Au proceeds only via an intermediary series mechanism with H_2O_2 as the reactant intermediate [**5.4**], see **Section 2.4.3.2**. This is often attributed to the relatively poor catalytic properties of Au for the decomposition of H_2O_2 compared to other noble metals (*e.g.* Pt). In alkaline solutions, O_2 is readily reduced to H_2O_2 (**Equation 5.8**) and partial peroxide reduction to water occurs on the Au surface [**5.4**,**5.7**].

$O_2 + 2H_2O + 2e^- \rightarrow H_2O_2 + 2OH^-$ E_r = –0.351 V (*vs.* Ag/AgCl, 3.5 M KCl) (5.8)

The region ***(C')*** in the negative potential range, between –0.200 V to the plateau at –0.700 V (*vs.* Ag/AgCl), shows a clear difference between the deaerated and aerated NaCl solution in **Figure 5.4**, thus demonstrating the occurrence of a well-defined wave of the ORR governed by **Equation 5.8**. The rate of the second step appears to be potential independent. This suggests that the reduction of O_2 to H_2O_2 is determined by a chemical step involving the adsorbed peroxide species [**5.4**].

$$H_2O_2 \rightarrow 2OH^{\bullet} \quad (5.9)$$

or

$$H_2O_2 \rightarrow H_2O + O^{\bullet} \quad (5.10)$$

$$O^{\bullet} + H_2O + e^- \leftrightarrows OH^{\bullet} + OH^- \quad (5.11)$$

Equation 5.9 or **Equations 5.10** and **5.11** are followed by the fast reaction:

$$OH^{\bullet} + e^- \leftrightarrows OH^- \quad (5.12)$$

Overall, the second step with adsorbed peroxide species, which corresponds to a second wave of ORR that is poorly defined in **Figure 5.4 (solid line)**, can be equivalent to **Equation 5.13**:

$$H_2O_2 + 2e^- \rightarrow 2OH^- \quad (5.13)$$

5.7 Summary of the CV analysis for the NaCl test condition

Overall, the electrochemical response in **Figure 5.4** (Au oxide formation and stripping in the anodic region, and also ORR in the cathodic region) was in good agreement with typical voltammogram of Au in a 3.5 % NaCl test solution [**5.4**], see **Table 5.3**. Importantly, a cathodically polarised Au electrode, between –0.200 V to the plateau at –0.700 V (*vs.* Ag/AgCl), can be used to monitor the ORR (this is the working principle of the Clark electrode [**5.8**,**5.9**]), whereas the anodic region can be informative of potential self-cleaning / generation process of the Au surface for in service conditions [**5.4**,**5.10**-**5.12**].

Table 5.3. Summary of detectable electrochemical process at the Au / 3.5 % NaCl interface (**Figure 5.4**) for a potential range of –1.000 to +1.000 V (*vs.* Ag/AgCl).

Potentials	**Regions**	**Description**	
≥ +0.750 V (*vs.* Ag/AgCl)	***(A')***	Au oxide formation	**self-cleaning of the Au surface**
around +0.550 V (*vs.* Ag/AgCl)	***(B')***	cathodic stripping of the Au oxide	
between –0.200 V to the plateau at –0.700 V (*vs.* Ag/AgCl)	***(C')***	**ORR wave**	

5.8 CV for the abiotic test condition

As with to the NaCl test solution in **Figure 5.4**, only the voltammogram for the 72 h data has been presented in **Section 5.8** arising from time-independent response for the abiotic test condition (containing organic materials, see **Section 4.4**). This behaviour can be attributed to no overall change / modification of the reaction kinetics at the Au / abiotic ASW interface.

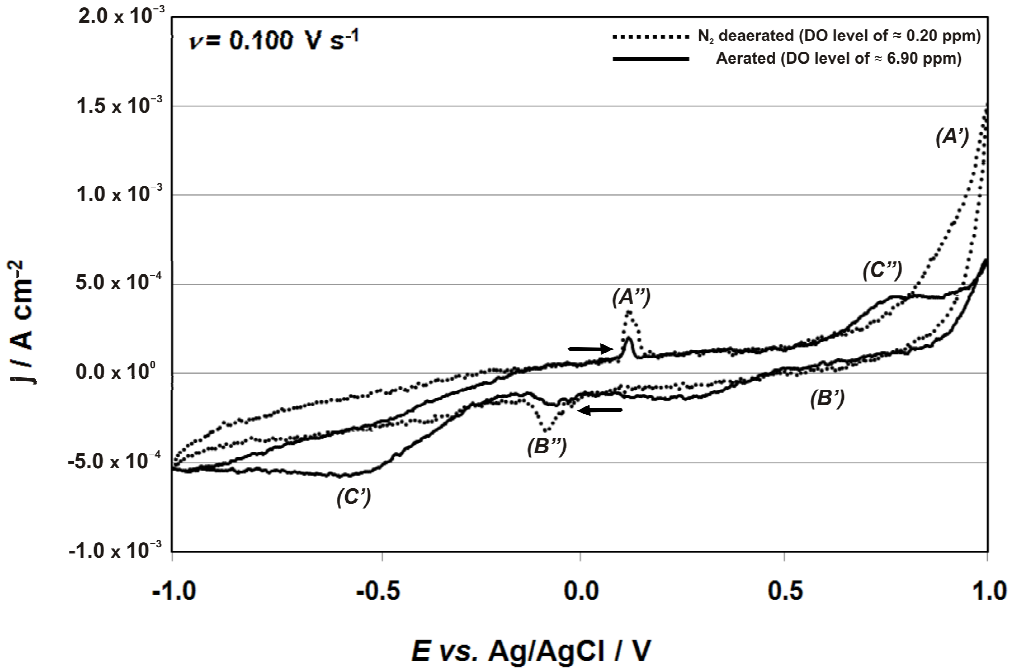

Figure 5.8. Comparison of cyclic voltammograms for a 0.2 mm diameter Au electrode in N_2 deaerated **(dashed line)** and aerated **(solid line)** abiotic ASW at a scan rate of 0.100 V s^{-1}.

Similarly in **Figure 5.8** for the ASW medium, the regions **(*A'*)** and **(*C'*)** were representative of the Au oxide formation and the ORR, thus consistent with **Figure 5.4**. However, anodic / cathodic peaks in the domains ***(A'')*** and ***(B'')*** were apparent for the abiotic ASW at ± 0.125 V (*vs.* Ag/AgCl), where an oxidation wave in the region ***(C'')***, between +0.500 to +0.900 V (*vs.* Ag/AgCl), was more pronounced for the aerated ASW medium (**Figure 5.8**) as observed by Hu *et al.* using a similar organic medium [**5.13**]. A direct comparison with the NaCl solution is shown in **Figure 5.9** and overall these responses were indicative of interfacial changes: adsorption / desorption process in the regions ***(A'')*** and ***(B'')*** and oxidation of organic material (favoured in aerated conditions) in the region ***(C'')***. Likewise, the regions **(*A'*)** and ***(B')*** of the Au oxide formation and stripping for the abiotic ASW (less prominent to that for the NaCl solution in **Figure 5.9**) were shifted / suppressed due to the presence of an adsorbed organic material on the Au surface [**5.14**-**5.16**].

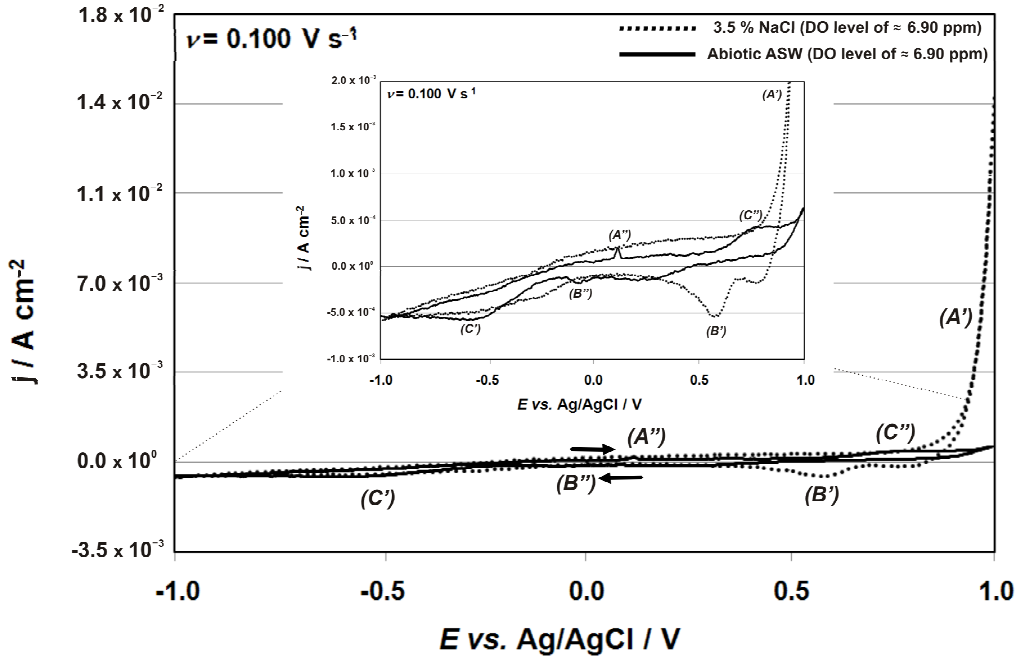

Figure 5.9. Comparison of cyclic voltammograms for a 0.2 mm diameter Au electrode in aerated **(dashed line)** 3.5% NaCl and **(solid line)** ASW medium at a scan rate of 0.100 V s^{-1}.

To address the nature of the electrochemical process for the abiotic ASW medium, a comparative study between a control ASW test solution (only composed of salts and metal-ions plus EDTA in **Section 4.4**) and abiotic ASW is presented in **Figures 5.10** and **5.11**. Overall, the voltammogram for the control ASW medium (**Figure 5.10**) was similar to that for the abiotic ASW in **Figure 5.8** with the regions ***(A')***, ***(C')***, ***(A'')*** and ***(B'')*** representative of the Au oxide formation, the ORR and the anodic / cathodic peaks (herein for the control ASW test solution) due to electro-active adsorption / desorption of metal ions. In contrast, the wave of ORR in the region ***(C')*** was more evident for the abiotic ASW in comparison with the control ASW (**Figure 5.11**), thus suggesting enhanced mass transport properties when an adsorbed organic layer (conditioning film) forms on the Au surface [**5.10**-**5.12**]. Similarly, the peaks for the regions ***(A'')*** and ***(B'')*** in **Figure 5.11** were depressed in the abiotic ASW, therefore explained by blocking effects of adsorbed organic material (exposed Au surface is lower) [**5.14**,**5.15**,**5.17**]. Whereas the oxidation wave in the region ***(C'')*** was more pronounced compared to that for the control ASW medium, as a consequence attributed to oxidation reaction of organic material and consistent with [**5.13**].

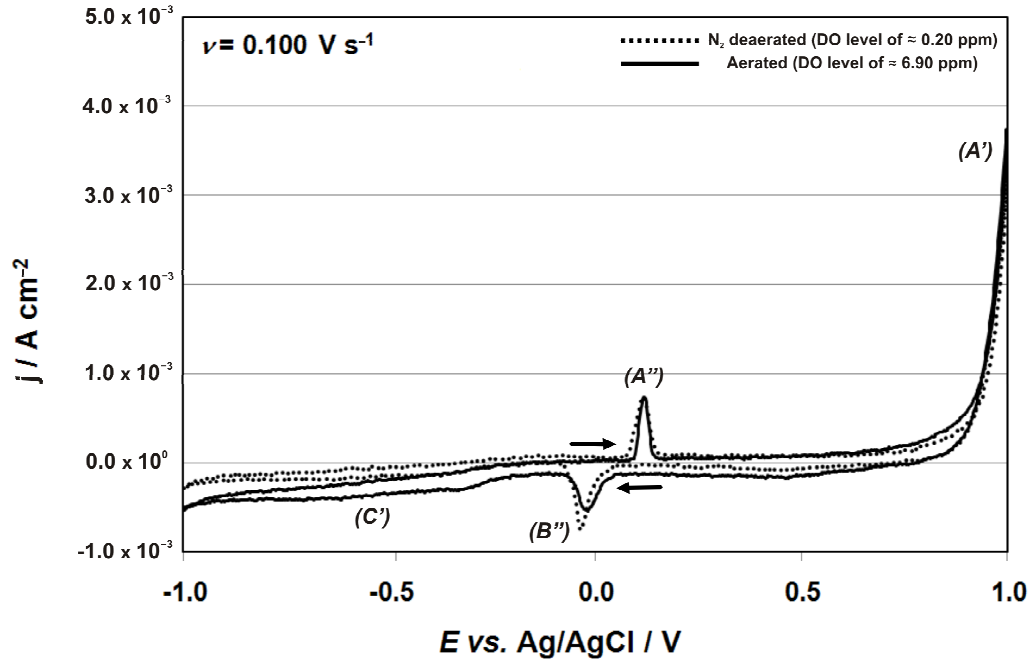

Figure 5.10. Comparison of cyclic voltammograms for a 0.2 mm diameter Au electrode in N_2 deaerated **(dashed line)** and aerated **(solid line)** control ASW at a scan rate of 0.100 V s^{-1}.

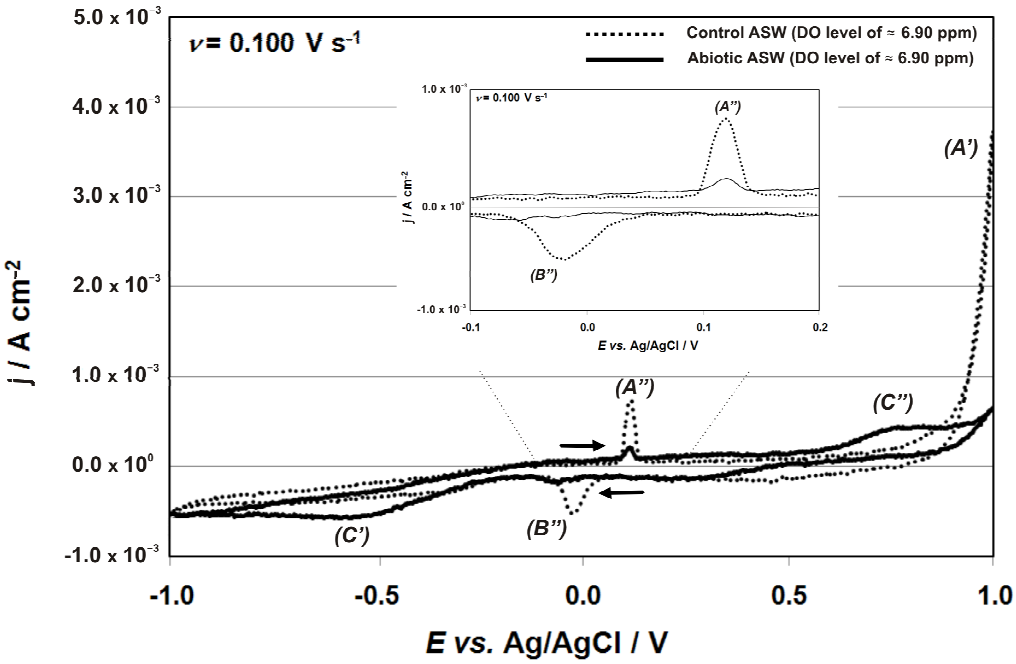

Figure 5.11. Comparison of cyclic voltammograms for a 0.2 mm diameter Au electrode in aerated control **(dashed line)** and abiotic **(solid line)** ASW at a scan rate of 0.100 V s^{-1}.

In addition, the anodic surface charge density (Q_a) in the region ***(A'')*** was calculated by integrating the area under the curve between 0.080 and 0.150 V (*vs.* Ag/AgCl) in **Figure 5.11**.

$$Q_a = \int_{t_1}^{t_2} j\mathrm{d}t \qquad (5.14)$$

where t_1 and t_2 are the times representative of 0.080 and 0.150 V (*vs.* Ag/AgCl), respectively.

The cathodic peak in the region ***(B'')*** for the abiotic ASW in **Figure 5.11** was not well-defined (thus not considered for percentage surface coverage studies), herein explained by the influence of oxygen, *i.e.* peak shift towards the region ***(C')*** of the ORR [**5.14**]. **Table 5.4** shows the Q_a values using **Equation 5.14** and the corresponding percentage surface coverage for the adsorbed organic materials.

Table 5.4. Summary of Q_a values for the region ***(A'')*** in **Figure 5.11** and the corresponding percentage surface coverage of adsorbed organic layers.

Media	Control ASW	Abiotic ASW
Q_a **/ C cm^{-2}**	1.25×10^{-2}	3.70×10^{-3}
Percentage surface coverage of adsorbed organic layers	**≈ 70 %**	

A percentage surface coverage of **70 %** (**Table 5.4**) was assessed when an adsorbed organic layer can significantly suppress the electron transfer process on the Au surface [**5.14**,**5.15**,**5.17**]. Overall, this represents a limited electrochemical interpretation of the surface process occurring when a conditioning film forms on the Au surface. Consequently, corroborative tests such as AFM and spectroscopy methods on Au electrode are necessary and can be insightful on the exact nature, composition and morphology of the adsorbed organic layer [**5.18**].

In addition, CV for the N_2 deaerated and aerated control, and also abiotic ASW were performed at scan rates of 0.050, 0.100, 0.200 and 0.500 V s^{-1}. This allowed the study of overall electron transfer processes (see **Equation 5.15** [**5.14**,**5.19**]) using plots of the anodic and cathodic peaks current density (absolute value), $|j_{pa}|$ and $|j_{pc}|$ *vs.* $\nu^{1/2}$, where j_{pa} and j_{pc} correspond to the magnitude of the anodic / cathodic peaks in **Figure 5.12**.

$$j_p = (2.99\times10^5)z\alpha^{1/2}cD^{1/2}\nu^{1/2} \qquad (5.15)$$

where j_p is the peak current density, α the transfer coefficient, c and D the concentration and the diffusion coefficient of the relevant species.

The (charging / discharging) baseline for the non-faradaic process (see the idealised plot to illustrate the curve analysis in **Figure 5.12**) shows a minimum variation between the aerated control and abiotic ASW in **Figure 5.11**, thereby suggesting that the adsorption layers (*i.e.* adsorbed organic materials) are electrochemical conductive [**5.14**].

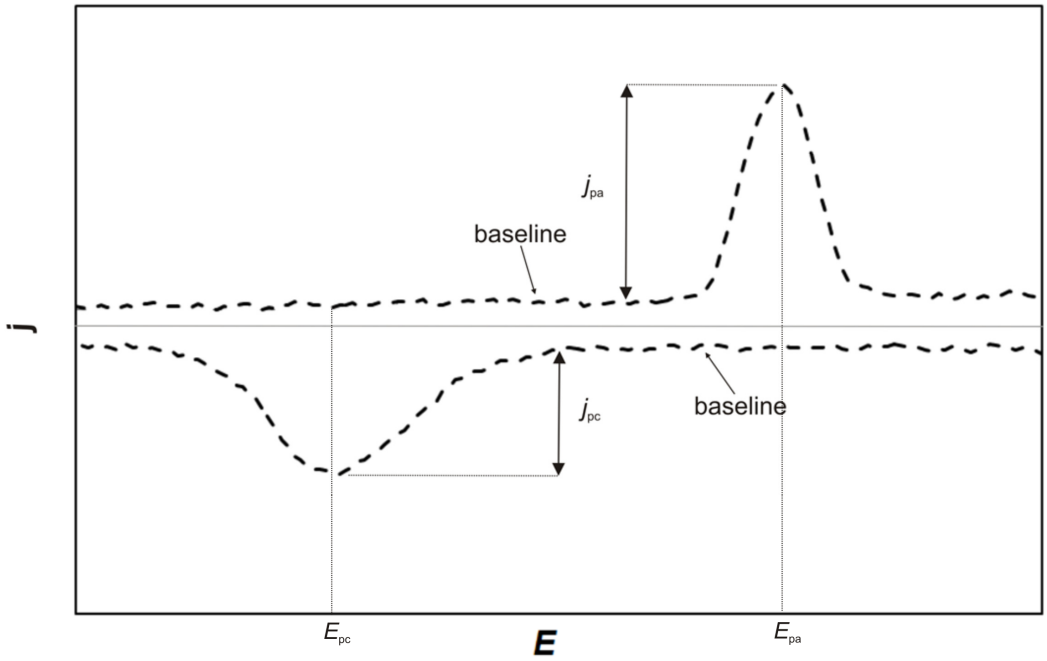

Figure 5.12. Methodology to determine anodic and cathodic peaks current density (j_{pa} and j_{pc}) and peak potentials (E_{pa} and E_{pc}) in the voltammograms for the control and abiotic ASW media – idealised plot to illustrate the curve analysis.

For clarity, only the plots $|j_{pa}|$ and $|j_{pc}|$ *vs.* $\nu^{1/2}$ for the aerated conditions were presented in **Figures 5.13** and **5.14** (similar trends were obtained for the N_2 deaerated ASW media). A linear relationship was apparent between $|j_p|$ and $\nu^{1/2}$ for the control ASW (r^2 = 0.99) in **Figure 5.13** in contrast with the abiotic ASW (r^2 = 0.93) in **Figure 5.14**, where the current density values were overall about 5-fold lower to that for the control ASW, thus demonstrating the occurrence of an overall diffusion dominant process associated with the peaks ***(A'')*** / ***(B'')*** (**Figure 5.11**), which is depressed by surface adsorption of organic materials (≈ 70 % surface coverage in **Table 5.4**).

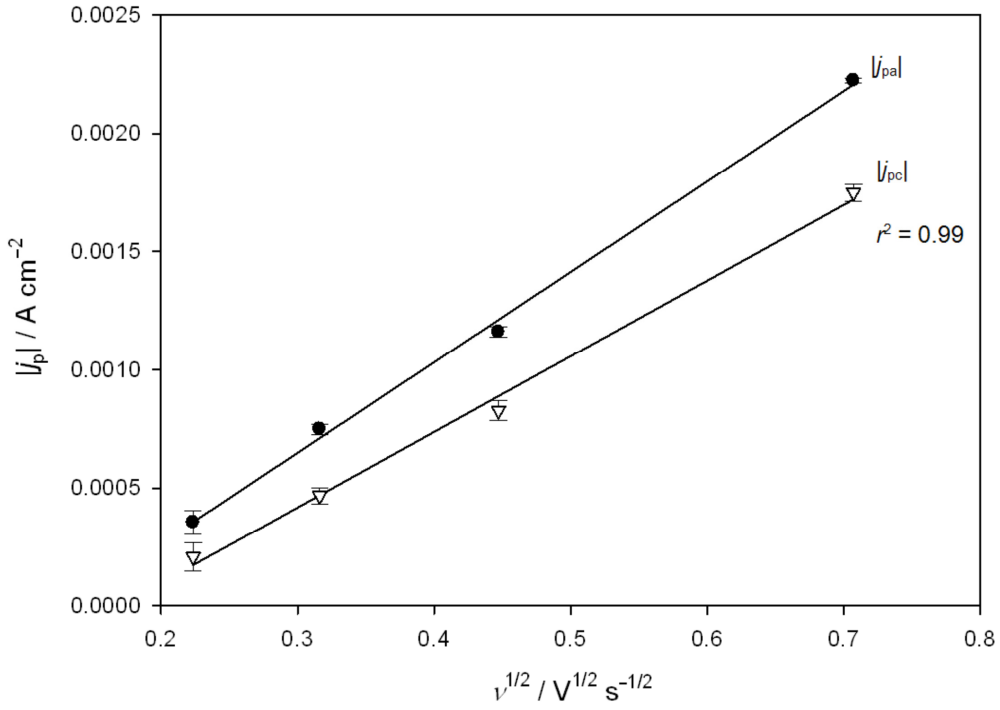

Figure 5.13. Plots of $|j_{pa}|$ and $|j_{pc}|$ *vs.* $\nu^{1/2}$ for the aerated control ASW.

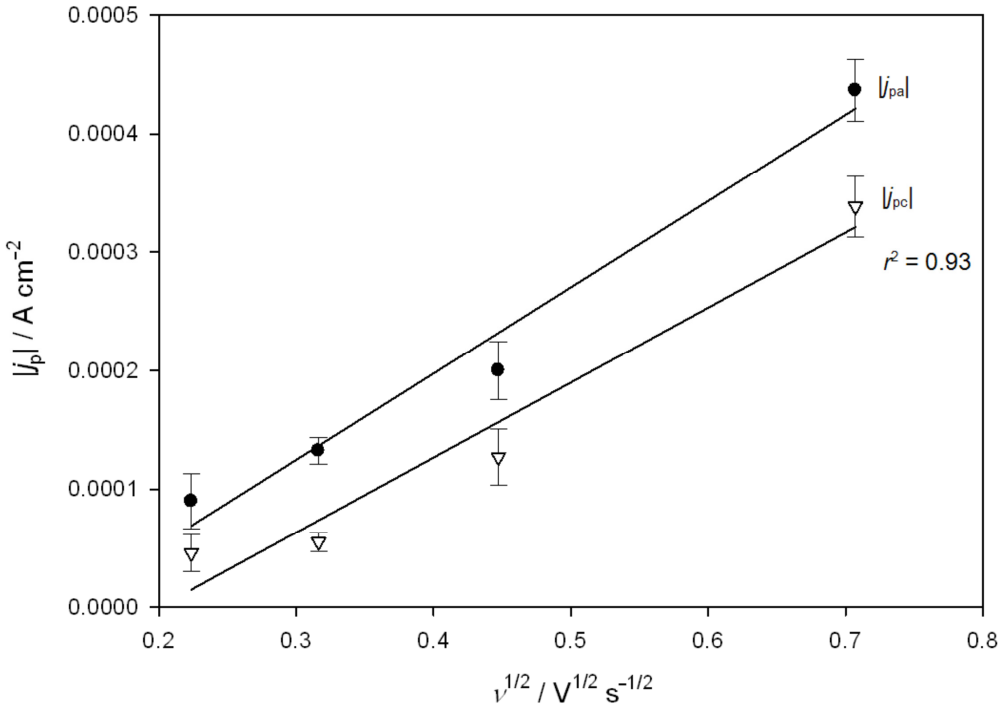

Figure 5.14. Plots of $|j_{pa}|$ and $|j_{pc}|$ *vs.* $\nu^{1/2}$ for the aerated abiotic ASW.

Using **Figure 5.13**, the ratio of $|j_{pa}|$ to $|j_{pc}|$ can be evaluated and is approximately equal to 1, thus informative of a quasi-reversible electron transfer process [**5.14**]. Likewise, the peak potential separation (ΔE_p) in **Equation 5.16** can be evaluated using CV for the aerated control ASW at scan rates of 0.050, 0.100, 0.200 and 0.500 V s^{-1}, see **Table 5.5**.

$$\Delta E_p = E_{pa} - E_{pc} = \frac{0.058}{z} \text{ V (}vs.\text{ Ag/AgCl)} \qquad (5.16)$$

where E_{pa} and E_{pc} are the anodic and cathodic peak potentials, see **Figure 5.12**.

Table 5.5. Summary of ΔE_p values for the aerated control ASW at scan rates of 0.050, 0.100, 0.200 and 0.500 V s^{-1}.

ν / V s^{-1}	0.050	0.100	0.200	0.500
E_{pa} / V (*vs.* Ag/AgCl)	0.098	0.117	0.120	0.136
E_{pc} / V (*vs.* Ag/AgCl)	–0.019	–0.018	–0.030	–0.048
ΔE_p / V (*vs.* Ag/AgCl)	0.117	0.135	0.150	0.184

The ΔE_p value (**Table 5.5**) is on average $\frac{0.145}{z}$ V (*vs.* Ag/AgCl) compared to the theoretical $\frac{0.058}{z}$ V (*vs.* Ag/AgCl) for a single electron transfer reaction (z = 1) in **Equation 5.16**. The difference between the experimental values (**Table 5.5**) and the theoretical prediction can be ascribed to the presence of EDTA amide ligands bound to the Au surface, thus forming coordinated metal ion complexes with an additional solution resistance [**5.14**,**5.20**].

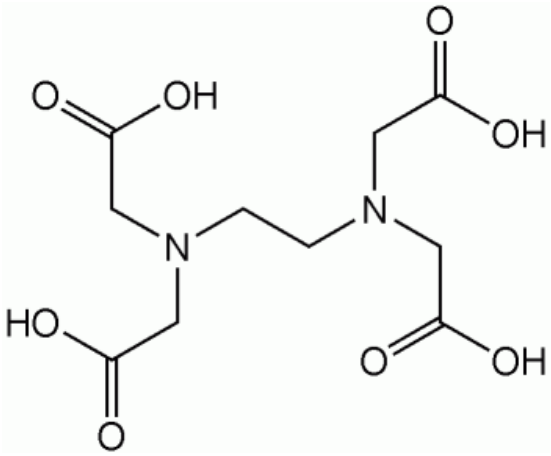

Figure 5.15. Chemical composition of EDTA.

This single electron transfer process (**Table 5.5**) can correspond to the ferric-EDTA complex (see reduction reaction in **Equation 5.17**) [**5.20**,**5.21**], where the concentration of $FeCl_3$ is similar to that for EDTA in **Table 4.3**.

Fe^{3+} EDTA + $e^- \rightarrow Fe^{2+}$ EDTA E_r = –0.085 V (*vs.* Ag/AgCl, 3.5 M KCl) (5.17)

The anodic and cathodic transfer coefficients (α_a and α_c) can be determined (**Equation 5.18** [**5.14**,**5.19**]) utilising the relationships E_{pa} and E_{pc} *vs.* $\ln \nu$ for the aerated control ASW in **Figure 5.16**.

$$E_p = E^{0'} + \frac{RT}{\alpha F}\left[0.780 + \ln\left(\frac{D^{1/2}}{k^0}\right) + \ln\left(\frac{\alpha F \nu}{RT}\right)^{1/2}\right] \quad (5.18)$$

where E_p is the peak potential, $E^{0'}$ is the formal potential of the electrode and k^0 the standard heterogeneous rate constant. **Figure 5.16** shows E_{pa} and E_{pc} *vs.* $\ln \nu$, where using **Equation 5.18** the slopes for E_{pa} and E_{pc} equal $\frac{RT}{2\alpha_a F}$ and $-\frac{RT}{2\alpha_c F}$, respectively.

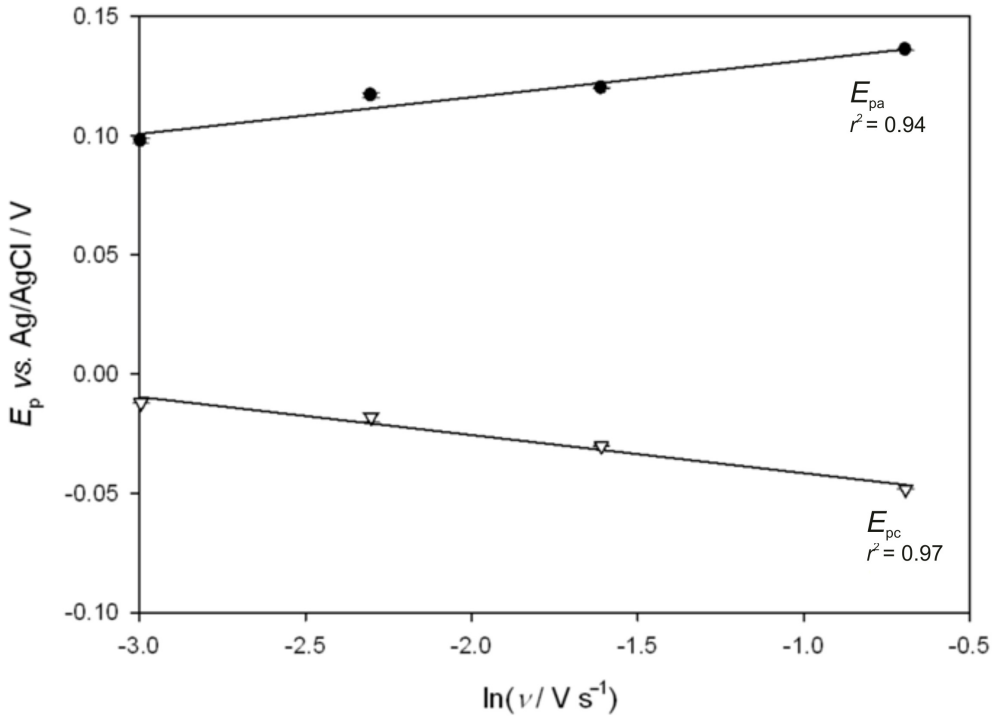

Figure 5.16. Plots of E_{pa} and E_{pc} *vs.* $\ln \nu$ for the aerated control ASW.

The transfer coefficient values can be deduced utilising **Figure 5.16**, where $\alpha_a \approx$ **0.82** and $\alpha_c \approx$ **0.79** (**Table 5.6**), thus showing symmetrical values informative of a quasi-reversible process (ideally $\alpha_a + \alpha_c = 1$ for a reversible process) [**5.14**].

Table 5.6. Summary of the transfer coefficient values for the aerated control ASW using **Figure 5.16**.

R **/ J K^{-1} mol^{-1}**	8.3144
T **/ K,** see **Table 4.5**	291.75
F **/ C mol^{-1}**	96,485
Slope for E_{pa} *vs.* ln ν / V	0.015
α_a **/ dimensionless**	**0.82**
Slope for E_{pc} *vs.* ln ν / V	–0.016
α_c **/ dimensionless**	**0.79**

Quantitative analyses using **Equation 5.15** would imply that corresponding j_p values are within the order of magnitude of 2.0×10^{-4} A cm^{-2} for $c = 1.0 \times 10^{-6}$ mol cm^{-3} (*i.e.* 1.0×10^{-3} mol L^{-1}) [**5.14**]. This is about 10^3-fold higher to the concentration of $FeCl_3$ and EDTA in **Table 4.3**, thus **Equation 5.15** is not applicable for this concentration in order to determine accurately the diffusion coefficient of the ferric-EDTA complex.

5.9 Summary of the CV analysis for the abiotic test condition

Overall, the performance of the sensor in the abiotic ASW medium was in agreement with typical electrochemical characteristics of a Au electrode in an abiotic seawater environment [**5.4**]. The analysis for the abiotic ASW medium was supported by a comparative study with a conventional behaviour of a Au electrode in 3.5 % NaCl and with the electrochemical response in a control ASW test solution (only consisting of metal-ions and salts, and also EDTA in **Section 4.4**).

Table 5.7. Summary of detectable electrochemical process at the Au / abiotic ASW interface (**Figure 5.8**) for a potential range of –1.000 to +1.000 V (*vs.* Ag/AgCl).

Potentials	Regions	Description	
≥ +0.750 V (*vs.* Ag/AgCl)	***(A')***	Au oxide formation	**self-cleaning of the Au surface**
around +0.550 V (*vs.* Ag/AgCl)	***(B')***	cathodic stripping of the Au oxide	
between –0.200 V to the plateau at –0.700 V (*vs.* Ag/AgCl)	***(C')***	**ORR wave**	
± 0.125 V (*vs.* Ag/AgCl)	***(A'') / (B'')***	electro-active adsorption / desorption of metal-ions suppressed by blocking organic material	
between +0.500 to +0.900 V (*vs.* Ag/AgCl)	***(C'')***	oxidation wave for organic material oxidation reaction	

Importantly, and as well as similar to the NaCl test solution, an electrode polarised in the cathodic region between –0.200 V to the plateau at –0.700 V (*vs.* Ag/AgCl), can detect the baseline ORR in a marine environment (Clark electrode) [**5.4**]. The oxidation reaction of organic material, corresponding to the wave between +0.500 to +0.900 V (*vs.* Ag/AgCl), can suppress the surface oxidation process beginning around +0.750 V (*vs.* Ag/AgCl) both in the NaCl test solution and control ASW medium [**5.14**-**5.16**]. This suggests that higher potentials may be required for the self-cleaning of the Au electrode immersed in seawater enriched with organic material. Likewise, it was demonstrated that metal-ions from the bulk ASW medium can diffuse and subsequently electro-actively adsorb / desorb on the Au surface, *i.e.* in the regions ***(A'')*** and ***(B'')*** at ± 0.125 V (*vs.* Ag/AgCl), and also overall this diffusion dominant process was depressed by the presence of blocking organic material (in the abiotic ASW) adsorbed / desorbed on the Au surface, which in turn represents about **70 %** percentage surface coverage. Although **Section 5.8** has outlined limited quantitative evaluation of the diffusion process in the region ***(A'')*** and ***(B'')***, it was shown that the electrochemical reaction involved was a quasi-reversible ($\alpha_a \approx$ **0.82** and $\alpha_c \approx$ **0.79**) and single electron process (z = 1) consistent with the redox couple Fe^{3+} EDTA / Fe^{2+} EDTA. Overall, this will have negligible influence on the interfacial response for the biotic test condition in **Section 5.10**. In contrast with surface modification treatment, this clearly shows that a

conditioning film on the Au surface is not representative of an impermeable and controllable coating but can consist of a monolayer with defects / pinholes facilitating charge diffusion process in analogy with self-assembled monolayers on Au microelectrodes [**5.14**,**5.15**,**5.22**].

5.10 CV for the biotic test condition

In contrast with the abiotic ASW, the electrochemical response for the biotic test condition (**Figure 5.17**) was time-dependent and showed of detectable modification of the reaction kinetics at the Au / biotic ASW interface after a 72 h immersion.

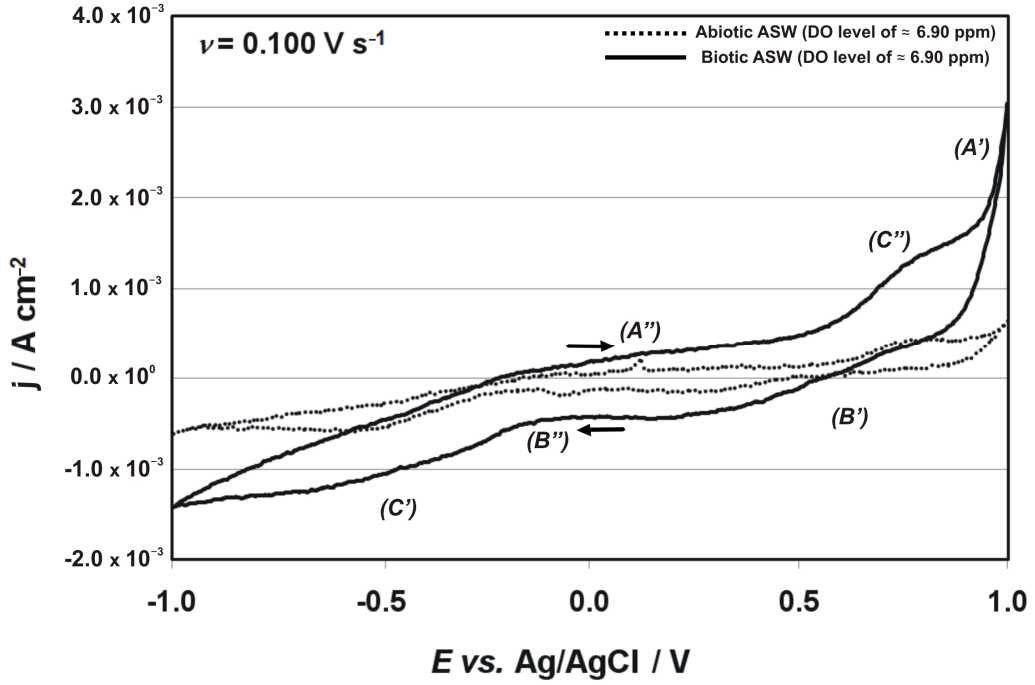

Figure 5.17. Comparison of cyclic voltammograms for a 0.2 mm diameter Au electrode in aerated **(dashed line)** abiotic and **(solid line)** biotic ASW medium after a 72 h immersion at a scan rate of 0.100 V s^{-1}.

Overall, the electrochemical characteristics obtained over 72 h in the biotic ASW medium (**Figure 5.17**) were more complex compared to the abiotic condition (**Figure 5.8**), thus consistent with [**5.13**,**5.23**]. As in the abiotic ASW medium, the domain **(*A'*)** represents the onset of the Au oxide formation, where the corresponding cathodic peak in the region **(*B'*)** was suppressed, thus indicative of an irreversible process [**5.6**]. Interestingly, the region ***(C')*** of the ORR was more pronounced for the biotic in comparison with the abiotic condition. This is representative of an increase of the current density (absolute value) in the presence of *Pseudoalteromonas* bacteria. This phenomenon can be explained by an enhancement of the ORR kinetics due to

enzymatic activities, thus consistent with [**5.24**-**5.27**] where specific enzymes (*e.g.* catalase) that are present in the EPS matrix could be responsible for an increase in cathodic currents. H_2O_2 in **Equation 5.8** (**Section 5.6**) can be decomposed by enzymatic processes to H_2O and O_2 (**Section 2.4.3.2**), see **Equation 5.19**. A higher concentration of reactants (*i.e.* O_2 species) is readily available at the cathode, therefore increasing the kinetics of the overall ORR.

$$2H_2O_2 \rightarrow 2H_2O + O_2 \qquad (5.19)$$

Conversely, the regions **(*A''*)** and **(*B''*)** corresponding to the electro-active adsorption / desorption of metal ions were completely suppressed as compared with the abiotic condition, thus explained by the inability of metal-ions to diffuse across the biofilm to the Au surface. This is in good agreement with the characteristics of aerobic bacteria to change the electrochemical properties of metallic surfaces [**5.24**,**5.28**]. In addition, a wave in the region ***(C'')*** was observed between about +0.300 to +0.800 V (*vs.* Ag/AgCl). This wave can be explained by anodic reaction mechanisms of electro-active *Pseudoalteromonas* biofilms [**5.29**-**5.31**] and was consistent with similar reports using adhered biofilms on a Au surface [**5.13**,**5.23**].

Although the exact pathway of interfacial charge transfer supported by bacterial cells remains to be clarified (see **Section 2.4.3.2**), it has been proposed that bacteria within electro-active biofilms can directly exchange electrons with a conductive material without a mediator [**5.29**,**5.30**,**5.32**-**5.34**]. One possible explanation is presented in analogy with the concept of mediator-less MFC or biological fuel cell, *i.e.* a system where electrochemically active bacteria can transfer electrons directly from the bacterial respiratory enzyme to the electrode [**5.29**,**5.30**,**5.32**-**5.34**]. When bacterial biofilms develop on the conditioning film, a gradient of DO level is generated (differential aeration cell), thus resulting in the formation of micro-galvanic anode and cathode on the electrode, see **Figure 2.19(c)*(ii)*** in **Section 2.6.5.3**. At the anodic site where O_2 is deficient, bacteria can oxidise organic material and produce CO_2 plus H_2O [**5.33**]. The oxidation reaction at the anode via respiratory enzymes generates electrons collected at the cathodic site where O_2 is prominent. In this process, bacteria can assist in the transfer of electrons, where the most active cells can be found at the biofilm / seawater interface [**5.27**]. Overall, the enzymatic enhanced ORR via catalase enzymes (**Figure 5.18**) is the prevailing reaction at the cathode.

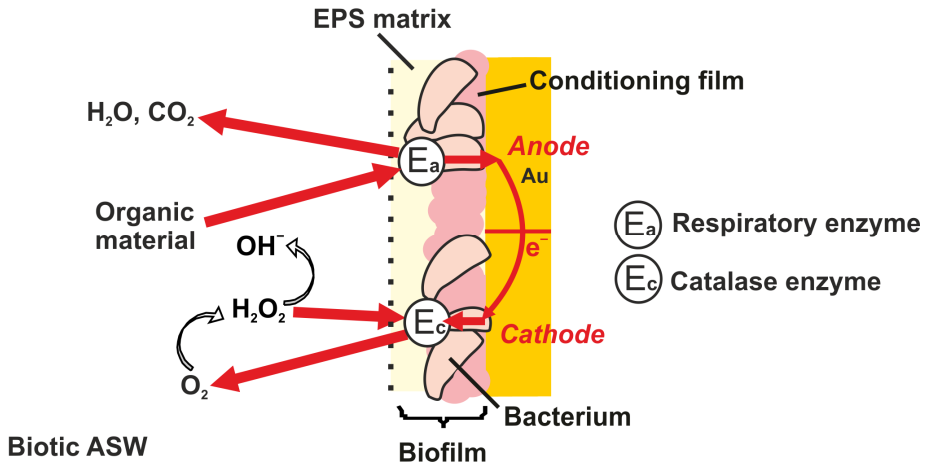

Figure 5.18. Schematic representation of electron transfers pathway within a *Pseudoalteromonas* biofilm in analogy with biological fuel cell – typical thickness of the bacterial biofilm ≈ a few microns [**5.7**,**5.24**,**5.35**,**5.36**].

5.11 Summary of electrochemical performance within abiotic and biotic ASW test media

Overall, the cyclic voltammograms between the abiotic and biotic ASW media demonstrated that bacterial biofilms can change the electrochemical properties at the interface, *i.e.* suppression of regions ***(B')***, ***(A'')*** and ***(B'')*** and enhance the overall ORR, and also the oxidation reaction of organic material, see **Table 5.8**. Herein, the results were consistent with [**5.13**,**5.24**,**5.25**]. By polarising in the negative direction, *i.e.* the cathodic domain **(*C'*)**, the overall and enhanced ORR due to enzymatic processes can be assessed. The working principle of commercialised electrochemical sensors for biofilm sensing, such as the BIoGEORGE and BioX (**Section 2.6.4.2**) relies on similar electrical polarisation method [**5.35**-**5.40**]. With the depression of the Au oxide stripping (**Table 5.8**), the self-cleaning of the biofilmed Au is debatable for a potential range of –1.000 to +1.000 V (*vs.* Ag/AgCl), where higher potentials to that for the NaCl test solution and ASW medium may be necessary. However, the essence of this scientific work is to sense for biofilms without imposing an electrical polarisation, which has been proven to influence biofilms [**5.41**] (**Section 2.6.6**). Consequently, the EIS at the OCP values has been chosen (see **Section 5.12**).

Table 5.8. Summary of detectable electrochemical process at the Au / biotic ASW interface (**Figure 5.17**) for a potential range of –1.000 to +1.000 V (*vs.* Ag/AgCl).

Potentials	Regions	Description
≥ +0.750 V (*vs.* Ag/AgCl)	***(A')***	Au oxide formation
around +0.550 V (*vs.* Ag/AgCl)	***(B')***	N/A
between –0.200 V to the plateau at –0.700 V (*vs.* Ag/AgCl)	***(C')***	**enzymatic enhanced ORR wave**
± 0.125 V (*vs.* Ag/AgCl)	***(A'') / (B'')***	N/A
between +0.500 to +0.900 V (*vs.* Ag/AgCl)	***(C'')***	enzymatic enhanced oxidation wave for organic material oxidation reaction

5.12 Qualitative analysis of the EIS data / confocal microscopy

The EIS data were presented in three forms: the Bode $|Z|$ (|impedance| *vs.* frequency) plots, the Bode $-\theta$ (the –phase *vs.* frequency) plots and the Nyquist (the –imaginary part *vs*. real components of the complex impedance) diagrams. The impedance data for the NaCl test solution in **Figures 5.19** to **5.21** represent the electrochemical behaviour of the Au electrode in a neutral – alkaline solution, pH 8.0 [**5.42**]. This has allowed establishing a framework of electrochemical characterisation for the abiotic test condition (**Figures 5.25** to **5.27**) to be used for a comparative study between the abiotic and biotic media (**Figures 5.30** to **5.32**) in order to evaluate the sensor performance. Importantly, the EIS response of the 500 nM NO donor SNP on a 72-h old biofilmed Au electrode is uniquely presented in **Figures 5.36** to **5.38** to assess the overall effectiveness of the natural biocide (continuous dosing) over a 24 h duration. In addition, a fine evaluation of the capacitive parameters for the NaCl test solution, the abiotic and biotic media, and also the 500 nM SNP in ASW is addressed in **Section 5.13**.

5.12.1 EIS analysis of the NaCl test condition

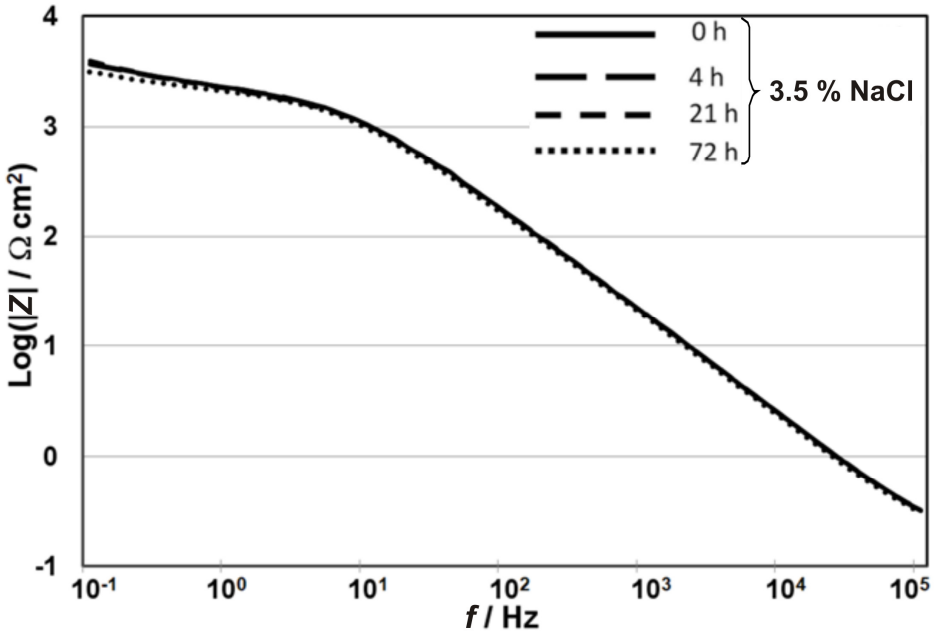

Figure 5.19. Bode (|*Z*| *vs. f*) plots at OCP for a 0.2 mm diameter Au electrode in the 3.5 % NaCl solution – OCP values: +0.090, –0.070, –0.215 and –0.225 V (*vs.* Ag/AgCl) after a 0, 4, 21 and 72 h immersion, respectively.

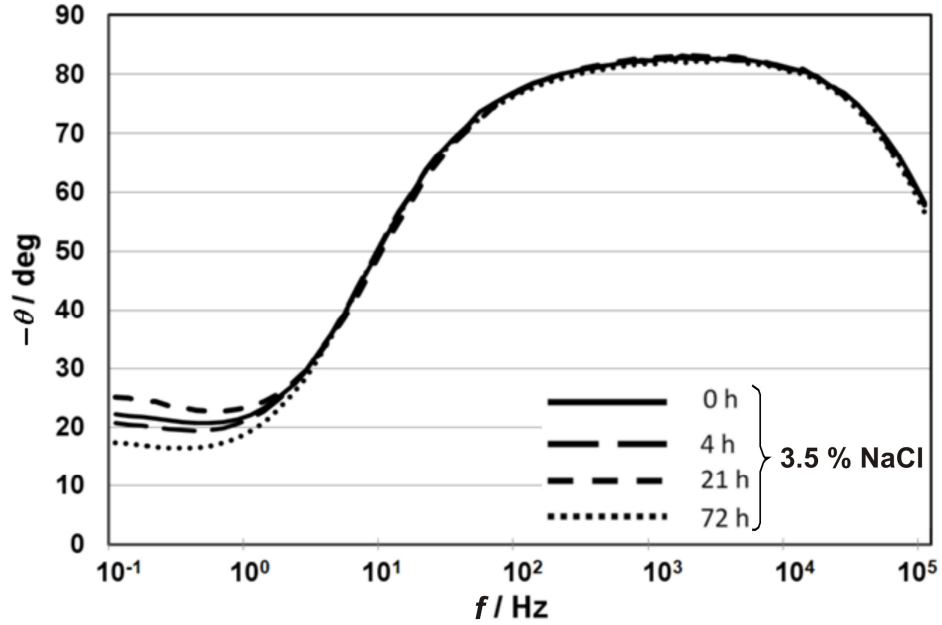

Figure 5.20. Bode (–θ *vs. f*) plots at OCP for a 0.2 mm diameter Au electrode in the 3.5 % NaCl solution – OCP values: +0.090, –0.070, –0.215 and –0.225 V (*vs.* Ag/AgCl) after a 0, 4, 21 and 72 h immersion, respectively.

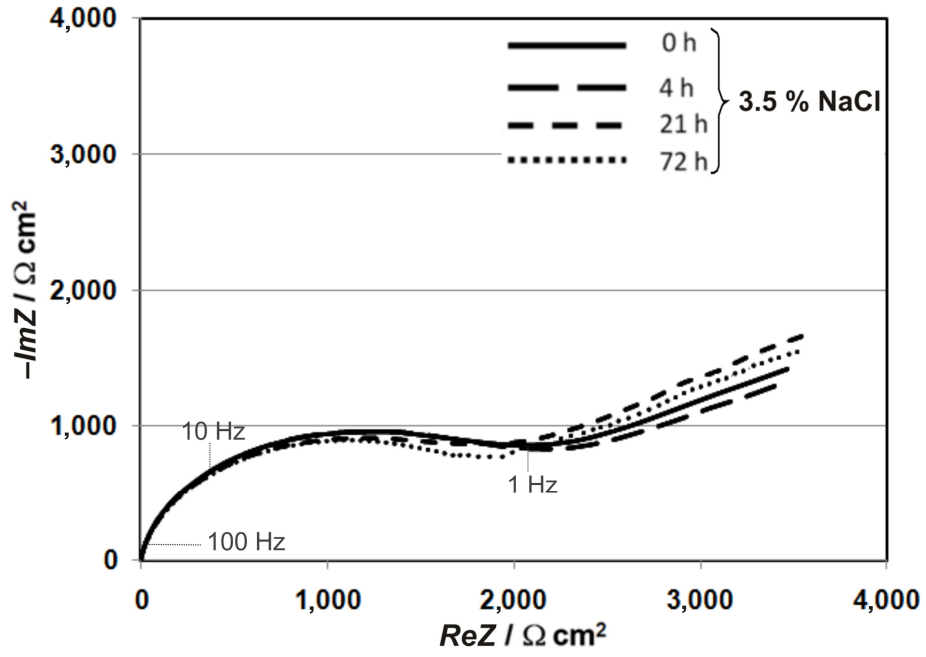

Figure 5.21. Nyquist diagrams at OCP for a 0.2 mm diameter Au electrode in the 3.5 % NaCl solution – OCP values: +0.090, –0.070, –0.215 and –0.225 V (*vs.* Ag/AgCl) after a 0, 4, 21 and 72 h immersion, respectively.

Overall, the EIS response in **Figure 5.19** was relatively uniform over time with two distinct regions. At higher frequencies, between 10 to 100,000 Hz, a linear relationship is apparent between the interfacial impedance modulus |*Z*| and frequency with a slope close to –1 (see **Section 5.13** for a fine assessment of the capacitive characteristics for the NaCl test solution), which corresponds to a plateau of the phase angle close to –90 degrees in **Figure 5.20** and partially resolved Nyquist plot semicircles in **Figure 5.21**. This is indicative of a predominantly capacitance behaviour and is consistent with a previous study using a similar experimental sterile configuration [**5.42**] and with the well-established double-layer concept (*i.e*. interfacial charge distribution) [**5.43**]. In this frequency region, the plots are perfectly overlapped, thus indicating good reproducibility of the EIS performance. At lower frequencies, between 0.1 to 10 Hz, an additional resistance / diffusive response (**Figure 5.19**) can be seen with negligible impedance changes over a 72 h immersion, thus demonstrating the absence of detectable modification of the interfacial charge transfer with time. The diffusive behaviour (**Figure 5.19**) is associated with linear features having a slope close to 45 degrees (representative of a Warburg impedance response, W) over the 72 h in **Figure 5.21**. This impedance characteristic can result from diffusion of the electro-active DO to the Au surface to participate in the ORR [**5.42**]. In a deaerated 3.5 % NaCl solution (see the idealised plot to illustrate the curve analysis in **Figure 5.22**), the

EIS response would be similar to a perfect capacitive behaviour without the low frequency resistive / diffusive characteristic [**5.42**].

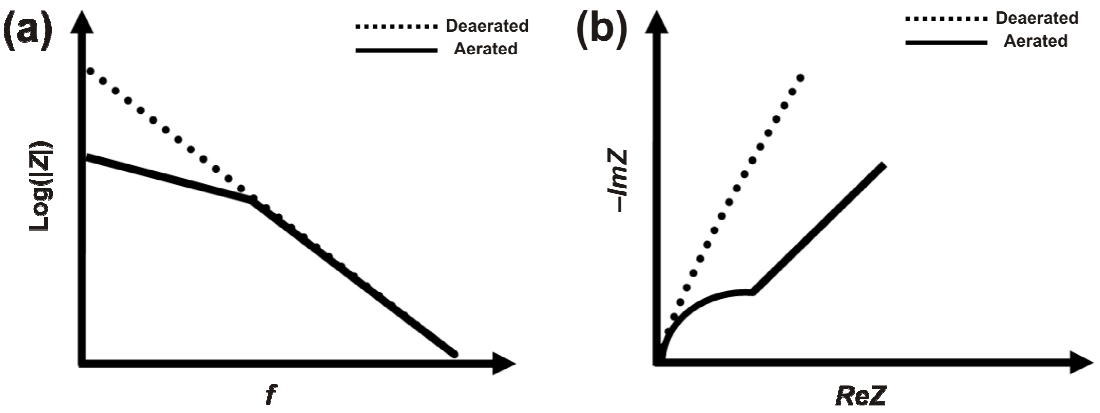

Figure 5.22. Qualitative **(a)** Bode (|*Z*| *vs. f*) and **(b)** Nyquist plots for a Au micro-electrode in N_2 **(dashed line)** and air **(solid line)** saturated, 3.5 % NaCl solution – idealised plot to illustrate the curve analysis, adapted from [**5.42**].

Figure 5.23 shows the confocal microscopy analyses of a Au electrode after a 72 h immersion in NaCl.

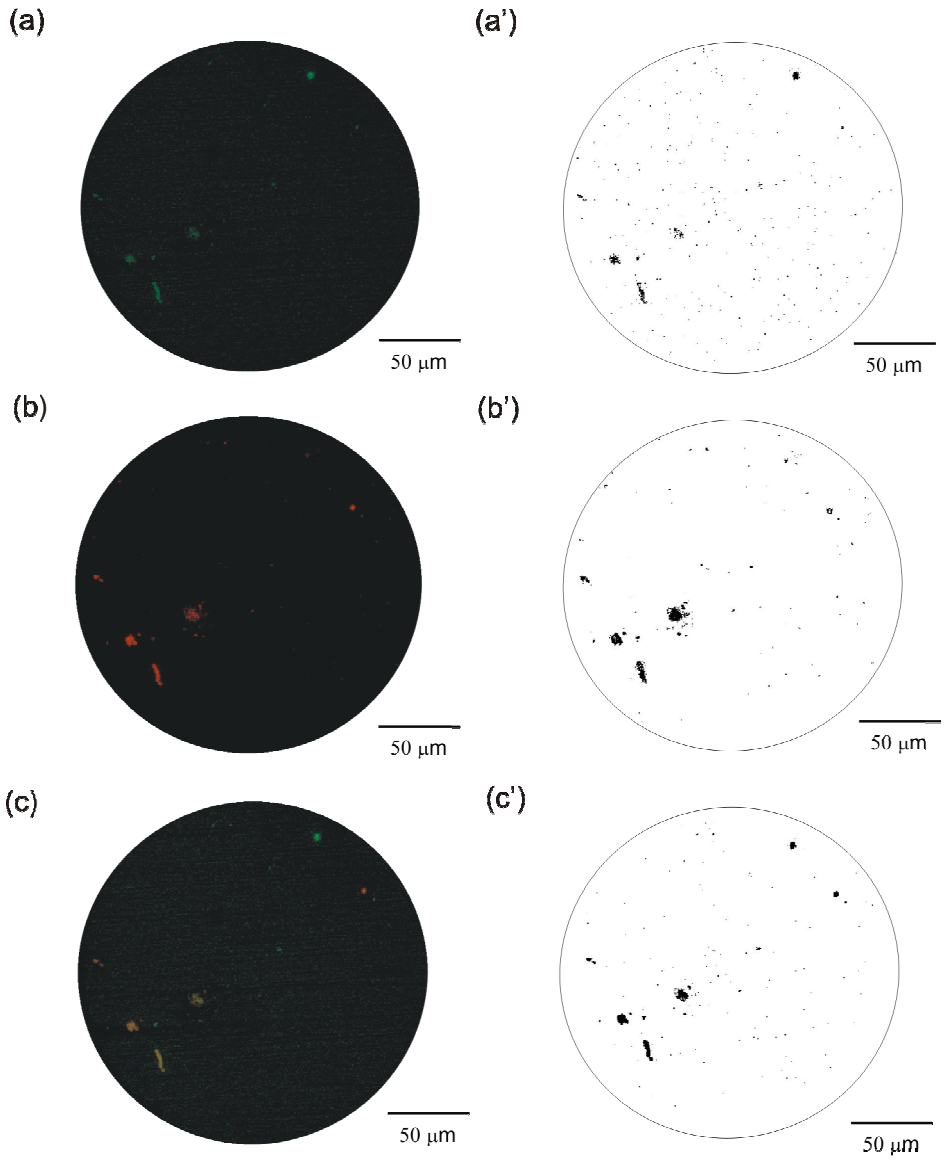

Figure 5.23. Confocal microscopy of a Au electrode stained with the *Bac*Light™ viability kit after a 72 h immersion in 3.5% NaCl: **(a)** Live, **(b)** Dead and **(c)** Live / Dead – corresponding binary (black and white) images in **(a')**, **(b')** and **(c')** using ImageJ software.

The presence of a few isolated spots in **Figure 5.23** is indicative of a minimum fouling on the Au surface in the NaCl. A control test with no *Bac*Light is necessary to fully address the nature of the fluorescent background signal (**Figure 5.23**). After discussions with Dr Stoodley (nCATS), it is usually attributed to processes of non-specific binding (where the stains are binding to receptors not of interest in order to achieve a more favourable chemical configuration) [**5.44**].

Overall, the prevailing processes in NaCl can be explained by DO from the bulk solution diffusing across the double layer to be reduced at the Au surface via the ORR, see **Figure 5.24**.

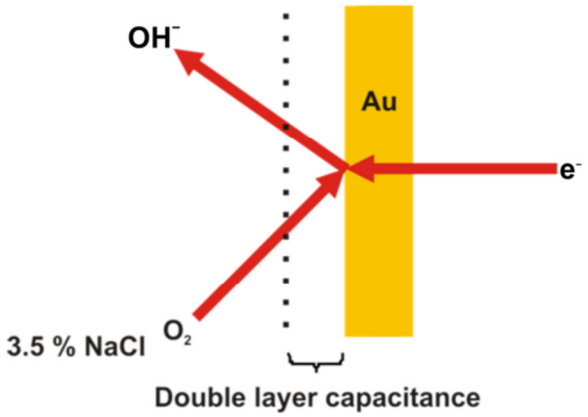

Figure 5.24. ORR mechanisms at the Au / NaCl interface – typical thickness of the double layer ≈ 0.5 nm [**5.8**].

5.12.2 EIS analysis of the abiotic test condition

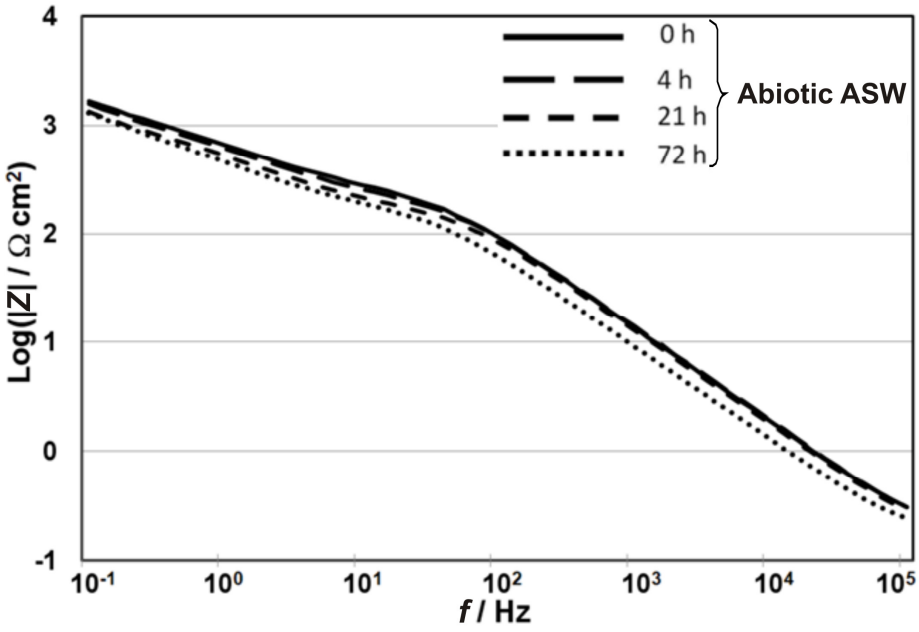

Figure 5.25. Bode (|*Z*| *vs. f*) plots at OCP for a 0.2 mm diameter Au electrode in the abiotic ASW medium – OCP values: +0.085, –0.070, –0.250 and –0.325 V (*vs.* Ag/AgCl) after a 0, 4, 21 and 72 h immersion, respectively.

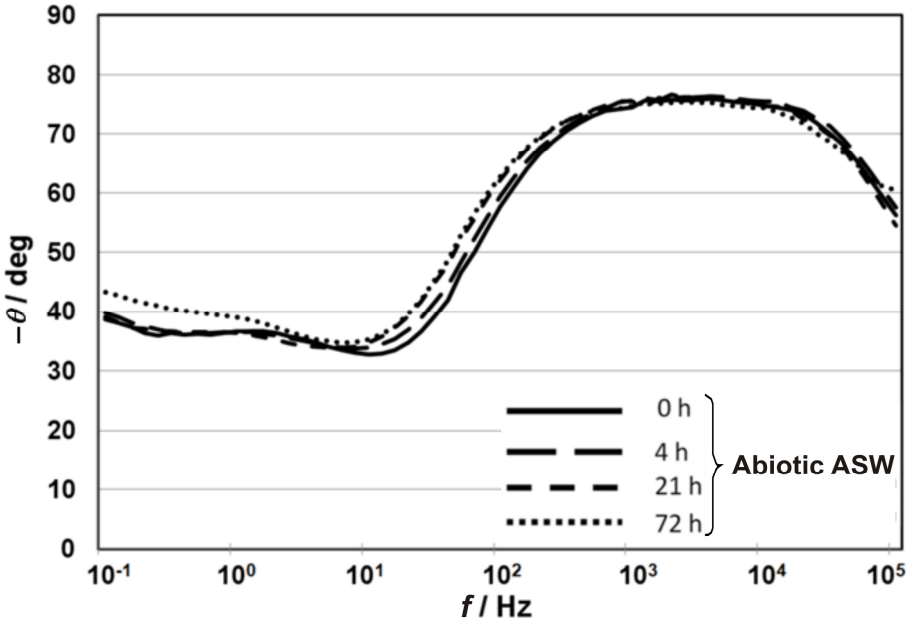

Figure 5.26. Bode (*–θ vs. f*) plots at OCP for a 0.2 mm diameter Au electrode in the abiotic ASW medium – OCP values: +0.085, –0.070, –0.250 and –0.325 V (*vs.* Ag/AgCl) after a 0, 4, 21 and 72 h immersion, respectively.

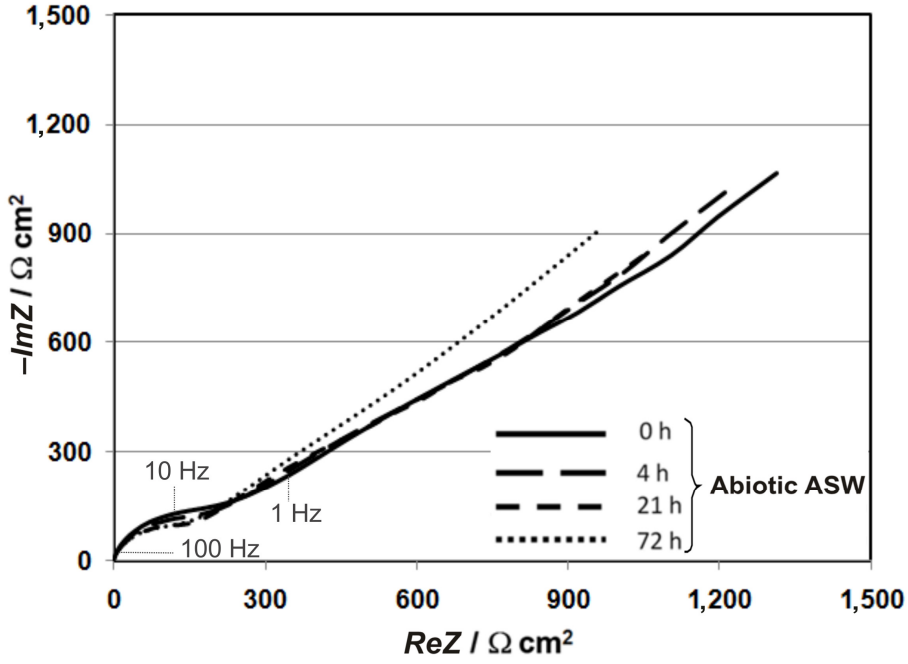

Figure 5.27. Nyquist diagrams at OCP for a 0.2 mm diameter Au electrode in the abiotic ASW medium – OCP values: +0.085, –0.070, –0.250 and –0.325 V (*vs.* Ag/AgCl) after a 0, 4, 21 and 72 h immersion, respectively.

Overall, the EIS response in the abiotic ASW medium (**Figures 5.25** and **5.26**) tends to shift with time towards lower frequencies. This behaviour is often associated with interfacial adsorption dominant processes [**5.45**,**5.46**]. In the high frequency part of the spectra, 100 to 100,000 Hz (**Figure 5.25**), a slope close to –1 (see **Section 5.13** for a fine study of the capacitive behaviour for the abiotic ASW) is evident corresponding to a plateau of the phase angle relatively close to –90 degrees in **Figure 5.26** and to partially resolved Nyquist semicircles in **Figure 5.27**. This can be explained by a capacitance characteristic associated with a conditioning film due to the rapid formation of an adsorbed layer of organic material (*i.e.* a conditioning film) on the Au surface [**5.36**,**5.47**,**5.48**]. In the low frequency part of the spectra, 0.1 to 100 Hz, a clear diffusive response can be seen in **Figure 5.25**. This coincides with the presence of a delineated linear feature having a slope of 45 degrees in **Figure 5.27**, which is characteristic of diffusion of dissolved species, such as electro-active DO to the Au surface.

Figure 5.28 represents the confocal microscopy analyses of a Au electrode after a 72 h immersion in abiotic ASW. Similar to the NaCl solution in **Figure 5.23**, the presence of faint coloured spots (**Figure 5.28**) is representative of minimum fouling and may be explained by non-specific binding [**5.44**].

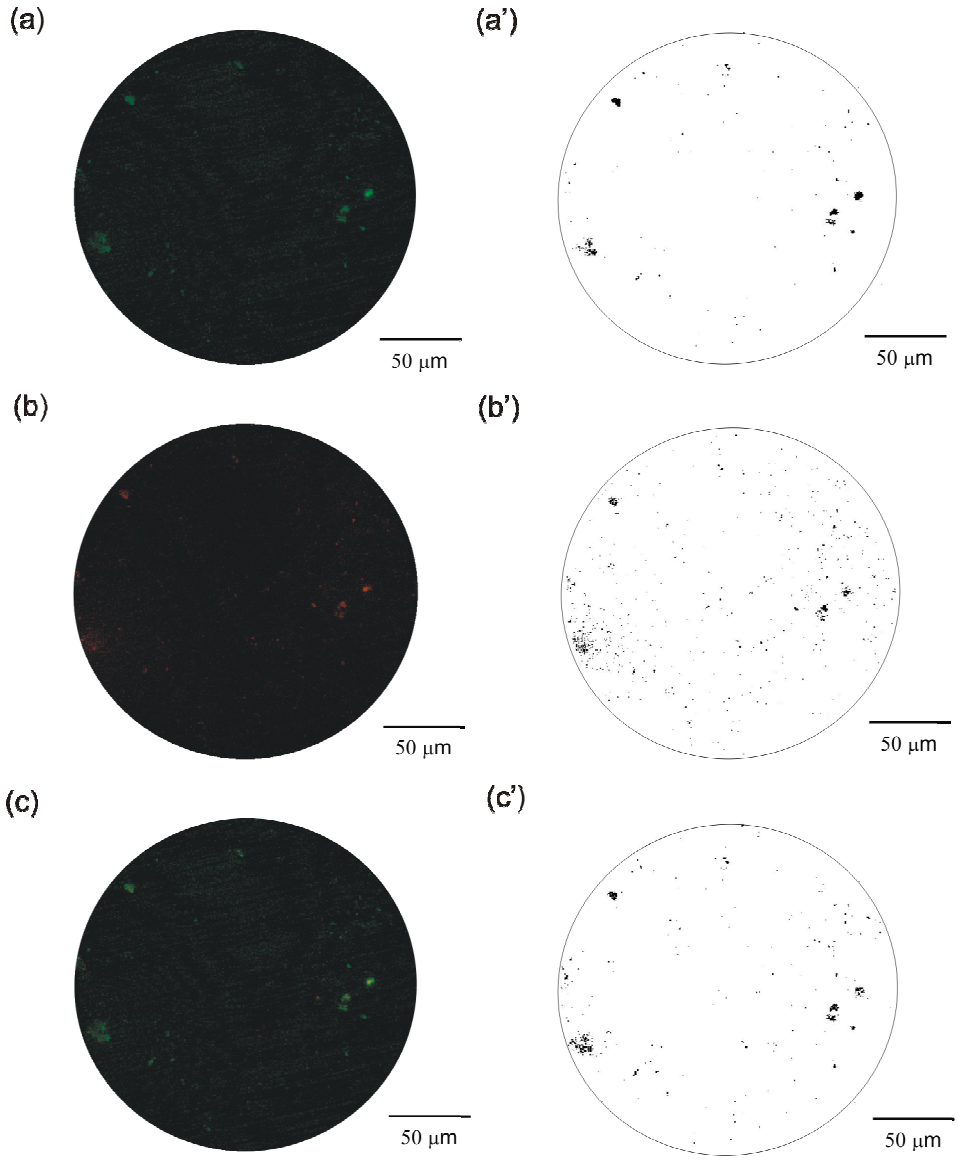

Figure 5.28. Confocal microscopy of a Au electrode stained with the *Bac*Light™ viability kit after a 72 h immersion in abiotic ASW: **(a)** Live, **(b)** Dead and **(c)** Live / Dead – corresponding binary (black and white) images in **(a')**, **(b')** and **(c')** using ImageJ software.

Overall, the mechanistic model in the ASW (**Figure 5.29**) is the diffusion of DO from the bulk across the conditioning layer to be reduced at the Au surface via the ORR.

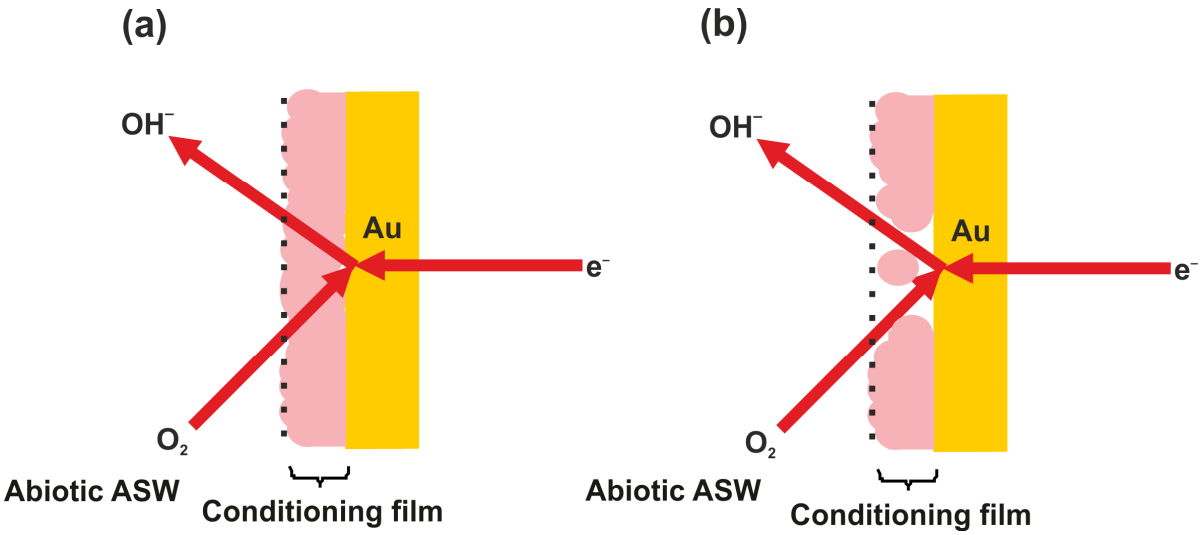

Figure 5.29. ORR mechanisms at the Au / ASW interface for **(a)** a homogeneous and **(b)** a heterogeneous adsorbed organic layer – typical thickness of the conditioning film ≈ 6 – 10 nm [**5.35**,**5.36**,**5.49**].

Herein, it is clear that the EIS response (at the Au / 3.5 % NaCl or abiotic ASW interface) was independent of time, *i.e.* there was no significant impedance change during the 72 h test. Thus, the results for the 3.5 % NaCl and abiotic ASW test solutions established that no detectable modification of the electron transfer or cathodic reduction reaction occurred.

5.12.3 EIS analysis of the biotic test condition

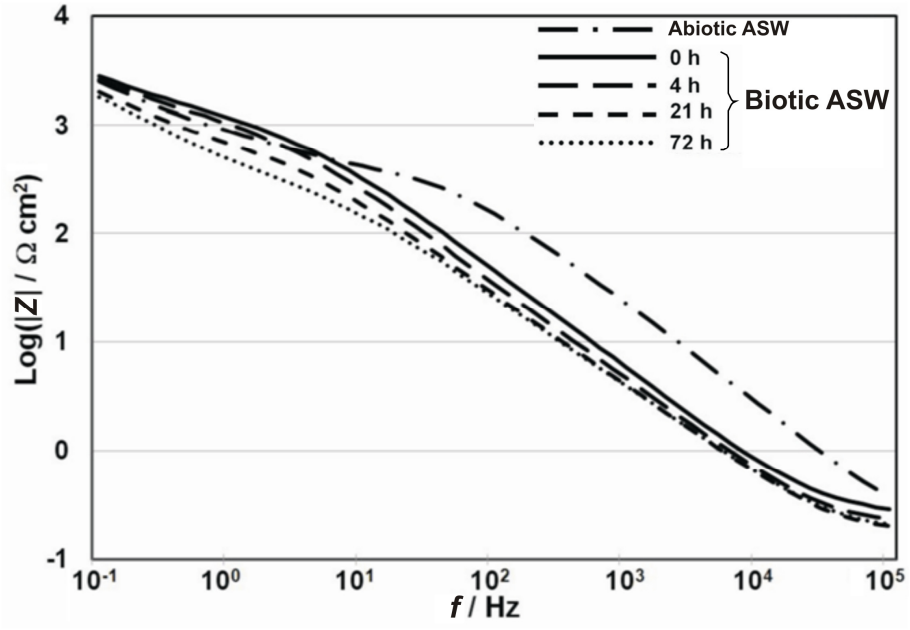

Figure 5.30. Bode (|*Z*| *vs. f*) plots for a 0.2 mm diameter Au electrode in the biotic ASW medium (abiotic: –1 h before inoculation) – OCP values: +0.090, +0.085, –0.075, –0.460 and –0.560 V (*vs.* Ag/AgCl) at –1 h (abiotic) and after a 0, 4, 21 and 72 h immersion, respectively.

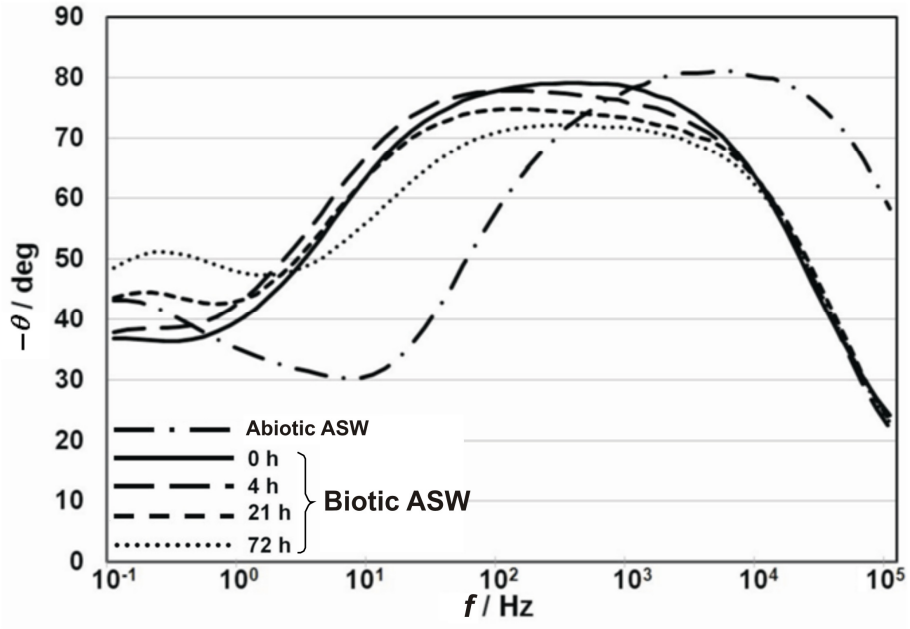

Figure 5.31. Bode (–θ *vs. f*) plots for a 0.2 mm diameter Au electrode in the biotic ASW medium (abiotic: –1 h before inoculation) – OCP values: +0.090, +0.085, –0.075, –0.460 and –0.560 V (*vs.* Ag/AgCl) at –1 h (abiotic) and after a 0, 4, 21 and 72 h immersion, respectively.

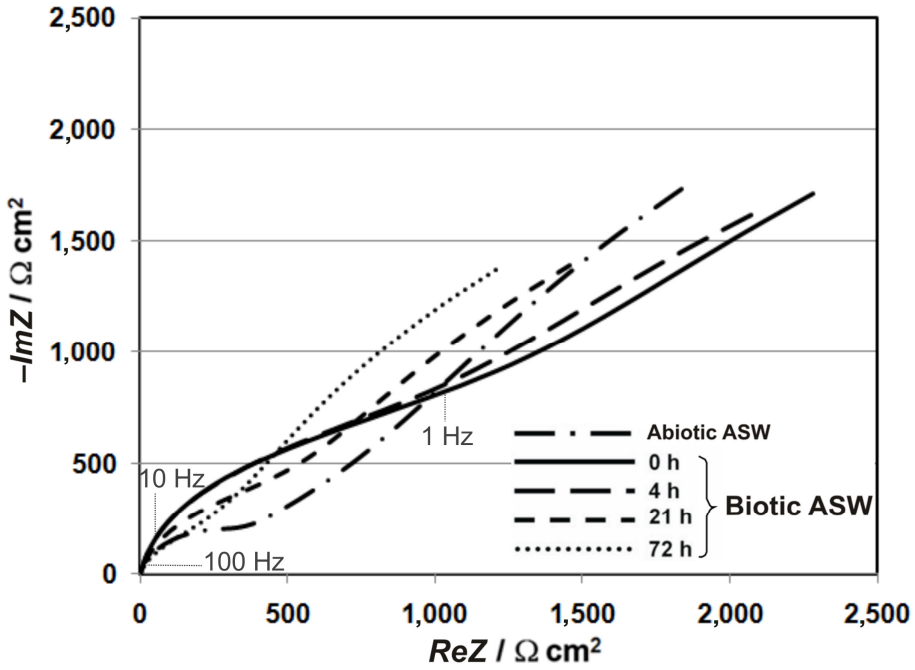

Figure 5.32. Nyquist diagrams for a 0.2 mm diameter Au electrode in the biotic ASW medium (abiotic: –1 h before inoculation) – OCP values: +0.090, +0.085, –0.075, –0.460 and –0.560 V (*vs.* Ag/AgCl) at –1 h (abiotic) and after a 0, 4, 21 and 72 h immersion, respectively.

In contrast to the abiotic ASW in **Section 5.12.2**, the EIS data show a more complex impedance response for the biotic ASW medium. Initially similar at –1 h to the abiotic condition, after inoculation (0 h) the capacitive region was clearly extended deeper into the low frequency part of the spectra (**Figures 5.30** and **5.31**) with an overall increase in the diameter of the resolved Nyquist semicircles observed in **Figure 5.32**. This is indicative of a greater influence of adsorption processes [**5.45**,**5.46**], associated with the adhesion of the pioneering bacteria on a conditioning film [**5.50**,**5.51**], thus consistent with [**5.52**]. At lower frequencies, 0.1 to 100 Hz (**Figure 5.30**), a diffusive behaviour with a subtle change in impedance over 72 h was observed compared to the abiotic condition. This coincides with a decrease of the depressed Nyquist semicircles with a tail having a slope close to 45 degrees, see **Figure 5.32**. It can probably be explained by an enhancement of the ORR by enzymatic processes via similar mechanisms presented in **Figure 2.19(c)*(ii)*** in **Section 2.6.5.3**, thus consistent with similar work using the same strain on 70 / 30 Cu-Ni alloys (although the corrosion products and oxide film formation also influenced the EIS response) [**5.53**].

Figure 5.33 shows the confocal microscopy analyses of a Au electrode after a 72 h immersion in biotic ASW. The bacterial clusters or patchy slime are clearly seen (**Figure 5.33**), thus corroborating the presence of bacterial biofilms established under low laminar flow conditions [**5.36**] (as opposed to filamentous / streamlined biofilms observed in turbulent flow regime [**5.54**]) and the EIS response for the biotic ASW medium in **Figures 5.30** to **5.32**. Using the LCS version 2.61, a biofilm thickness of 3.0 $\pm$ 0.5 μm was measured (**Figure 5.34**), consistent with the occurrence of a thin physical diffusion barrier [**5.55**,**5.56**], which has been reported to be 4 – 8 μm thick on a Au surface after a 10 days exposure in seawater [**5.7**].

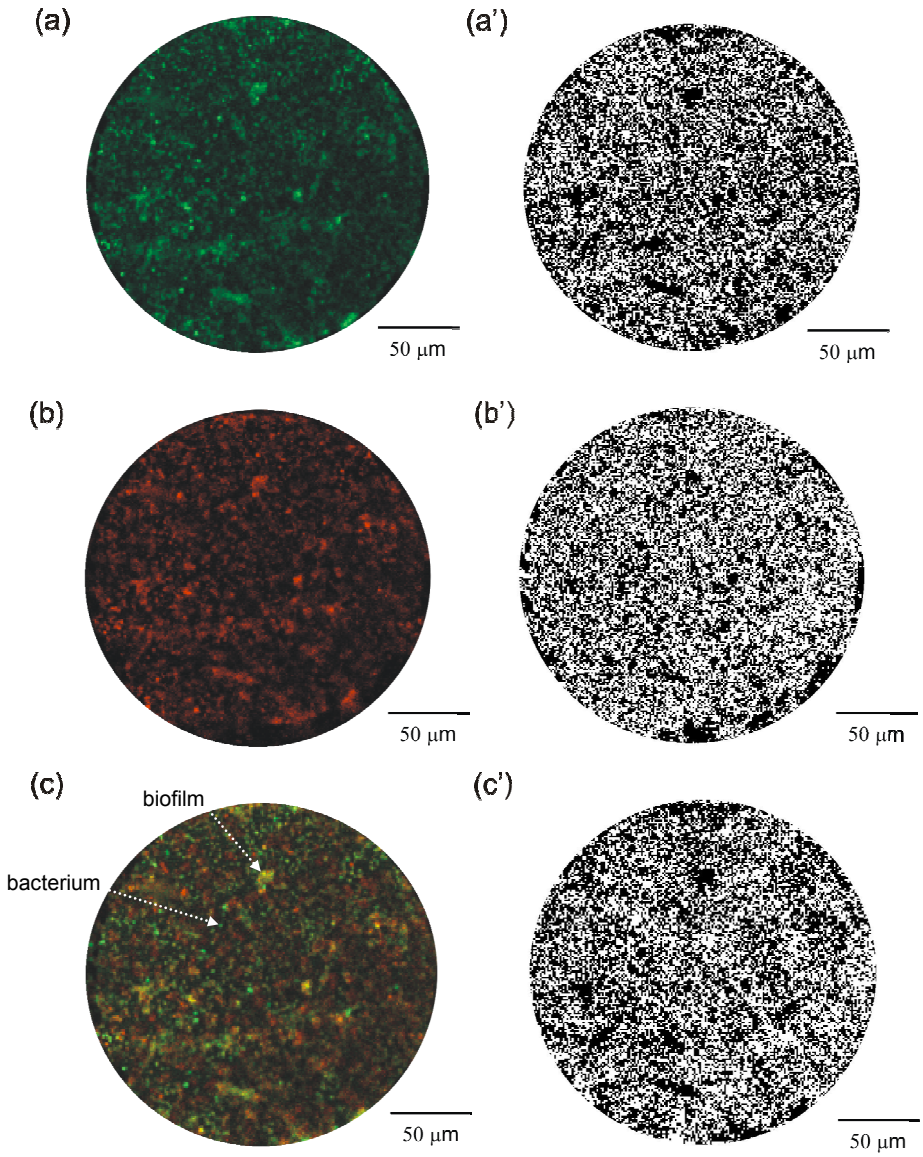

Figure 5.33. Confocal microscopy of a Au electrode stained with the *Bac*Light™ viability kit after a 72 h immersion in biotic ASW: **(a)** Live, **(b)** Dead and **(c)** Live / Dead – corresponding binary (black and white) images in **(a')**, **(b')** and **(c')** using ImageJ software.

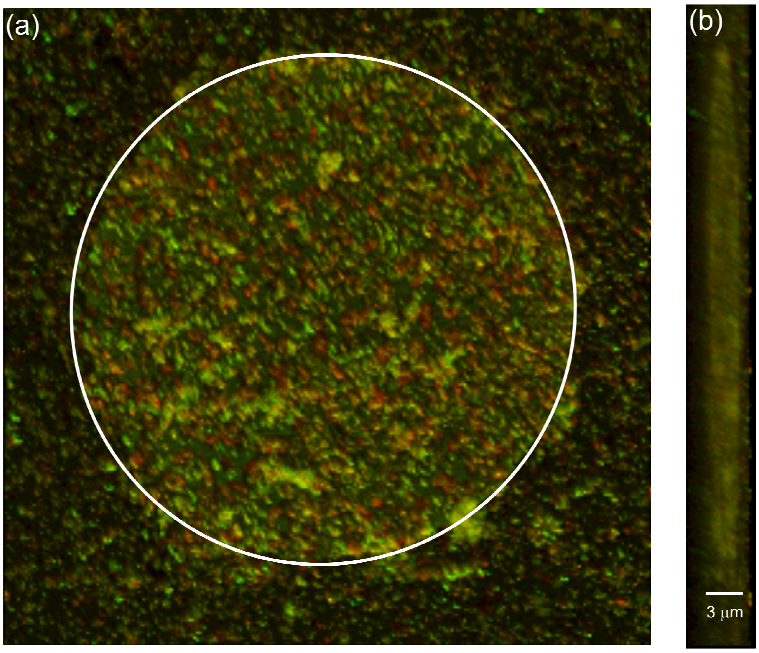

Figure 5.34. **(a)** Confocal microscopy of a 72 h-old biofilmed Au electrode stained with the *Bac*Light™ viability kit and (**b)** the corresponding cross section.

In agreement with the EIS data, this confirms that bacterial biofilm formation and its extent is a dynamic and complex process [**5.47**]. Initially, pioneering bacteria will settle on the conditioning film formed on the Au surface. Subsequent bacterial growth, colonisation and EPS secretion will follow the initial bacterial adhesion using available nutrients within the EPS and bulk solution. Similarly, enzymes (*e.g.* catalase in **Section 2.4.3.2**) will be produced to assist in the ORR enhancement, see **Figure 5.35**.

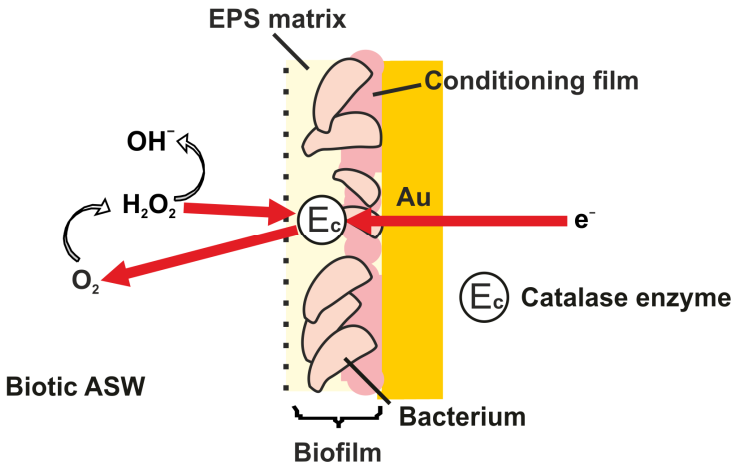

Figure 5.35. ORR enhancement mechanisms for the biotic condition – typical thickness of the bacterial biofilm ≈ a few microns [**5.7**,**5.24**,**5.35**,**5.36**].

5.12.4 EIS analysis of the NO donor SNP

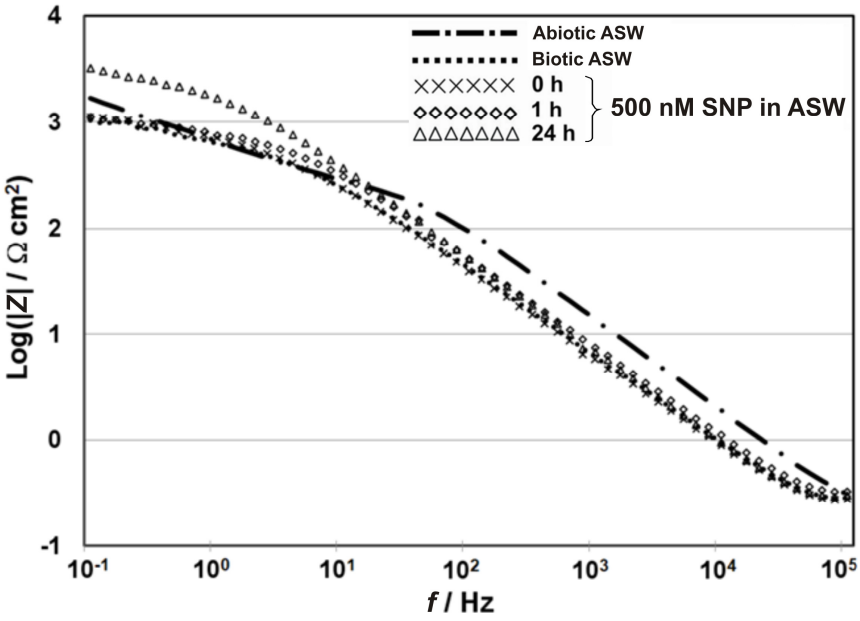

Figure 5.36. Bode (|*Z*| *vs. f*) plots for a 0.2 mm diameter Au electrode with 500 nM NO donor SNP in ASW medium for 24 h (abiotic: –1 h before inoculation and biotic growth for 72 h) – OCP values: +0.080, –0.470, –0.470, –0.470 and –0.325 V (*vs.* Ag/AgCl) at –1 h (abiotic) and 72 h (biotic) after a 0, 1 and 24 h treatment with SNP, respectively.

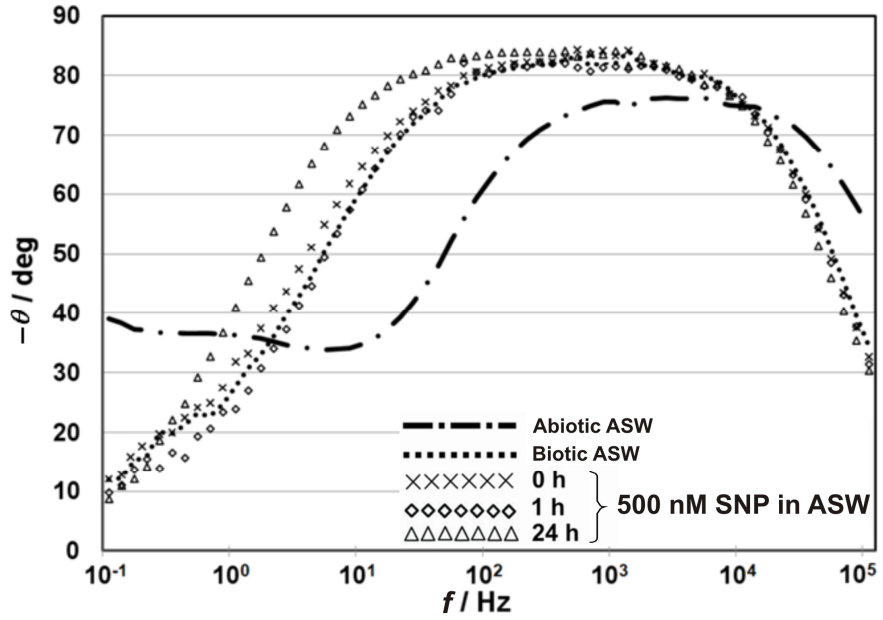

Figure 5.37. Bode (*–θ vs. f*) plots for a 0.2 mm diameter Au electrode with 500 nM NO donor SNP in ASW medium for 24 h (abiotic: –1 h before inoculation and biotic growth for 72 h) – OCP values: +0.080, –0.470, –0.470, –0.470 and –0.325 V (*vs.* Ag/AgCl) at –1 h (abiotic) and 72 h (biotic) after a 0, 1 and 24 h treatment with SNP, respectively.

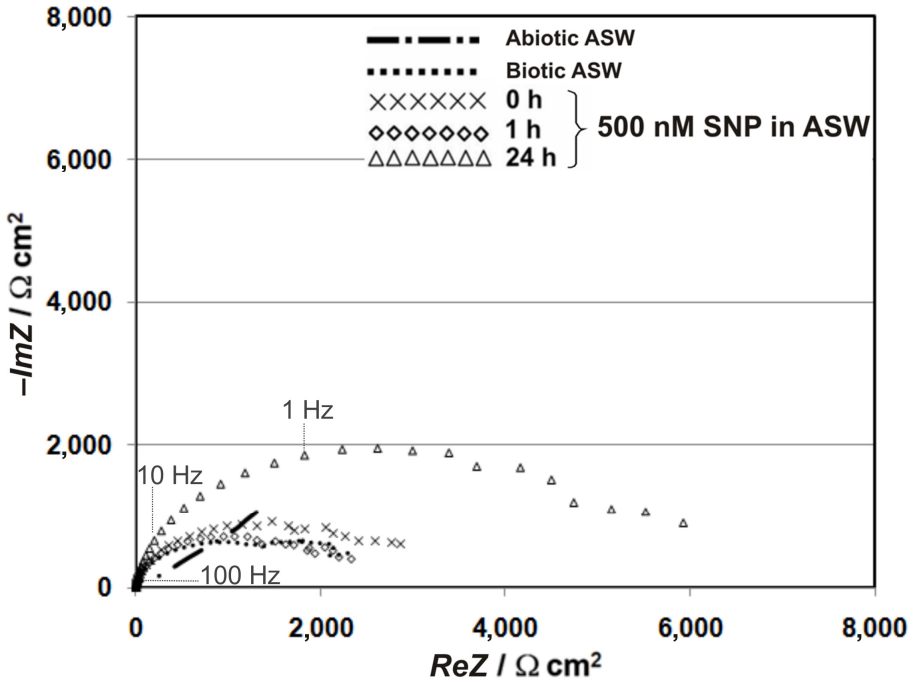

Figure 5.38. Nyquist diagrams for a 0.2 mm diameter Au electrode with 500 nM NO donor SNP in ASW medium for 24 h (abiotic: –1 h before inoculation and biotic growth for 72 h) – OCP values: +0.080, –0.470, –0.470, –0.470 and –0.325 V (*vs.* Ag/AgCl) at –1 h (abiotic) and 72 h (biotic) after a 0, 1 and 24 h treatment with SNP, respectively.

Overall, the EIS response in the abiotic and biotic conditions (**Figures 5.36** to **5.38**) was qualitatively comparable with the electrochemical performances in **Figures 5.30** to **5.32**. These include the impedance shift towards lower frequencies (**Figures 5.36** and **5.37**), the diffusive / resistive behaviour and the subtle change in impedance (**Figure 5.36**) in the low frequency part of the spectra, 0.1 to 100 Hz. Initially at 0 h, after addition of SNP on the 72-h old biofilmed Au surface, no marked change in impedance was observed. Importantly, a detectable modification of the EIS response (increase in the interfacial resistance at lower frequencies) was evident after prolonged exposure. This can be explained by a significant suppression of the interfacial charge transfer resulting from stress induced by NO on the bacterial biofilms [**5.57**,**5.58**]. Although the exact dispersal mechanism of NO action remains to be elucidated [**5.57**,**5.59**] (herein further electrochemical are required to understand the exact nature of the interfacial process involved), the detectable increase in impedance can presumably be associated with biofilm sloughing. Likewise, subtle interfacial charge transfer (smaller depressed Nyquist semi-circle after 1 h of exposure to that for 0 h) in **Figure 5.38** can account for residual ORR via enzymatic processes. In this overall process, it is possible that adsorbed NO and O_2 compete on electro-active sites, thereby affecting the Au interface [**5.60**].

The confocal microscopy in **Figure 5.39** has enabled, for the first time, an assessment of the performance of a 500 nM of the NO donor SNP on a 72 h-old *Pseudoalteromonas* biofilmed Au surface. Conversely, the presence of bacterial clusters in **Figure 5.39** has been greatly reduced on the Au electrode. This clearly demonstrates, in agreement with the NO biofilm dispersal approach at Southampton in **Section 2.9**, that continuous exposure to low, non-toxic concentrations of NO donor SNP; in the nanomolar range (500 nM) [**5.57**,**5.58**], can induce effective and efficient dispersal in marine bacterial biofilms. These results are consistent with [**5.57**] where greatest antifouling effects (decrease in biofilm biomass and an increase in planktonic biomass) were observed with 500 nM of the NO donor SNP.

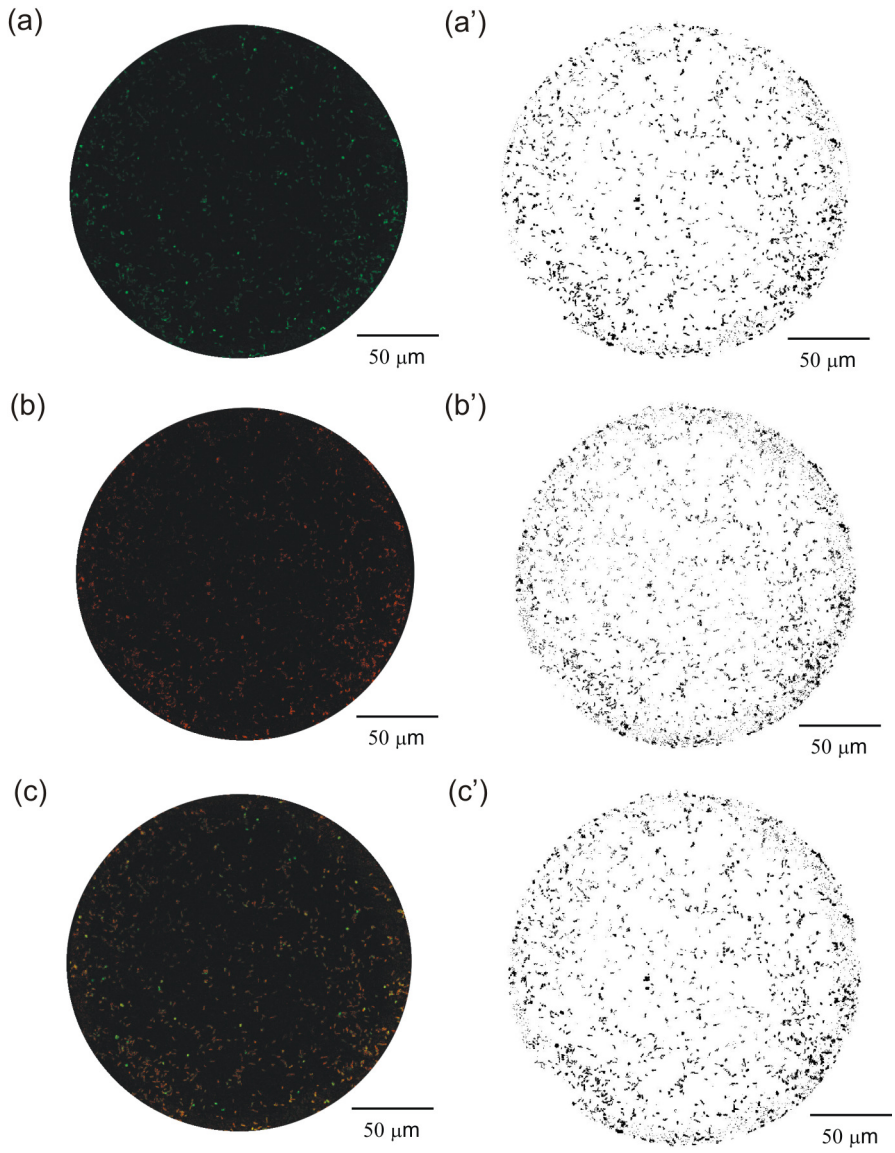

Figure 5.39. Confocal microscopy of a Au 72 h-old biofilmed electrode stained with the *Bac*Light™ viability kit after a 24 h immersion using 500 nM of the NO donor SNP: **(a)** Live, **(b)** Dead and **(c)** Live / Dead – corresponding binary (black and white) images in **(a')**, **(b')** and **(c')** using ImageJ software.

In that process, small molecules of NO will diffuse across the interface and induce biological stresses, causing potential damages to DNA, lipids and proteins of bacterial cells [**5.57**,**5.58**]. This can occur when the production of NO overwhelms the capacity of cells to remove the reactive nitrogen intermediates, *i.e.* the NO molecules [**5.57**,**5.58**]. This leads to biofilm dispersal from the Au surface at low, non-toxic concentrations of NO donor SNP, see **Figure 5.40**.

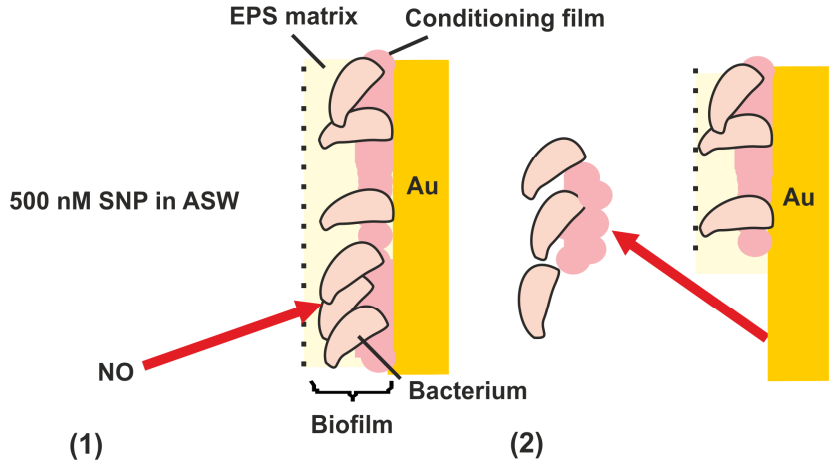

Figure 5.40. Detachment mechanism induced by NO on a biofilmed Au surface: **(1)** diffusion of NO molecule across the interface and **(2)** subsequent biofilm dispersal – typical thickness of the bacterial biofilm ≈ a few microns [**5.7**,**5.24**,**5.35**,**5.36**].

5.12.5 Surface percentage coverage

A comparative study (percentage coverage) of the fouling performances of the Au surface in NaCl, abiotic and biotic ASW, and also biotic ASW with SNP is addressed in **Figure 5.41**. Whereas the fouling properties in NaCl and abiotic ASW are negligible (close to a few percent), a significant biofilm coverage has accumulated on the Au surface in biotic ASW. Overall, the histograms for the biotic conditions show that the biofilm is composed of live (≈ 55 %) and dead (≈ 50 %) cells. This can be explained by the lifespan (≈ 72 h) of the *Pseudoalteromonas* strain [**5.1**] with the occurrence of growing and aging cells forming the biofilm [**5.61**]. After exposure to SNP, a marked decrease of biofouling from about 50 % to 5 % was observed.

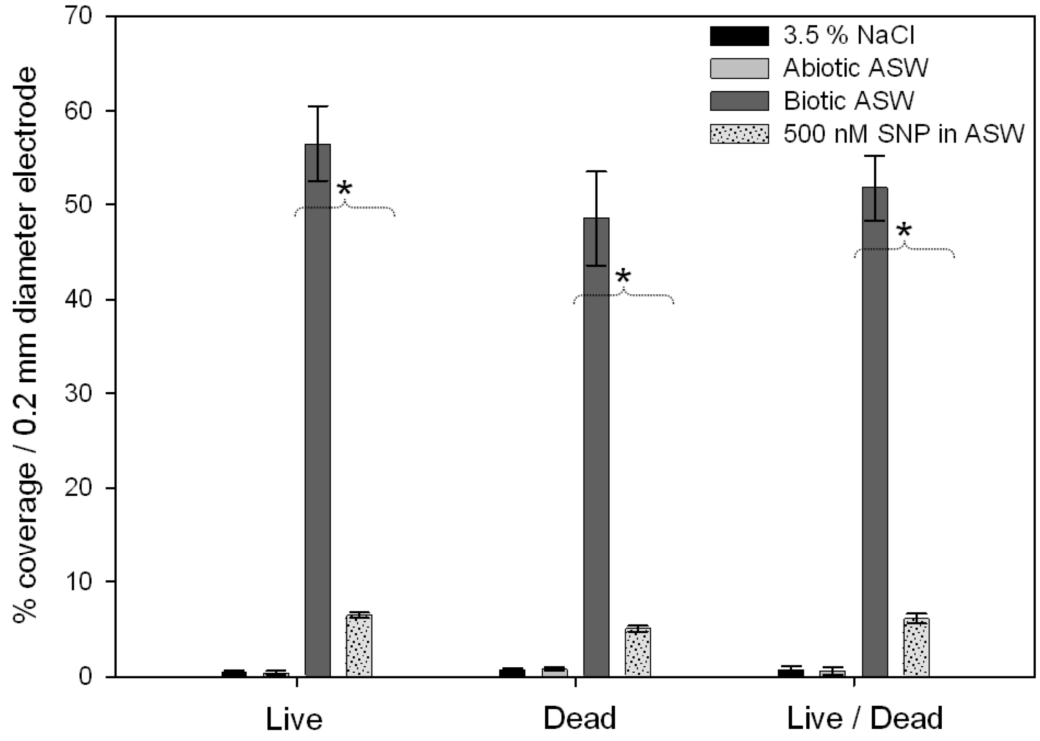

Figure 5.41. Surface coverage analyses on Au electrodes using the Live / Dead *Bac*Light™ viability kit after immersion in NaCl, abiotic and biotic ASW, and also SNP on biofilmed surfaces – * represents $P < 0.05$.

5.12.6 Estimation of the number of sessile bacterial cells

Numbers of attached bacterial cells for the biotic ASW (72 h-old biofilm in **Figure 5.33**) and 500 nM SNP in ASW (24 h exposure to NO donor SNP in **Figure 5.39**) are presented in **Table 5.9**. Results in **Table 5.9** have been outlined assuming the occurrence of a monolayer of bacterial cells on the Au surfaces (with cells in direct contact to the surface likely to influence the electrochemistry, see **Section 2.4.3.2**), where the exact distribution of cells is non-uniform along the *z*-direction (different biofilm layer stacks), see **Section 2.7.1**.

Table 5.9. Numbers of attached bacterial cells for the biotic ASW (72 h-old biofilmed Au surface) and 500 nM SNP in ASW (24 h exposure).

Au (0.2 mm diameter) electrode area / cm^2		3.14×10^{-4}	
Area covered by one *Pseudoalteromonas* sp. NCIMB 2021 / cm^2 – using cell dimensions in [5.62]		$0.95 \pm 0.55 \times 10^{-8}$	
Au surface		**Number of sessile bacterial cells / Au electrode**	**Number of sessile bacterial cells / cells cm^{-2}**
Estimation of sessile bacterial cells assuming complete surface coverage		49,740 ± 28,800	$1.6 \pm 0.9 \times 10^8$
Biotic ASW **(Figure 5.41)**	Live	28,100 ± 1,990	$8.9 \pm 0.6 \times 10^7$
	Dead	24,175 ± 2,485	$7.7 \pm 0.8 \times 10^7$
	Live / Dead	25,765 ± 1,740	$8.2 \pm 0.5 \times 10^7$
	Mean value	26,015 ± 2,485	$8.3 \pm 0.8 \times 10^7$
500 nM SNP in ASW **(Figure 5.41)**	Live	3,210 ± 150	$10.2 \pm 0.5 \times 10^6$
	Dead	2,510 ± 150	$8.0 \pm 0.5 \times 10^6$
	Live / Dead	3,035 ± 250	$9.6 \pm 0.8 \times 10^6$
	Mean value	2,920 ± 250	$9.3 \pm 0.8 \times 10^6$

The standard deviation in **Table 5.9** can be explained by different contact surface areas for the sessile bacterial cells, where bacteria in **Figure 5.42(a)*(i)*** / **Figure 5.42(b)*(i)*** will undergo greater interfacial mechanisms to those in **Figure 5.42(a)*(ii)*** / **Figure 5.42(b)*(ii)***.

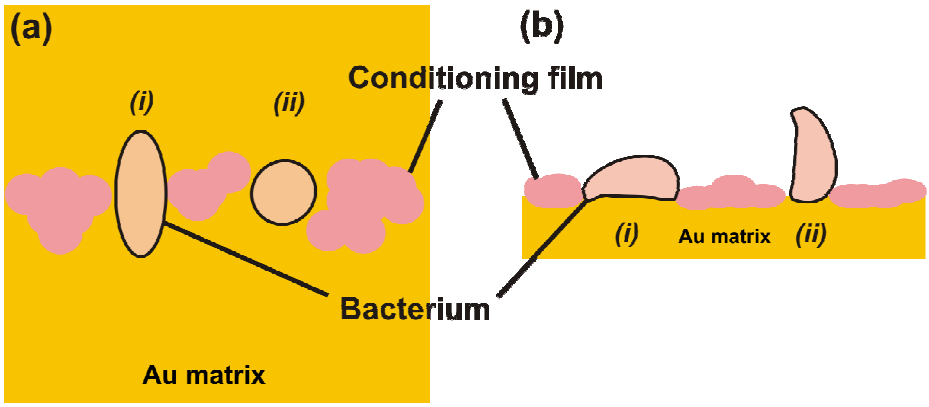

Figure 5.42. **(a)** Plan view of sessile bacterial cells on a Au matrix and **(b)** the corresponding cross section.

An estimation of 26,015 ± 2,485 bacterial cells for the mean value (corresponding to $8.3 \pm 0.8 \times 10^7$ cells cm^{-2}) was assessed on the 72 h-old biofilmed Au surface, whereas 2,920 ± 250 adhered bacterial cells (representative of $9.3 \pm 0.8 \times 10^6$ cells cm^{-2}) remained on the Au surface, thus showing approximately a 10-fold decrease of overall biofouling after treatment with 500 nM of the NO donor SNP. Although the methodology used in **Table 5.9** to quantify numbers of adhered bacteria is limited (it assumes that black features in **Figures 5.33** and **5.39** are biofilm cell clusters, see **Section 4.9**), it represents relevant quantifiable data to support the quantitative analysis of the EIS measurements (see **Section 5.13**).

5.12.7 OCP values of the EIS data

Figure 5.43 shows the variation of the OCP values of the EIS data over 72 h for the 3.5 % NaCl solution, the abiotic and biotic media. Overall, the OCP values shifted towards the cathodic region of the ORR, between about +0.100 and –0.225 V (*vs.* Ag/AgCl) for the NaCl test solution, and –0.325 V (*vs.* Ag/AgCl) for the abiotic ASW, and also –0.550 V (*vs.* Ag/AgCl) for the biotic ASW. Whereas the OCP values (for the NaCl test solution and abiotic ASW) gradually stabilise over the first few 4 – 8 h, those for the biotic conditions exhibit more pronounced variation towards higher negative potentials. This can be explained by the development of an interfacial charge distribution to achieve a stable state [**5.46**], *i.e.* double layer for the NaCl solution [**5.43**] where Cl^- ions can negatively charge the Au surface and potentially yield chloro complexes (under low flowing conditions in **Section 4.6**, thus affecting the Au interface) [**5.63**], and electrode polarisation due to the presence of adsorbed organic material (the conditioning film) associated with an overall change in the adsorbed species and the kinetics of the ORR for the abiotic ASW [**5.59**,**5.64**]. For the biotic ASW, it can be attributed to a natural polarisation process of the Au surface due to the biofilm formation and is consistent with [**5.27**,**5.31**]. In particular, the slow negative shift in **Figure 5.43** reflects an increased surface heterogeneity in the presence of an adsorption film or biofilm (for the abiotic and biotic ASW), thereby the surface active area decreases and can subsequently influence the ORR [**5.14**]. Similarly, the exact interfacial mechanism may be more complex with the potential influence of the catalase to the shift of the OCP values towards the cathodic region [**5.65**,**5.66**]. After addition of the NO donor SNP in the biotic condition, an increase of the OCP value was observed towards a plateau of potentials at about –0.300 V (*vs.* Ag/AgCl). This plateau corresponds to cathodic potentials recorded in the abiotic ASW, thus suggesting a depolarisation process of the Au electrode associated with biofilm dispersal.

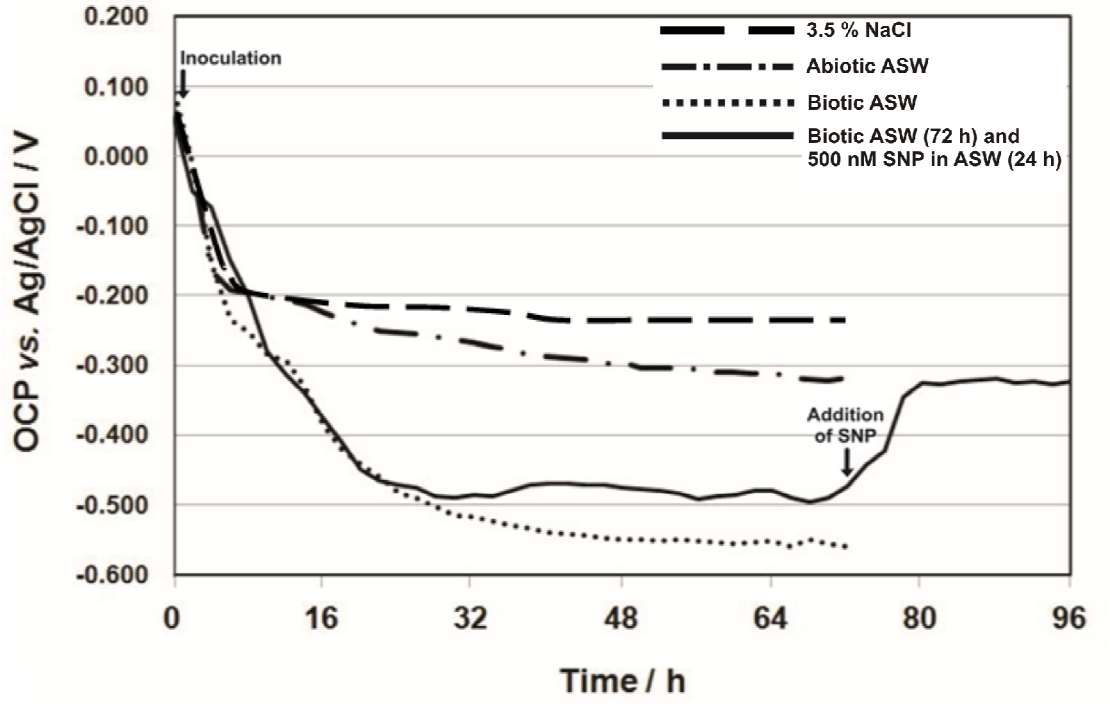

Figure 5.43. Comparison of the OCP values for the 3.5 % NaCl solution, the abiotic and biotic ASW media recorded over 72 h, and also after 24 h prolonged exposure with the NO donor SNP in the biotic ASW medium.

Although the EIS data in **Section 5.12** have been addressed for different OCP values (see **Figure 5.43**), herein this current study has outlined the naturally occurring bacterial biofilm (without polarisation) on a Au surface.

5.13 Quantitative analysis of the EIS measurements

5.13.1 Study of the capacitive parameters using imaginary impedance plots

The imaginary impedance plots (**Figures 5.44** to **5.47**) in the form logarithm of the –imaginary part *vs.* logarithm of the frequency were presented to justify the use of the CPE parameters in the EC model for Au in the chloride media (see **Section 2.6.7**) in **Table 4.4** [**5.67**]. This representation can often lead to a fine description of the capacitive behaviour in contrast with the qualitative assessment utilising the Bode (|*Z*| *vs. f*) plots (see **Section 5.12**) since the slopes can be associated with the CPE behaviour, in addition any peaks reveal characteristic time constants [**5.67**].

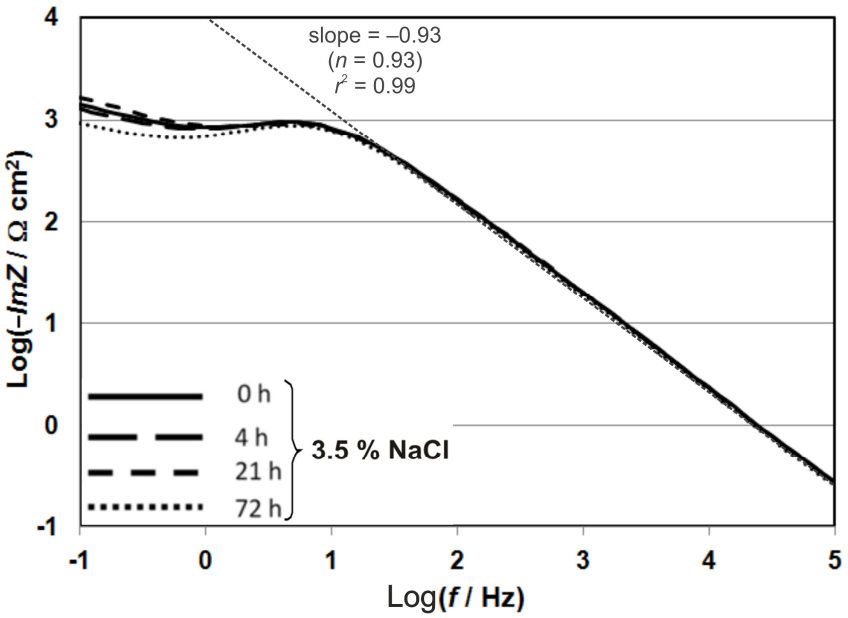

Figure 5.44. Representation of the logarithm of the –imaginary part *vs.* the logarithm of the frequency at OCP for a 0.2 mm diameter Au electrode in the 3.5 % NaCl solution – OCP values: +0.090, –0.070, –0.215 and –0.225 V (*vs.* Ag/AgCl) after a 0, 4, 21 and 72 h immersion, respectively.

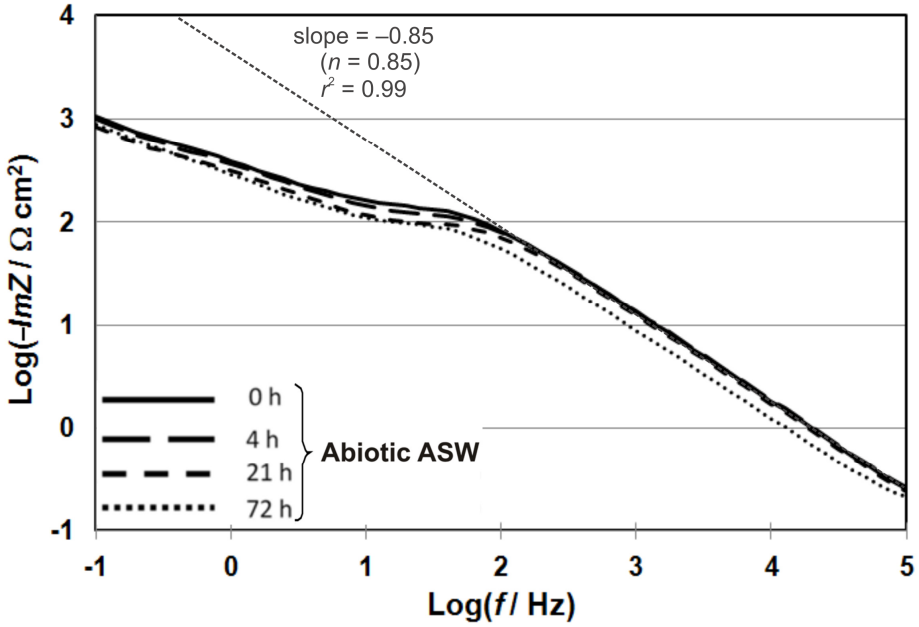

Figure 5.45. Representation of the logarithm of the –imaginary part *vs.* the logarithm of the frequency at OCP for a 0.2 mm diameter Au electrode in the abiotic ASW medium – OCP values: +0.085, –0.070, –0.250 and –0.325 V (*vs.* Ag/AgCl) after a 0, 4, 21 and 72 h immersion, respectively.

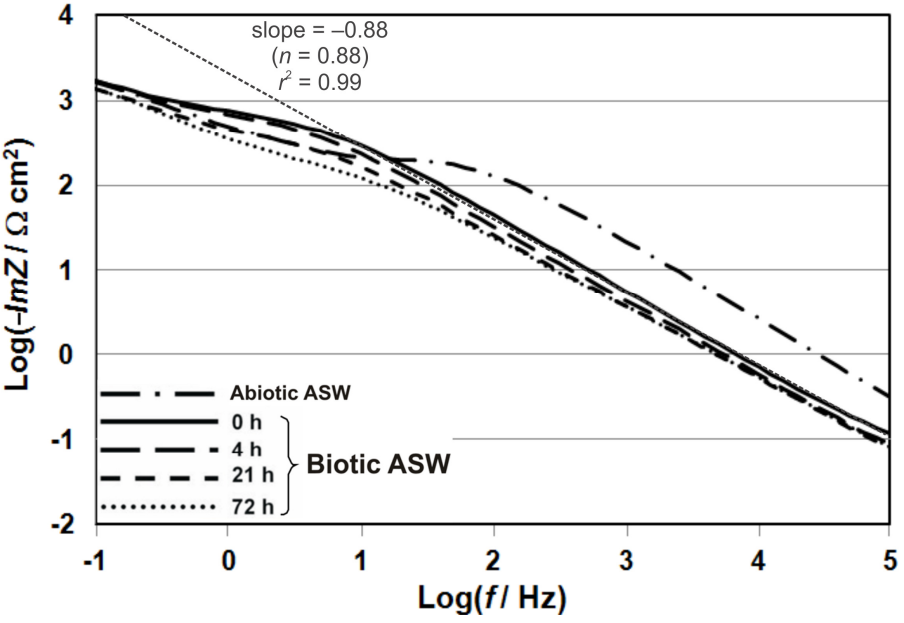

Figure 5.46. Representation of the logarithm of the –imaginary part *vs.* the logarithm of the frequency at OCP for a 0.2 mm diameter Au electrode in the biotic ASW medium (abiotic: –1 h before inoculation) – OCP values: +0.090, +0.085, –0.075, –0.460 and –0.560 V (*vs.* Ag/AgCl) at –1 h (abiotic) and after a 0, 4, 21 and 72 h immersion, respectively.

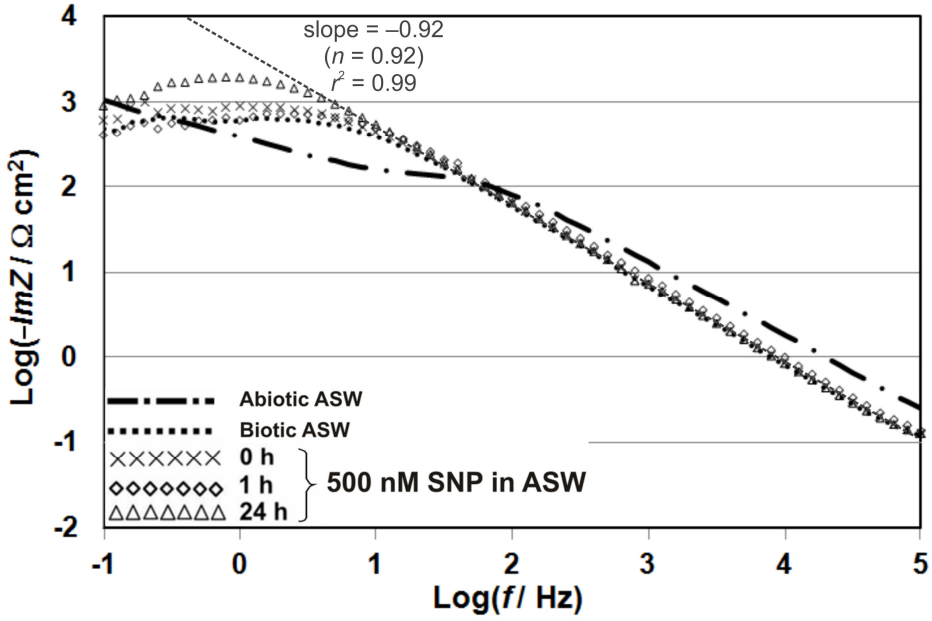

Figure 5.47. Representation of the logarithm of the –imaginary part *vs.* the logarithm of the frequency at OCP for a 0.2 mm diameter Au electrode with 500 nM NO donor SNP in ASW medium for 24 h (abiotic: –1 h before inoculation and biotic growth for 72 h) – OCP values: +0.080, –0.470, –0.470, –0.470 and –0.325 V (*vs.* Ag/AgCl) at –1 h (abiotic) and 72 h (biotic) after a 0, 1 and 24 h treatment with SNP, respectively.

For clarity, only the slope at 0 h computed at higher frequencies, between 100 to 100,000 Hz, has been labelled with the corresponding value of the empirical exponent of the CPE for the NaCl test solution, the abiotic and biotic ASW, and also 500 nM SNP in ASW in **Figures 5.44** to **5.47**. Overall, the values of the n coefficients calculated using this graphical method for the whole experimental duration in **Figures 5.44** to **5.47** are presented alongside with the regression procedure in **Tables 5.10** to **5.13**, thus confirm the presence of the CPE in the high frequency part of the spectra, 100 to 100,000 Hz, and is consistent with [**5.67**].

5.13.2 EC fitting

Tables 5.10 to **5.13** show the results of the EC modelled data for all the Au / chloride media interfaces fitted using the Gamry Echem Analyst software (version 5.30). The values were normalised to the sensing area of the 0.2 mm diameter Au electrode. All the interfaces were modelled using an EC with mixed kinetic and charge transfer control (**Figure 2.20** in **Section 2.6.7**), *i.e.* for the interfacial current exchange in the presence of diffusion [**5.24**,**5.28**,**5.31**,**5.43**]. Whereas the double layer capacitance C_{dl} was used to describe the interfacial charge distribution for the NaCl solution, C_{con} and C_{EPS} represent the conditioning film (adsorbed organic layer) for the abiotic ASW and the biofilm for the biotic ASW, respectively. A W component for DO diffusion to the Au surface (from the bulk solution and / or enhanced by enzymatic activity) was added to the model (*i.e.* in series with R_{ct}), see **Figure 2.20** in **Section 2.6.7**.

The quality of the EC fit was quantified by assessing the χ^2 error, which has to be suitably low ($\chi^2 \leq 10^{-4}$) to achieve good fit [**5.68**], see **Section 4.7**. In contrast, χ^2 errors significantly larger than 10^{-3} are usually explained by the presence of partially localised aberrant points due to random and spikes in the impedance spectra [**5.68**]. Overall, the χ^2 errors in **Tables 5.10** to **5.13** were reasonably low, thus showing reliable EC fit of the impedance data. In addition, the R_{s} values of the chloride media in **Tables 5.10** to **5.13** were between 0.163 and 0.170 Ω cm², thus corresponding to values of σ = 47.0 $\pm$ 1.0 mS cm^{-1} at 19 °C (see **Equation 2.25** in **Section 2.6.7**) for salinity values of 35 ‰, and also clearly demonstrating the minimum effect of the external reference capacitance (C_{ref}) on the measurements in **Tables 5.10** to **5.13** (see **Section 2.6.7**). From the surface charge density, an estimate of the number sessile bacteria can be determined after subtraction of the abiotic response, see **Equation 2.32** in **Section 2.8.2.2**.

Whereas the standard deviations for the R_{s}, R_{ct} and Y_0 parameters were obtained using the regression procedure of the Gamry Echem Analyst software (version 5.30), those for the C_{eff} values were estimated utilising the analytical expression for the relative uncertainty of **Equation 2.27** (with R_{f} similar to R_{ct} for a thin biofilm in **Section 2.6.7**) where the R_{ct} and Y_0 components can correspond to measured data, see **Equation 5.20** [**5.69**]. In contrast, no standard deviation was computed for the Q_{ADS} values (and

the deduced numbers of bacterial cells) since those derived parameters result from computed (and non-measured) data.

$$\frac{\sigma_{C_{\text{eff}}}}{C_{\text{eff}}} = \frac{1-n}{n}\left(\frac{\sigma_{R_{\text{ct}}}}{R_{\text{ct}}}\right) + \frac{1}{n}\left(\frac{\sigma_{Y_0}}{Y_0}\right) \tag{5.20}$$

where $\sigma_{C_{\text{eff}}}$, $\sigma_{R_{\text{ct}}}$ and σ_{Y_0} are the calculated uncertainty values for the C_{eff} , R_{ct} and Y_0 parameters. These expressions of measurement uncertainty represent estimated standard deviation values in **Tables 5.10** to **5.13**.

Table 5.10. Impedance data for the Au / 3.5 % NaCl interface.

Conditioning		OCP / V (*vs.* Ag/AgCl)	R_s / Ω cm^2	R_{ct} / Ω cm^2	$Z_{C_{dl}}$			C_{eff} (C_{dl})	Z_W		χ^2 / 10^{-4}
					Y_0 / (Ω^{-1} cm^{-2} s^n) × 10^{-6}	n	r^2	(F cm^{-2}) × 10^{-6}	Y_0 / (Ω^{-1} cm^{-2} s^n) × 10^{-6}	n	
3.5 % NaCl	0 h	+0.090	0.165 ± 0.006	1605 ± 83	14.5 ± 0.3	0.93	0.99	10.9 ± 0.1	517 ± 21	0.38	1.6
	4 h	–0.070	0.163 ± 0.006	1579 ± 95	14.8 ± 0.3	0.93	0.99	11.2 ± 0.1	541 ± 25	0.36	2.1
	21 h	–0.215	0.167 ± 0.006	1508 ± 71	14.1 ± 0.3	0.93	0.99	10.6 ± 0.1	464 ± 15	0.41	1.7
	72 h	–0.225	0.164 ± 0.006	1505 ± 89	14.0 ± 0.4	0.93	0.99	10.5 ± 0.2	475 ± 17	0.40	2.9

Table 5.11. Impedance data for the Au / abiotic ASW interface.

Conditioning		OCP / V (*vs.* Ag/AgCl)	R_s / Ω cm^2	R_{ct} / Ω cm^2	$Z_{C_{con}}$			C_{eff} (C_{con})	Q_{ADS}	Z_W		χ^2 / 10^{-4}
					Y_0 / (Ω^{-1} cm^{-2} s^n) × 10^{-6}	n	r^2	(F cm^{-2}) × 10^{-6}	(C cm^{-2}) × 10^{-6}	Y_0 / (Ω^{-1} cm^{-2} s^n) × 10^{-6}	n	
Abiotic ASW	0 h	+0.085	0.167 ± 0.008	220 ± 8	28.8 ± 0.9	0.85	0.99	11.8 ± 0.1	4.7	792 ± 9	0.49	7.6
	4 h	–0.070	0.169 ± 0.006	180 ± 8	26.2 ± 0.9	0.85	0.99	10.2 ± 0.1	4.1	837 ± 10	0.49	8.1
	21 h	–0.250	0.170 ± 0.005	161 ± 6	28.1 ± 0.9	0.85	0.99	10.8 ± 0.1	4.4	987 ± 12	0.50	10.5
	72 h	–0.325	0.166 ± 0.008	172 ± 6	43.7 ± 1.5	0.83	0.99	16.0 ± 0.2	6.5	1020 ± 13	0.52	14.8

Table 5.12. Impedance data for the Au / biotic ASW interface (abiotic: –1 h before inoculation).

Conditioning		OCP / V (*vs.* Ag/AgCl)	R_s / Ω cm^2	R_{ct} / Ω cm^2	$Z_{C_{con}}$			C_{eff} (C_{con})	$Z_{C_{EPS}}$			C_{eff} (C_{EPS})	Q_{ADS}	Number of cells	Z_W		χ^2 / 10^{-4}
					Y_0 / (Ω^{-1} cm^{-2} s^n) × 10^{-6}	n	r^2	(F cm^{-2}) × 10^{-6}	Y_0 / (Ω^{-1} cm^{-2} s^n) × 10^{-6}	n	r^2	(F cm^{-2}) × 10^{-6}	(C cm^{-2}) × 10^{-6}	(cells cm^{-2}) × 10^6	Y_0 / (Ω^{-1} cm^{-2} s^n) × 10^{-6}	n	
Abiotic ASW	–1 h	+0.090	0.163 ± 0.007	331 ± 13	20.1 ± 0.4	0.89	0.99	10.8 ± 0.1	N/A	N/A	N/A	N/A	4.3	N/A	567 ± 20	0.53	3.1
Biotic ASW	0 h	+0.085	0.170 ± 0.004	950 ± 60	N/A	N/A	N/A	N/A	76.2 ± 1.6	0.88	0.99	53.3 ± 0.5	21.4	17.1	582 ± 15	0.54	4.9
	4 h	–0.075	0.168 ± 0.003	876 ± 45	N/A	N/A	N/A	N/A	103.2 ± 1.5	0.87	0.99	72.1 ± 0.5	28.9	24.6	636 ± 11	0.55	4.8
	21 h	–0.460	0.165 ± 0.003	618 ± 31	N/A	N/A	N/A	N/A	142.8 ± 2.1	0.85	0.99	93.0 ± 0.6	37.4	33.1	707 ± 13	0.56	5.4
	72 h	–0.560	0.169 ± 0.003	296 ± 26	N/A	N/A	N/A	N/A	167.6 ± 2.8	0.85	0.99	98.6 ± 0.9	39.7	35.3	680 ± 11	0.59	4.1

Table 5.13. Impedance data for the Au / biotic ASW interface after treatment with 500 nM of NO donor SNP (abiotic: –1 h before inoculation and biotic growth for 72 h).

Conditioning		OCP / V (*vs.* Ag/AgCl)	R_s / Ω cm^2	R_{ct} / Ω cm^2	$Z_{C_{con}}$			C_{eff} (C_{con})	$Z_{C_{EPS}}$			C_{eff} (C_{EPS})	Q_{ADS}	Number of cells	Z_W		χ^2 / 10^{-4}
					Y_0 / (Ω^{-1} cm^{-2} s^n) × 10^{-6}	n	r^2	(F cm^{-2}) × 10^{-6}	Y_0 / (Ω^{-1} cm^{-2} s^n) × 10^{-6}	n	r^2	(F cm^{-2}) × 10^{-6}	(C cm^{-2}) × 10^{-6}	(cells cm^{-2}) × 10^6	Y_0 / (Ω^{-1} cm^{-2} s^n) × 10^{-6}	n	
Abiotic ASW	–1 h	+0.080	0.162 ± 0.006	233 ± 9	31.1 ± 0.9	0.85	0.99	13.0 ± 0.5	N/A	N/A	N/A	N/A	5.2	N/A	795 ± 10	0.49	6.5
Biotic ASW	72 h	–0.470	0.164 ± 0.003	759 ± 66	N/A	N/A	N/A	N/A	95.3 ± 0.8	0.92	0.99	75.8 ± 1.3	30.5	25.3	662 ± 78	0.24	12.5
500 nM SNP in ASW	0 h	–0.470	0.160 ± 0.003	886 ± 57	N/A	N/A	N/A	N/A	55.1 ± 0.6	0.92	0.99	42.4 ± 0.7	17.0	11.8	564 ± 10	0.24	11.5
	1 h	–0.470	0.169 ± 0.004	946 ± 60	N/A	N/A	N/A	N/A	37.9 ± 0.5	0.93	0.99	29.5 ± 0.6	11.9	6.6	636 ± 11	0.19	8.1
	24 h	–0.325	0.168 ± 0.004	3251 ± 150	N/A	N/A	N/A	N/A	32.2 ± 0.4	0.93	0.99	27.2 ± 0.5	10.9	5.7	427 ± 13	0.19	15.2

5.13.2.1 EC fitting for the NaCl solution

The impedance data in **Table 5.10** was relatively constant over the 72 h test in 3.5 % NaCl. These include the R_{ct} values *circa* 1500 Ω cm^2, thus demonstrating the absence of a detectable change of charge transfer (interfacial ORR) with time at the Au / 3.5 % NaCl interface. Likewise, the CPE parameters relative to C_{dl} were constant with n = 0.9, indicative of a capacitive behaviour (Helmholtz theory in electrochemistry) [**5.43**,**5.70**]. The values of C_{dl} were on average equal to 10.8 ± 0.2 μF cm^{-2} using **Equation 2.27** in **Section 2.6.7**, thereby consistent with the mean value of C_{dl} (14.25 μF cm^{-2}) reported for a bare Au electrode immersed in a standard solution [**5.17**]. For the Warburg impedance, the CPE parameters had values of n relatively close to 0.5, consistent with a diffusion layer of infinite thickness.

5.13.2.2 EC fitting for the abiotic test solution

Similar to the 3.5 % NaCl, the EIS data for the abiotic ASW in **Table 5.11** did not show significant changes in impedance over a 72 h duration. However, the R_{ct} values (with approximately a 10-fold decrease) for the ASW were lower to that for the NaCl. In analogy with protein adsorption on metallic surfaces [**5.46**,**5.71**,**5.72**], this can be explained by the presence of blocking organic material, *i.e.* a conditioning layer on the Au electrode (consistent with **Section 5.8**), thus affecting the overall interfacial charge transfer (decrease of the resistance parameters) [**5.64**]. In this instance, the values of Q_{ADS} (**Table 5.11**) representative of the surface charge density corresponding to adsorbed organic material were assessed using **Equation 2.31** in **Section 2.8.2.2** [**5.45**,**5.71**-**5.73**]. Overall, the values (in analogy with adsorbed proteins on an Au surface) were within the same order of magnitude as in [**5.71**]. Additionally, the CPE parameters for the Warburg impedance with values of n = 0.5 were indicative of more pronounced DO diffusion across the interface, suggesting that the conditioning layer (thin porous membrane) may be suitable for enhanced mass transport properties from the bulk solution [**5.10**-**5.12**]. Overall, this process corresponds to the ORR at the Au / abiotic ASW interface.

5.13.2.3 EC fitting for the biotic test solution

Whereas the impedance data for the abiotic ASW in **Table 5.12** were similar to that in **Table 5.11**, changes in the EIS data (increase in the capacitance and R_{ct} values) were observed (**Table 5.12**) at 0 h, *i.e* after inoculation with bacteria. This can be explained by an initial complex modification of the interfacial properties when pioneering bacteria colonise the Au surface (discharge electrons and thus charge the interface) [**5.50**,**5.51**], coinciding with an early stage of microfouling (adaptation to changing environment [**5.27**]) preceding redox processes, *i.e.* enzymatic activity. After prolonged exposure, a gradual increase of the capacitive parameters was apparent in contrast with a gradual decrease in the R_{ct} values, thus consistent with **Section 2.8.2.2**. This can be attributed to an enhancement of electrons discharge induced by bacterial cells (within the biofilm) to the Au electrode, which support the charge transfer process associated with the enhanced enzymatic ORR at the Au / biotic ASW interface [**5.33**,**5.74**]. The CPE parameters for diffusion had values of n = 0.5, thus showing that the overall kinetic process is mixed with DO diffusion from the bulk solution.

5.13.2.4 EC fitting for the NO donor SNP

Similarly, when the initial EIS data for the abiotic and biotic ASW in **Table 5.13** were comparable to that in **Table 5.12**, an increase of the R_{ct} values was observed with time in contrast with a decrease of the capacitive parameters to reach values of 27.2 $\pm$ 0.5 μF cm^{-2} after addition of the NO donor SNP. The decrease in capacitance can be explained by a degradation of the biofilm exposed to the biocide, where affected and lysed bacterial cells can modify the biofilm structure [**5.51**]. Likewise, the increase in R_{ct} values is indicative of suppressed interfacial charge transfer (enhanced ORR via enzymatic process) with presumably a physical modification of the interface (*e.g.* biofilm sloughing confirmed by the confocal analyses in **Section 5.12.4**).

5.13.2.5 Significance of the capacitive parameters

The C_{eff} parameters for the seawater solutions have a relatively complex behaviour (see **Section 2.6.7**). The capacitance values depend on the dielectric properties (*i.e.* the effective dielectric constant) and the thickness of the capacitive layer, which have dual effects. During adhesion, it is more likely that the overall ionic charge across the capacitance increases, thus enhancing the dielectric effective constant and decreasing the film thickness [**5.74**]. Nevertheless, the capacitance is not just dependent of the extent of the adsorbed organic material, it is also a complex function of other parameters related to the Au / solution interface, which may also be dependent (in analogy with protein adsorption on a metal surface [**5.45**,**5.46**]) on the structural, physical and chemical properties of the organic material (thickness and structure of the biofilm and the Au / biofilm / solution interface).

5.13.3 Relationship for the bacterial biofilm sensor

The capacitance parameters have shown promise in quantifying planktonic / suspended bacteria. Herein, the interfacial capacitance was proposed as an electrochemical parameter to study bacterial attachment to metallic surfaces [**5.50**,**5.51**,**5.75**]. Previous studies on protein attached on metallic surfaces demonstrated that the surface charge density was proportional to the amount of adsorbed protein [**5.45**]. Using **Equation 2.32** in **Section 2.8.2.2**, a relationship between the surface charge density of sessile cells and their adhered population can be addressed in analogy with adsorbed protein on a metal surface [**5.45**,**5.76**]. These considerations were based on the assumptions in **Section 2.8.2.2**, such as the reported total surface charge of bacterial strains ($\approx 10^{-12}$ C per bacterium) during adhesion [**5.77**] used in **Figure 5.48 (data in the absence of *)**.

The dependence between the surface charge density accounting for bacterial biofilm (values in **Tables 5.12** and **5.13**) and the corresponding number of adhered bacterial cells is shown in **Figure 5.48 (data in the absence of *)**. A few values for the abiotic ASW (ranging between 4.1 and 6.5 μC cm^{-2} in **Tables 5.11** to **5.13**) have been added to represent the conditioning film formation, where there is no adhered bacterial cell. The estimated number of attached bacterial cells (mean value) utilising the *ex situ* confocal microscopy in **Table 5.9** have been used in **Figure 5.48 (data in the presence of *)**, where the corresponding deduced values (based on the hypotheses in **Section 2.8.2.2**) lie in close to the ± standard deviation or are within the same order of magnitude of the data in the presence of *, see **Figure 5.48**. In addition, the percentage coverage for the abiotic and biotic ASW, and also the 500 nM SNP in ASW (mean value in **Figure 5.41**, see **Section 5.12.5**) are shown for a direct comparison with the data in the presence of * in **Figure 5.48** assuming that a complete surface coverage (100 %) / bacterial monolayer biofilm on the Au surface can correspond to 1.6×10^8 cells cm^{-2}, see **Table 5.9** in **Section 5.12.6**.

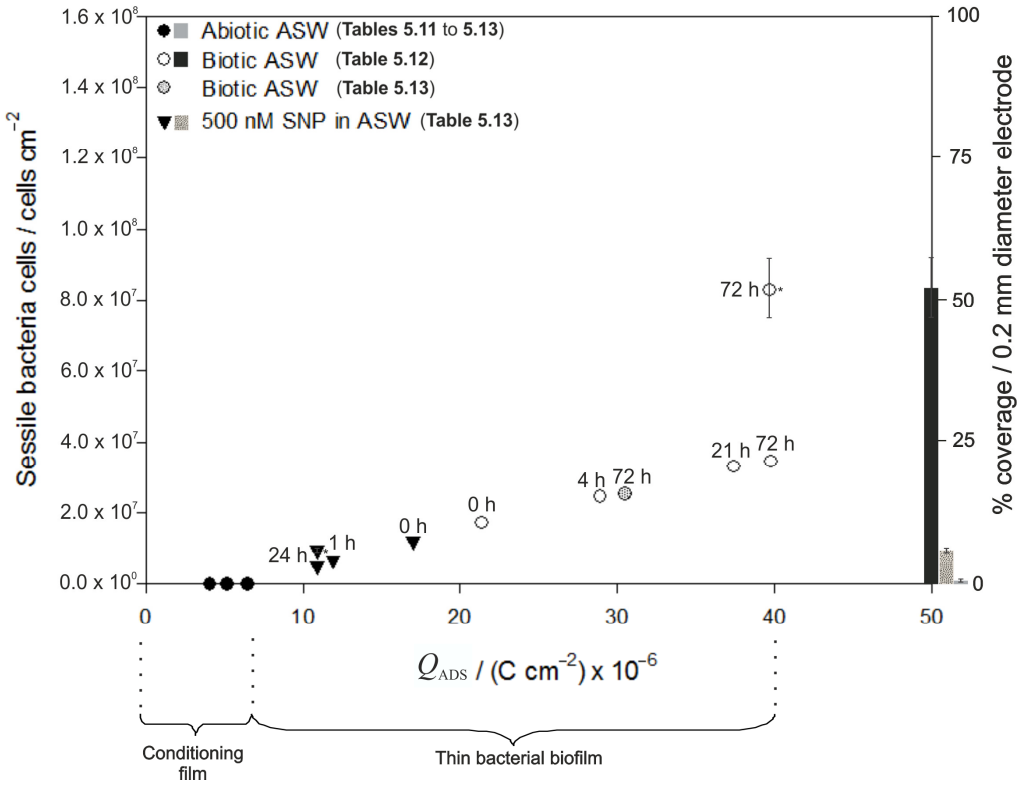

Figure 5.48. Number of sessile bacterial cells as a function of the surface charge density – data in the presence of * represent the estimations of number of attached bacterial cells (*y*-axis) using the *ex situ* confocal microscopy studies in **Table 5.9**, together with the bacterial cell population (data in the absence of *) deduced utilising the hypotheses in **Section 2.8.2.2**, corresponding to the experimental impedance data (*x*-axis) – surface coverage analyses (P < 0.05) in **Section 5.12.5** are shown for a direct comparison with the data in the presence of *.

After inoculation (0 h) for the biotic ASW, the overall surface charge density increases (*i.e.* modification of the adsorbed organic layer and pioneering bacterial adhesion at the interface, see **Section 5.12.3**) and can range between 21.4 and 39.7 $\mu C\ cm^{-2}$ in **Tables 5.12** and **5.13** over a 72 h immersion, therefore explained by the occurrence of a growing bacterial biofilm. Using **Figure 5.48 (data in the absence of *)**, the corresponding number of sessile bacterial cells for the 72 h biofilmed Au surface (**Table 5.12**) is approximately 3.5×10^7 cells cm^{-2}, thus consistent with the estimation of $8.3 \pm 0.8 \times 10^7$ cells cm^{-2} utilising *ex situ* confocal microscopy analyses in **Table 5.9**, see **Figure 5.48 (data in the presence of *)**.

Although within the same order of magnitude, the difference observed between the 72 h biotic ASW data for **Tables 5.12** (39.7 $\mu C\ cm^{-2}$) and **5.13** (30.5 $\mu C\ cm^{-2}$) in **Figure 5.48 (data in the absence of *)** was expected due to stochastic / random effects incurred by biological systems [**5.78**] and the presence of different Au surface active areas per testing [**5.79**]. In contrast, the overall charge density decreases after treatment with 500 nM of NO donor SNP (between 17.0 and 10.9 $\mu C\ cm^{-2}$ in **Table 5.13** after a 24 h immersion), thereby associated with bacterial biofilm dispersal, see **Section 5.12.4**. Similar to the 72 h biotic Au surface, estimate of sessile bacterial cells for the 500 nM SNP in ASW leads to 5.7×10^6 cells cm^{-2} in **Figure 5.48 (data in the absence of *)**, *i.e.* it is in good agreement with the estimation of $9.3 \pm 0.8 \times 10^6$ cells cm^{-2} in **Table 5.9**, see **Figure 5.48 (data in the presence of *)**.

Variations noticed between estimations for the EIS response and confocal microscopy analyses can be explained by the nature of the experiments. Whereas *in situ* EIS monitoring was performed (non-attached bacterial cells can potentially influence the EIS response), *ex situ* confocal microscopy was employed (occurrence of an overall more mature bacterial biofilm), see **Sections 4.7** and **4.9**.

Although the validity of the relationship (between the surface charge density and the number of sessile bacterial cells) obtained in **Figure 5.48 (data in the absence of *)** needs to be further investigated (see **Section 2.8.2.2**), a correlation with the results using the *ex situ* confocal microscopy was demonstrated for the data at 72 h (**Table 5.12**) and 24 h (**Table 5.13**), see **Figure 5.48**. This clearly suggests that the surface charge density can be utilised as a quantifiable biofouling indicator, wherein the capacitance can be the main parameter and ultimately the measurement procedure could be tailored to obtain it (the capacitance) using a specific frequency range, *i.e.* between 100 to 100,000 Hz in **Section 5.13.1**.

Overall, **Figure 5.48** has demonstrated that the electrochemical impedance data (*i.e.* surface charge density) have potentially the capability of providing accurate quantifiable values of number of adhered bacterial cells (in good agreement with the confocal microscopy analyses in **Table 5.9**). Although assessment of sessile bacterial population should ideally be done for a range of times (between 0 and 72 h), the relationship between the number of adhered bacterial cells and Q_{ADS} in a biotic environment in **Figure 5.48 (data in the absence of *)** can be informative of potential quantitative inhibition strategy / control of bacterial biofilm (*e.g.* using a threshold Q_{ADS} value in order to control the extent of bacterial biofilm).

5.14 Summary of EIS analysis

Overall, the EIS response in **Section 5.12** demonstrated clear differences between abiotic and biotic media. Herein, the qualitative EIS analysis has shown that initial marine bacterial biofilms can be electrochemically detected under a controlled flow cell environment. Importantly, a main parameter of the EIS response in the quantitative analysis (**Section 5.13**), which is a capacitive component (100 to 100,000 Hz), can be used to quantify biofilm and subsequently gauge the extent of biofouling. For the first time, the number of attached bacterial cells on the Au surface (after a 72 h biofilm growth and a 24 h exposure to 500 nM of the NO donor SNP) estimated from the impedance data (*in situ* sensing) were in good agreement with an *ex situ* assessment using confocal microscopy analyses. Consequently, this reinforces that the relationship between the surface charge density induced by biofilm and their corresponding sessile bacterial population can provide greater insight into sensor calibration curves used for real time biofilm monitoring devices.

Similarly, the impedance response after addition of 500 nM of the NO donor SNP in biotic condition uniquely demonstrated a significant change in impedance, which was corroborated (using confocal microscopy) by important biofilm detachment on the Au surface. This was clearly indicative of an effective and efficient biofilm dispersal using low, non-toxic concentration of NO donor SNP, therefore consistent with [**5.57**,**5.58**].

These considerations may support the studies on the antifouling efficiency and the molecular mechanisms inherent to the nanomolar range NO donor SNP dosed on a metal surface. Little is known about the main factors that can influence the bacterial dispersal mechanisms due to chemical stresses [**5.59**,**5.80**]. Overall, the mechanisms of biofilm maturation, structuring and detachment may be controlled by quorum

sensing, where gene expression can trigger enzymatic degradation of proteins or detergent-like peptides within the biofilm [**5.81**]. Likewise, the gene expression distribution was shown to be markedly different between sessile and planktonic mode of growth [**5.81**], thus suggesting that a suitable cleaning procedure for flowing cells would be inappropriate against biofilms [**5.36**,**5.59**].

In addition, it was shown that the biocide concentration is a critical parameter for biofouling control [**5.57**,**5.82**]. For instance, concentrations below the threshold required to inhibit growth can enhance biofilm formation [**5.82**]. In this current project and as proposed by Barraud *et al.* [**5.57**], 500 nM of the NO donor SNP can be the optimum concentration to clean a substratum; *i.e.* a metallic surface. This low, non-toxic concentration of NO donor SNP consists in an environmentally friendly biocide employed to keep costs at a minimum and it represents a good alternative to non-efficient and toxic chlorine widely used in industrial fouling [**5.36**]. In practice, the duration (ideally short) and frequency of dosing (continuous dosing, shock treatment and pulse dosing), and also the flow regime (allowable flow rate) are of great importance to define suitable biocide dosing strategies for biofilm control [**5.82**]. Ideally, an intelligent combination of these three factors should be addressed to maintain the operating systems and reduce the capital costs incurred. However, it is still unclear how this can be achieved since biofilms are competent biological systems that can constantly adapt to extremely different environmental conditions [**5.36**,**5.47**,**5.48**].

Therefore, these results suggest new perspectives to trigger a biocide strategy when necessary using Au multi-microelectrode arrays for enhanced sensitivity, objectivity and rapidity of analysis, and also biofouling quantification in seawater piping systems [**5.10**,**5.83**-**5.85**]. In real systems, the Au multi-microelectrode arrays have to be located on likely biofouling positions such as in low turbulent regions within the seawater systems, *e.g.* stagnation zones [**5.86**].

Chapter 6 – Conclusions and further work

6.1 Conclusions

6.1.1 Thesis overview

Uniquely, this thesis has addressed a qualitative and quantitative microbial biofilm study combining microbiological and engineering expertise to embed a 0.2 mm diameter Au electrode into a once through microbial flow cell in order to: *(i)* measure and explore in detail the enzymatic enhancement of the ORR over 72 h; and *(ii)* monitor (after a 24 h exposure) the subsequent biofilm detachment induced by 500 nM of the NO donor SNP. Confocal microscopy imaging has also been utilised to provide insightful corroboration of the bacterial biofilm / Au electrode interfacial processes. It was demonstrated, for the first time, that the numbers of sessile bacterial cells estimated from the EIS response (72 h biotic ASW and 24 h treatment with 500 nM of the NO donor SNP) were consistent with those for the confocal microscopy analyses.

Testing was undertaken using well-defined conditions (**Table 6.1**):

Table 6.1. Summary of the experimental conditions for this current study.

Experimental conditions	Effect on bacterial biofilms / measurable signal
low laminar flow regime ($R_e \approx 1$)	flow
light irradiance of 0.12 ± 0.01 μmol photons m^{-2} s^{-1}	light radiation
controlled room temperature at 18 ± 1 °C	temperature
NOC laboratory facilities (under atmospheric pressure)	water depth
Faraday cage	electromagnetic interference
continuous fresh, flush and aerated conditions (6.90 ppm)	DO level
enriched carbon source ASW of known composition	nutrient / carbon source supply
35 ‰ ASW	osmotic pressure
pH 8.1	pH
200 μL aliquot of 2 h-old *Pseudoalteromonas* sp. strain NCIMB 2021 culture, corresponding to an initial bacterial fouling population of approximately 3.5×10^6 cells mL^{-1} having a growth rate of 0.15 h^{-1} and a mean generation time of 4.52 h	physiology

6.1.2 Main thesis thrusts

Chapters 2 and **3** have established the main scientific and engineering concerns to assist and justify the development of this investigations experimental methodology (as outlined in **Chapter 4**).

6.1.2.1 Summary of Chapter 1

This study has been motivated by the detrimental effects (and the unsolved problems to reduce capital costs) of biofouling and biocorrosion on metallic surfaces directly exposed to seawater, such as can be found in marine heat exchangers and seawater handling systems. In this instance, both the fluid flow and heat transfer performance of seawater systems can be dramatically affected, potentially resulting in blockages and failures of fluid handling components. Additionally, existing inhibition strategies are often costly and inappropriate, leading to subsequent microorganism resistance and / or toxicity problems (*i.e.* toxic by-products discharge in seawater), plus there in greater concerns due to increased environmental legislature. Developing an alternative means of controlling all biofoulers is a great challenge, however, there are substantial benefits to be gained. Herein, this thesis has focused on the development of a reliable, accurate and quantitative biofilm sensing approach.

6.1.2.2 Summary of Chapter 2

It is often reported that bacterial biofilms play a fundamental role (the initial development and cohesion of marine communities) in the complex biofouling process on metallic surfaces. In particular for this study, the genus *Pseudoalteromonas* can trigger larval attachment and subsequent macrofouling inside heat exchangers. Although corrosion studies on anaerobic bacteria (*e.g.* SRB) are well documented, the literature for aerobic microbes is sparse. Perhaps, the most established mechanism for aerobic bacteria on a metal surface is the enzymatic enhancement of ORR using *Pseudoalteromonas* sp. (of relevance for this investigation) but this still needs to be fully addressed. Although Cu-based pipes (traditionally used for marine heat exchangers) are known for their antifouling properties against macrofouling, microfouling (preceding macrofouling) remains an issue, thus emphasising the importance of early warning bacterial biofilm detection (*i.e.* using a 72 h immersion for the current study). Likewise, laboratory experiments have enabled to demonstrate the

viscoelastic properties of a biofilm, where a fundamental understanding of the flow effect on a biofilm established inside pipes is limited. Consequently, a low laminar flow regime was chosen (for the proposed approach) to minimise the overall influence of flow at the interface.

A broad range of techniques is available for biofilm detection but a few are applicable to seawater systems, where a clear understanding of the significance of the measurable signal can easily be subject to debate. In this thesis, EIS using a 0.2 mm diameter Au electrode was selected as an *in situ*, non-destructive (no applied polarisation) biofilm monitoring technique rarely used for ocean sensing. This was representative of a starting point to sense interfacial properties (*i.e.* enzymatic enhanced ORR) and the mass transport near the interface, when a bacterial biofilm grows on the Au surface. In corroboration with the electrochemical investigation, CLSM was identified as a mature characterisation method for quantitative biofilm evaluation (*i.e.* biofilm thickness and magnitude number of sessile cell population) and assessment of the effectiveness of a biofilm disruption strategy. For the current study, it was decided to transfer the knowledge on the novel and attractive approach to marine NO inhibition strategy developed at Southampton (where NO can be involved in natural biofilm dispersal) to establish an environmentally friendly NO dosing strategy with the ultimate goal to control *in situ* NO generation.

6.1.2.3 Summary of Chapter 3

In a diverse and complex environment such as in seawater, substantial knowledge of physico-chemical and biological properties is required. For instance, bacterial communities can affect the marine ecology (*e.g.* pH and DO gradients across a biofilmed metallic surface) but also they are sensitive to environmental stresses, such as changes in DO level for aerobic species. A flow cell device was chosen as a suitable continuous culturing growth system for this investigation, *i.e.* allowing embedment of the Au electrode. The aerobic bacterial fouling *Pseudoalteromonas* sp. NCIMB 2021 widespread in ocean was selected for the electrochemical biofilm study, where a NOC marine flow cytometer would be used for bacterial growth characterisation. Overall, **Chapter 3** has enabled the justification of the experimental conditions for this proposed approach in **Table 6.1**.

6.1.2.4 Summary of Chapter 4

A modified once through flow system (using a 0.2 mm diameter embedded Au electrode with a 0.3 μm Al_2O_3 powder final polishing) was developed to electrochemically monitor initial bacterial biofilm development and extent, and also disruption under a controlled low laminar flow condition ($R_e \approx 1$). A critical review of the published literature has established the limitations of flow cell channel designs for bacterial biofilm culturing, where engineering concepts, together with microbiological expertise, are necessary. For this study, the flow cell (with similar dimensions to flow cell devices proposed in the literature) was designed to:

- minimise flow separation and pressure losses at the inlet / outlet,
- operate in fully developed flow conditions (*i.e.* L_e = 0.33 × 10^{-3} m for a 40.0 × 10^{-3} m flow channel length) with substantially low wall shear stress (0.31 × 10^{-3} Pa) and pressure drop (1.99 × 10^{-3} Pa) for a clean rectangular flow channel, and
- allow initial bacterial adhesion and subsequent development using a relatively long residence time of 351.6 s.

The test solutions were composed of:

- 3.5 % NaCl (baseline for the ORR),
- abiotic ASW (baseline for a conditioning film),
- control ASW (baseline for complex metal-ions),
- biotic ASW (biofilm) and,
- 500 nM of the NO donor SNP in biotic ASW (biofilm dispersal)

The physico-chemical properties of these solutions before testing (0 h), *i.e.* salinity close to 35 ‰, pH ≈ 8, temperature of 18 ± 1 °C and DO level of ≈ 6.90 ppm, were representative of surface seawater from the North Atlantic equilibrated with the atmosphere.

The bacterial growth characteristics (growth rate, mean generation time and initial growth phase, and also the overall number of planktonic cells at 0 h) of the *Pseudoalteromonas* sp. NCIMB 2021 were determined using a NOC marine flow cytometer to address the bacterial fouling properties inside the flow channel. CV tests were performed to support the use of the EIS at OCP values for biofilm monitoring. A comparative methodology between abiotic and biotic conditions was employed to address detectable modifications of the interfacial response. Overall, the qualitative electrochemical investigation was corroborated with confocal microscopy examinations for a visual and a quantitative assessment of the presence and extent of bacterial biofilms on the Au surface.

6.1.2.5 Summary of Chapter 5

Bacterial growth curve

It has been demonstrated in **Sections 5.1** and **5.2** that:

- The modified flow cell for this study was suitable for bacterial biofilm culturing with a growth rate of 0.15 h^{-1} and a mean generation time of 4.52 h.
- Growth variability between the flow cell and the batch culture was minimal, *i.e.* the growth curves were similar.

CV

Sections 5.4 to **5.7** have shown that:

- The electrochemical response of Au in 1 M H_2SO_4 was consistent with a typical Au electrode acid voltammogram.
- The CV analysis for the 3.5 % NaCl test solution was in good agreement with a conventional voltammogram at the interface Au / 3.5 % NaCl, where the ORR can be monitored between –0.200 V to the plateau at –0.700 V (*vs.* Ag/AgCl) and self-cleaning / generation process of the Au surface can be achieved in the anodic region.

Results in **Sections 5.8** and **5.9** have proven that:

- The electrochemical behaviour for the abiotic ASW was overall similar to that for a Au surface immersed in an abiotic seawater system.
- For the NaCl test solution, the ORR can be detected between –0.200 V to the plateau at –0.700 V (*vs.* Ag/AgCl), whereas the anodic region can be used for self-cleaning of the Au electrode.
- An oxidation wave between +0.500 to +0.900 V (*vs.* Ag/AgCl) corresponding to the oxidation of organic material was detectable.
- Bulk solution metal-ions can electro-actively adsorb / desorb on the Au surface at ± 0.125 V (*vs.* Ag/AgCl) via an overall diffusion dominant process, which can be suppressed by blocking organic material (representing ≈ 70 % percentage surface coverage).
- Although quantitative analyses could not be fully addressed, this diffusion process was quasi-reversible ($\alpha_a \approx 0.82$ and $\alpha_c \approx 0.79$) with $z = 1$ for a single electron transfer process, thus corresponding to the redox couple Fe^{3+} EDTA / Fe^{2+} EDTA.
- The interface for the abiotic ASW was ascribed to a non-controllable and permeable coating similar to a monolayer with defects / pinholes favouring charge diffusion process in analogy with self-assembled monolayers on Au microelectrodes.

The main conclusions for **Sections 5.10** and **5.11** are:

- A clear difference between the abiotic and biotic ASW was evident with a modification of the interfacial properties by bacterial biofilms (suppression of electro-active adsorbed / desorbed metal-ions due to the presence of a biofilm on the Au surface) and both an enzymatic enhanced ORR, and also oxidation reaction of organic material.
- The results in the cathodic region (enhanced ORR) were consistent with typical characteristics of commercialised electrochemical sensors using polarisation methods, such as the BioGEORGE and BioX.
- The self-cleaning of the biofilmed Au surface would not be straightforward for a potential range of –1.000 to +1.000 V (*vs.* Ag/AgCl), therefore higher potentials to that for the NaCl and abiotic ASW would be required.

- The CV analysis for the biotic ASW has demonstrated the significance of polarisation on a biofilmed Au electrode, where herein EIS at OCP values has been chosen for bacterial biofilm study without imposing an electrical polarisation.

Qualitative EIS / CLSM analysis

It has been shown in **Section 5.12** that:

- The EIS response for the NaCl test solution was relatively uniform with time and consistent with a typical interfacial impedance for a similar experimental sterile configuration, *i.e.* a capacitance behaviour at higher frequencies, between 10 to 100,000 Hz (interfacial charge distribution), and a diffusive / resistive characteristic at lower frequencies, between 0.1 to 10 Hz (diffusion of bulk DO across the Au surface to undergo the ORR).
- Similar to the NaCl test solution (where no detectable modification of the ORR occurred), a capacitance characteristic at higher frequencies, between 100 to 100,000 Hz (adsorbed organic layer or conditioning film), and a diffusive response at lower frequencies, between 0.1 to 100 Hz (diffusion of DO to the Au surface) were monitored for the abiotic ASW.
- The corroborative confocal images for the NaCl solution and abiotic ASW were indicative of minimum fouling potentially ascribed to non-specific binding.
- The EIS response for the biotic ASW was more complex with a clear extension of the capacitive region at higher frequencies, between 100 to 100,000 Hz (greater influence of adsorption processes / adhesion of pioneering bacteria), and a diffusive behaviour and subtle change in impedance over 72 h at lower frequencies, between 0.1 to 100 Hz (enzymatic enhanced ORR).
- Bacterial clusters were clearly seen on the CLSM images for the biotic ASW, thus consistent with the presence of a thin biofilm established at low laminar flow regime.
- The qualitative EIS / CLSM analysis has confirmed that bacterial biofilm growth and extent are a dynamic and complex process, where pioneering bacteria will initially colonise and develop on the Au surface in order to subsequently secrete EPS and favour enzymatic reactions for the enhanced ORR.
- Initial marine bacterial biofilms can be electrochemically detected under a controlled flow cell environment.
- A detectable increase in the interfacial resistance at lower frequencies, between 0.1 to 100 Hz (significant suppression of the interfacial ORR resulting from NO

induced stress on the bacterial biofilms), was evident after a 24 h exposure to 500 nM of the NO donor SNP on the 72 h-old biofilmed Au surface.

- Although the exact interfacial mechanism of NO action remains to be elucidated, the corresponding confocal images (after NO treatment) have revealed significant bacterial biofilm dispersal on the Au surface, thereby consistent with previous studies using the nanomolar range (500 nM) NO donor SNP.
- The fouling performances of the Au surface (using percentage coverage analysis) were greater for the biotic ASW (≈ 50 %) compared to that for the NaCl and abiotic ASW (a few percents for a minimum biofouling), and were significantly reduced (≈ 5 %) after a 24 h exposure to 500 nM of the NO donor SNP.
- The OCP values of the EIS data varied overall towards the cathodic region of the ORR (consistent with a previous study for Au in a seawater environment), thus suggesting a natural polarisation process associated with biofilm formation that is substantially suppressed after exposure to the 500 nM of the NO donor SNP (increase in the OCP values).

Quantitative EIS / CLSM analysis

Results in **Section 5.13** have demonstrated that:

- An important parameter of the EIS response can be used to quantify bacterial biofilm and gauge the extent of biofouling, *i.e.* capacitive component (between 100 to 100,000 Hz) for assessment of a number of sessile bacteria.
- The bacterial biofilm thickness was approximately 3.0 μm (within the same order of magnitude of 4 – 8 μm thick biofilms reported for Au in seawater), when the corresponding sessile bacterial population was $\approx 8.3 \times 10^7$ cells cm^{-2} after a 72 h immersion.
- Uniquely, a method for assessing the number of sessile bacterial cells (on the Au surface) using *in situ* EIS monitoring has been addressed, where the results were in good agreement with a reliable *ex situ* investigation utilising confocal microscopy analyses.
- The relationship for the surface charge density (capacitive component / number of sessile bacterial density) can potentially provide valuable insight into calibration of real time biofilm monitoring devices.

6.1.3 Bacterial biofilm: a fascinating concept

As mentioned by Flemming *et al.* (and in particular for this thesis), a bacterial biofilm can be viewed as a bioreactor in the wrong place and time causing detrimental effects to engineering systems. However, it can also be regarded as a competent entity encompassing physico-chemical and biological properties, see **Figure 6.1**.

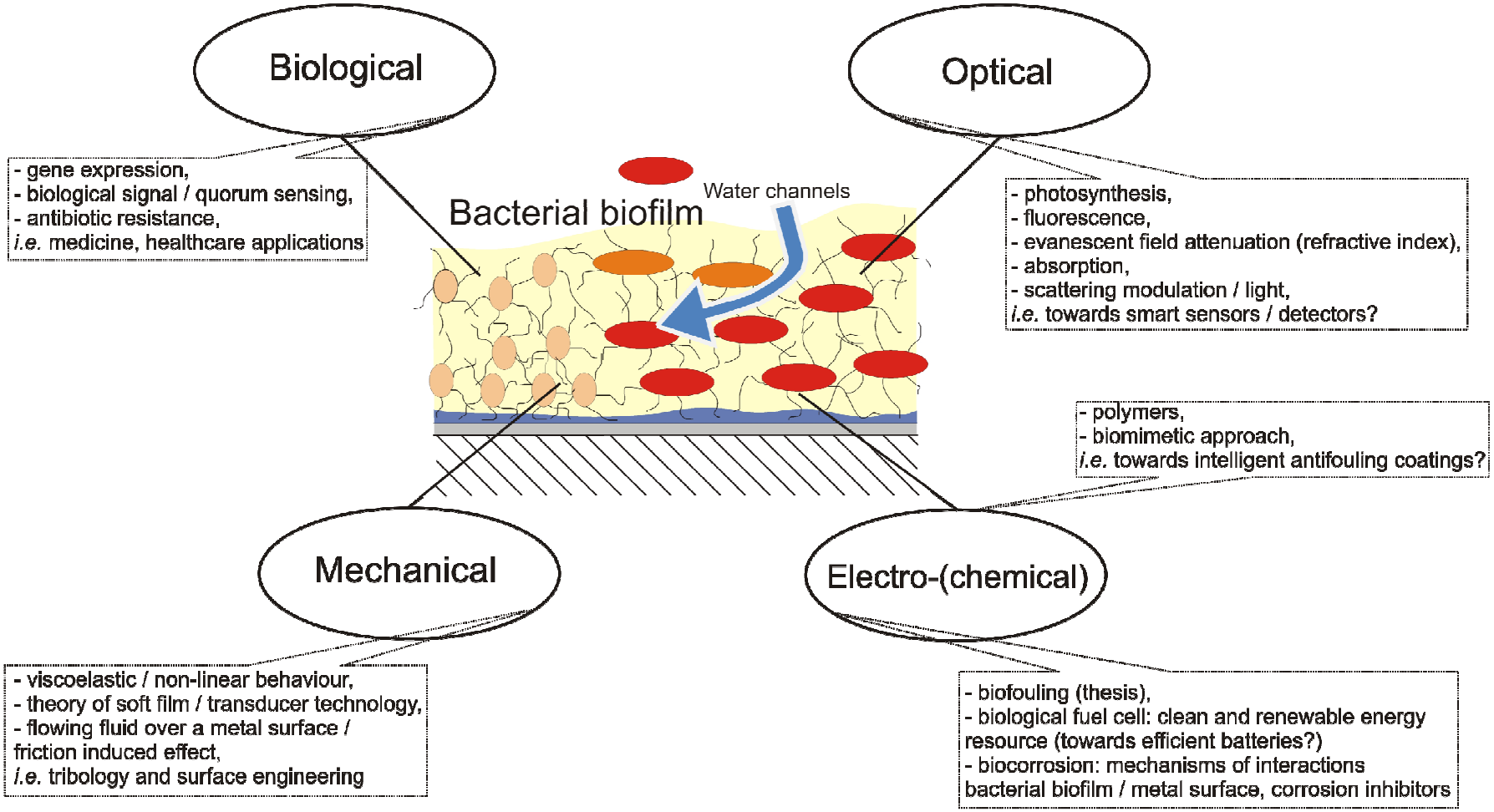

Figure 6.1. Schematic of the physico-chemical and biological properties of a bacterial biofilm.

In the context of fundamental research (**Figure 6.1**), a bacterial biofilm is a fascinating concept with biological, optical, mechanical and electro-(chemical) characteristics, which could inspire and revolution future generations in science and engineering, *e.g.* towards efficient biological fuel cells? From an engineering standpoint, the author believes that a holistic approach is necessary to understand a bacterial biofilm in details but it is extremely challenging. Herein, this thesis has focused on the electrochemical properties of bacterial biofilms, which can correspond to only one piece of the puzzle (**Figure 6.1**) and further corroborative studies are required for a complete story in the exciting field of bacterial biofilm.

6.2 Further work

Section 6.2.1 outlines the next step for this investigation, while **Section 6.2.2** describes further fundamental approaches for bacterial biofilm studies.

6.2.1 Future studies born directly from this work

6.2.1.1 Sensor sensitivity

Further testing should be focused on the sensor sensitivity to amplify the measurable signal:

- Robust Au multi-microelectrode arrays could be developed and tested for enhanced bacterial biofilm quantification, where their performance could be compared to single electrodes used in-service.
- After validation of the robustness and reliability of Au multi-microelectrode arrays, mapping could be an attractive detection strategy (using a combination of different electrochemical techniques) to understand in detail the interactions between a bacterial biofilm and a metallic surface.

6.2.1.2 Sensing / operating system

The bacterial biofilm sensing approach (*i.e.* the sensor itself) only has significance when it is incorporated into a monitoring system (herein a flow cell device), thus:

- Microbiologists and engineers need greater consensus: *(i)* on the flow channel design for enhanced controllability of laboratory biofilm studies; and *(ii)* on the necessary addition of a chemostat / bioreactor in the flow system for nutrient supply and bacterial growth rate control.
- *In situ* microscopic observations inside the modified flow cell channel, *i.e.* using EIS [**6.1**], could provide insight into the kinetics of bacterial biofilm formation and development.
- A smart flow cell monitoring device (in analogy with corrosion monitoring systems [**6.2**]) could be developed for *in situ* measurement of important factors, such as pH, DO level, H_2O_2 concentration, mass transfer coefficient and temperature for correlation with bacterial biofilm growth and extent.
- Where the channel electrode is reported to be non-uniformly accessible (*i.e.* the current density distribution over the electrode is non-uniform [**6.3**]) in contrast with the RDE, a comparative study between the channel electrode and a RDE modified flow cell could be informative of an improved controllable (uniform) sensing surface.
- Steady-state dc EIS experiments in order to choose the suitable amplitude of the stimulus excitation [**6.4**], could be performed and compared with the ac EIS tests to search for variability in the sensing response / influence on bacterial biofilm.
- The effect of pulsative flow (peristaltic pump) on the electrochemical response could be investigated, for instance using static followed by hydrodynamic followed by static flow conditions.
- Corroborative electrochemical and biological studies could be carried out to establish a mode of action mechanism of 500 nM of the NO donor SNP (dosed on a biofilmed surface) to understand in details the NO induced biofilm dispersal.
- The test matrix for the inhibition biocide strategy could be completed using NO donor SNP (25 and 500 nM, 50 μM, 50 and 100 mM), sodium hypochlorite (0.6, 2, 3, 5 and 10 mg L^{-1} Cl_2), 0.1 and 1 % (w/v) tri(ethylene glycol) and sodium azide (10 mM), see **Table 6.2**.

Table 6.2. Proposed test matrix for the biocide / biocide-free antifouling dosing strategy.

Biocide / biocide-free antifouling solution	**Concentrations (in seawater)**	**Effects / predictions**	
NO donor SNP	25 nM	Bacterial biofilm dispersal / increase in planktonic cell density	
	500 nM	Bacterial biofilm dispersal / increase in planktonic cell density	**Optimum concentration (thesis)**
	50 μM	Bacterial biofilm dispersal / increase in planktonic cell density	
	50 mM	Increase in biofilm biomass / decrease in planktonic biomass	Converse effect
	100 mM		
Sodium hypochlorite	0.6 mg L^{-1} Cl_2	Comparison with the performance of the BioGeorge™ sensor (control of biofilm buildup by pulse-chlorination using a 30 min dosing) / do not induce biofilm sloughing	
	2 mg L^{-1} Cl_2	Presence of respiratory activity in biofilms / do not induce biofilm sloughing	
	3 mg L^{-1} Cl_2	Biofilm disruption	
	5 mg L^{-1} Cl_2		
	10 mg L^{-1} Cl_2		
Tri(ethylene glycol)	0.1 % (w/v)	Inhibition of biofilm formation	
	1 % (w/v)		
Sodium azide	10 mM	Inhibition of enzymatic activity (shut down the respiratory activity resulting in bacterial cell death)	

This also applies for an operating (in-service) system, therefore:

- The hydrodynamic performance of the biofilm sensor could be characterised using a corrosion loop system and an in-service marine heat exchanger tube, where the most likely biofouling locations (*e.g.* stagnation zones) could be assessed for target based determination of sensing areas, *i.e.* the inside favourable biofilmed surfaces.
- Once a clear understanding on biocide inhibition strategy / antifouling solution is gained (**Table 6.2**), it could be tested in-service to establish the optimum concentration, duration and frequency of dosing at a given allowable flow rate.

6.2.2 Potential new routes for investigation

6.2.2.1 Bacterial biofilm system

Probably the least controllable factor for this engineering investigation, the biological properties (**Biological** in **Figure 6.1**) are also tremendously fundamental:

- Studies on the gene expression for bacterial adhesion and EPS matrix secretion, and also natural dispersal could help to define suitable countermeasures for the control of bacterial biofilms.
- DNA and RNA analyses could be utilised to quantify bacterial growth and the corresponding metabolic activity, for instance to study the expression and specific activity of catalase.
- Investigation on bacterial selectivity and the influence of environmental variability, for example on the production of catalase isoforms, could be informative on the metabolic process involved during bacterial growth and extent.
- The influence of catalase on a bacterial biofilm, *i.e.* both changes in chemistry and stickiness of the EPS matrix, together with the corresponding electrochemical response, could be investigated.
- A mixed population of bacteria species (*i.e.* marine aerobic and / or anaerobic microbes) and fungi / yeasts, spores of macroalgae, and also protozoa could be used to understand their interactions on a metal surface.
- Analytical studies / modelling of bacterial biofilm attachment within a flow channel and inside pipe stagnation zones could help to support experimental tests.

- Quantification software, such as COMSTAT, ISA and PHLIP could be used to study the internal properties of a bacterial biofilm (*e.g.* diffusion, porosity and biovolume) for corroboration with electrochemical investigations in **Chapter 5**.
- A detailed description of bacterial biofilm spatial distribution and composition could be achieved using a corroboration of microscopy and spectroscopy techniques.

6.2.2.2 Bio-inspired engineering systems

In correlation with **Section 6.2.2.1**, greater understanding of the biological characteristics of competent bacterial biofilms could lead to the design and development of new biologically inspired sensors, actuators and engineering systems:

- Optical fibre devices utilising a modified biological membrane (with a bacterial biofilm) could be a great tool to study the optical properties of a bacterial biofilm, thus suggesting new sensing applications (**Optical** in **Figure 6.1**).
- The non-linear and viscoelastic behaviour of a bacterial biofilm could be investigated using a QCM and compared with the corresponding results in a flow cell system (**Mechanical** in **Figure 6.1**).
- SECM could be used for investigation on the redox activity within an aerobic bacterial biofilm and subsequent potential correlations with the catalase (**Electrochemical** in **Figure 6.1**).

References

References to Chapter 1

[**1.1**] A.I. Railkin, *Marine Biofouling: Colonization Processes and Defenses*, 1st ed., CRC Press LLC, USA (2004).

[**1.2**] H.-C. Flemming, P. Sriyutha Murthy, R. Venkatesan and K.E. Cooksey, *Marine and Industrial Biofouling*, Springer, Germany (2009).

[**1.3**] J.E. Duddridge, C.A. Kent and J.F. Laws, Effect of Surface Shear Stress on the Attachment of *Pseudomonas fluorescens* to Stainless Steel under Defined Flow Conditions, *Biotechnology and Bioengineering*, **24**(1), 153-164 (1982).

[**1.4**] C. Hellio and D.M. Yebra, *Advances in marine antifouling coatings and technologies*, Woodhead Publishing Limited, UK (2009).

[**1.5**] J. Starosvetsky, D. Starosvetsky and R. Armon, Identification of microbiologically influenced corrosion (MIC) in industrial equipment failures, *Engineering Failure Analysis*, **14**(8), 1500-1511 (2007).

[**1.6**] S. Kakaç, *Boilers, Evaporators, and Condensers*, John Wiley and Sons, Inc., USA (1991).

[**1.7**] H.A. Videla, *Manual of Biocorrosion*, 1st ed., CRC Press, USA (1996).

[**1.8**] M. Whestone, Biofouling: Searching for Answers, *Sea Technonology,* **33**(8), 35-39 (1992).

[**1.9**] V. Scotto and M.E. Lai, The ennoblement of stainless steel in seawater: a likely explanation coming from the field, *Corrosion Science*, **40**(6), 1007-1018 (1998).

[**1.10**] C.S. Rangan, G.R. Sarma and V.S.V. Mani, *Instrumentation Devices and Systems*, Tata McGraw-Hill Publishing Company Limited, India (1983).

[**1.11**] G. Ash et collaborateurs, *Les capteurs en instrumentation industrielle*, 5e éd., Dunod, France (1999).

[**1.12**] T. Coradin and J. Livage, Aqueous Silicates in Biological Sol-Gel Applications: New Perspectives for Old Precursors, *Accounts of Chemical Research*, **40**(9), 819-826 (2007).

[**1.13**] N. Barraud, D.J. Hassett, S.-H. Hwang, S.A. Rice, S. Kjelleberg and J.S. Webb, Involvement of Nitric Oxide in Biofilm Dispersal of *Pseudomonas aeruginosa*, *Journal of Bacteriology*, **188**(21), 7344–7353 (2006).

[**1.14**] J.B. Xavier, C. Picioreanu, S.A. Rani, M.C.M. van Loosdrecht and P.S. Stewart, Biofilm-control strategies based on enzymic disruption of the extracellular polymeric substance matrix - a modelling study, *Microbiology*, **151**(12), 3817-3832 (2005).

[**1.15**] C. Johansen, P. Falholt and L. Gram, Enzymatic Removal and Disinfection of Bacterial Biofilms, *Applied and Environmental Microbiology*, **63**(9), 3724-3728 (1997).

References to Chapter 2

[**2.1**] A.I. Railkin, *Marine Biofouling: Colonization Processes and Defenses*, 1st ed., CRC Press LLC, USA (2004).

[**2.2**] H.A. Videla, *Manual of Biocorrosion*, 1st ed., CRC Press, USA (1996).

[**2.3**] H.-C. Flemming, P. Sriyutha Murthy, R. Venkatesan and K.E. Cooksey, *Marine and Industrial Biofouling*, Springer, Germany (2009).

[**2.4**] C. Hellio and D.M. Yebra, *Advances in marine antifouling coatings and technologies*, Woodhead Publishing Limited, UK (2009).

[**2.5**] L.F. Melo and T.R. Bott, Biofouling in Water Systems, *Experimental Thermal and Fluid Science*, **14**(4), 375-381 (1997).

[**2.6**] M. Fletcher, *Bacterial Adhesion: Molecular and Ecological*, 1st ed., Wiley Series in Ecological and Applied Microbiology, USA (1996).

[**2.7**] J.B. McClintock and B.J. Baker, *Marine Chemical Ecology (Marine Science)*, 1st ed., CRC Press LLC, USA (2001).

[**2.8**] U. Szewzyk, C. Holmström, M. Wrangstadh, M.-O. Samuelson, J.S. Maki and S. Kjelleberg, Relevance of the exopolysaccharide of marine *Pseudomonas* sp. strain S9 for the attachment of *Ciona intestinalis* larvae, *Marine Ecology Progress Series*, **75**(2-3), 259-265 (1991).

[**2.9**] J.R. Lawrence, D.R. Korber, B.D. Hoyle, J.W. Costerton and D.E. Caldwell, Optical Sectioning of Microbial Biofilms, *Journal of Bacteriology,* **173**(20), 6558-656 (1991).

[**2.10**] J.R. Lawrence, G.M. Wolfaardt and D.R. Korber, Determination of Diffusion Coefficients in Biofilms by Confocal Laser Microscopy, *Applied and Environmental Microbiology*, **60**(4), 1166-1173 (1994).

[**2.11**] F. Mansfeld, The interaction of bacteria and metal surfaces, *Electrochimica Acta*, **52**(27), 7670-7680 (2007).

[**2.12**] B.J. Little, J.S. Lee and R.I. Ray, Diagnosing Microbiologically Influenced Corrosion: A State-of-the-Art Review, *Corrosion*, **62**(11), 1006-1017 (2006).

[**2.13**] Woods Hole Oceanographic Institution (WHOI), *Marine Fouling and its Prevention*, Annapolis: United States Naval Institute, USA (1952).

[**2.14**] J.E. Duddridge, C.A. Kent and J.F. Laws, Effect of Surface Shear Stress on the Attachment of *Pseudomonas fluorescens* to Stainless Steel under Defined Flow Conditions, *Biotechnology and Bioengineering*, **24**(1), 153-164 (1982).

[**2.15**] M. Whestone, Biofouling: Searching for Answers, *Sea Technonolgy*, **33**(8), 35-39 (1992).

[**2.16**] S.C. Dexter and J.P. Lafontaine, Effect of Natural Marine Biofilms on Galvanic Corrosion, *Corrosion*, **54**(11), 851-861 (1998).

[**2.17**] B.J. Little, P.A. Wagner and F. Mansfeld, *Microbiologically Influenced Corrosion*, NACE International, Houston, Texas, Vol.5, USA (1997).

[**2.18**] G.J. Brankevich, M.L.F. De Mele and H.A. Videla, Biofouling and Corrosion in Coastal Power Plant Cooling Water Systems, *Marine Technology Society Journal*, **24**(3), 18-28 (1990).

[**2.19**] J. Starosvetsky, D. Starosvetsky and R. Armon, Identification of microbiologically influenced corrosion (MIC) in industrial equipment failures, *Engineering Failure Analysis*, **14**(8), 1500-1511 (2007).

[**2.20**] E. Denkhaus, S. Meisen, U. Telgheder and J. Wingender, Chemical and physical methods for characterisation of biofilms. *Microchimica Acta*, **158**(1-2), 1-27 (2007).

[**2.21**] T.E. Cloete, L. Jacobs and V.S. Brözel, The chemical control of biofouling in industrial water systems, *Biodegradation*, **9**(1), 23-37 (1998).

[**2.22**] P.S. Stewart, G.A. McFeters and C.T. Huang, *Biofilm control by antimicrobial agents*, In Biofilms II: Process Analysis and Applications, pp. 373-405, Edited by J. D. Bryers, Wiley, USA (2000).

[**2.23**] W.G. Characklis and K.C. Marshall, *Biofilms*, Wiley, USA (1990).

[**2.24**] L.D. Chambers, K.R. Stokes, F.C. Walsh and R.J.K. Wood, Modern approaches to marine antifouling coatings, *Surface and Coatings Technology*, **201**(6), 3642–3652 (2006).

[**2.25**] E. Almeida, T.C. Diamantino, O. de Sousa, Marine paints: The particular case of antifouling paints, *Progress in Organic Coatings*, **59**(1), 2-20 (2007).

[**2.26**] J.B. Xavier, C. Picioreanu, S.A. Rani, M.C.M. van Loosdrecht and P.S. Stewart, Biofilm-control strategies based on enzymic disruption of the extracellular polymeric substance matrix - a modelling study, *Microbiology*, **151**(12), 3817-3832 (2005).

[**2.27**] R.M. Donlan, Biofilms: Microbial Life on Surfaces, *Emerging Infectious Diseases*, **8**(9), 881-890 (2002).

[**2.28**] L.D. Chambers, F.C. Walsh, R.J.K Wood and K.R. Stokes, *Biomimetic approach to the design of the marine antifouling coatings*, In World Maritime Technology Conference, ICMES Proceedings, The Institute of Marine Engineering, Science and Technology (2006).

[**2.29**] C. Rubio, *Compréhension des mécanismes d'adhésion des biofilms en milieu marin en vue de la conception de nouveaux moyens de prevention*, Thèse de doctorat de l'Université de Paris 6, Spécialité: Métallurgie et Matériaux (2002).

[**2.30**] W. Wang, J. Wang, X. Li, H. Xu and J. Wu, Influence of biofilms growth on corrosion potential of metals immersed in seawater, *Materials and Corrosion*, **55**(1), 30-35 (2004).

[**2.31**] H.A. Videla and L.K. Herrera, Microbiologically influenced corrosion: looking to the future, *International Microbiology*, **8**(3), 169-180 (2005).

[**2.32**] A. Homas and D.L. Hillis, *Biofouling and corrosion research for marine heat exchangers*, 38-41, In Oceans 89, Vol. 1, New York, IEEE. 1719, USA (1989).

[**2.33**] R.H. Perry and D.W. Green, *Perry's Chemical Engineers' Handbook*, 6th ed., McGraw-Hill, USA (1984).

[**2.34**] J.H. Lienhard IV and J.H. Lienhard V, *A Heat Transfer Textbook*, 3rd ed., Cambridge, Massachusetts – Phlogiston Press, USA (2004).

[**2.35**] S. Kakaç, *Boilers, Evaporators, and Condensers*, John Wiley and Sons, Inc., USA (1991).

[**2.36**] Boat Parts Info, *Marine Cooling Systems and Heat Exchangers*, Retrieved 09/07/2010, from http://www.boatpartsinfo.com/images/fresh-water-cooling-system.gif, © 2010 Boat Parts Info.

[**2.37**] D. Féron, *Corrosion behaviour and protection of copper and aluminium alloys in seawater*, European Federation of Corrosion Publications Number 50, Woodhead Publishing Limited and CRC Press LLC,UK (2007).

[**2.38**] H.A. Videla, M.F.L. DeMele and G. Brankevich, Assessment of corrosion and microfouling of several metals in polluted seawater, *Corrosion*, **44**(7), 423-426 (1988).

[**2.39**] K.D. Efird, Interrelation of corrosion and fouling for metals in sea-water, *Materials Performance*, **15**(4), 16-25 (1976).

[**2.40**] V.J. Harwood and A.S. Gordon, Regulation of Extracellular Copper-Binding Proteins in Copper-Resistant and Copper-Sensitive Mutants of *Vibrio alginolyticus*, *Applied and Environmental Microbiology*, **60**(6), 1749-1753 (1994).

[**2.41**] R.C. Barik, *Environmental factors affecting the marine corrosion performance of nickel aluminium bronze*, PhD Thesis, University of Southampton, Faculty of Engineering, Science and Mathematics, School of Engineering Sciences (2006).

[**2.42**] D. Pletcher and F. Walsh, *Industrial Electrochemistry*, 2nd ed., Blackie A. & P., An Imprint of Chapman & Hall, UK (1993).

[**2.43**] M.G. Fontana and N.D. Greene, *Corrosion Engineering*, 2nd ed., John Wiley & Sons, Inc., USA (1978).

[**2.44**] K.R. Trethewey and J. Chamberlain, *Corrosion for Science and Engineering*, 2nd ed., Longman, UK (1995).

[**2.45**] J.A. Wharton and K.R. Stokes, Analysis of nickel–aluminium bronze crevice solution chemistry using capillary electrophoresis, *Electrochemistry Communications,* **9**(5), 1035-1040 (2007).

[**2.46**] J.A. Wharton, R.C. Barik, G. Kear, R.J.K. Wood, K.R. Stokes, and F.C. Walsh, The corrosion of nickel–aluminium bronze in seawater, *Corrosion Science,* **47**(12), 3336-3367 (2005).

[**2.47**] A.V. Benedetti, P.T.A. Sumodjo, K. Nobe, P.L. Cabot and W.G. Proud, Electrochemical studies of copper, copper-aluminium and copper-aluminium-silver alloys: impedance results in 0.5 M NaCl, *Electrochimica Acta*, **40**(16), 2657-2668 (1995).

[**2.48**] H. Siedlarek, D. Wagner, W.R. Fisher and H.H. Paradies, Microbiologically influenced corrosion of copper: The ionic transport properties of biopolymers, *Corrosion Science*, **36**(10), 1751-1763 (1994).

[**2.49**] R. Baboian, *Corrosion Tests and Standards: Application and Interpretation*, 2nd ed, ASTM International, USA (2005).

[**2.50**] K. Rabaey, J. Rodríguez, L.L. Blackall, J. Keller, P. Gross, D. Batstone, W. Verstraete and K.H. Nealson, Microbial ecology meets electrochemistry: electricity-driven and driving communities, *The International Society for Microbial Ecology*, **1**(1), 9-18 (2007).

[**2.51**] L.P. Nielsen, N. Risgaard-Petersen, H. Fossing, P.B. Christensen and M. Sayama, Electric currents couple spatially separated biogeochemical processes in marine sediment, *Nature*, **463**(7284), 1071-1074 (2010).

[**2.52**] A.K. Shukla, P. Suresh, S. Berchmans and A. Rajendran, Biological fuel cells and their application, *Current Science*, **87**(4), 455-468 (2004).

[**2.53**] F. Zhao, R.C.T. Slade and J.R. Varcoe, Techniques for the study and development of microbial fuel cells: an electrochemical perspective, *Chemical Society Reviews*, **38**(7), 1926-1939 (2009).

[**2.54**] C.I. Torres, A.K. Marcus, H-S. Lee, P. Parameswaran, R. Krajmalnik-Brown and B.E. Rittmann, A kinetic perspective on extracellular electron transfer by anode-respiring bacteria, *FEMS Microbiology Review*, **34**(1), 3-17 (2010).

[**2.55**] S. Bayoudh, A. Othmane, L. Ponsonnet and H. Ben Ouada, Electrical detection and characterization of bacterial adhesion using electrochemical impedance spectroscopy-based flow chamber, *Colloids and Surfaces A: Physicochemical and Engineering Aspects*, **318**(1-3), 291-300 (2008).

[**2.56**] A.T. Poortinga, R. Bos and H.J. Busscher, Measurement of charge transfer during bacterial adhesion to an indium tin oxide surface in a parallel plate flow chamber, *Journal of Microbiological Methods*, **38**(3), 183-189 (1999).

[**2.57**] D.J. Schiffrin and S.R. de Sánchez, The Effect of Pollutants and Bacterial Microfouling on the Corrosion of Copper Base Alloys in Seawater, *Corrosion*, **41**(1), 31-38 (1985).

[**2.58**] V. Scotto and M.E. Lai, The ennoblement of stainless steel in seawater: a likely explanation coming from the field, *Corrosion Science*, **40**(6), 1007-1018 (1998).

[**2.59**] J.P. Busalmen, M. Vázquez and S.R. de Sánchez. New evidences on the catalase mechanism of microbial corrosion, *Electrochimica Acta*, **47**(12), 1857-1865 (2002).

[**2.60**] V.M. Vazquez, S.R. de Sánchez, E.J. Calvo and D.J. Schiffrin, The electrochemical reduction of oxygen on polycrystalline copper in borax solution, *Journal of Electroanalytical Chemistry*, **374**(1-2), 189-197 (1994).

[**2.61**] D. Nercessian, F.B. Duville, M. Desimone, S. Simison and J.P. Busalmen, Metabolic turnover and catalase activity of biofilms of *Pseudomonas fluorescens* (ATCC 17552) as related to copper corrosion, *Water Research*, **44**(8), 2592-2600 (2010).

[**2.62**] T. Kocha, M. Yamaguchi, H. Ohtaki, T. Fukuda and T. Aoyagi, Hydrogen peroxide-mediated degradation of protein: different oxidation modes of copper- and iron-dependent hydroxyl radicals on the degradation of albumin, *Biochimica et Biophysica Acta*, **1337**(2), 319-326 (1997).

[**2.63**] E. Eguia, A. Trueba, A. Girón, B. Rio-Calonge, F. Otero and C. Bielva, Optimisation of biocide dose as a function of residual biocide in a heat exchanger pilot plant effluent, *Biofouling*, **23**(3-4), 231-247 (2007).

[**2.64**] E. Eguia, A. Trueba, B. Rio-Calonge, A. Girón, J.J. Amieva and C. Bielva, Combined monitor for direct and indirect measurement of biofouling, *Biofouling*, **24**(2), 75-86 (2008).

[**2.65**] J.A. Wharton and R.J.K Wood, Influence of flow conditions on the corrosion of AISI 304L stainless steel, *Wear*, **256**(5), 525-536 (2004).

[**2.66**] P. Stoodley, Z. Lewandowski, J.D. Boyle and H.M. Lappin-Scott, Oscillation Characteristics of Biofilm Streamers in Turbulent Flowing Water as Related to Drag and Pressure Drop, *Biotechnology and Bioengineering*, **57**(5), 537-544 (1998).

[**2.67**] M. Salta, J.A. Wharton, P. Stoodley, S.P. Dennington, L.R. Goodes, S. Werwinski, U. Mart, R.J.K. Wood and K.R. Stookes, Designing biomimetic antifouling surfaces, *Philosophical Transactions of the Royal Society A*, **368**(1929), 4729-4754 (2010).

[**2.68**] Q. Zhao, Y. Liu, C. Wang, S. Wang and H. Müller-Steinhagen, Effect of surface free energy on the adhesion of biofouling and crystalline fouling, *Chemical Engineering Science*, **60**(17), 4858-4865 (2005).

[**2.69**] H.-C. Flemming, Biofouling in water systems – cases, causes and countermeasures, *Applied Microbiology and Biotechnology*, **59**(6), 629-640 (2002).

[**2.70**] L. Lemoine, J. Guezennec, D. Festy and P. Fera, *Corrosion and biofouling of OTEC heat exchangers: IFREMER researches*, In Oceans 85, volume 2, Washington D.C.: Marine Technology Society/IEEE, 1260-1266 (1985).

[**2.71**] R.A. Brizzolara, D.J. Nordham, M. Walch, R.M. Lennen, R. Simmons, E. Burnett and M.S. Mazzola, Non-Chemical Biofouling Control in Heat Exchangers and Seawater Piping Systems Using Acoustic Pulses Generated by an Electrical Discharge, *Biofouling*, **19**(1), 19-35 (2003).

[**2.72**] A.H. Tuthill, Guidelines For the Use of Copper Alloys in Seawater, *Materials Performance*, **26**(9), 12-22 (1987).

[**2.73**] H.J. Busscher and H.C. van der Mei, Microbial Adhesion in Flow Displacement Systems, *Clinical Microbiology Reviews*, **19**(1), 127-141 (2006).

[**2.74**] Y.A. Çengel and J.M. Cimbala, *Fluid mechanics: fundamentals and applications*, 1st ed., McGraw-Hill, USA (2006).

[2.75] P. Bradshaw, A note on "critical roughness height" and "transitional roughness", *Physics of Fluids*, **12**(6), 1611 (2000).

[**2.76**] D. Herbert-Guillou, B. Tribollet, D. Festy and L. Kienel, In situ detection and characterization of biofilm in waters by electrochemical methods, *Electrochimica Acta*, **45**(7), 1067-1075 (1999).

[**2.77**] D. Herbert-Guillou, B. Tribollet, D. Festy, Influence of the hydrodynamics on the biofilm formation by mass transport analysis, *Bioelectrochemistry*, **53**(1), 119-125 (2000).

[**2.78**] P. Stoodley, S. Yang, H. Lappin-Scott and Z. Lewandowski, Relationship Between Mass Transfer Coefficient and Liquid Flow Velocity in Heterogenous Biofilms Using Microelectrodes and Confocal Microscopy, *Biotechnology and Bioengineering*, **56**(6), 682-688 (1997).

[**2.79**] B.C. Dunsmore, A. Jacobsen, L. Hall-Stoodley, C.J. Bass, H.M. Lappin-Scott and P. Stoodley, The influence of fluid shear on the structure and material properties of sulphate-reducing bacterial biofilms, *Journal of Industrial Microbiology and Biotechnology*, **29**(6), 347-353 (2002).

[**2.80**] J.F. Douglas, J.M. Gasiorek and J.A.Swaffield, *Fluid mechanics*, 3rd ed., Longman Scientific & Technical, UK (1995).

[**2.81**] M. Mehdi Salek, S.M. Jones and R.J. Martinuzzi, The influence of flow cell geometry related shear stresses on the distribution, structure and susceptibility of *Pseudomonas aeruginosa* 01 biofilms, *Biofouling*, **25**(8), 711-725 (2009).

[**2.82**] D.E. Nivens, R.J. Palmer Jr and D.C. White, Continuous nondestructive monitoring of microbial biofilms: a review of analytical techniques, *Journal of Industrial Microbiology and Biotechnology*, **15**(4), 263-276 (1995).

[**2.83**] W.G. Characklis, *Biofilm development: A process analysis*, In: Marshall, K.C., ed., Microbial Adhesion and Aggregation, Vol. 31, Life Sciences Research Report, Springer-Verlag, Germany (1984).

[**2.84**] K. Sauer, A.K. Camper, G.D. Ehrlich, J.W. Costerton and D.G. Davies, *Pseudomonas aeruginosa* Displays Multiple Phenotypes during Development as a Biofilm, *Journal of Bacteriology,* **184**(4), 1140-1154 (2002).

[**2.85**] M.R. Parsek and E.P. Greenberg, Acyl-homoserine lactone quorum sensing in Gram-negative bacteria: A signalling mechanism involved in associations with higher organisms, *Proceedings of the National Academy of Sciences of the United States of America,* **97**(16), 8789-8793 (2000).

[**2.86**] P.S. Stewart and J.W. Costerton, Antibiotic resistance of bacteria in biofilms, *Lancet*, **358**(9276), 135-138 (2001).

[**2.87**] K.J. Grobe, J. Zahller and P.S. Stewart, Role of dose concentration in biocide efficacy against *Pseudomonas aeruginosa* biofilms, *Journal of Industrial Microbiology and Biotechnology,* **29**(1), 10-15 (2002).

[**2.88**] O.O. Babalola, Molecular techniques: An overview of methods for the detection of bacteria, *African Journal of Biotechnology*, **2**(12), 710-713 (2003).

[**2.89**] S.B. Surman, J.T. Walker, D.T. Goddard, L.H.G. Morton, C. W. Keevil, W. Weaver, A. Skinner, K. Hanson, D. Caldwell and J. Kurtz, Comparison of microscope techniques for the examination of biofilms, *Journal of Microbiological Methods,* **25**(1), 57-70 (1996).

[**2.90**] C.S. Rangan, G.R. Sarma and V.S.V. Mani, *Instrumentation Devices and Systems*, Tata McGraw-Hill Publishing Company Limited, India (1983).

[**2.91**] G. Ash et collaborateurs, *Les capteurs en instrumentation industrielle*, 5^{e} éd., Dunod, France (1999).

[**2.92**] G. Denuault, Microelectrodes, *Chemistry and Industry*, **18**, 678-680 (1996).

[**2.93**] G. Denuault, Electrochemical techniques and sensors for ocean research, *Ocean Science Discussions*, **6**(2), 1857-1893 (2009).

[**2.94**] C.W. Keevil, Rapid detection of biofilms and adherent pathogens using scanning confocal laser microscopy and episcopic differential interference contrast microscopy, *Water Science and Technology*, **47**(5), 105-116 (2003).

[**2.95**] J.W. Schultze, T. Osaka and M. Datta, *Electrochemical microsystem technologies*, in: New Trends in Electrochemical Technology Series, Vol. 2, Taylor and Francis, UK (2002).

[**2.96**] A. Bressel, J.W. Schultze, W. Khan, G.M. Wolfaardt, H.-P. Rohns, R. Irmscher and M.J. Schöning, High resolution gravimetric, optical and electrochemical investigations of microbial biofilm formation in aqueous systems, *Electrochimica Acta*, **48**(20-22), 3363-3372 (2003).

[**2.97**] H. Beyenal, Z. Lewandowski, C. Yakymyshyn, B. Lemley and J. Wehri, Fiber-optic microsensors to measure backscattered light intensity in biofilms, *Applied Optics*, **39**(19), 3408-3412 (2000).

[**2.98**] C. Gabrielli, M. Keddam, N. Portail, P. Rousseau, H. Takenouti and V. Vivier, Electrochemical impedance spectroscopy investigations of a microelectrode behavior in a thin-layer cell: Experimental and theoretical studies, *Journal of Physical Chemistry B*, **110**(41), 20478-20485 (2006).

[**2.99**] X. Bai, S.C. Dexter and G.W. Luther III, Application of EIS with Au–Hg microelectrode in determining electron transfer mechanisms, *Electrochimica Acta*, **51**(8-9), 1524-1533 (2005).

[**2.100**] S. Lomperski and M.T. Farmer, Experimental evaluation of the water ingression mechanism for corium cooling, *Nuclear Engineering and Design*, **237**(9), 905-917 (2006).

[**2.101**] P. Cady, Impedimetric screening for bacteriuria, *Journal of Clinical Microbiology*, **7**(), 273-278 (1978).

[**2.102**] M. Veiseh, O. Veiseh, M.C. Martin, C. Bertozzi and M. Zhang, Single cell based sensors and synchrotron FTIR spectroscopy: a hybrid system towards bacterial detection, *Biosensors and Bioelectronics*, **23**(2), 253-260 (2007).

[**2.103**] D.E. Nivens, J.Q. Chambers, T.R. Anderson and D.C. White, Long-Term, On-Line Monitoring of Microbial Biofilms Using a Quartz Crystal Microbalance, *Analytical Chemistry*, **65**(1), 65-69 (1993).

[**2.104**] C. Ruan, K. Zeng, O.K. Varghese and C.A. Grimes, Magnetoelastic Immunosensors: Amplified Mass Immunosorbent Assay for Detection of *Escherichia coli* O157:H7, *Analytical Chemistry*, **75**(23), 6494-6498 (2003).

[**2.105**] R. Guntupalli, J. Hu, R.S. Lakshmanan, T.S. Huang, J.M. Barbaree and B.A. Chin, A magnetoelastic resonance biosensor immobilized with polyclonal antibody for the detection of *Salmonella typhimurium*, *Biosensors and Bioelectronics,* **22**(7), 1474-1479 (2007).

[**2.106**] R. Guntupalli, R.S. Lakshmanan, J. Hu , T.S. Huang, J.M. Barbaree, V. Vodyanoy and B. A. Chin, Rapid and sensitive magnetoelastic biosensors for the detection of *Salmonella typhimurium* in a mixed microbial population, *Journal of Microbiological Methods*, **70**(1), 112-118 (2007).

[**2.107**] S. Kröger and R.J. Law, Biosensors for marine applications: We all need the sea, but does the sea need biosensors?, *Biosensors and Bioelectronics*, **20**(10), 1903-1913 (2005).

[**2.108**] H. Beyenal, C.C. Davis and Z. Lewandowski, An improved Severinghaus-type carbon dioxide microelectrode for use in biofilms, *Sensors and Actuators B*, **97**(2-3) 202-210 (2003).

[**2.109**] M. Kühl, Optical Microsensors for Analysis of Microbial Communities, *Methods in Enzymology*, **397**, 166-199 (2005).

[**2.110**] H. Beyenal, C. Yakymyshyn, J. Hyungnak, C.C. Davis and Z. Lewandowski, An optical microsensor to measure fluorescent light intensity in biofilms, *Journal of Microbiological Methods,* **58**(3), 367-374 (2004).

[**2.111**] D. Le Coq, K. Michel, J. Keirsse, C. Boussard-Plédel, G. Fonteneau, B. Bureau, J.-M. Le Quéré, O. Sire and J. Lucas, Infrared glass fibers for in-situ sensing, chemical and biochemical reactions, *Comptes Rendus Chimie*, **5**(12), 907-913 (2002).

[**2.112**] J. Keirsse, C. Boussard-Plédel, O. Loréal, O. Sire, B. Bureau, P. Leroyer, B. Turlin and J. Lucas, IR optical fiber sensor for biomedical applications, *Vibrational Spectroscopy*, **32**(1), 23-32 (2003).

[**2.113**] R. Philip-Chandy, P.J. Scully, P. Eldridge, H.J. Kadim, G. Grapin, G. Jonca, G. D'Ambrosio, and F. Colin, An Optical Fiber Sensor for Biofilm Measurement Using Intensity Modulation and Image Analysis, *IEEE Journal on Selected Topics in Quantum Electronics*, **6**(5), 764-772 (2000).

[**2.114**] A. Kerr, M.J. Cowling, C.M. Beveridge, M.J. Smith, A.C.S. Parr, R.M. Head, J. Davenport and T. Hodgkiess, The early stages of marine biofouling and its effect on two types of optical sensors, *Environment International*, **24**(3), 331-343 (1998).

[**2.115**] T.E. Cloete, Biofouling control in industrial water systems: What we know and what we need to know, *Materials and Corrosion,* **54**(7), 520-526 (2003).

[**2.116**] V. Reipa, J. Almeida and K.D. Cole, Long-term monitoring of biofilm growth and disinfection using a quartz crystal microbalance and reflectance measurements, *Journal of Microbiological Methods,* **66**(3), 449-459 (2006).

[**2.117**] P. Miečinskas, K. Leinartas, V. Uksienė, and E. Juzeliūnas, QCM study of microbiological activity during long-term exposure to atmosphere – aluminium colonisation by *Aspergillus Niger*, *Journal of Solid State Electrochemistry*, **11**(7), 909-913 (2007).

[**2.118**] P. Janknecht and L.F. Melo, Online biofilm monitoring, *Reviews in Environmental Science and Biotechnology*, **2**(2-4), 269-283 (2003).

[**2.119**] K.S. Chang, C.K. Chang and C.Y. Chen, A surface acoustic wave sensor modified from a wireless transmitter for the monitoring of the growth of bacteria, *Sensors and Actuators B*, **125**(1), 207-213 (2007).

[**2.120**] W. Wang, J. Wang, H. Xu and X. Li, Electrochemical techniques used in MIC studies, *Materials and Corrosion*, **57**(10), 800-804 (2006).

[**2.121**] A. Pereira, J. Mendes and L.F. Melo, Using Nanovibrations to Monitor Biofouling, *Biotechnology and Bioengineering*, **99**(6), 1407-1415 (2008).

[**2.122**] D. Herbert-Guillou, B. Tribollet, D. Festy and L. Kienel, In situ detection and characterization of biofilm in waters by electrochemical methods, *Electrochimica Acta*, **45**(7), 1067-1075 (1999).

[**2.123**] M. Basu, S. Seggerson, J. Henshaw, J. Jiang, R. del A Cordona, C. Lefave, P. J. Boyle, A. Miller, M. Pugia and S. Basu, Nano-biosensor development for bacterial detection during human kidney infection: Use of glycoconjugate-specific antibody-bound gold NanoWire arrays (GNWA), *Glycoconjugate Journal*, **21**(8-9), 487-496 (2004).

[**2.124**] E. Spiller, A. Schöll, R. Alexy, K. Kümmerer and G.A. Urban, A sensitive microsystem as biosensor for cell growth monitoring and antibiotic testing, *Sensors and Actuators A*, **130**-**131**, 312-321 (2006).

[**2.125**] L.M. Oliver, P.S. Dunlop, J.A.M Byrne, I.S. Blair, M. Boyle, K.G. McGuigan and E.T. McAdams, An impedimetric sensor for monitoring the growth of Staphylococcus epidermidis, *Proceedings of the 28th IEEE EMBS Annual International Conference New York City*, USA, Aug 30-Sept 3, (2006).

[**2.126**] L.M. Oliver, E.T. McAdams, P.S.M Dunlop, J.A. Byrne, I.S. Blair, M. Boyle and K.G. McGuigan, *Electrical Impedance Spectroscopy as a Powerful Analytical Tool for Monitoring Microbiological Growth on Medical Implants*, In: N. Wickramasinghe and E. Geisler, Encyclopedia of healthcare information systems, Vol. 2, Hershey, PA, Medical Information Science, USA, 487-496 (2008).

[**2.127**] N. Washizu, Y. Katada and T. Kodama, Role of H_2O_2 in microbially influenced ennoblement of open circuit potentials for type 316L stainless steel in seawater, *Corrosion Science*, **46**(5), 1291-1300 (2004).

[**2.128**] B. Tribollet, Electrochemical sensors for biofilm and biocorrosion, *Materials and Corrosion*, **54**(7), 527-534 (2003).

[**2.129**] F. Mansfeld, The use of electrochemical techniques for the investigation and monitoring of microbiologically influenced corrosion and its inhibition – a review, *Materials and Corrosion*, **54**(7), 489-502 (2003).

[**2.130**] P. Cristiani, A. Mollica and G. Ventura, *On-line monitoring of biofilm and T.R.O. by a new ENEL'S system*, In: T.R. Bott (Ed.), Understanding Heat Exchanger Fouling and Its Mitigation Conference, 11-16 May, Castel Pascoli, Italy, Begell House, inc., New York, 323-329, USA (1997).

[**2.131**] M.C.M. Bruijs, L.P. Venhuis, H.A. Jenner, G.J. Licina and D. Daniels, Biocide Optimization Using On-Line Biofilm Monitor, *PowerPlant Chemistry*, **3**(7), 400-405 (2001).

[**2.132**] P. Cristiani, Solutions to fouling in power station condensers, *Applied Thermal Engineering*, **25**(16), 2630-2640 (2005).

[**2.133**] J.P. Busalmen and S.R. de Sánchez, Changes in the Electrochemical Interfaces as a Result of the Growth of *Pseudomonas fluorescens* Biofilms on Gold, *Biotechnology and Bioengineering*, **82**(5), 619-624 (2003).

[**2.134**] J.P. Busalmen, A. Berná and J.M. Feliu, Spectroelectrochemical Examination of the Interaction between Bacterial Cells and Gold Electrodes, *Langmuir*, **23**(11), 6459-6466 (2007).

[**2.135**] P. Stoodley, D. DeBeer and H.M. Lappin-Scott, Influence of Electric Fields and pH on Biofilm Structure as Related to the Bioelectric Effect, *Antimicrobial Agents and Chemotherapy*, **41**(9), 1876-1879 (1997).

[**2.136**] J.P. Busalmen and S.R. de Sánchez, Electrochemical Polarization-Induced Changes in the Growth of Individual Cells and Biofilms of *Pseudomonas fluorescens* (ATCC 17552), *Applied and Environmental Microbiology*, **71**(10), 6235-6240 (2005).

[**2.137**] J.W. Costerton, B. Ellis, K. Lam, F. Johnson and A.E. Khoury, Mechanism of Electrical Enhancement of Efficacy of Antibiotics in Killing Biofilm Bacteria, *Antimicrobial Agents and Chemotherapy*, **38**(12), 2803-2809 (1994).

[**2.138**] X. Muñoz-Berbel, F.J. Muñoz, N. Vigués and J. Mas, On-chip impedance measurements to monitor biofilm formation in the drinking distribution network, *Sensors and Actuators B*, **118**(1-2), 129-134 (2006).

[**2.139**] X. Muñoz-Berbel, N. Vigués, J. Mas, A.T.A. Jenkins and F.J. Munoz, Impedimetric characterization of the changes produced in the electrode-solution interface by bacterial attachment, *Electrochemistry Communications*, **9**(11), 2654-2660 (2007).

[**2.140**] A. Dheilly, I. Linossier, A. Darchen, D. Hadjiev, C. Corbel and V. Alonso, Monitoring of microbial adhesion and biofilm growth using electrochemical impedancemetry, *Applied Microbiology and Biotechnology*, **79**(1), 157-164 (2008).

[**2.141**] T. Roßteuscher, *Online monitoring of biofilm in microchannels with thermal lens microscopy*, Doktorarbeit, Fakultät für Chemie der Technischen Universität München, Lehrstuhl für Analytische Chemie Institut für Wasserchemie und Chemische Balneologie (2009).

[**2.142**] E. Barsoukov and J.R. Macdonald, *Impedance Spectroscopy, Theory, Experiment, and Applications*, 2nd ed., John Wiley & Sons, USA (2005).

[**2.143**] M.E. Orazem and B.Tribollet, *Electrochemical Impedance Spectroscopy*, John Wiley & Sons, USA (2008).

[**2.144**] M. Sluyters-Rehbach, Impedances of electrochemical systems: Terminology, nomenclature and representation. Part I: Cells with metal electrodes and liquid solutions, *Pure and Applied Chemistry*, **66**(9), 1831-1891 (1994).

[**2.145**] E.T. McAdams, A. Lackermeier, J.A. McLaughlin, D. Macken and J. Jossinet, The linear and the non-linear electrical properties of the electrode-electrolyte interface, *Biosensors and Bioelectronics,* **10**(1-2), 67-74 (1995).

[**2.146**] I.O. K'Owino and O.A. Sadik, Impedance Spectroscopy: A Powerful Tool for Rapid Biomolecular Screening and Cell Culture Monitoring, *Electroanalysis*, **17**(23), 2101-2113 (2005).

[**2.147**] E.T. McAdams and J. Jossinet, Tissue impedance: a historical overview, *Physiological Measurement*, **16**, A1-A13 (1995).

[**2.148**] E.T. McAdams and J. Jossinet, Problems in equivalent circuit modeling of the electrical properties of biological tissues, *Bioelectrochemistry and Bioenergetics*, **40**(2), 147-152 (1996).

[**2.149**] R.P. Ramasamy, V. Gadhamshetty, L.J. Nadeau and G.R. Johnson, Impedance Spectroscopy as a Tool for Non-Intrusive Detection of Extracellular Mediators in Microbial Fuel Cells, *Biotechnology and Bioengineering*, **104**(5), 882-891 (2009).

[**2.150**] F. Walsh, *A First Course in Electrochemical Engineering*, 1st ed., The Electrochemical Consultancy, UK (1993).

[**2.151**] C. Gabrielli, *Use and Application of Electrochemical Impedance Techniques* – Solartron analytical technical report n°24, UK (1997).

[**2.152**] B.A. Boukamp, *Equivalent Circuit Users Manual*, 2nd revised ed., University of Twente, The Netherlands (1988 / 89).

[**2.153**] W. Franks, I. Schenker, P. Schmutz and A. Hierlemann, Impedance Characterization and Modeling of Electrodes for Biomedical Applications, *IEEE Transactions on Biomedical Engineering*, **52**(7), 1295-1302 (2005).

[**2.154**] C. Díaz, P.L. Schilardi, R.C. Salvarezza and M. Fernández Lorenzo de Mele, Nano/Microscale Order Affects the Early Stages of Biofilm Formation on Metal Surfaces, *Langmuir*, **23**(22), 11206-11210 (2007).

[**2.155**] C. Díaz, P.L. Schilardi and M. Fernández Lorenzo de Mele, Influence of Surface Sub-micropattern on the Adhesion of Pioneer Bacteria on Metals, *Artificial Organs*, **32**(4), 292-298 (2008).

[**2.156**] X. Muñoz-Berbel, C. García-Aljaro and F.J. Muñoz, Impedimetric approach for monitoring the formation of biofilms on metallic surfaces and the subsequent application to the detection of bacteriophages, *Electrochimica Acta*, **53**(19), 5739-5744 (2008).

[**2.157**] R.-I. Stefan, J.F. van Staden, H. Y. Aboul-Enein, *Electrochemical Sensors in Bioanalysis*, Marcel Dekker, Inc., USA (2001).

[**2.158**] S. Ben-Ali, D.A. Cook, S.A.G. Evans, A. Thienpont, P.N. Bartlett and A. Kuhn, Electrocatalysis with monolayer modified highly organized macroporous electrodes, *Electrochemistry Communications*, **5**(9), 747-751 (2003).

[**2.159**] R. Szamocki, A. Velichko, C. Holzapfel, F. Mücklich, S. Ravaine, P. Garrigue, N. Sojic, R. Hempelmann and A. Kuhn, Macroporous Ultramicroelectrodes for Improved Electroanalytical Measurements, *Analytical Chemistry*, **79**(2), 533-539 (2007).

[**2.160**] M. Sosna, *Oxygen Reduction at Electrodes: Application to the Dissolved Oxygen Sensor for in situ Oceanographic Measurements*, PhD Thesis, University of Southampton, Faculty of Engineering, Science and Mathematics, School of Chemistry (2006).

[**2.161**] M.F.L. de Mele, R.C. Salvarezza, V.D. Vasquez Moll, H.A. Videla and A.J. Arvia, Kinetics and Mechanism of Silver Chloride Electroformation during the Localized Electrodissolution of Silver in Solutions Containing Sodium Chloride, *Journal Electrochemical Society*, **133**(4), 746-752 (1986).

[**2.162**] H.H. Hassan, M.A.M. Ibrahim, S.S. Abd El Rehim and M.A. Amin, Comparative Studies of the Electrochemical Behavior of Silver Electrode in Chloride, Bromide and Iodide Aqueous Solutions, *International Journal of Electrochemical Science*, **5**(2), 278-294 (2010).

[**2.163**] S.S. Abd El Rehim, H.H. Hassan, M.A.M. Ibrahim and M.A. Amin, Electrochemical Behavior of a Silver Electrode in NaOH Solutions, *Monatshefte für Chemie*, **129**(11), 1103-1117 (1998).

[**2.164**] S.Y. Lee, H.J. Kim, R. Patel, S.J. Im, J.H. Kim and B.R. Min, Silver nanoparticles immobilized on thin film composite polyamide membrane: characterization, nanofiltration, antifouling properties, *Polymers for Advanced Technologies*, **18**(7), 562-568 (2007).

[**2.165**] A. Dror-Ehre, A. Adin, G. Markovich and H. Mamane, Control of biofilm formation in water using molecularly capped silver nanoparticles, *Water Research*, **44**(8), 2601-2609 (2010).

[**2.166**] G. Neser and A. Kaçar, The antifouling performance of gelcoats containing biocides and silver ions in seawater environment, *Journal of Coatings Technology and Research*, **7**(1), 139-143 (2010).

[**2.167**] M. Sosna, G. Denuault, R.W. Pascal, R.D. Prien and M. Mowlem, Field assessment of a new membrane-free microelectrode dissolved oxygen sensor for water column profiling, *Limnology and Oceanography: Methods*, **6**, 180-189 (2008).

[**2.168**] M. Sosna, G. Denuault, R.W. Pascal, R.D. Prien and M. Mowlem, Development of a reliable microelectrode dissolved oxygen sensor, *Sensors and Actuators B*, **123**(1), 344-351 (2007).

[**2.169**] J. Sokolowski, J. M. Czajkowski and M. Turowska, Zero charge potential measurement of solid electrodes by inversion immersion method, *Electrochimica Acta*, **35**(9), 1393-1398 (1990).

[**2.170**] L.D. Chambers, *The Development of a Marine Antifouling System Using Environmentally Acceptable and Naturally Occurring Products*, PhD Thesis, University of Southampton, Faculty of Engineering, Science and Mathematics, School of Engineering Sciences, Surface Engineering and Tribology Research Group (2008).

[**2.171**] D. Loveday, P. Peterson and B. Rodgers – Gamry Instruments, Evaluation of Organic Coatings with Electrochemical Impedance Spectroscopy, *Part 2: Application of EIS to Coatings*, *JCT CoatingsTech*, 88-93 (2004).

[**2.172**] D. Loveday, P. Peterson and B. Rodgers – Gamry Instruments, Evaluation of Organic Coatings with Electrochemical Impedance Spectroscopy, *Part 3: Protocols for Testing Coatings with EIS*, *JCT CoatingsTech*, 22-27 (2005).

[**2.173**] F. Mansfeld, F. Huet and O.R. Mattos, *New trends in electrochemical impedance spectroscopy (EIS) and electrochemical noise analysis (ENA) proceedings of the international symposium*, Vol. 2000-24, The Electrochemical Society, Inc. Pennington, NJ, (2001).

[**2.174**] P.L. Bonora, F. Deflorian and L. Fedrizzi, Electrochemical impedance spectroscopy as a tool for investigating underpaint corrosion, *Electrochimica Acta*, **41**(7-8), 1073-1082 (1996).

[**2.175**] R.C. Barik, J.A. Wharton, R.J.K. Wood, K.R. Stokes and R.L. Jones, Corrosion, erosion and erosion-corrosion performance of plasma electrolytic oxidation (PEO) deposited Al_2O_3 coatings, *Surface & Coatings Technology*, **199**(2-3), 158-167 (2005).

[**2.176**] J.E.G. González, F.J.H. Santana and J.C. Mirza-Rosca, Effect of bacterial biofilm on 316 SS corrosion in natural seawater by EIS, *Corrosion Science*, **40**(12), 2141-2154 (1998).

[**2.177**] G. Gabrielli, M. Keddam, N. Portail, P. Rousseau, H. Takenouti and V. Vivier, Electrochemical Impedance Spectroscopy Investigations of a Microelectrode Behavior in a Thin-Layer Cell: Experimental and Theoretical Studies, *Journal of Physical Chemistry B*, **110**(41), 20478-20485 (2006).

[**2.178**] X. Muñoz-Berbel, N. Vigués, A.T.A. Jenkins, J. Mas and F.J. Muñoz, Impedimetric approach for quantifying low bacteria concentrations based on the changes produced in the electrode-solution interface during the pre-attachment stage, *Biosensors and Bioelectronics*, **23**(10), 1540-1546 (2008).

[**2.179**] L. Yang, C. Ruan and Y. Li, Detection of viable *Salmonella typhimurium* by impedance measurement of electrode capacitance and medium resistance, *Biosensors and Bioelectronics*, **19**(5), 495-502 (2003).

[**2.180**] L. Yang, Y. Li, C.L. Griffis and M.G. Johnson, Interdigitated microelectrode (IME) impedance sensor for the detection of viable *Salmonella typhimurium*, *Biosensors and Bioelectronics*, **19**(10), 495-502 (2004).

[**2.181**] S.J. Yuan, S.O. Pehkonen, Y.P. Ting, E.T. Kang and K.G. Neoh, Corrosion Behavior of Type 304 Stainless Steel in a Simulated Seawater-Based Medium in the Presence and Absence of Aerobic *Pseudomonas* NCIMB 2021 Bacteria, *Industrial & Engineering Chemistry Research*, **47**(9), 3008-3020 (2008).

[**2.182**] S.J. Yuan, A.M.F. Choong and S.O. Pehkonen, The influence of the marine aerobic *Pseudomonas* strain on the corrosion of 70/30 Cu–Ni alloy, *Corrosion Science*, **49**(12), 4352-4385 (2007).

[**2.183**] X.T. Chang, Y.S. Yin, G.H. Niu, T. Liu, S.Cheng and S.B. Sun, The electrochemical behavior of oceanic microbiological influenced corrosion on carbon steel, *Acta Metallurgica Sinica (English Letters)*, **20**(5), 334-340 (2007).

[**2.184**] E. Juzeliūnas, R. Ramanauskas, A. Lugauskas, K. Leinartas, M. Samulevičienė and A Sudavičius, Influence of wild strain *Bacillus mycoides* on metals: From corrosion acceleration to environmentally friendly protection, *Electrochimica Acta*, **51**(27), 6085-6090 (2006).

[**2.185**] E. Juzeliūnas, R. Ramanauskas, A. Lugauskas, K. Leinartas, M. Samulevičienė, A Sudavičius and R. Juškėnas, Microbially influenced corrosion of zinc and aluminium – Two-year subjection to influence of *Aspergillus Niger*, *Corrosion Science*, **49**(11), 4098-4112 (2007).

[**2.186**] H. Castaneda, X.D. Benetton, SRB-biofilm influence in active corrosion sites formed at the steel-electrolyte interface when exposed to artificial seawater conditions, *Corrosion Science*, **50**(4), 1169-1183 (2008).

[**2.187**] J.S. Daniels and N. Pourmand, Label-Free Impedance Biosensors: Opportunities and Challenges, *Electroanalysis*, **19**(12), 1239-1257 (2007).

[**2.188**] W.H. Mulder, J.H. Sluyters, T. Pajkossy and I. Nyikos, Tafel current at fractal electrodes: Connection with admittance spectra, *Journal of Electroanalytical Chemistry*, **285**(1-2), 103-115 (1990).

[**2.189**] C.-H. Kim, S.-I. Pyun and J.-H. Kim, An investigation of the capacitance dielectric dispersion on the fractal carbon electrode with edge and basal orientations, *Electrochimica Acta*, **48**(23), 3455-3463 (2003).

[**2.190**] C.A. Schiller and W. Strunz, The evaluation of experimental dielectric data of barrier coatings by means of different models, *Electrochimica Acta*, **46**(24-25), 3619-3625 (2001).

[**2.191**] J-B Jorcin, M.E. Orazem, N. Pebere and B. Tribollet, CPE analysis by local impedance analysis, *Electrochimica Acta*, **51**(8-9), 1473-1479 (2006).

[**2.192**] K.B. Oldham, The *RC* time "constant" at a disk electrode, *Electrochemistry Communications*, **6**(2), 210-214 (2004).

[**2.193**] B. Hirschorn, M.E. Orazem, B. Tribollet, V. Vivier, I. Frateur and M. Musiani, Determination of effective capacitance and film thickness from constant-phase-element parameters, *Electrochimica Acta*, **55**(21), 6218-6227 (2010).

[**2.194**] G.J. Brug, A.L.G. van den Eeden, M. Sluyters-Rehbach and J.H. Sluyters, The analysis of electrode impedances complicated by the presence of a constant phase element, *Journal of Electroanalytical Chemistry and Interfacial Electrochemistry*, **176**(1-2), 275-295 (1984).

[**2.195**] M. Metikos-Hukovic, Z. Pilic, R. Babic and D. Omanovic, Influence of alloying elements on the corrosion stability of CoCrMo implant alloy in Hank's solution, *Acta Biomaterialia*, **2**(6), 693-700 (2006).

[**2.196**] J. Gamby, A. Pailleret, C.B. Clodic, C.-M. Pradier and B. Tribollet, In situ detection and characterization of potable water biofilms on materials by microscopic, spectroscopic and electrochemistry methods, *Electrochimica Acta*, **54**(1), 66-73 (2008).

[**2.197**] J.J. Harrison, H. Ceri, J. Yerly, C.A. Stremick, Y. Hu, R. Martinuzzi and R.J. Turner, The use of miscroscopy and three-dimensional visualization to evaluate the structure of microbial biofilms cultivated in the Calgary Biofilm Device, *Biological Procedures Online*, **8**(1), 194-215 (2006).

[**2.198**] J. Warner, *Novel Techniques for the in situ detection of bacteria on salad leaf surfaces,* PhD Thesis, University of Southampton, Faculty of Medicine, Health and Life Sciences, School of Biological Sciences (2009).

[**2.199**] D.J. Stokes, Recent advances in electron imaging, image interpretation and applications: environmental scanning electron microscopy, *Philosophical Transactions of the Royal Society of London A*, **361**(1813), 2771-2787 (2003).

[**2.200**] J.R. Lawrence, G.D.W. Swerhone, G.G. Leppard, T. Araki, X. Zhang, M.M. West and A.P. Hitchcock, Scanning Transmission X-Ray, Laser Scanning, and Transmission Electron Microscopy Mapping of the Exopolymeric Matrix of Microbial Biofilms, *Applied and Environmental Microbiology*, **69**(9), 5543-5554 (2003).

[**2.201**] Z. Aslam, M. Abraham, R. Brydson, A. Brown and B. Rand, Initial Studies Using a Combined TEM – Scanning Tunnelling Microscopy (STM) Side Entry Sample Holder, *Journal of Physics: Conference Series*, **26**(26), 54-58 (2006).

[**2.202**] I.B. Beech, The Potential Use of Atomic Force Microscopy for Studying Corrosion of Metals in the Presence of Bacterial Biofilms – an Overview, *International Biodeterioration and Biodegradation*, **37**(3-4), 141-149 (1996).

[**2.203**] I.B. Beech, J.R. Smith, A.A. Steele, I. Penegar and S.A. Campbell, The use of atomic force microscopy for studying interactions of bacterial biofilms with surfaces, *Colloids and Surfaces B: Biointerfaces*, **23**(2-3), 231-247 (2002).

[**2.204**] Y. Hu, J. Zhang and J. Ulstrup, Interfacial Electrochemical Electron Transfer Processes in Bacterial Biofilm Environments on Au(111), *Langmuir*, **26**(11), 9094-9103 (2010).

[**2.205**] S.M. Flores and J.L. Toca-Herrera, The new future of scanning probe microscopy: Combining atomic force microscopy with other surface-sensitive techniques, optical microscopy and fluorescence techniques, *Nanoscale*, **1**(1), 40-49 (2009).

[**2.206**] P.K. Hansma, B. Drake, O. Marti, S.A. Gould and C.B. Prater, The scanning ion-conductance microscope, *Science*, **243**(4891), 641-643 (1989).

[**2.207**] Y.E. Korchev, C.L. Bashford, M. Milovanovic, I. Vodyanoy and M.J. Lab, Scanning Ion Conductance Microscopy of Living Cells, *Biophysical Journal*, **73**(2), 653-658 (1997).

[**2.208**] Y.E. Korchev, M. Milovanovic, C.L .Bashford, D.C. Bennett, E.V. Sviderskaya, I. Vodyanoy and M.J. Lab, Specialized scanning ion conductance microscopy of living cells, *Journal of Microscopy*, **188**(1), 17-23 (1997).

[**2.209**] Y.E. Korchev, Y.A. Negulyaev, C.R.W. Edwards, I. Vodyanoy and M.J. Lab, Functional localization of single active ion channels on the surface of a living cell, *Nature Cell Biology*, **2**(9), 616-619 (2000).

[**2.210**] Y.E. Korchev, J. Gorelik, M.J. Lab, E.V. Sviderskaya, C.L. Johnston, C.R. Coombes, I. Vodyanoy and C.R.W. Edwards, Cell Volume Measurement Using Scanning Ion Conductance Microscopy, *Biophysical Journal*, **78**(1), 451-457 (2000).

[**2.211**] J. Gorelik, Y. Zhang, A.I. Shevchuk, G.I. Frolenkov, D. Sánchez, M.J. Lab, I. Vodyanoy, C.R.W. Edwards, D. Klenerman and Y.E. Korchev, The use of scanning ion conductance microscopy to image A6 cells, *Molecular and Cellular Endocrinology*, **217**(1-2), 101-108 (2004).

[**2.212**] A.J. Bard, G. Denuault, C. Lee, D. Mandler and D.O. Wipf, Scanning Electrochemical Microscopy: A New Technique for the Characterization and Modification of Surfaces, *Accounts of Chemical Research*, **23**(11), 357-363 (1990).

[**2.213**] J.L. Amphlett and G. Denuault, Scanning Electrochemical Microscopy (SECM): An Investigation of the Effects of Tip Geometry on Amperometric Tip Response, *Journal of Physical Chemistry B*, **102**(49), 9946-9951 (1998).

[**2.214**] Z. Hu, J. Jin, H.D. Abruña, P.L. Houston, A.G. Hay, W.C. Ghiorse, M.L. Shuler, G. Hidalgo and L.W. Lion, Spatial Distributions of Copper in Microbial Biofilms by Scanning Electrochemical Microscopy, *Environmental Science and Technology*, **41**(3), 936-941 (2007).

[**2.215**] B. Liu, S.A. Rotenberg and M.V. Mirkin, Scanning electrochemical microscopy of living cells: Different redox activities of nonmetastatic and metastatic human breast cells, *Proceedings of the National Academy of Sciences of the United States of America*, **97**(18), 9855-9860 (2000).

[**2.216**] B. Liu, W. Cheng, S.A. Rotenberg and M.V. Mirkin, Scanning electrochemical microscopy of living cells: Part 2. Imaging redox and acid/basic reactivities, *Journal of Electroanalytical Chemistry*, **500**(1-2), 590-597 (2001).

[**2.217**] C. Cai, B. Liu, M.V. Mirkin, H.A. Frank and J.F. Rusling, Scanning Electrochemical Microscopy of Living Cells. 3. *Rhodobacter sphaeroides*, *Analytical Chemistry*, **74**(1), 114-119 (2002).

[**2.218**] B. Liu, S.A. Rotenberg and M.V. Mirkin, Scanning Electrochemical Microscopy of Living Cells. 4. Mechanistic Study of Charge Transfer Reactions in Human Breast Cells, *Analytical Chemistry*, **74**(24), 6340-6348 (2002).

[**2.219**] W. Feng, S.A. Rotenberg and M.V. Mirkin, Scanning Electrochemical Microscopy of Living Cells. 5. Imaging of Fields of Normal and Metastatic Human Breast Cells, *Analytical Chemistry*, **75**(16), 4148-4154 (2003).

[**2.220**] W. Wang, X. Zhang and J. Wang, Heterogeneous electrochemical characteristics of biofilm/metal interface and local electrochemical techniques used for this purpose, *Materials and Corrosion*, **60**(12), 957-962 (2009).

[**2.221**] R. Bakke and P.Q. Olsson, Biofilm thickness measurements by light microscopy, *Journal of Microbiological Methods*, **5**(2), 93-98 (1986).

[**2.222**] D. Murphy, Differential interference contrast (DIC) microscopy and modulation contrast microscopy, in *Fundamentals of Light Microscopy and Digital Imaging*, Wiley-Liss, New York, pp. 153–168 (2001).

[**2.223**] Leica Microsystems, *Leica Confocal Systems, Product and Technology Guide*, Leica Microsystems Heidelberg GmbH, Germany (2002).

[**2.224**] K. König, K. Schenke-Layland, I. Riemann and U.A. Stock, Multiphoton autofluorescence imaging of intratissue elastic fibers, *Biomaterials*, **26**(5), 495-500 (2005).

[**2.225**] C. Xu, W. Zipfel, J.B. Shear, R.M. Williams and W.W. Webb, Multiphoton fluorescence excitation: New spectral windows for biological nonlinear microscopy, *Proceedings of the National Academy of Sciences of the United States of America*, **93**(20), 10763-10768 (1996).

[**2.226**] K. König, Multiphoton microscopy in life sciences, *Journal of Microscopy-Oxford*, **200**(2), 83-104 (2000).

[**2.227**] C. Xu and W.W. Webb, Measurement of two-photon excitation cross sections of molecular fluorophores with data from 690 to 1050 nm, *Journal of the Optical Society of America B – Optical Physics*, **13**(3), 481-491 (1996).

[**2.228**] B. Manz, F. Volke, D. Goll and H. Horn, Measuring Local Flow Velocities and Biofilm Structure in Biofilm Systems With Magnetic Resonance Imaging (MRI), *Biotechnology and Bioengineering*, **84**(4), 424-432 (2003).

[**2.229**] U. Metzger, U. Lankes, E.H. Hardy, B.C. Gordalla, F.H. Frimmel, Monitoring the formation of an Aureobasidium pullulans biofilm in a bead-packed reactor via flow-weighted magnetic resonance imaging, *Biotechnology Letters*, **28**(16), 1305-1311 (2006).

[**2.230**] J. Morató, F. Codony and J. Mas, *Microscopy techniques applied for monitoring the development of aquatic biofilms*, In: Current Issues on Multidisciplinary Microscopy Research and Education, Formatex Microscopy Book Series,Vol. 2, pp. 93-100 (2004).

[**2.231**] H.-J. Shin and M.K. Lee, Scanning soft X-ray spectromicroscopy at the Pohang Light Source: commissioning results, *Nuclear Instruments and Methods in Physics Research Section A: Accelerators, Spectrometers, Detectors and Associated Equipment* , **467-468**(2), 909-912 (2001).

[**2.232**] Molecular Probes invitrogen detection technologies, *LIVE/DEAD® BacLight™ Bacterial Viability Kits*, Molecular Probes, Inc., 1-8, USA, (2004).

[**2.233**] J.S. Webb, L.S. Thompson, S. James, T. Charlton, T. Tolker-Nielsen, B. Koch, M. Givskov and S. Kjelleberg, Cell Death in *Pseudomonas aeruginosa* Biofilm Development, *Journal of Bacteriology*, **185**(15), 4585-4592 (2003).

[**2.234**] N. Barraud, D.J. Hassett, S.-H. Hwang, S.A. Rice, S. Kjelleberg and J.S. Webb, Involvement of Nitric Oxide in Biofilm Dispersal of *Pseudomonas aeruginosa*, *Journal of Bacteriology*, **188**(21), 7344-7353 (2006).

[**2.235**] P. Stoodley, S. Wilson, L. Hall-Stoodley, J.D. Boyle, H.M. Lappin-Scott and J.W. Costerton, Growth and detachment of cell clusters from mature mixed-species biofilms, *Applied and Environmental Microbiology*, **67**(12), 5608-5613 (2001).

[**2.236**] J.T. Walker, D.J. Bradshaw, M.R. Fulford and P.D. Marsh, Microbiological Evaluation of a Range of Disinfectant Products To Control Mixed-Species Biofilm Contamination in a Laboratory Model of a Dental Unit Water System, *Applied and Environmental Microbiology*, **69**(6), 3327-3332 (2003).

[**2.237**] H. Beyenal, C. Donovan, Z. Lewandowski and G. Harkin, Three-dimensional biofilm structure quantification, *Journal of Microbiological Methods*, **59**(3), 395-413 (2004).

[**2.238**] J.B. Xavier, A. Schnell, S. Wuertz, R. Palmer, D.C. White and J.S. Almeida, Objective threshold selection procedure (OTS) for segmentation of scanning laser confocal microscope images, *Journal of Microbiological Methods*, **47**(2), 169-180 (2001).

[**2.239**] J.B. Xavier, C. Picioreanu and M.C.M. van Loosdrecht, A framework for multidimensional modeling of activity and structure of multispecies biofilms, *Environmental Microbiology*, **7**(8), 1085-1103 (2005).

[**2.240**] A. Heydorn, A.T. Nielsen, M. Hentzer, C. Sternberg, M. Givskov, B.K. Ersboll and S. Molin, Quantification of biofilm structures by the novel computer program COMSTAT, *Microbiology*, **146**(10), 2395-2407 (2000).

[**2.241**] H. Beyenal, Z. Lewandowski and G. Harkin, Quantifying Biofilm Structure: Facts and Fiction, *Biofouling*, **20**(1), 1-23 (2004).

[**2.242**] X. Yang, H. Beyenal, G. Harkin and Z. Lewandowski, Quantifying biofilm structure using image analysis, *Journal of Microbiological Methods*, **39(**2), 109-119 (2000).

[**2.243**] L.N. Mueller, J. FC. de Brouwer, J.S. Almeida, L.J. Stal and J.B. Xavier, Analysis of a marine phototrophic biofilm by confocal laser scanning microscopy using the new image quantification software PHLIP, *BMC Ecology (BioMed Central)*, **6**(1), 1-15 (2006).

[**2.244**] A. Bogomolova, E. Komarova, K. Reber, T. Gerasimov, O. Yavuz, S. Bhatt and M. Aldissi, Challenges of Electrochemical Impedance Spectroscopy in Protein Biosensing, *Analytical Chemistry*, **81**(10), 3944-3949 (2009).

[**2.245**] J.E.I. Wright, N.P. Cosman, K. Fatih, S. Omanovic and S.G. Roscoe, Electrochemical impedance spectroscopy and quartz crystal nanobalance (EQCN) studies of insulin adsorption on Pt, *Journal of Electroanalytical Chemistry*, **564**(1-2), 185-197 (2004).

[**2.246**] S. Omanovic and S.G. Roscoe, Electrochemical Studies of the Adsorption Behavior of Bovine Serum Albumin on Stainless Steel, *Langmuir*, **15**(23), 8315-8321 (1999).

[**2.247**] D.R. Jackson, S. Omanovic and S.G. Roscoe, Electrochemical Studies of the Adsorption Behavior of Serum Proteins on Titanium, *Langmuir*, **16**(12), 5449-5457 (2000).

[**2.248**] S.E. Moulton, J.N. Barisci, A. Bath, R. Stella and G.G. Wallace, Studies of double layer capacitance and electron transfer at a gold electrode exposed to protein solutions, *Electrochimica Acta*, **49**(24), 4223-4230 (2004).

[**2.249**] M.F Smiechowski, V.F. Lvovich, S. Roy, A. Fleischman, W.H. Fissell and A.T. Riga, Electrochemical detection and characterization of proteins, *Biosensors and Bioelectronics*, **22**(5), 670-677 (2006).

[**2.250**] D. Sun, *Abrasion-corrosion of Cast CoCrMo in Simulated Hip Joint Environments*, PhD Thesis, University of Southampton, Faculty of Engineering, Science and Mathematics, School of Engineering Sciences (2009).

[**2.251**] Z. Qian, P. Stoodley and W.G. Pitt, Effect of low-intensity ultrasound upon biofilm structure from confocal scanning laser microscopy observation, *Biomaterials*, **17**(20), 1975-1980 (1996).

[**2.252**] J. Jass and H.M. Lappin-Scott, The efficacy of antibiotics enhanced by electrical currents against *Pseudomonas aeruginosa* biofilms, *Journal of Antimicrobial Chemotherapy*, **38**(6), 987-1000 (1996).

[**2.253**] M. Pasmore and J.W. Costerton, Biofilms, bacterial signaling, and their ties to marine biology, *Journal of Industrial Microbiology and Biotechnology*, **30**(7), 407-413 (2003).

[**2.254**] Mexel Industries SAS, *Water Cooling Circuits/MEXEL® 432*, Retrieved 09/07/2010, from http://www.mexel.fr/, © 2009 Mexel Industries SAS.

[**2.255**] L. Arehmouch, *Embryo-Toxicologie des Poissons, Les salissures biologiques, Toxicité du Mexel® 432, un agent anti-salissure industriel, vis-à-vis du développement précoce de la carpe commune (Cyprinus carpio L.)*, Thèse de doctorat de l'Université de Metz, UFR Sciences Fondamentales et Appliquées, Spécialité : Toxicologie de l'Environnement (1997).

[**2.256**] A.S. Allonier and M. Khalanski, *Biodégradation du Mexel 432 par des bactéries de la Seine*, Département Environnement, Groupe Gestion de l'Eau et Environnement, Electricité de France, Direction des Etudes et Recherches, Rapport n° HE-31/96-020 (1996).

[**2.257**] L. Arehmouch, F. Ghillebaert, C. Chaillou and P. Roubaud, Lethal effects of Mexel 432, an antifouling agent, on embryolarval development of common carp (*Cyprinus carpio* L.), *Ecotoxicology and environmental safety*, **42**(2), 110-118 (1999).

[**2.258**] A. Whelan and F. Regan, Antifouling strategies for marine and riverine sensors, *Journal of Environmental Monitoring*, **8**(9), 880-886 (2006).

[**2.259**] K. Nandakumar, H. Obika, A. Utsumi, T. Ooie and T. Yano, In Vitro Laser Ablation of Natural Marine Biofilms, *Applied and Environmental Microbiology*, **70**(11), 6905-6908 (2004).

[**2.260**] R.A. Brizzolara, D.J. Nordham, M. Walch, R.M. Lennen, R. Simmons, E. Burnett and M.S. Mazzola, Non-Chemical Biofouling Control in Heat Exchangers and Seawater Piping Systems Using Acoustic Pulses Generated by an Electrical Discharge, *Biofouling*, **19**(1), 19-35 (2003).

[**2.261**] R. Caubet, F. Pedarros-Caubet, M. Chu, E. Freye, M. de Belém Rodrigues, J.M. Moreau and W.J. Ellison, A Radio Frequency Electric Current Enhances Antibiotic Efficacy against Bacterial Biofilms, *Antimicrobial Agents and Chemotherapy*, **48**(12), 4662-4664 (2004).

[**2.262**] C. Johansen, P. Falholt and L. Gram, Enzymatic Removal and Disinfection of Bacterial Biofilms, *Applied and Environmental Microbiology*, **63**(9), 3724-3728 (1997).

[**2.263**] C. Leroy, C. Delbarre, F. Ghillebaert, C. Compere and D. Combes, Effects of commercial enzymes on the adhesion of a marine biofilm-forming bacterium, *Biofouling*, **24**(1), 11-22 (2008).

[**2.264**] P. Chaignon, I. Sadovskaya, Ch. Ragunah, N. Ramasubbu, J.B. Kaplan and S. Jabbouri, Susceptibility of staphylococcal biofilms to enzymatic treatments depends on their chemical composition, *Applied Microbiology and Biotechnology*, **75**(1), 125-132 (2007).

[**2.265**] Y. Xiong and Y. Liu, Biological control of microbial attachment: a promising alternative for mitigating membrane biofouling, *Applied Microbiology and Biotechnology*, **86**(3), 825-837 (2010).

[**2.266**] M.C. Frost, M.M. Reynolds and M.E. Meyerhoff, Polymers incorporating nitric oxide releasing/generating substances for improved biocompatibility of blood-contacting medical devices, *Biomaterials*, **26**(14), 1685-1693 (2005).

[**2.267**] N. Barraud, M.V. Storey, Z.P. Moore, J.S. Webb, S.A. Rice and S. Kjelleberg, Nitric oxide-mediated dispersal in single- and multi-species biofilms of clinically and industrially relevant microorganisms, *Microbial Biotechnology*, **2**(3), 370-378 (2009).

[**2.268**] V.N. Bernshtein and V.G. Belikov, Sodium nitroprusside and its use in analysis, *Russian Chemical Reviews*, **30**(4), 227-236 (1961).

[**2.269**] P.T. Manoharan and W.C. Hamilton, The Crystal Structure of Sodium Nitroprusside, *Inorganic Chemistry*, **2**(5), 1043-1047 (1963).

[**2.270**] A.R. Butler and I.L. Megson, Non-Heme Iron Nitrosyls in Biology, *Chemical Reviews*, **102**(4), 1155–1165 (2002).

[**2.271**] P. Coppens, I. Novozhilova and A. Kovalevsky, Photoinduced Linkage Isomers of Transition-Metal Nitrosyl Compounds and Related Complexes, *Chemical Reviews*, **102**(4), 861–883 (2002).

[**2.272**] M. Boualam, F. Quilès, L. Mathieu and J.-C. Block, Monitoring the Effect of Organic Matter on Biofilm Growth in Low Nutritive Waters by ATR/FT-IR Spectroscopy, *Biofouling*, **18**(1), 73-81 (2002).

[**2.273**] R.M. Donlan, J.A. Piede, C.D. Heyes, L. Sanii, R. Murga, P. Edmonds, I. El-Sayed and M.A. El-Sayed, Model System for Growing and Quantifying *Streptococcus pneumonia* Biofilms In Situ and in Real Time, *Applied and Environmental Microbiology*, **70**(8), 4980-4988 (2004).

[**2.274**] S. Hou, E.A. Burton, K.A. Simon, D. Blodgett, Y.-Y. Luk and D. Ren, Inhibition of *Escherichia coli* Biofilm Formation by Self-Assembled Monolayers of Functional Alkanethiols on Gold, *Applied and Environmental Microbiology*, **73**(13), 4300-4307 (2007).

[**2.275**] J.A. Hrabie and L.K. Keefer, Chemistry of the Nitric Oxide-Releasing Diazeniumdiolate ("Nitrosohydroxylamine") Functional Group and Its Oxygen-Substituted Derivatives, *Chemical Reviews*, **102**(4), 1135-1154 (2002).

[**2.276**] Y. Wu, A.P. Rojas, G.W. Griffith, A.M. Skrzpchak, R.H. Bartlett and M.E. Meyerhoff, Improving Blood Compatibility of Intravascular Oxygen Sensors Via Catalytic Decomposition of S-Nitrosothiols to Generate Nitric Oxide In Situ, *Sensors and Actuators B: Chemical*, **121**(1), 36-46 (2007).

[**2.277**] D.M. Grant and T.R. Bott, Biocide Dosing Strategies for Biofilm Control, *Heat Transfer Engineering*, **26**(1), 44-50 (2005).

References to Chapter 3

[**3.1**] M.J., Kennish, *CRC Practical Handbook of Marine Science*, 2nd ed., CRC Press, Boca Raton, FL, USA (1994).

[**3.2**] D.M. Yebra, S. Kiil and K. Dam-Johansen, Antifouling technology – past, present and future steps towards efficient and environmentally friendly antifouling coatings, *Progress in Organic Coatings*, **50**(2), 75-104 (2004).

[**3.3**] E. Brown, A. Colling, D. Park, J. Phillips, D. Rothery and J. Wright (Open University Course Team), *Seawater: its composition, properties and behaviour*, 2nd ed., The Open University, UK (1997).

[**3.4**] A.C. Redfield, *On the proportions of organic derivations in sea water and their relation to the composition of plankton*, In: James Johnstone Memorial Volume, ed. R.J. Daniel, University Press of Liverpool, UK (1934).

[**3.5**] Woods Hole Oceanographic Institution (WHOI), *Marine Fouling and its Prevention*, Annapolis: United States Naval Institute, USA (1952).

[**3.6**] R. Parsons, M. Takahashi and B. Hargrave, *Biological Oceanographic Processes*, 3rd ed., Pergamon Press, UK, (1990).

[**3.7**] R.C. Barik, Environmental factors affecting the marine corrosion performance of nickel aluminium bronze, PhD Thesis, University of Southampton, Faculty of Engineering, Science and Mathematics, School of Engineering Sciences (2006).

[**3.8**] A.L. Bradshaw and K.E. Schleicher, Electrical Conductivity of Seawater, *IEEE Journal of Oceanic Engineering*, OE-**5**(1), 50-62 (1980).

[**3.9**] Hanna instruments, Portable waterproof microprocessor dissolved oxygen meters, www.hannainst.com (2003).

[**3.10**] A.I. Railkin, *Marine Biofouling: Colonization Processes and Defenses*, 1st ed., CRC Press LLC, USA (2004).

[**3.11**] J.W. Costerton, Introduction to biofilm, *International Journal of Antimicrobial Agents*, **11**(3-4), 217-221 (1999).

[**3.12**] H.A. Videla, *Manual of Biocorrosion*, 1st ed., CRC Press, USA (1996).

[**3.13**] J. Warner, *Novel Techniques for the in situ detection of bacteria on salad leaf surfaces,* PhD Thesis, University of Southampton, Faculty of Medicine, Health and Life Sciences, School of Biological Sciences (2009).

[**3.14**] M. Pasmore and J.W. Costerton, Biofilms, bacterial signaling, and their ties to marine biology, *Journal of Industrial Microbiology and Biotechnology*, **30**(7), 407-413 (2003).

[**3.15**] D.B. Roszak and R.R. Colwell, Survival Strategies of Bacteria in the Natural Environment, *Microbiological Reviews*, **51**(3), 365-379 (1987).

[**3.16**] C. Hellio and D.M. Yebra, *Advances in marine antifouling coatings and technologies*, Woodhead Publishing Limited, UK (2009).

[**3.17**] B.J. Little, P.A. Wagner and F. Mansfeld, *Microbiologically Influenced Corrosion*, NACE International, Houston, Texas, Vol.5, USA (1997).

[**3.18**] J.W. Costerton, Z. Lewandowski, D.E. Caldwell, D.R. Korber and H.M. Lappin-Scott, Microbial Biofilms, *Annual Review of Microbiology,* **49**, 711-745 (1995).

[**3.19**] H.M. Lappin-Scott and J.W. Costerton, *Microbial biofilms*, 1st ed., Cambridge University Press, UK (1995).

[**3.20**] I.Klimant, M. Kühl, R.N. Glud and G. Holst, Optical measurement of oxygen and temperature in microscale: strategies and biological applications, *Sensors and Actuators B*, **38**(1-3), 29-37 (1997).

[**3.21**] H.-C. Flemming, P. Sriyutha Murthy, R. Venkatesan and K.E. Cooksey, *Marine and Industrial Biofouling*, Springer, Germany (2009).

[**3.22**] E. Denkhaus, S. Meisen, U. Telgheder and J. Wingender, Chemical and physical methods for characterisation of biofilms. *Microchimica Acta*, **158**(1-2), 1-27 (2007).

[**3.23**] D.E. Nivens, R.J. Palmer Jr and D.C. White, Continuous nondestructive monitoring of microbial biofilms: a review of analytical techniques, *Journal of Industrial Microbiology and Biotechnology*, **15**(4), 263-276 (1995).

[**3.24**] P. Janknecht and L.F. Melo, Online biofilm monitoring, *Reviews in Environmental Science and Biotechnology*, **2**(2-4), 269-283 (2003).

[**3.25**] W. Wang, J. Wang, H. Xu and X. Li, Electrochemical techniques used in MIC studies, *Materials and Corrosion*, **57**(10), 800-804 (2006).

[**3.26**] B. Tribollet, Electrochemical sensors for biofilm and biocorrosion, *Materials and Corrosion*, **54**(7), 527-534 (2003).

[**3.27**] F. Mansfeld, The use of electrochemical techniques for the investigation and monitoring of microbiologically influenced corrosion and its inhibition – a review, *Materials and Corrosion*, **54**(7), 489-502 (2003).

[**3.28**] C. Rubio, *Compréhension des mécanismes d'adhésion des biofilms en milieu marin en vue de la conception de nouveaux moyens de prevention*, Thèse de doctorat de l'Université de Paris 6, Spécialité: Métallurgie et Matériaux (2002).

[**3.29**] H.-J. Jördening and J. Winter, Environmental Biotechnology: Concepts and Applications, Wiley-Vch Verlag GmbH & Co. KGaA, Germany (2005).

[**3.30**] J. Owicki and J.Parce, Biosensors based on the energy metabolism of living cells: the physical chemistry and cell biology of extracellular acidification, *Biosensors and Bioelectronics*, **7**(4), 255-272 (1992).

[**3.31**] M.D. Iglesias-Rodriguez, P.R. Halloran, R.E.M. Rickaby, I.R. Hall, E. Colmenero-Hidalgo, J.R. Gittins, D.R.H. Green, T. Tyrrell, S.J. Gibbs, P. von Dassow, E. Rehm, E.V. Armbrust and K.P. Boessenkool, Phytoplankton Calcification in a High-CO_2 World, *Science*, **320**(5874), 336-340 (2008).

[**3.32**] A. Balaji Ganesh and T.K. Radhakrishnan, Fiber-optic sensors for the estimation of pH within the natural biofilms on metals, *Sensors and Actuators B* **123**(2), 1107-1112 (2007).

[**3.33**] L.M. Prescott, J.P. Harley and D.A. Klein, *Microbiology*, 3rd ed., Wm. C. Brown Publishers, USA (1996).

[**3.34**] N. Le Bozec, *Réaction de réduction de l'oxygène sur les aciers inoxydables en eau de mer naturelle. Influence du biofilm sur les processus de corrosion*, Thèse de doctorat (Spécialité Chimie Fine), Université de Bretagne Occidentale (2000).

[**3.35**] L.F. Melo and T.R. Bott, Biofouling in Water Systems, *Experimental Thermal and Fluid Science*, **14**(4), 375-381 (1997).

[**3.36**] A.M. Shams El Din, M.E. El-Dahshan and A.M. Tag El Din, Bio-film formation on stainless steels. Part 2. The role of seasonal changes, seawater composition and surface roughness, *Desalination*, **154**(3), 267-276 (2003).

[**3.37**] S.L. McCallister, J.E. Bauer, J.E. Bauer, J. Kelly and H.W. Ducklow, Effects of sunlight on decomposition of estuarine dissolved organic C, N and P and bacterial metabolism, *Aquatic Microbial Ecology*, **40**(1), 25-35 (2005).

[**3.38**] T. Reinthaler and G.J. Herndl, Seasonal dynamics of bacterial growth efficiencies in relation to phytoplankton in the southern North Sea, *Aquatic Microbial Ecology*, **39**(1), 7-16 (2005).

[**3.39**] C. Leroy, C. Delbarre, F. Ghillebaert, C. Compere and D. Combes, Effects of commercial enzymes on the adhesion of a marine biofilm-forming bacterium, *Biofouling*, **24**(1), 11-22 (2008).

[**3.40**] Y. Xiong and Y. Liu, Biological control of microbial attachment: a promising alternative for mitigating membrane biofouling, *Applied Microbiology and Biotechnology*, **86**(3), 825-837 (2010).

[**3.41**] B.C. Dunsmore, A. Jacobsen, L. Hall-Stoodley, C.J. Bass, H.M. Lappin-Scott and P. Stoodley, The influence of fluid shear on the structure and material properties of sulphate-reducing bacterial biofilms, *Journal of Industrial Microbiology and Biotechnology*, **29**(6), 347-353 (2002).

[**3.42**] K. Horikoshi, Barophiles: deep-sea microorganisms adapted to an extreme environment, *Current Opinion in Microbiology*, **1**(3), 291-295 (1998).

[**3.43**] P.S. Stewart and M.J. Franklin, Physiological heterogeneity in biofilms, *Nature Review Microbiology*, **6**(3), 199-21 (2008).

[**3.44**] I.B. Beech, Corrosion of technical materials in the presence of biofilms – current understanding and state-of-the art methods of study, *International Biodeterioration and Biodegradation*, **53**(3), 177-183 (2004).

[**3.45**] S.J. Yuan, Amy M.F. Choong and S.O. Pehkonen, The influence of the marine aerobic Pseudomonas strain on the corrosion of 70/30 Cu–Ni alloy, *Corrosion Science,* **49**(12), 4352-4355 (2007).

[**3.46**] C. Hellio, C. Simon-Colin, A.S. Clare and E. Deslandes, Isethionic acid and floridoside isolated from the red alga, Grateloupia turuturu, inhibit settlement of Balanus amphitrite cyprid larvae, *Biofouling*, **20**(3), 139-145 (2004).

[**3.47**] T. Nyström, K. Flärdh and S. Kjelleberg, Responses to Multiple-Nutrient Strarvation in Marine *Vibrio* sp. Strain CCUG 15956, *Journal of Bacteriology*, **172**(12), 7085-7097 (1990).

[**3.48**] K. Flärdh, T. Axberg, N.H. Albertson and S. Kjelleberg, Stringent Control during Carbon Starvation of Marine *Vibrio* Sp. Strain S14: Molecular Cloning, Nucleotide Sequence, and Deletion of the *relA* Gene, *Journal of Bacteriology*, **176**(19), 5949-5957 (1994).

[**3.49**] I.B. Beech and C.C. Gaylarde, Recent advances in the study of biocorrosion - an overview, *Revista de Microbiologia*, **30**(3), 177-190 (1999).

[**3.50**] M. Fletcher and G.D. Floodgate, An Electron-microscopic Demonstration of an Acidic Polysaccharide Involved in the Adhesion of a Marine Bacterium to Solid Surfaces, *Journal of General Microbiology*, **74**(FEB), 325-334 (1973).

[**3.51**] J.P. Busalmen, M. Vázquez and S.R. de Sánchez, New evidences on the catalase mechanism of microbial corrosion, *Electrochimica Acta*, **47**(12), 1857-1865 (2002).

[**3.52**] M.P. Dawson, B.A. Humphrey and K.C. Marshall, Adhesion: a tactic in the survival strategy of a marine vibrio during starvation, *Current Microbiology*, **6**(4), 195-199 (1981).

[**3.53**] S. Kjelleberg, B.A. Humphrey and K.C. Marshall, Effect of interfaces on small starved marine bacteria, *Applied and Environmental Microbiology*, **43**(5), 1166-1172 (1982).

[**3.54**] M. Fletcher, The Effects of Proteins on Bacterial Attachment to Polystyrene, *Journal of General Microbiology*, **94**(6), 400-404 (1976).

[**3.55**] M. Fletcher, The effects of culture concentration and age, time, and temperature on bacterial attachment to polystyrene, *Canadian Journal of Microbiology*, **23**(1), 1-6 (1977).

[**3.56**] M. Fletcher and G.I. Loeb, Influence of Substratum Characteristics on the Attachment of a Marine Pseudomonad to Solid Surfaces, *Applied and Environmental Microbiology*, **37**(1), 67-72 (1979).

[**3.57**] S.J. Yuan, S.O. Pehkonen, Y.P. Ting, E.T. Kang and K.G. Neoh, Corrosion Behavior of Type 304 Stainless Steel in a Simulated Seawater-Based Medium in the Presence and Absence of Aerobic *Pseudomonas* NCIMB 2021 Bacteria, *Industrial and Engineering Chemistry Research*, **47**(9), 3008-3020 (2008).

[**3.58**] I. Beech, L. Hanjagsit, M. Kalaji, A.L. Neal and V. Zinkevich, Chemical and structural characterization of exopolymers produced by *Pseudomonas* sp. NCIMB 2021 in continuous culture, *Microbiology*, **145**(6), 1491-1497 (1999).

[**3.59**] S.J. Yuan and S.O. Pehkonen, Microbiologically influenced corrosion of 304 stainless steel by aerobic *Pseudomonas* NCIMB 2021 bacteria: AFM and XPS study, *Colloids and Surfaces B: Biointerfaces*, **59**(1), 87-99 (2007).

[**3.60**] K. Rasmussen and K. Østgaard, Adhesion of the marine bacterium *Pseudomonas* sp. NCIMB 2021 to different hydrogel surfaces, *Water Research*, **37**(3), 519-524 (2003).

[**3.61**] B.E. Christensen, J. Kjosbakken and O. Smidsrød, Partial Chemical and Physical Characterization of Two Extracellular Polysaccharides Produced by Marine, Periphytic *Pseudomonas* sp. Strain NCMB 2021, *Applied and Environmental Microbiology*, **50**(4), 837-845 (1985).

[**3.62**] M. Salta, J.A. Wharton, P. Stoodley, S.P. Dennington, L.R. Goodes, S. Werwinski, U. Mart, R.J.K. Wood and K.R. Stookes, Designing biomimetic antifouling surfaces, *Philosophical Transactions of the Royal Society A*, **368**(1929), 4729-4754 (2010).

[**3.63**] W.G. Characklis, *Biofilm development: A process analysis*, In: Marshall, K.C., Ed., Microbial Adhesion and Aggregation, Vol. 31, Life Sciences Research Report, Springer-Verlag, Germany (1984).

[**3.64**] C.W. Keevil, Continuous Culture Models to Study Pathogens in Biofilms, *Methods in Enzymology: Microbial Growth in Biofilms Part B*, **337**, 104-122 (2001).

[**3.65**] D.E. Dykhuizen and D.L. Hartl, Selection in Chemostats, *Microbiological Re*views, **47**(2), 150-168 (1983).

[**3.66**] J.P. Grivet, Nonlinear Population Dynamics in the Chemostat, *Computing in Science and Engineering*, **3**(1), 48-55 (2001).

[**3.67**] J.T. Walker, D.J. Bradshaw, M.R. Fulford and P.D. Marsh, Microbiological Evaluation of a Range of Disinfectant Products To Control Mixed-Species Biofilm Contamination in a Laboratory Model of a Dental Unit Water System, *Applied and Environmental Microbiology*, **69**(6), 3327-3332 (2003).

[**3.68**] N.F. Azevedo, M.J. Vieira and C.W. Keevil, Establishment of a continuous model system to study *Helicobacter pylori* survival in potable water biofilms, *Water Science and Technology*, **47**(5), 155-160 (2003).

[**3.69**] R.Bos, H.C. van der Mei and H.J. Busscher, Physico-chemistry of initial microbial adhesive interactions – its mechanisms and methods for study, *FEMS Microbiology Reviews*, **23**(2), 179-230 (1999).

[**3.70**] J.S. Webb, L.S. Thompson, S. James, T. Charlton, T. Tolker-Nielsen, B. Koch, M. Givskov and S. Kjelleberg, Cell Death in *Pseudomonas aeruginosa* Biofilm Development, *Journal of Bacteriology*, **185**(15), 4585-4592 (2003).

[**3.71**] P. Stoodley, Z. Lewandowski, J.D. Boyle and H.M. Lappin-Scott, Oscillation characteristics of biofilm streamers in turbulent flowing water as related to drag and pressure drop, *Biotechnology and Bioengineering*, **57**(5), 537-544 (1998).

[**3.72**] H.J. Busscher and H.C. van der Mei, Microbial Adhesion in Flow Displacement Systems, *Clinical Microbiology Reviews*, **19**(1), 127-141 (2006).

[**3.73**] R.J. Holland, *NOCS Flow Cytometry Facility User Guide BD FACSort and FACSCalibur Instruments*, UK (2008).

[**3.74**] D. Marie, F. Partensky, S. Jacquet and D. Vaulot, Enumeration and Cell Cycle Analysis of Natural Populations of Marine Picoplankton by Flow Cytometry Using the Nucleic Acid Stain SYBR Green I, *Applied and Environmental Microbiology*, **63**(1), 186-193 (1997).

[**3.75**] J.L. Collier, Flow cytometry and the single cell in phycology, *Journal of Phycology*, **36**(4), 628-644 (2000).

References to Chapter 4

[**4.1**] M.Fletcher and G.D. Floodgate, An Electron-microscopic Demonstration of an Acidic Polysaccharide Involved in the Adhesion of a Marine Bacterium to Solid Surfaces, *Journal of General Microbiology*, **74**(FEB), 325-334 (1973).

[**4.2**] M.C. Frost, M.M. Reynolds and M.E. Meyerhoff, Polymers incorporating nitric oxide releasing/generating substances for improved biocompatibility of blood-contacting medical devices, *Biomaterials*, **26**(14), 1685-1693 (2005).

[**4.3**] V.N. Bernshtein and V.G. Belikov, Sodium nitroprusside and its use in analysis, *Russian Chemical Reviews*, **30**(4), 227-236 (1961).

[**4.4**] R. Riegman, W. Stolte, A.A.M. Noordeloos and D. Slezak, Nutrient uptake and alkaline phosphatase (EC 3:1:3:1) activity of *Emiliania huxleyi* (Prymnesiophyceae) during growth under N and P limitation in continuous cultures, *Journal of Phycology*, **36**(1), 87-96 (2000).

[**4.5**] M.Fletcher, The effects of culture concentration and age, time, and temperature on bacterial attachment to polystyrene, *Canadian Journal of Microbiology*, **23**(1), 1-6 (1977).

[**4.6**] X. Bai, S.C. Dexter and G.W. Luther III, Application of EIS with Au–Hg microelectrode in determining electron transfer mechanisms, *Electrochimica Acta*, **51**(8-9), 1524-1533 (2005).

[**4.7**] A.I. Railkin, *Marine Biofouling: Colonization Processes and Defenses*, 1st ed., CRC Press LLC, USA (2004).

[**4.8**] H.-C. Flemming, P. Sriyutha Murthy, R. Venkatesan and K.E. Cooksey, *Marine and Industrial Biofouling*, Springer, Germany (2009).

[**4.9**] N. Barraud, D. J. Hassett, S.-H. Hwang, S. A. Rice, S. Kjelleberg and J. S. Webb, Involvement of Nitric Oxide in Biofilm Dispersal of Pseudomonas *aeruginosa*, *Journal of Bacteriology,* **188**(21), 7344-7353 (2006).

[**4.10**] R.C. Barik, *Environmental factors affecting the marine corrosion performance of nickel aluminium bronze*, PhD Thesis, University of Southampton, Faculty of Engineering, Science and Mathematics, School of Engineering Sciences (2006).

[**4.11**] M.J., Kennish, *CRC Practical Handbook of Marine Science*, 2nd ed., CRC Press, Boca Raton, FL, USA (1994).

[**4.12**] H.A. Videla, *Manual of Biocorrosion*, 1st ed., CRC Press, USA (1996).

[**4.13**] I.O. K'Owino and O.A. Sadik, Impedance Spectroscopy: A Powerful Tool for Rapid Biomolecular Screening and Cell Culture Monitoring, *Electroanalysis*, **17**(23), 2101-2113 (2005).

[**4.14**] K.R. Trethewey and J. Chamberlain, *Corrosion for Science and Engineering*, 2nd ed., Longman, UK (1995).

[**4.15**] D.J.G. Ives and G.J. Janz, *Reference Electrodes, Theory and Practice*, UK ed., Academic Press Inc., USA (1961).

[**4.16**] F. Zhao, R.C.T. Slade and J.R. Varcoe, Techniques for the study and development of microbial fuel cells: an electrochemical perspective, *Chemical Society Reviews*, **38**(7), 1926-1939 (2009).

[**4.17**] M. Sosna, *Oxygen Reduction at Electrodes: Application to the Dissolved Oxygen Sensor for in situ Oceanographic Measurements*, PhD Thesis, University of Southampton, Faculty of Engineering, Science and Mathematics, School of Chemistry (2006).

[**4.18**] R.Bos, H.C. van der Mei and H.J. Busscher, Physico-chemistry of initial microbial adhesive interactions – its mechanisms and methods for study, *FEMS Microbiology Reviews*, **23**(2), 179-230 (1999).

[**4.19**] J.S. Webb, L.S. Thompson, S. James, T. Charlton, T. Tolker-Nielsen, B. Koch, M. Givskov and S. Kjelleberg. Cell Death in *Pseudomonas aeruginosa* Biofilm Development. *Journal of Bacteriology*, **185**(15), 4585-4592 (2003).

[**4.20**] J.F. Douglas, J.M. Gasiorek and J.A.Swaffield. *Fluid Mechanics*, 3rd. ed., Longman Scientific & Technical, UK (1995).

[**4.21**] Y.A. Çengel and J.M. Cimbala, *Fluid mechanics: fundamentals and applications*, 1st ed., McGraw-Hill, USA (2006).

[**4.22**] D.J. Shaughnessy, Jr., I.M. Katz and J.P. Schaffer, *Introduction to Fluid Mechanics*, Oxford University Press, Inc., UK (2005).

[**4.23**] S. Bayoudh, A. Othmane, L. Ponsonnet and H. Ben Ouada, Electrical detection and characterization of bacterial adhesion using electrochemical impedance spectroscopy-based flow chamber, *Colloids and Surfaces A: Physicochemical and Engineering Aspects*, **318**(1-3), 291-300 (2008).

[**4.24**] M. Mehdi Salek, S.M. Jones and R.J. Martinuzzi, The influence of flow cell geometry related shear stresses on the distribution, structure and susceptibility of *Pseudomonas aeruginosa* 01 biofilms, *Biofouling*, **25**(8), 711-725 (2009).

[**4.25**] P. Stoodley, Z. Lewandowski, J.D. Boyle and H.M. Lappin-Scott, Oscillation Characteristics of Biofilm Streamers in Turbulent Flowing Water as Related to Drag and Pressure Drop, *Biotechnology and Bioengineering*, **57**(5), 537-544 (1998).

[**4.26**] P. Stoodley, S. Wilson, L. Hall-Stoodley, J.D. Boyle, H.M. Lappin-Scott and J.W. Costerton, Growth and detachment of cell clusters from mature mixed-species biofilms, *Applied and Environmental Microbiology*, **67**(12), 5608-5613 (2001).

[**4.27**] D. Pletcher and F. Walsh, *Industrial Electrochemistry*, 2nd ed., Blackie A. & P., An Imprint of Chapman & Hall, UK (1993).

[**4.28**] J.A. Wharton and R.J.K Wood, Influence of flow conditions on the corrosion of AISI 304L stainless steel, *Wear*, **256**(5), 525-536 (2004).

[**4.29**] B.C. Dunsmore, A. Jacobsen, L. Hall-Stoodley, C.J. Bass, H.M. Lappin-Scott and P. Stoodley, The influence of fluid shear on the structure and material properties of sulphate-reducing bacterial biofilms, *Journal of Industrial Microbiology and Biotechnology*, **29**(6), 347-353 (2002).

[**4.30**] P. Stoodley, D. DeBeer and H.M. Lappin-Scott, Influence of Electric Fields and pH on Biofilm Structure as Related to the Bioelectric Effect, *Antimicrobial Agents and Chemotherapy*, **41**(9), 1876-1879 (1997).

[**4.31**] P. Stoodley, S. Yang, H. Lappin-Scott and Z. Lewandowski, Relationship Between Mass Transfer Coefficient and Liquid Flow Velocity in Heterogenous Biofilms Using Microelectrodes and Confocal Microscopy, *Biotechnology and Bioengineering*, **56**(6), 682-688 (1997).

[**4.32**] R.J. Cornish, Flow in Pipe of Rectangular Cross-Section, *Proceedings of the Royal Society of London. Series A, Containing Papers of a Mathematical and Physical Character*, **120**(786), 691-700 (1928).

[**4.33**] A.C. Fisher, *Electrode Dynamics*, Oxford University Press Inc., USA (2006).

[**4.34**] M. Salta, J.A. Wharton, P. Stoodley, S.P. Dennington, L.R. Goodes, S. Werwinski, U. Mart, R.J.K. Wood and K.R. Stookes, Designing biomimetic antifouling surfaces, *Philosophical Transactions of the Royal Society A*, **368**(1929), 4729-4754 (2010).

[**4.35**] F. Ghirelli and B. Leckner, Transport equation for the local residence time of a fluid, *Chemical Engineering Science*, **59**(3), 513-523 (2004).

[**4.36**] N. Le Bozec, *Réaction de réduction de l'oxygène sur les aciers inoxydables en eau de mer naturelle. Influence du biofilm sur les processus de corrosion*, Thèse de doctorat (Spécialité Chimie Fine), Université de Bretagne Occidentale (2000).

[**4.37**] Watson Marlow Pumps, *Watson-Marlow Bredel Manuals: Watson-Marlow 323E, 323S, 323U and 323Du pumps*, Watson-Marlow Limited, UK (2008).

[**4.38**] Y. Le Duigou and W. Leidert, Effect of Residual Amounts of Oxygen on the Accuracy of Coulometric Titrations of Uranium, *Fresenius' Zeitschrift für Analytische Chemie*, **285**(3-4), 264-265 (1977).

[**4.39**] E.C. Slater, Phosphorylation Coupled with the Oxidation of α-Ketoglutarate by Heart-Muscle Sarcosomes. 3 Experiments with Ferricytochrome *C* as Hydrogen Acceptor, *Biochemical Journal*, **59**(3), 392-405 (1955).

[**4.40**] LI-COR, *LI-189 Quantum/Radiometer/Photometer Instruction Manual*, LI-COR, Inc., USA (1990).

[**4.41**] L.D. Chambers, *The Development of a Marine Antifouling System Using Environmentally Acceptable and Naturally Occurring Products*, PhD Thesis, University of Southampton, Faculty of Engineering, Science and Mathematics, School of Engineering Sciences, Surface Engineering and Tribology Research Group (2008).

[**4.42**] J.B. Pawley, *Handbook of Biological Confocal Microscopy*, 3rd ed., Springer, USA (2006).

[**4.43**] S.J. Yuan and S.O. Pehkonen, Microbiologically influenced corrosion of 304 stainless steel by aerobic *Pseudomonas* NCIMB 2021 bacteria: AFM and XPS study, *Colloids and Surfaces B: Biointerfaces*, **59**(1), 87-99 (2007).

References to Chapter 5

[**5.1**] M.Fletcher, The effects of culture concentration and age, time, and temperature on bacterial attachment to polystyrene, *Canadian Journal of Microbiology*, **23**(1), 1-6 (1977).

[**5.2**] C.W. Keevil, Continuous Culture Models to Study Pathogens in Biofilms, *Methods in Enzymology: Microbial Growth in Biofilms Part B*, **337**, 104-122 (2001).

[**5.3**] K. Rasmussen and K. Østgaard, Adhesion of the marine bacterium *Pseudomonas* sp. NCIMB 2021 to different hydrogel surfaces, *Water Research*, **37**(3), 519-524 (2003).

[**5.4**] M. Sosna, *Oxygen Reduction at Electrodes: Application to the Dissolved Oxygen Sensor for in situ Oceanographic Measurements*, PhD Thesis, University of Southampton, Faculty of Engineering, Science and Mathematics, School of Chemistry (2006).

[**5.5**] L.D. Burke and P.F. Nugent, The Electrochemistry of Gold: I The Redox Behaviour of the Metal in Aqueous Media, *Gold Bulletin*, **30**(2), 43-53 (1997).

[**5.6**] Y. Ling, J.C. Elkenbracht, W.F. Flanagan and B.D. Lichter, The Electrochemical Oxidation of Gold in 0.6 M NaCl and 0.3 M Na_2SO_4, *Journal of The Electrochemical Society*, **144**(8), 2689-2697 (1997).

[**5.7**] N. Le Bozec, *Réaction de réduction de l'oxygène sur les aciers inoxydables en eau de mer naturelle. Influence du biofilm sur les processus de corrosion*, Thèse de doctorat (Spécialité Chimie Fine), Université de Bretagne Occidentale (2000).

[**5.8**] D. Pletcher and F. Walsh, *Industrial Electrochemistry*, 2nd ed., Blackie A. & P., An Imprint of Chapman & Hall, UK (1993).

[**5.9**] F. Walsh, *A First Course in Electrochemical Engineering*, 1st ed., The Electrochemical Consultancy, UK (1993).

[**5.10**] G. Denuault, Electrochemical techniques and sensors for ocean research, *Ocean Science Discussions*, **6**(2), 1857-1893 (2009).

[**5.11**] M. Sosna, G. Denuault, R.W. Pascal, R.D. Prien and M. Mowlem, Field assessment of a new membrane-free microelectrode dissolved oxygen sensor for water column profiling, *Limnology and Oceanography: Methods*, **6**, 180-189 (2008).

[**5.12**] M. Sosna, G. Denuault, R.W. Pascal, R.D. Prien and M. Mowlem, Development of a reliable microelectrode dissolved oxygen sensor, *Sensors and Actuators B*, **123**(1), 344-351 (2007).

[**5.13**] Y. Hu, J. Zhang and J. Ulstrup, Interfacial Electrochemical Electron Transfer Processes in Bacterial Biofilm Environments on Au(111), *Langmuir*, **26**(11), 9094-9103 (2010).

[**5.14**] A.J. Bard and L.R. Faulkner, *Electrochemical Methods: Fundamentals and Applications*, 2nd ed., John Wiley and Sons, USA (2004).

[**5.15**] M. Sheffer, V. Vivier and D. Mandler, Self-assembled monolayers on Au microelectrodes, *Electrochemistry Communications*, **9**(12), 2827-2832 (2007).

[**5.16**] K.L. Davis, B.J. Drews, H. Yue, D. H. Waldeck, K. Knorr and R.A. Clark. Electron-Transfer Kinetics of Covalently Attached Cytochrome *c*/SAM/Au Electrode Assemblies, *Journal of Physical Chemistry C*, **112**(16), 6571-6576 (2008).

[**5.17**] S.E. Moulton, J.N. Barisci, A. Bath, R. Stella and G.G. Wallace, Studies of double layer capacitance and electron transfer at a gold electrode exposed to protein solutions, *Electrochimica Acta*, **49**(24), 4223-4230 (2004).

[**5.18**] J. Gamby, A. Pailleret, C.B. Clodic, C.-M. Pradier and B. Tribollet, In situ detection and characterization of potable water biofilms on materials by microscopic, spectroscopic and electrochemistry methods, *Electrochimica Acta*, **54**(1), 66-73 (2008).

[**5.19**] C. Barus, P. Gros, M. Comtat, S. Daunes-Marion and R. Tarroux, Electrochemical behaviour of *N*-acetyl-L-cysteine on gold electrode – A tentative reaction mechanism, *Electrochimica Acta*, **52**(28), 7978-7985 (2007).

[**5.20**] R.M. Dilmore, *Evaluation of the kinetics of biologically catalyzed treatment and regeneration of NO_x scrubbing process waters*, PhD thesis, University of Pittsburgh, Graduate Faculty of the School of Engineering (2004).

[**5.21**] K.L. Straub, M. Benz and B. Schink, Iron metabolism in anoxic environments at near neutral pH, *FEMS Microbiology Ecology*, **34**(3), 181-186 (2001).

[**5.22**] C-H. Huang, N.D. McClenaghan, A. Kuhn, G. Bravic and D.M. Bassani, Hierarchical self-assembly of all-organic photovoltaic devices,*Tetrahedron*, **62**(9), 2050-2059 (2006).

[**5.23**] J.P. Busalmen, A. Berná and J.M. Feliu, Spectroelectrochemical Examination of the Interaction between Bacterial Cells and Gold Electrodes, *Langmuir*, **23**(11), 6459-6466 (2007).

[**5.24**] A. Bressel, J.W. Schultze, W. Khan, G.M. Wolfaardt, H.-P. Rohns, R. Irmscher and M.J. Schöning, High resolution gravimetric, optical and electrochemical investigations of microbial biofilm formation in aqueous systems, *Electrochimica Acta*, **48**(20-22) 3363-3372 (2003).

[**5.25**] J.P. Busalmen, M. Vázquez and S.R. de Sánchez. New evidences on the catalase mechanism of microbial corrosion, *Electrochimica Acta*, **47**(12), 1857-1865 (2002).

[**5.26**] I.B. Beech and J. Sunner, Biocorrosion: towards understanding interactions between biofilms and metals, *Current Opinion in Biotechnology*, **15**(3), 181-186 (2004).

[**5.27**] D. Nercessian, F.B. Duville, M. Desimone, S. Simison and J.P. Busalmen, Metabolic turnover and catalase activity of biofilms of *Pseudomonas fluorescens* (ATCC 17552) as related to copper corrosion, *Water Research*, **44**(8), 2592-2600 (2010).

[**5.28**] B. Tribollet, Electrochemical sensors for biofilm and biocorrosion, *Materials and Corrosion*, **54**(7), 527-534 (2003).

[**5.29**] S. Parot, *Biofilms électroactifs: formation, caractérisation et mécanismes*, Thèse de doctorat (Spécialité: Génie des Procédés et de l'Environnement), Institut National Polytechnique de Toulouse (2007).

[**5.30**] S. Dulon, S. Parot, M.-L. Delia and A. Bergel, Electroactive biofilms: new means for electrochemistry, *Journal of Applied Electrochemistry*, **37**(1), 173-179 (2007).

[**5.31**] J.P. Busalmen and S.R. de Sánchez, Changes in the Electrochemical Interfaces as a Result of the Growth of *Pseudomonas fluorescens* Biofilms on Gold, *Biotechnology and Bioengineering*, **82**(5), 619-624 (2003).

[**5.32**] A.K. Shukla, P. Suresh, S. Berchmans and A. Rajendran, Biological fuel cells and their application, *Current Science*, **87**(4), 455-468 (2004).

[**5.33**] F. Zhao, R.C.T. Slade and J.R. Varcoe, Techniques for the study and development of microbial fuel cells: an electrochemical perspective, *Chemical Society Reviews*, **38**(7), 1926-1939 (2009).

[**5.34**] C.I. Torres, A.K. Marcus, H-S. Lee, P. Parameswaran, R. Krajmalnik-Brown and B.E. Rittmann, A kinetic perspective on extracellular electron transfer by anode-respiring bacteria, *FEMS Microbiology Review*, **34**(1), 3-17 (2010).

[**5.35**] H.A. Videla, *Manual of Biocorrosion*, 1st ed., CRC Press, USA (1996).

[**5.36**] H.-C. Flemming, P. Sriyutha Murthy, R. Venkatesan and K.E. Cooksey, *Marine and Industrial Biofouling*, Springer, Germany (2009).

[**5.37**] M. Salta, J.A. Wharton, P. Stoodley, S.P. Dennington, L.R. Goodes, S. Werwinski, U. Mart, R.J.K. Wood and K.R. Stookes, Designing biomimetic antifouling surfaces, *Philosophical Transactions of the Royal Society A*, **368**(1929), 4729-4754 (2010).

[**5.38**] P. Cristiani, A. Mollica and G. Ventura, *On-line monitoring of biofilm and T.R.O. by a new ENEL'S system*, In: T.R. Bott (Ed.), Understanding Heat Exchanger Fouling and Its Mitigation Conference, 11-16 May, Castel Pascoli, Italy, Begell House, inc., New York, 323-329 (1997).

[**5.39**] M.C.M. Bruijs, L.P. Venhuis, H.A. Jenner, G.J. Licina and D. Daniels, Biocide Optimization Using On-Line Biofilm Monitor, *PowerPlant Chemistry*, **3**(7), 400-405 (2001).

[**5.40**] P. Cristiani, Solutions to fouling in power station condensers, *Applied Thermal Engineering*, **25**(16), 2630-2640 (2005).

[**5.41**] D.E. Nivens, R.J. Palmer Jr and D.C. White, Continuous nondestructive monitoring of microbial biofilms: a review of analytical techniques, *Journal of Industrial Microbiology and Biotechnology*, **15**(4), 263-276 (1995).

[**5.42**] X. Bai, S.C. Dexter and G.W. Luther III, Application of EIS with Au–Hg microelectrode in determining electron transfer mechanisms, *Electrochimica Acta*, **51**(8-9), 1524-1533 (2005).

[**5.43**] E. Barsoukov and J.R. Macdonald, *Impedance Spectroscopy, Theory, Experiment, and Applications*, 2nd ed., John Wiley & Sons, USA (2005).

[**5.44**] C.M Mendel and D.B. Mendel, 'Nom-specific' binding. The problem, and a solution, *Biochemical Journal*, **228**(1), 269-272 (1985).

[**5.45**] D.R. Jackson, S. Omanovic and S.G. Roscoe, Electrochemical Studies of the Adsorption Behavior of Serum Proteins on Titanium, *Langmuir*, **16**(12), 5449-5457 (2000).

[**5.46**] D. Sun, *Abrasion-corrosion of Cast CoCrMo in Simulated Hip Joint Environments*, PhD Thesis, University of Southampton, Faculty of Engineering, Science and Mathematics, School of Engineering Sciences (2009).

[**5.47**] A.I. Railkin, *Marine Biofouling: Colonization Processes and Defenses*, 1st ed., CRC Press LLC, USA (2004).

[**5.48**] C. Hellio and D.M. Yebra, *Advances in marine antifouling coatings and technologies*, Woodhead Publishing Limited, UK (2009).

[**5.49**] B. Bonanni, D. Alliata, A.R. Bizzarri and S. Cannistraro, Topological and Electron-Transfer Properties of Yeast Cytochrome c Adsorbed on Bare Gold Electrodes, ChemPhysChem, **4**(11), 1183-1188 (2003).

[**5.50**] X. Muñoz-Berbel, N. Vigués, A.T.A. Jenkins, J. Mas and F.J. Muñoz, Impedimetric approach for quantifying low bacteria concentrations based on the changes produced in the electrode-solution interface during the pre-attachment stage, *Biosensors and Bioelectronics*, **23**(10), 1540-1546 (2008).

[**5.51**] X. Muñoz-Berbel, C. García-Aljaro and F.J. Muñoz, Impedimetric approach for monitoring the formation of biofilms on metallic surfaces and the subsequent application to the detection of bacteriophages, *Electrochimica Acta*, **53**(19), 5739-5744 (2008).

[**5.52**] H.L. Gomes, R.B. Leite, R. Afonso, P. Stallinga and M.L. Cancela, A microelectrode impedance method to measure interaction of cells, *Proceedings of the IEEE Sensors 2004,* Vienna, Austria, Vols 1-3, 1011-1013, Oct 24-27, (2004).

[**5.53**] S.J. Yuan, Amy M.F. Choong and S.O. Pehkonen, The influence of the marine aerobic *Pseudomonas* strain on the corrosion of 70/30 Cu–Ni alloy, *Corrosion Science*, **49**(12), 4352-4385 (2007).

[**5.54**] P. Stoodley, S. Yang, H. Lappin-Scott and Z. Lewandowski, Relationship Between Mass Transfer Coefficient and Liquid Flow Velocity in Heterogenous Biofilms Using Microelectrodes and Confocal Microscopy, *Biotechnology and Bioengineering*, **56**(6), 682-688 (1997).

[**5.55**] G.J. Brankevich, M.L.F. De Mele and H.A. Videla, Biofouling and Corrosion in Coastal Power Plant Cooling Water Systems, *Marine Technology Society Journal*, **24**(3), 18-28 (1990).

[**5.56**] Q. Zhao, Y. Liu, C. Wang, S. Wang and H. Müller-Steinhagen, Effect of surface free energy on the adhesion of biofouling and crystalline fouling, *Chemical Engineering Science*, **60**(17), 4858-4865 (2005).

[**5.57**] N. Barraud, D. J. Hassett, S.-H. Hwang, S. A. Rice, S. Kjelleberg and J. S. Webb, Involvement of Nitric Oxide in Biofilm Dispersal of *Pseudomonas aeruginosa*, *Journal of Bacteriology*, **188**(21), 7344–7353 (2006).

[**5.58**] J.S. Webb, L.S. Thompson, S. James, T. Charlton, T. Tolker-Nielsen, B. Koch, M. Givskov and S. Kjelleberg. Cell Death in *Pseudomonas aeruginosa* Biofilm Development. *Journal of Bacteriology*, **185**(15), 4585-4592 (2003).

[**5.59**] R.M. Donlan, Biofilms: Microbial Life on Surfaces, *Emerging Infectious Diseases*, **8**(9), 881-890 (2002).

[**5.60**] E.M. Hetrick and M.H. Schoenfisch, Analytical Chemistry of Nitric Oxide, *Annual Review of Analytical Chemistry*, **2**, 409-433 (2009).

[**5.61**] W.G. Characklis and K.C. Marshall, *Biofilms*, Wiley, USA (1990).

[**5.62**] S.J. Yuan and S.O. Pehkonen, Microbiologically influenced corrosion of 304 stainless steel by aerobic *Pseudomonas* NCIMB 2021 bacteria: AFM and XPS study, *Colloids and Surfaces B: Biointerfaces*, **59**(1), 87-99 (2007).

[**5.63**] Y.-R. Wang, P. Hu, Q.-L. Liang, G.-A. Luo and Y.-M. Wang, Transport Properties of Bovine Serum Albumin in Gold Nanotubule Membrane Modified with Cl^-, *Chinese Journal of Analytical Chemistry*, **35**(4), 583-585 (2007).

[**5.64**] W. Franks, I. Schenker, P. Schmutz and A. Hierlemann, Impedance Characterization and Modeling of Electrodes for Biomedical Applications, *IEEE Transactions on Biomedical Engineering*, **52**(7), 1295-1302 (2005).

[**5.65**] N. Washizu, Y. Katada and T. Kodama, Role of H_2O_2 in microbially influenced ennoblement of open circuit potentials for type 316L stainless steel in seawater, *Corrosion Science*, **46**(5), 1291-1300 (2004).

[**5.66**] R.C. Barik, *Environmental factors affecting the marine corrosion performance of nickel aluminium bronze*, PhD Thesis, University of Southampton, Faculty of Engineering, Science and Mathematics, School of Engineering Sciences (2006).

[**5.67**] O. Devos, C. Gabrielli and B. Tribollet, Simultaneous EIS and in situ microscope observation on a partially blocked electrode application to scale electrodeposition, *Electrochimica Acta*, **51**(8-9), 1413-1422 (2006).

[**5.68**] M. Metikos-Hukovic, Z. Pilic, R. Babic and D. Omanovic, Influence of alloying elements on the corrosion stability of CoCrMo implant alloy in Hank's solution, *Acta Biomaterialia*, **2**(6), 693-700 (2006).

[**5.69**] *Guide to the expression of uncertainty in measurement (GUM)*, International Organization for Standardization (1993).

[**5.70**] E.T. McAdams, A. Lackermeier, J.A. McLaughlin and D. Macken, The linear and the non-linear electrical properties of the electrode-electrolyte interface, *Biosensors and Bioelectronics,* **10**(1-2), 67-74 (1995).

[**5.71**] M.F Smiechowski, V.F. Lvovich, S. Roy, A. Fleischman, W.H. Fissell and A.T. Riga, Electrochemical detection and characterization of proteins, *Biosensors and Bioelectronics*, **22**(5), 670-677 (2006).

[**5.72**] S. Omanovic and S.G. Roscoe, Electrochemical Studies of the Adsorption Behavior of Bovine Serum Albumin on Stainless Steel, *Langmuir*, **15**(23), 8315-8321 (1999).

[**5.73**] J.E.I. Wright, N.P. Cosman, K. Fatih, S. Omanovic and S.G. Roscoe, Electrochemical impedance spectroscopy and quartz crystal nanobalance (EQCN) studies of insulin adsorption on Pt, *Journal of Electroanalytical Chemistry*, **564**(1-2), 185-197 (2004).

[**5.74**] S. Bayoudh, A. Othmane, L. Ponsonnet and H. Ben Ouada, Electrical detection and characterization of bacterial adhesion using electrochemical impedance spectroscopy-based flow chamber, *Colloids and Surfaces A: Physicochemical and Engineering Aspects*, **318**(1-3), 291-300 (2008).

[**5.75**] X. Muñoz-Berbel, N. Vigués, J. Mas, A.T.A. Jenkins and F.J. Muñoz, Impedimetric characterization of the changes produced in the electrode-solution interface by bacterial attachment, *Electrochemistry Communications*, **9**(11), 2654-2660 (2007).

[**5.76**] M. Basu, S. Seggerson, J. Henshaw, J. Jiang, R. del A Cordona, C. Lefave, P. J. Boyle, A. Miller, M. Pugia and S. Basu, Nano-biosensor development for bacterial detection during human kidney infection: Use of glycoconjugate-specific antibody-bound gold NanoWire arrays (GNWA), *Glycoconjugate Journal*, **21**(8-9), 487-496 (2004).

[**5.77**] A.T. Poortinga, R. Bos and H.J. Busscher, Measurement of charge transfer during bacterial adhesion to an indium tin oxide surface in a parallel plate flow chamber, *Journal of Microbiological Methods*, **38**(3), 183-189 (1999).

[**5.78**] P.S. Stewart and M.J. Franklin, Physiological heterogeneity in biofilms, *Nature Review Microbiology*, **6**(3), 199-21 (2008).

[**5.79**] A.C. Fisher, *Electrode Dynamics*, Oxford University Press Inc., USA (2006).

[**5.80**] J.B. Kaplan, Biofilm dispersal: Mechanisms, clinical implications, and potential therapeutic uses, *Journal of Dental Research*, **89**(3), 205-218 (2010).

[**5.81**] M. Otto, Staphylococcus epidermidis – the 'accidental' pathogen, *Nature Reviews Microbiology*, **7**(8), 555-567 (2009).

[**5.82**] D.M. Grant and T.R. Bott, Biocide Dosing Strategies for Biofilm Control, *Heat Transfer Engineering*, **26**(1), 44-50 (2005).

[**5.83**] R.-I. Stefan, J.F. van Staden and H. Y. Aboul-Enein, *Electrochemical Sensors in Bioanalysis*, Marcel Dekker, Inc., USA (2001).

[**5.84**] S. Ben-Ali, D.A. Cook, S.A.G. Evans, A. Thienpont, P.N. Bartlett and A. Kuhn, Electrocatalysis with monolayer modified highly organized macroporous electrodes, *Electrochemistry Communications*, **5**(9), 747-751 (2003).

[**5.85**] R. Szamocki, A. Velichko, C. Holzapfel, F. Mücklich, S. Ravaine, P. Garrigue, N. Sojic, R. Hempelmann and A. Kuhn, Macroporous Ultramicroelectrodes for Improved Electroanalytical Measurements, *Analytical Chemistry*, **79**(2), 533-539 (2007).

[**5.86**] H.-C. Flemming, Biofouling in water systems – cases, causes and countermeasures, *Applied Microbiology and Biotechnology*, **59**(6), 629-640 (2002).

References to Chapter 6

[**6.1**] O. Devos, C. Gabrielli and B. Tribollet, Simultaneous EIS and in situ microscope observation on a partially blocked electrode application to scale electrodeposition, *Electrochimica Acta*, **51**(8-9), 1413-1422 (2006).

[**6.2**] J.A. Wharton and K.R. Stokes, Analysis of nickel–aluminium bronze crevice solution chemistry using capillary electrophoresis, *Electrochemistry Communications*, **9**(5), 1035-1040 (2007).

[**6.3**] A.C. Fisher, *Electrode Dynamics*, Oxford University Press Inc., USA (2006).

[**6.4**] F. Zhao, R.C.T. Slade and J.R. Varcoe, Techniques for the study and development of microbial fuel cells: an electrochemical perspective, *Chemical Society Reviews*, **38**(7), 1926-1939 (2009).